p-ISSN 1607-3274
e-ISSN 2313-688X

Радіоелектроніка
Інформатика
Управління

Radio Electronics
Computer Science
Control

Радиоэлектроника
Информатика
Управление

9 771607 327005 33

2023/3

Національний університет «Запорізька політехніка»

Радіоелектроніка, інформатика, управління

Науковий журнал
Виходить чотири рази на рік
№ 3(66) 2023
Заснований у 1998 році, видається з 1999 року.
Засновник і видавець – Національний університет «Запорізька політехніка».
ISSN 1607-3274 (друкований), ISSN 2313-688X (електронний).
Запоріжжя
НУ «Запорізька політехніка»
2023

National University «Zaporizhzhia Polytechnic»

Radio Electronics, Computer Science, Control

The scientific journal
Published four times per year
№ 3(66) 2023
Founded in 1998, published since 1999.
Founder and publisher – National University «Zaporizhzhia Polytechnic».
ISSN 1607-3274 (print), ISSN 2313-688X (on-line).
Zaporizhzhia
NU «Zaporizhzhia Polytechnic»
2023

Национальный университет «Запорожская политехника»

Радиоэлектроника, информатика, управление

Научный журнал
Выходит четыре раза в год
№ 3(66) 2023
Основан в 1998 году, издается с 1999 года.
Основатель и издатель – Национальный университет «Запорожская политехника».
ISSN 1607-3274 (печатный), ISSN 2313-688X (электронный).
Запорожье
НУ «Запорожская политехника»
2023

Науковий журнал «Радіоелектроніка, інформатика, управління» (скорочена назва – РІУ) видається Національним університетом «Запорізька політехніка» (НУ «Запорізька політехніка») з 1999 р. періодичністю чотири номери на рік.

Зареєстровано у Міністерстві юстиції України 19.11.2019 р. (Свідоцтво про державну реєстрацію друкованого засобу масової інформації серія КВ № 24220-14060 ПР.)

ISSN 1607-3274 (друкований), **ISSN** 2313-688X (електронний).

Наказом Міністерства освіти і науки України № 409 від 17.03.2020 р. «Про затвердження рішень Атестаційної колегії Міністерства щодо діяльності спеціалізованих вчених рад від 06 березня 2020 року» **журнал включений до переліку наукових фахових видань України в категої «А» (найвищій рівень),** в яких можуть публікуватися результати дисертаційних робіт на здобуття наукових ступенів доктора наук і доктора філософії (кандидата наук).

Журнал включений до польського Переліку наукових журналів та рецензованих матеріалів міжнародних конференцій з присвоєною кількістю балів (додаток до оголошення Міністра науки та вищої освіти Республіки Польща від 31 липня 2019 р.: № 16981).

В журналі безкоштовно публікуються наукові статті англійською, російською та українською мовами.

Правила оформлення статей подано на сайті: http://ric.zntu.edu.ua/information/authors.

Журнал забезпечує **безкоштовний відкритий он-лайн доступ** до повнотекстових публікацій.

Журнал дозволяє авторам мати авторські права і зберігати права на видання без обмежень. Журнал дозволяє користувачам читати, завантажувати, копіювати, поширювати, друкувати, шукати або посилатися на повні тексти своїх статей. Журнал дозволяє повторне використання його вмісту у відповідності Creative Commons ліцензією CC BY-SA..

Опублікованим статтям присвоюється унікальний ідентифікатор цифрового об'єкта DOI.

Журнал входить до наукометричної бази Web of Science.

Журнал реферується та індексується у провідних міжнародних та національних реферативних журналах і наукометричних базах даних, а також розміщується у цифрових архівах та бібліотеках з безкоштовним доступом у режимі on-line, повний перелік яких подано на сайті: http://ric.zntu.edu.ua/about/editorialPolicies#custom-0.

Журнал розповсюджується за Каталогом періодичних видань України (передплатний індекс – 22914).

Тематика журналу: телекомунікації та радіоелектроніка, програмна інженерія (включаючи теорію алгоритмів і програмування), комп'ютерні науки (математичне і комп'ютерне моделювання, оптимізація і дослідження операцій, управління в технічних системах, міжмашинна і людино-машинна взаємодія, штучний інтелект, включаючи системи, засновані на знаннях, і експертні системи, інтелектуальний аналіз даних, розпізнавання образів, штучні нейронні і нейро-нечіткі мережі, нечітку логіку, колективний інтелект і мультиагентні системи, гібридні системи), комп'ютерна інженерія (апаратне забезпечення обчислювальної техніки, комп'ютерні мережі), інформаційні системи та технології (структури та бази даних, системи, засновані на знаннях та експертні системи, обробка даних і сигналів).

Усі статті, пропоновані до публікації, одержують **об'єктивний розгляд**, що оцінюється за суттю без урахування раси, статі, віросповідання, етнічного походження, громадянства або політичної філософії автора(ів).

Усі статті проходять двоступінчасте закрите (анонімне для автора) **резензування** штатними редакторами і незалежними рецензентами – провідними вченими за профілем журналу.

РЕДАКЦІЙНА КОЛЕГІЯ

РЕДАКЦІЙНО-КОНСУЛЬТАТИВНА РАДА

Рекомендовано до видання Вченою радою НУ «Запорізька політехніка», протокол № 2 від 25.09.2023.

Журнал зверстаний редакційно-видавничим відділом НУ «Запорізька політехніка».

Веб-сайт журналу: http://ric.zntu.edu.ua.

Адреса редакції: Редакція журналу «РІУ», Національний університет «Запорізька політехніка», вул. Жуковського, 64, м. Запоріжжя, 69063, Україна.

Тел: (061) 769-82-96 – редакційно-видавничий відділ Факс: +38-061-764-46-62

E-mail: rvv@zntu.edu.ua

The scientific journal «Radio Electronics, Computer Science, Control» is published by the National University «Zaporizhzhia Polytechnic» NU «Zaporizhzhia Polytechnic» since 1999 with periodicity four numbers per year.

The journal is registered by the Ministry of Justice of Ukraine in 19.11.2019. (State Registration Certificate of printed mass media series КВ № 24220-14060 ПР).

ISSN 1607-3274 (print), **ISSN** 2313-688X (on-line).

By the Order of the Ministry of Education and Science of Ukraine from 17.03.2020 № 409 "On approval of the decision of the Certifying Collegium of the Ministry on the activities of the specialized scientific councils dated 06 March 2020" **journal is included in the list of scientific specialized periodicals of Ukraine in category "A" (highest level),** where the results of dissertations for Doctor of Science and Doctor of Philosophy may be published.

The journal is included to tne Polish List of scientific journals and peer-reviewed materials from international conferences with assigned number of points (Annex to the announcement of the Minister of Science and Higher Education of Poland from July 31, 2019: Lp. 16981).

The journal publishes scientific articles in English, Russian, and Ukrainian free of charge.

The **article formatting rules** are presented on the site: http://ric.zntu.edu.ua/information/authors.

The journal provides policy of **on-line open (free of charge) access** for full-text publications. The journal allow the authors to hold the copyright without restrictions and to retain publishing rights without restrictions. The journal allow readers to read, download, copy, distribute, print, search, or link to the full texts of its articles. The journal allow reuse and remixing of its content, in accordance with Creative Commons license CC BY-SA.

Published articles have a unique digital object identifier (DOI).

The journal is included into Web of Science.

The journal is abstracted and indexed in leading international and national abstractig journals and scientometric databases, and also placed to the digital archives and libraries with a free on-line access, full list of which is presented at the site: http://ric.zntu.edu.ua/about/editorialPolicies#custom-0.

The journal is distributed:by the Catalogue of Ukrainian periodicals (the catalog number is 22914).

The journal scope: telecommunications and radio electronics, software engineering (including algorithm and programming theory), computer science (mathematical modeling and computer simulation, optimization and operations research, control in technical systems, machine-machine and man-machine interfacing, artificial intelligence, including data mining, pattern recognition, artificial neural and neuro-fuzzy networks, fuzzy logic, swarm intelligence and multiagent systems, hybrid systems), computer engineering (computer hardware, computer networks), information systems and technologies (data structures and bases, knowledge-based and expert systems, data and signal processing methods).

All articles proposed for publication receive an **objective review** that evaluates substantially without regard to race, sex, religion, ethnic origin, nationality, or political philosophy of the author(s).

All articles undergo a two-stage **blind peer review** by the editorial staff and independent reviewers – the leading scientists on the profile of the journal.

EDITORIAL BOARD

EDITORIAL-ADVISORY COUNCIL

Recommended for publication by the Academic Council of NU «Zaporizhzhia Polytechnic», protocol № 2 dated 25.09.2023.

The journal is imposed by the editorial-publishing department of NU «Zaporizhzhia Polytechnic».

The journal web-site is http://ric.zntu.edu.ua.

The address of the editorial office: Editorial office of the journal «Radio Electronics, Computer Science, Control», National University «Zaporizhzhia Polytechnic», Zhukovskiy street, 64, Zaporizhzhia, 69063, Ukraine.

Tel.: +38-061-769-82-96 – the editorial-publishing department. Fax: +38-061-764-46-62

E-mail: rvv@zntu.edu.ua

ЗМІСТ

CONTENTS

РАДІОЕЛЕКТРОНІКА ТА ТЕЛЕКОМУНІКАЦІЇ

RADIO ELECTRONICS AND TELECOMMUNICATIONS

UDC 621.396.67

POWER SUPPLY OF RING ANTENNA USING DIRECTIONAL COUPLERS

Ilnitskyi L. Ya. – Dr. Sc., Honored Worker of Science and Technology of Ukraine, National Aviation University, Kyiv, Ukraine.

Shcherbyna O. A. – Dr. Sc., Professor of the Department of Electronics, Robotics and Technology of Monitoring and Internet of Things, National Aviation University, Kyiv, Ukraine.

Zaliskyi M. Yu.– Dr. Sc., Professor of the Department of Telecommunication and Radio Electronic Systems, National Aviation University, Kyiv, Ukraine.

Mykhalchuk I. I. – PhD, Assistant of the Department of Cyber Security and Information Protection, Taras Shevchenko National University, Kyiv, Ukraine.

Kozhokhina O. V. – PhD, Associate Professor of the Department of Avionics, National Aviation University, Kyiv, Ukraine.

ABSTRACT

Context. The circular polarization of radio waves is used in various electronic systems. This includes, for example, space communications stations, some radio relay communication systems, radar stations, data transmission systems and others. The characteristics of radio wave propagation are studied by using electromagnetic waves separated by circular orthogonal polarization in radiomonitoring and radiocontrol systems. Compared to other antenna types, circularly polarized antennas, such as rings, have superior design simplicity and excellent electrodynamics properties.

Objective. The objective of this study is to analyse the characteristics and application of directional microstrip couplers for supplying power to ring antennas.

Method. To better the performance of microstrip ring antennas, the reasons for their limited operating frequency range are analysed. These causes include the frequency-dependent parameters of the coupler, errors in calculating the directional coupler circuit, and radiation from asymmetric strip lines. To understand how supply lines, affect antenna characteristics, correlations between radiation fields determined in both its coordinate system and that of the primary axis are taken into account.

Results. An analysis of the dependence graphs of the main characteristics of ring microstrip antennas with intricate power supply circuits for directional couplers and comparison with similar characteristics for simple circuits revealed that the shape of the radiation pattern in the higher radiation hemisphere became symmetrical about the axis, especially when symmetrically supplying the ring with branch-line couplers. The frequency band has also widened, at which there was an acceptable degree of deviation in the ellipticity coefficient from unity.

Conclusions. The simulation results of microstrip ring antennas with power lines connected to directional couplers of different types showed that supplying the ring antenna with electricity via the directional coupler ensures circular polarization for the emitted electromagnetic waves. Additionally, the range of operating frequencies where there is only a small discrepancy in ellipticity coefficient remains at an acceptable level of –3 dB is quite broad. By utilizing directional branch-line couplers to power a ring antenna, it is possible to simultaneously emit both right and left circularly polarized waves with the same antenna.

KEYWORDS: microstrip ring antenna, directional microstrip coupler, supply lines, ellipticity coefficient, main coordinate system, individual coordinate system.

ABBREVIATIONS

AA is an antenna array;

RHCP is right-handed circular polarization;

VSWR is the voltage standing wave ratio.

NOMENCLATURE

$C = 30kl_{eff}$ is the constant value for the emitter;

F (θ, φ) is the directivity characteristic of linear conductors in the main coordinate system;

$F_\theta(\theta)$ and $F_\theta(\varphi)$ are directivity characteristics of the ring antenna in different planes;

$F(\alpha, \beta)$ is the directivity characteristic of linear conductors in the individual coordinate system;

I_0 is current amplitude of the ring antenna at φ = 0.

$\dot{I}_{s.l}$ is the complex amplitude of the current flowing around the emitter;

$J_0(\sin\theta)$, $J_1(\sin\theta)$, $J_2(\sin\theta)$ are Bessel functions of the 0th, 1st and 2nd order;

DOI 10.15588/1607-3274-2023-3-1

$k = 2\pi\lambda$ is the wave number;

K_e is the ellipticity coefficient;

$\vec{l}_0'$ and $\vec{m}_0'$ are unit vectors of the rectangular coordinate system $l'0_1m'$;

l_{eff} is the effective length of the linear emitter;

m is the ratio of the meridional component of the field intensity to the azimuthal value;

q is the radiation efficiency factor of the strip line transmission;

α, β, ρ are coordinates of the individual spherical coordinate system;

α_0, β_0, ρ_0 are unit vectors of the individual spherical coordinate system;

θ, φ, r are coordinates of the main spherical coordinate system;

θ_0, φ_0, r_0 are unit vectors of the main spherical coordinate system;

λ is the length of the electromagnetic wave.

$\xi = c/\nu_f$ is the ratio of the speed of electromagnetic wave propagation in free space to the speed of wave in the strip line.

ρ is the distance from the phase center 0_1 to the observation point M.

ψ is the phase shift of the emitter current $\dot{I}_{s.l}$ relative to the current phase of the ring antenna in the cross-section of the conductor with the coordinate φ = 0;

INTRODUCTION

The circular polarization of radio waves is used in various electronic systems. This includes, for example, space communications stations, some radio relay communication systems, radar stations, data transmission systems and others. The characteristics of radio wave propagation are studied by using electromagnetic waves separated by circular orthogonal polarization in radiomonitoring and radiocontrol systems. Compared to other antenna types, circularly polarized antennas, such as rings, have superior design simplicity and excellent electrodynamic properties.

The ring antenna stands out for its uncomplicated construction and excellent electrical features when it comes to sending and receiving circularly or rotational polarized electromagnetic waves. It is composed of a conductor twisted in a loop, usually about the same length as the wavelength of an electric current. An antenna of this type can separate the wave that hits it into two components with circular polarization [1, 2], a phenomenon which is crucial to understanding the polarization properties of the radiation field. However, when it comes to actually constructing a ring antenna, it can be difficult to develop and construct the appropriate supplying device. One potential way of constructing the necessary circuitry for supplying the ring antenna is through using directional couplers.

Considering the current trend toward the prevalent utilization of PCB technology to make ring radiators and their supplying systems, this study examines the principles of constructing microstrip ring antennas on couplers with electromagnetic coupling and branch-line couplers.

The object of this study is the process of separating an electromagnetic wave into two components with different directions of circular polarization orientations.

The subject of this study is the method for constructing directional couplers for the power circuit of a microstrip ring antenna.

The objective of this study is to analyse the characteristics and application of directional microstrip couplers for supplying power to ring antennas.

1 REVIEW OF THE LITERATURE

Scientific papers provide information on a wide variety of ring antenna designs. The article [3] considers a basic slotted microstrip antenna with a capacitive as an element to generate radiation with circular polarization. Articles [4, 5] discuss a slotted ring antenna array (AA), which can switch between the S- and C-bands or between the S, C, and X bands, respectively. The 2x2 AA diagonal supplying process is used when operating in C-band mode. This technique offers the maximum level of decoupling for both vertical and horizontal polarizations. The article [6] presents a dual-band annular slot AA for both L and C bands. The aperture of the L-band slot antenna can be transformed into a 2×2 AA for the C-band using pin diodes. The design presented in the study [7] is a broadband single-layer ring antenna with a low level of cross-polarization. The ring elements can be combined into an AA to address different issues, such as measuring electromagnetic field parameters. In the paper [8] a double annular-ring microstrip antenna, split into six sectors, is proposed to achieve multiband operation with high gain and impedance bandwidth. The gaps on the driven and parasitic patches excite resonant frequencies that are located in the Ku-, K-, and Ka-bands thus making the antenna capable of these multiband applications. In the article [9] the design process of an annular ring microstrip antenna using graphene material for dualband applications is proposed. The microstrip antenna is modified using graphene-based annular ring microstrip layers for patch and ground plane with FR-4 epoxy substrate in between. The design process applied the short-pin technique for the estimation of the return loss, which leads to the analysis of the resonant frequency and the dual-band directions. Meanwhile, paper [10] outlines the principles of constructing the AA using ring elements.

It is widely recognized that a directional coupler, when connected to an electromagnetic wave transmission line, extracts a specific amount of electromagnetic energy from the transmission line and separates the incident and reflected waves in a predetermined power ratio. This property of the directional coupler can be applied to feed the ring antenna or receive electromagnetic waves while separating them in a circular orthogonal polarization basis.

Studies [1, 2] indicate that during the receiving mode, the electrical processes in the conductor of the ring

DOI 10.15588/1607-3274-2023-3-1

antenna can be regarded as two waves that move towards each other. These waves run around the antenna in a circular orthogonal polarization basis, with one wave rotating in a clockwise direction and the other in a counter clockwise direction. Consequently, the ring antenna can be considered as a transmission line in which the incident and reflected waves propagate during the receiving mode. To select the wave with the appropriate right or left direction around the ring antenna, it is recommended to use a directional coupler.

2 PROBLEM STATEMENT

Fig. 1 depicts a directional coupler with electromagnetic coupling where the conductor segment of the ring represents the primary line of the device. The primary line (numbered 1–2 in Fig. 1) is connected to the secondary line (numbered 3–4). Since the coupler formed by the stripline segments of the transmission lines is backward, a voltage is generated in shoulder 3 that is proportional to the current wave running counter clockwise around the ring. To ensure proper operation of the directional coupler, port 4 must be loaded with an impedance equal to the wave impedance of strip 3–4.

The operational principle of the circuit suggests that it is advisable to utilize the directional coupler with electromagnetic coupling only in the mode of receiving radio waves. This is due to the device's low efficiency, as a portion of the energy supplied to lines 3–4 is lost at the matched impedance of port 4.

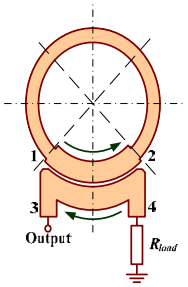

Figure 1 – The ring antenna with supplying by a directional coupler with electromagnetic coupling

In contrast, the branch-line directional coupler is a more efficient option, as depicted in Fig. 2.

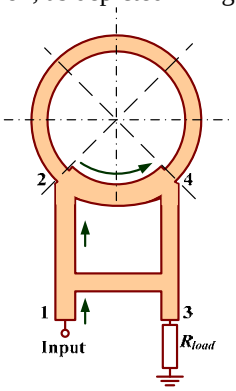

Figure 2 – The ring antenna with supplying by a branch-line directional coupler

Ports 1 and 3 of the branch-line directional coupler are electrically isolated, enabling the supply of current to both ports from two generators of identical frequency in the antenna transmission mode. This allows for the formation of a radiation field with any desired ellipticity coefficient. During the receiving mode, voltages are generated in ports 1 and 4, which are proportional to the intensity vectors of the electric fields rotating in the right and left directions. When the ring antenna is powered by a single generator connected to port 1 in the transmission mode, port 3 is loaded with a matched impedance. However, with the correct construction of the coupler, no energy enters or is absorbed into a load of port 4. Consequently, the efficiency of the device approaches unity.

The devices shown in Fig. 1 and Fig. 2 were studied using a specialized simulation program in the radiation mode of electromagnetic waves with right-handed circular polarization (RHCP). For the study, the operating frequency of f = 1.2 GHz (λ = 0.25 m) was selected, and the substrate for microstrip models was a dielectric with relative permittivity of ε_r = 4.4, a dielectric loss tangent of tgδ = 0.002, and a substrate thickness of h = 1.6 mm.

The results of the simulation are illustrated by the radiation patterns in two planes (Fig. 3), and the frequency dependence of the wave ellipticity coefficients, as shown in Fig. 4. In both cases, the voltage standing wave ratio (VSWR) within the operating frequency band did not exceed 1.5. Moreover, the directivity factor for the investigated right-handed circular polarization (RHCP) type was not less than 4 dBi.

Based on the results obtained from modelling ring antennas connected by directional couplers with an electromagnetic oscillation generator, the following conclusions can be drawn:

1. Supplying the ring with the directional coupler facilitates the study of electromagnetic waves on a circular orthogonal polarization basis. For the directional branch-line coupler to provide circular polarization with the directional branch-line coupler, it is necessary to design it with a power division factor of 3 dB.

2. The acceptable range operating frequency with a permissible deviation of the ellipticity coefficient from unity is significantly wide. This range can fulfill the requirements for the ellipticity of radiated waves in communication systems in certain cases.

3. Supplying a ring antenna with devices constructed using directional couplers allows for the creation of antennas with controlled polarization characteristics of the radiation field. This observation pertains to power devices constructed on branch-line directional couplers.

4. The simple power schemes, depicted in Fig. 1 and Fig. 2 tend to limit the operating frequency range of the ring antenna. This outcome is undesired, particularly when using these antennas for metrological purposes.

DOI 10.15588/1607-3274-2023-3-1

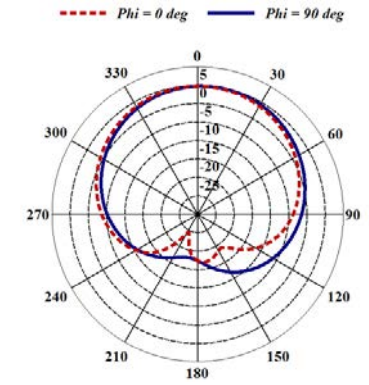

a

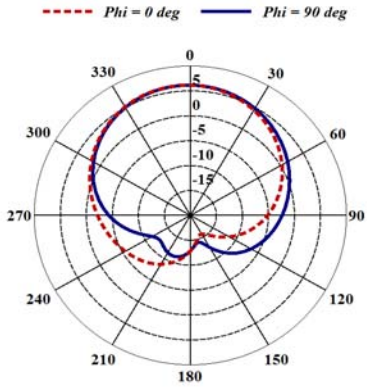

b

Figure 3 – Radiation patterns of ring antennas in two planes (φ = 0 and φ = 90º): a – powered by a directional coupler with electromagnetic coupling; b – powered by a branch-line directional coupler

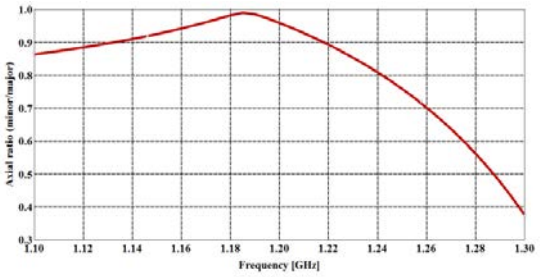

a

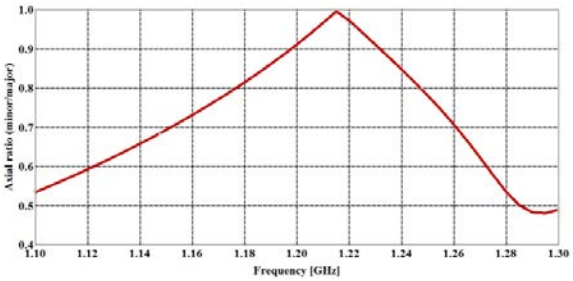

b

Figure 4 – Dependencies of the ellipticity coefficient of ring antennas on the operating frequency in the direction θ = 0: a – powered by a directional coupler with electromagnetic coupling; b – powered by a branch-line directional coupler

To enhance power devices and improve their properties, it is essential to examine the primary factors that contribute to the narrowing of the operating frequency range of the antenna. The most significant factor that influences the frequency response of the ring with the power supply is the frequency dependence of the parameters of the directional coupler. It is therefore evident that it is necessary to use coupler designs that ensure the stability of the primary parameters within specific frequency ranges.

The second significant factor is the accuracy of the directional coupler circuit calculation. Since one of the directional coupler components is the ring segment, determining the wave impedance of this segment poses a challenge. The radiation of electromagnetic waves by an annular strip line complicates the calculation of wave impedance.

The third factor that affects the structure of the radiation field of the ring antenna is the radiation of asymmetric strip lines [11, 12], which are utilized in constructing the power supply devices for the ring. The radiation intensity of strip lines is usually negligible, so in most cases, this can be neglected. However, when designing measurement antennas with stringent requirements for metrological characteristics, it is necessary to consider possible deformations of the radiation field structure due to the superposition of the fields of the ring antenna and segments of strip lines.

3 MATERIALS AND METHODS

As is known [1], the radiation field of the ring antenna is analytically described in the spherical coordinate system r, θ, φ, the polar axis of which coincides with the circle axis and the 0z axis of the rectangular coordinate system x, y, z. The antenna itself is located in the x0y plane of the rectangular coordinate system. Both coordinate systems are considered primary. Without considering the specific power supply system of the ring antenna, it is assumed that the radiation of the transmission line segment, which is part of the power supply system, is similar to the radiation of a short linear dipole. When the output impedance of the directional coupler is fully matched with the wave impedance of the ring, the current flowing through the elements of the power supply is determined uniquely through the current in the conductors of the ring.

To utilize the dipole radiation field formula, it is necessary to assign a coordinate system (both spherical and rectangular) to the power supply element, in which electromagnetic processes in the dipole are analysed. Consequently, the polar axis of this coordinate system, designated as 0_1l, must coincide with the axis of the supply line. Since the axis of the segment of the power circuit element, as well as the element itself, is in the x0y plane of the main coordinate system, it is advisable to place another coordinate axis in the same plane, for example, the 0_1m axis, in the coordinate system associated with the radiating element, and the third axis 0_1n parallel axis 0z (θ = 0). The new coordinate systems are denoted

DOI 10.15588/1607-3274-2023-3-1

as follows: rectangular *l*, *m*, *n* and spherical ρ, α, β, where $0_1 l$ is the polar axis (α = 0). In spherical coordinate system, α is the meridional angle, β is the azimuth angle. Such coordinate systems are considered to be the emitter's own coordinate systems. The mutual position of the coordinate systems is shown in Fig. 5.

The origin of the main coordinate system (point 0) coincides with the phase center of the ring antenna, and point 0_1 is the phase center of the interference emitter, that is, a segment of the strip line of the power device. In the general case, the axis of the interference emitter will not be parallel to the axes 0*x* and 0*y*, therefore, Fig. 5 shows the axes $0_1 l'$ and $0_1 m'$, which are parallel to the axes of the main coordinate system and are shifted from the corresponding axes of the own coordinate system by an angle Δ.

Fig. 5 also shows the observation point *M*, the position of which in the main coordinate system is defined as *M*(*r*, θ, φ), and in the emitter's own system as *M*(ρ, α, β).

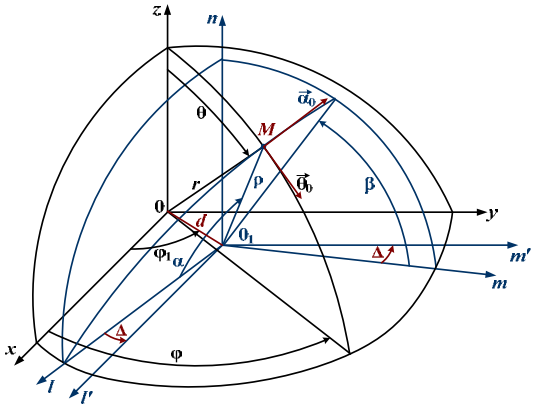

Figure 5 – The mutual position of the main and individual coordinate systems

The intensity of the interference electric field at point *M* in its coordinate system is written as

$$\dot{E}_{int} = \vec{\alpha}_0 \frac{qC\dot{I}_{s.l}}{\rho} F(\alpha,\beta) e^{-ik\rho}. \qquad (1)$$

To evaluate the impact of such field on the ring antenna radiation, it is necessary to determine the vector $\vec{\alpha}_0$ from expression (1), and the angles α and β using the quantities $\vec{\theta}_0$, $\vec{\varphi}_0$ and r, θ, φ. To accomplish this, the polar axis in its individual coordinate system must be altered, with the $0_1 n$ axis designated as the polar axis. The meridional angle will be measured from the $0_1 n$ axis, while the azimuthal angle τ –will be measured from the $0_1 l$ axis (Fig. 5 and Fig. 6).

In the own coordinate system ρ, α, β, the unit vector $\vec{\rho}_0$ is determined by the coordinates of the rectangular coordinate system *m*, *n*, *l*, which can be expressed as:

$$\vec{\rho}_0 = \vec{m}_0 \sin\alpha\cos\beta + \vec{n}_0 \sin\alpha\sin\beta + \vec{l}_0 \cos\alpha. \qquad (2)$$

In the ρ, σ, τ system, the value of the unit vector can be determined using the following expression:

$$\vec{\rho}_0 = \vec{l}_0 \sin\sigma\cos\tau + \vec{m}_0 \sin\sigma\sin\tau + \vec{n}_0 \cos\sigma. \qquad (3)$$

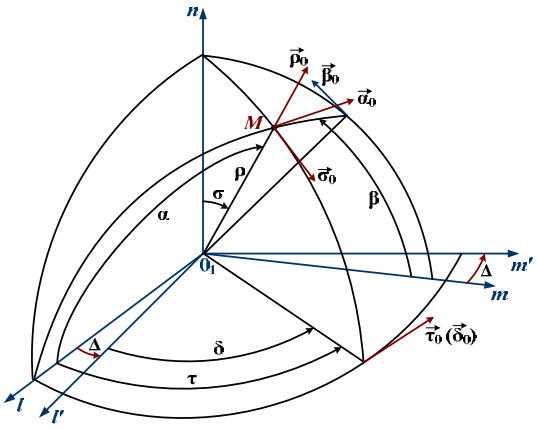

Figure 6 – The mutual position of two coordinate systems *m*, *n*, *l* and *m*′, *n*, *l*′ with angular shift Δ

As the right parts of expressions (2) and (3) represent the same value, it is possible to find the relation between the angles α, β and σ, τ. So

$$\left.\begin{aligned} \sin\alpha\cos\beta &= \sin\sigma\sin\tau; \\ \sin\alpha\sin\beta &= \cos\sigma; \\ \cos\alpha &= \sin\sigma\cos\tau. \end{aligned}\right\} \qquad (4)$$

From the equations system (4):

$$\left.\begin{aligned} \cos\alpha &= \sin\sigma\cos\tau; \\ \sin\alpha &= \sqrt{1-\cos^2\tau\sin^2\sigma}; \\ \cos\beta &= \frac{\sin\sigma\sin\tau}{\sqrt{1-\cos^2\tau\sin^2\sigma}}; \\ \sin\beta &= \frac{\cos\sigma}{\sqrt{1-\cos^2\tau\sin^2\sigma}}. \end{aligned}\right\} \qquad (5)$$

Transforming to the rectangular coordinate system *m*, *n*, *l*, the expression for the unit vector $\vec{\alpha}_0$ in the own coordinate system can be written as follows:

$$\vec{\alpha}_0 = \vec{m}_0 \cos\alpha\cos\beta + \vec{n}_0 \cos\alpha\sin\beta - \vec{l}_0 \sin\alpha. \qquad (6)$$

Equations (5) and (6) determine the values of the vector $\vec{\alpha}_0$ in the new coordinate system, where the polar axis aligns with the $0_1 n$ axis:

$$\vec{\alpha}_0 = \left(1-\cos^2\tau\sin^2\sigma\right)^{-\frac{1}{2}} \begin{bmatrix} \vec{m}_0 \cos\tau\sin^2\sigma\sin\tau + \\ + \vec{n}_0 \cos\sigma\cos\tau\sin\sigma - \\ - \vec{l}_0 \left(1-\cos^2\tau\sin^2\sigma\right) \end{bmatrix}. \qquad (7)$$

DOI 10.15588/1607-3274-2023-3-1

After shifting the coordinate system by an angle Δ (Fig. 6), the new coordinate system can be obtained with axes $0_1l'$ and $0_1m'$ parallel to the axes $0x$ and $0y$ of the main system, by using the following equations:

$$\left.\begin{aligned}\vec{l}_0 &= \vec{l}_0'\cos\Delta - \vec{m}_0'\sin\Delta;\\ \vec{m}_0 &= \vec{l}_0'\sin\Delta + \vec{m}_0'\cos\Delta.\end{aligned}\right\} \quad (8)$$

Using relation (8), the dependence of the vector $\vec{\alpha}_0$ (7) on the unit vectors of the coordinate system $l'0_1m'$ can be found:

$$\begin{aligned}\vec{\alpha}_0 = \vec{l}_0' &\frac{\sin^2\sigma\cos(\delta+\Delta)\cos\delta - \cos\Delta}{\sqrt{1-\cos^2(\delta+\Delta)\sin^2\sigma}} +\\ +\vec{m}_0' &\frac{\sin^2\sigma\cos(\delta+\Delta)\sin\delta + \sin\Delta}{\sqrt{1-\cos^2(\delta+\Delta)\sin^2\sigma}} +\\ +\vec{n}_0 &\frac{\cos\sigma\sin\sigma\cos(\delta+\Delta)}{\sqrt{1-\cos^2(\delta+\Delta)\sin^2\sigma}}.\end{aligned} \quad (9)$$

The spherical coordinate system ρ, σ, δ is combined with the rectangular coordinate system (Fig. 6). To express the formula (9) in the spherical coordinate system, the formula (9) is substituted with the values of orts $\vec{l}_0'$, $\vec{m}_0'$ and $\vec{n}_0$ expressed in terms of the coordinates and orts of the system ρ, σ, δ:

$$\left.\begin{aligned}\vec{l}_0' &= \vec{\rho}_0\sin\sigma\cos\delta + \vec{\sigma}_0\cos\sigma\cos\delta - \vec{\delta}_0\sin\delta;\\ \vec{m}_0' &= \vec{\rho}_0\sin\sigma\sin\delta + \vec{\sigma}_0\cos\sigma\sin\delta + \vec{\delta}_0\cos\delta;\\ \vec{n}_0 &= \vec{\rho}_0\cos\sigma - \vec{\sigma}_0\sin\sigma.\end{aligned}\right\}$$

After substituting and rearranging the expressions, we obtain:

$$\begin{aligned}\vec{\alpha}_0 = -\vec{\sigma}_0 &\frac{\cos\sigma\cos(\delta+\Delta)}{\sqrt{1-\cos^2(\delta+\Delta)\sin^2\sigma}} +\\ +\vec{\delta}_0 &\frac{\sin(\delta+\Delta)}{\sqrt{1-\cos^2(\delta+\Delta)\sin^2\sigma}}.\end{aligned} \quad (10)$$

So, the vector $\vec{\alpha}_0$ in the spherical coordinate system ρ, σ, δ has two mutually perpendicular components that are orthogonal to the vector $\vec{\rho}_0$. One component is in the meridional plane and the other is in the azimuth plane.

The impact of the interference field (1) on the field of the ring antenna can be estimated only by determining the relationship between the values ρ, σ, δ included in the formula (1) and the values r, θ, φ of the main coordinate system. To establish this connection, it is necessary to refer to Fig. 5, where the position of the phase center of the interference source in the main coordinate system is denoted by x_1 and y_1. The distance between the phase centers of the ring antenna and interference sources is defined as:

$$d = \sqrt{x_1^2 + y_1^2}\ .$$

The distance between the phase center of the ring antenna and the observation point M in the main rectangular coordinate system can be expressed as:

$$r = \sqrt{x^2 + y^2 + z^2}\ , \quad (11)$$

where x, y, z are the coordinates of point M.

The distance from the phase center of the interference source 0_1 to the observation point M can be calculated as follows:

$$\rho = \sqrt{(x-x_1)^2 + (y-y_1)^2 + z^2} \quad (12)$$

In the spherical coordinate system, the coordinates of the observation point M can be expressed as follows:

$$\left.\begin{aligned}x &= r\sin\theta\cos\varphi;\\ y &= r\sin\theta\sin\varphi.\end{aligned}\right\} \quad (13)$$

The position of the phase center of the interference source in the spherical coordinate system is as follows:

$$\left.\begin{aligned}x_1 &= d\cos\varphi_1;\\ y_1 &= d\sin\varphi_1.\end{aligned}\right\} \quad (14)$$

Using relations (11), (15) and (16), the right-hand side of equation (12) can be simplified to the following form:

$$\rho = \sqrt{r^2 + d^2 - 2dr\sin\theta\cos(\varphi-\varphi_1)}$$

or

$$\rho = r\sqrt{1 + \left(\frac{d}{r}\right)^2 - 2\frac{d}{r}\sin\theta\cos(\varphi-\varphi_1)}\ . \quad (15)$$

If the observation point is in the far field, then $d << r$ and the formula (15) can be written as follows:

$$\rho = r - d\sin\theta\cos(\varphi-\varphi_1) \quad (16)$$

In the case when the distance ρ is used in the calculation of quantities in which the slight difference between the distance ρ and the distance r can be neglected, it can be assumed that

$$\rho \approx r\ . \quad (17)$$

Therefore, the value ρ from formula (16) should be taken into account in the exponent in expression (1), and in other cases, the approximate value (17) is used.

DOI 10.15588/1607-3274-2023-3-1

To establish a relation between the meridional angles θ and σ can be found through the expression:

$$\sigma = \arccos(z/\rho). \quad (18)$$

Since the *z*-coordinate in the main coordinate system is equal to

$$z = r\cos\theta, \quad (19)$$

then expression (18), in which relations (15) and (19) are used, becomes a function of the meridional angle σ of the coordinate system ρ, σ, δ which depends on the parameters θ and φ of the main coordinate system:

$$\sigma = \arccos\left(\frac{\cos\theta}{\sqrt{1+\left(\frac{d}{r}\right)^2 - 2\frac{d}{r}\sin\theta\cos(\varphi-\varphi_1)}}\right)$$

or it can be written approximately that $\sigma \approx \theta$.

The azimuthal angle δ of the observation point *M* in the main coordinate system can be determined as shown in Fig. 7:

$$\delta = \operatorname{arctg}\left((y-y_1)/(x-x_1)\right). \quad (20)$$

As depicted in Fig. 7, the meridional planes passing through point *M* in both coordinate systems intersect at an angle Ω. Therefore, it can be written that:

$$\delta = \varphi - \Omega. \quad (21)$$

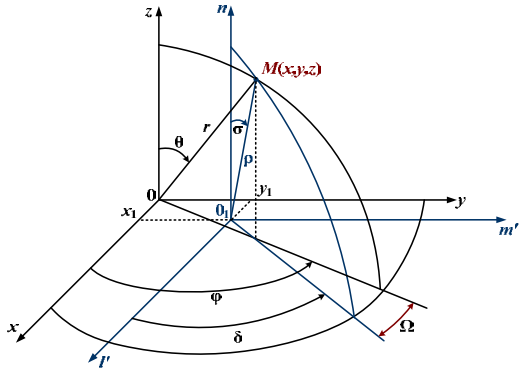

Figure 7 – The mutual position of two coordinate systems *x*, *y*, *z* and *l′*, *m′*, *n*

Since the angle φ can be determined through the coordinates of the observation point as $\varphi = \operatorname{arctg}(x/y)$, then the value of the angle Ω can be found as the difference between the angles φ and δ:

$$\Omega = \operatorname{arctg}(x/y) - \operatorname{arctg}\left((y-y_1)/(x-x_1)\right). \quad (22)$$

By using expressions (15) and (14), it is possible to represent expression (22) in terms of the observation point's coordinates in the basic spherical coordinate system as follows:

$$\Omega = \chi\pi + \operatorname{arctg}\frac{d\sin(\varphi_1-\varphi)}{r\sin\theta - d\cos(\varphi_1-\varphi)}, \quad (23)$$

where $\chi = 0$ if $A > -1$; $\chi = +1$ if $A < -1$ and $\operatorname{tg}\varphi > 0$; $\chi = -1$ if $A < -1$ and $\operatorname{tg}\varphi < 0$;

$$A = \operatorname{tg}\varphi\frac{r\sin\theta\sin\varphi - d\sin\varphi_1}{r\sin\theta\cos\varphi - d\cos\varphi_1}.$$

If the inequalities $y >> y_1$ and $x >> x_1$ are valid, it can be assumed that:

$$\delta \approx \varphi. \quad (24)$$

The spherical surfaces $r = \text{const}$ and $\rho = \text{const}$ intersect at point *M* as shown in Fig. 7. As a result, the tangent planes at point *M* are not parallel to each other. Only at significant distances from points 0 and 0_1, where condition (20) is satisfied, it can be assumed that the planes θ*M*φ and σ*M*δ coincide. In this case, the corresponding unit vectors of the polar coordinate system in the plane tangent to point *M* (Fig. 8) will be displaced from one another by an angle Ω.

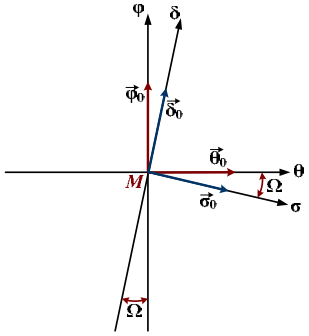

Figure 8 – The shift of unit vectors of the spherical coordinate system

In this regard, expression (10) in the coordinates θ and φ can be rewritten as follows:

$$\vec{\alpha}_0 = \vec{\theta}_0 A_\theta + \vec{\varphi}_0 A_\varphi, \quad (25)$$

where

$$A_\theta = \frac{\sin(\varphi+\Delta-\Omega)\sin\Omega}{\sqrt{1-\cos^2(\varphi+\Delta-\Omega)\sin^2\theta}} - \frac{\cos\theta\cos(\varphi+\Delta-\Omega)\cos\Omega}{\sqrt{1-\cos^2(\varphi+\Delta-\Omega)\sin^2\theta}};$$

$$A_\varphi = \frac{\sin(\varphi+\Delta-\Omega)\cos\Omega}{\sqrt{1-\cos^2(\varphi+\Delta-\Omega)\sin^2\theta}} - \frac{\cos\theta\cos(\varphi+\Delta-\Omega)\sin\Omega}{\sqrt{1-\cos^2(\varphi+\Delta-\Omega)\sin^2\theta}}.$$

The directivity characteristic is another factor present in expression (1), and its content is dependent on the chosen coordinate system. To determine the directivity characteristic, the reasons for the radiation of the power

DOI 10.15588/1607-3274-2023-3-1

supply elements must be considered and specified. The traveling wave mode is established in the transmission line segments with the correct construction of the device. When asymmetric strip lines are used for energy transfer, surface waves arise, leading to the generation of a radiation field. The directivity characteristic of linear conductors with a traveling wave of current is known and can be expressed as follows for our case:

$$F(\alpha,\beta)=\cos\alpha\frac{\sin\left[\frac{kl}{2}(\xi-\cos\alpha)\right]}{\frac{kl}{2}(\xi-\cos\alpha)}. \qquad (26)$$

Formula (26) needs to be modified in the general case to account for the screen effect.To transform this formula into the dependence of the noise field intensity on the coordinates of the main polar coordinate system, we can use expressions (5), (17), (20), (21), (23), or (24).

Since the strip lines are designed to minimize or eliminate radiation, the value of q in formula (1), which represents the radiation efficiency coefficient, is much less than unity. Therefore, the efficiency coefficient characterizes the losses in asymmetric strip lines due to the radiation of electromagnetic energy.

Considering all the obtained relationships between the coordinates of the individual and the main coordinate systems, the radiation field of the interference source can be expressed as follows:

$$\dot{\vec{E}}_{int}=\left(\vec{\theta}_0A_\theta+\vec{\varphi}_0A_\varphi\right)qCI_{s.l}F(\theta,\varphi)e^{i\psi}e^{-ikr}.$$

For the ring antenna, the radiation field is defined as:

$$\dot{\vec{E}}_{ring}=\left(\vec{\theta}_0F_\theta(\theta)-i\vec{\varphi}_0F_\varphi(\theta)\right)\frac{30\pi I_0}{r}e^{-ikr},$$

where $F_\theta(\theta)=2\mathrm{ctg}\theta J_1(\sin\theta)$;
$F_\varphi(\theta)=J_0(\sin\theta)-J_2(\sin\theta)$.

In the meridional plane, the electric field intensity of both the antenna and the interference is equal:

$$\dot{E}_\theta=\dot{E}^\theta_{ring}+\dot{E}^\theta_{int}e^{-i\psi}=E_\theta e^{i\psi_\theta}e^{i\omega t}, \qquad (27)$$

where $E^\theta_{ring}=\frac{30\pi I_0}{r}F_\theta(\theta)$; $E^\theta_{int}=qA_\theta CI_{s.l}F(\theta)$;

$$E_\theta=\sqrt{\left(E^\theta_{ring}\right)^2+2E^\theta_{ring}E^\theta_{int}\cos\psi+\left(E^\theta_{int}\right)^2};$$

$$\psi_\theta=\arccos\left(\frac{E^\theta_{ring}+E^\theta_{int}\cos\psi}{E_\theta}\right)=\arcsin\left(-\frac{E^\theta_{int}\sin\psi}{E_\theta}\right).$$

In the horizontal plane, the sum of the intensities is determined as follows:

$$\dot{E}_\varphi=\dot{E}^\varphi_{ring}e^{-i\frac{\pi}{2}}+\dot{E}^\varphi_{int}e^{-i\psi}=E_\theta e^{i\psi_\varphi}e^{i\omega t}, \qquad (28)$$

where $E^\varphi_{ring}=\frac{30\pi I_0}{r}F_\varphi(\theta)$; $E^\varphi_{int}=qA_\varphi CI_{s.l}F(\theta)$;

$$E_\varphi=\sqrt{\left(E^\varphi_{ring}\right)^2+2E^\varphi_{ring}E^\varphi_{int}\sin\psi+\left(E^\varphi_{int}\right)^2};$$

$$\psi_\varphi=\arccos\left(\frac{E^\varphi_{int}\cos\psi}{E_\varphi}\right)=\arcsin\left(-\frac{E^\varphi_{ring}+E^\varphi_{int}\sin\psi}{E_\varphi}\right).$$

The ellipticity coefficient can be calculated using the following formula:

$$K_e=\pm\sqrt{\frac{m\sin^2\gamma-\sin2\gamma\cos\psi_0+(1/m)\cos^2\gamma}{m\cos^2\gamma+\sin2\gamma\cos\psi_0+(1/m)\sin^2\gamma}},$$

where $m=E_\theta/E_\varphi$; $\psi_0=\psi_\theta-\psi_\varphi$; $\mathrm{tg}2\gamma=\frac{2m\cos\psi_0}{m^2-1}$.

The polarization of the wave due to the interference radiation will not be circular in the direction of the polar axis ($\theta = 0$) as it can be inferred from expressions (27) and (28), where $E_\theta \neq E_\varphi$ and $E_\theta/E_\varphi \neq 1$. In case q has a significantly small value (q<<1), the ellipticity coefficient of the radiation along the annular antenna axis will be close to unity, satisfying the polarization requirements in communication lines. However, for metrological purposes, more stringent requirements for circular polarization quality should be met, and additional circuit or design solutions must be employed to reduce interference radiation.

4 EXPERIMENTS

The radiation in the direction of the ring axis of the ring antenna can serve as a standard reference for studying polarization characteristics of antennas. In such instances, the waves emitted by the power devices should be compensated. This can be achieved by designing the power supply circuit in such a way that its identical components form an anti-phase system of emitters. As a result, waves of equal intensity but opposite phases will be emitted in the direction of the ring axis, resulting in almost complete suppression of the interference intensity. Fig. 9 depicts the circuit diagram for supplying the ring antenna with two directional couplers placed symmetrically around the center of the circuit.

As shown in the diagram, all directional coupler elements are symmetrical in pairs concerning point *O* and are fed in an antiphase. The diagram indicates the phase shifts of the currents, and the arrows indicate the directions of the current wave propagation in the strip line segments.

DOI 10.15588/1607-3274-2023-3-1

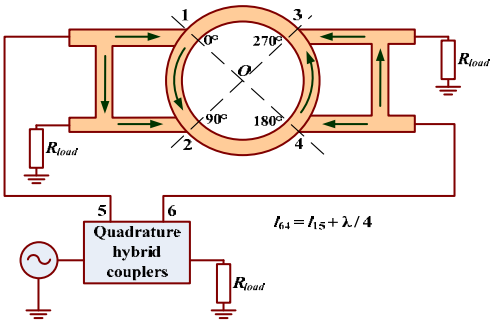

Figure 9 – The ring antenna with feeding by two branch-line directional couplers

The emission of interference radiation can also be mitigated through partial shielding of the power supply. Fig. 10 illustrates the ring antenna diagram with the opposite directional coupler's primary line placed behind the ring strip. In this configuration, the surface electromagnetic wave that may occur during the current wave propagation along the primary line will be contained within the dielectric layer between the two strips, there by considerably reducing unwanted radiation.

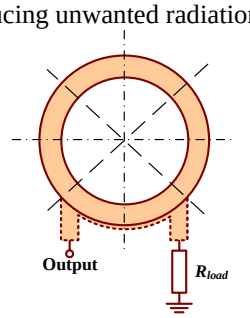

Figure 10 – The ring antenna in which the primary line of the directional coupler is located behind the ring strip

5 RESULTS

After analyzing the model shown in Fig. 9, the radiation pattern in two planes (as shown in Fig. 11) and the relationship between the wave ellipticity coefficient and frequency (as demonstrated in Fig. 12) were obtained. The VSWR did not exceed 1.4 within the operating frequency band. Moreover, the gain for the examined RHCP was not less than 6 dBi.

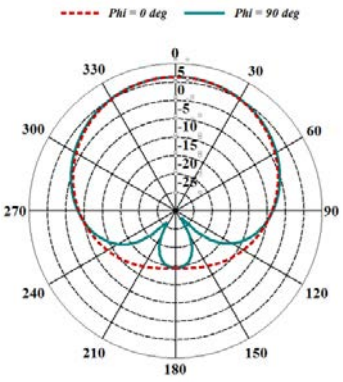

Figure 11 – The radiation patterns of ring antennas in two planes (φ = 0 and φ = 90º) when supplied by two branch-line directional couplers

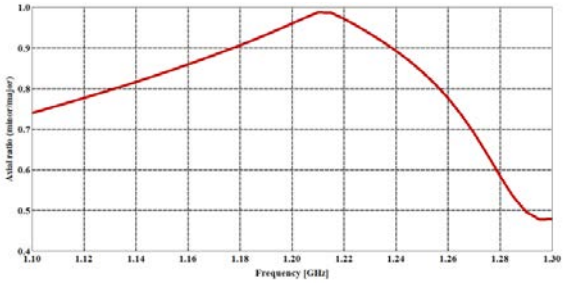

Figure 12 – Dependence of the ellipticity coefficient of ring antennas with supplying by two branch-line directional couplers on the operating frequency in the direction θ = 0

The study results of the ring microstrip antenna with front electromagnetic coupling (as illustrated in Fig. 10) are presented in Fig. 13 and 14. The radiation pattern and the ellipticity coefficient as a function of frequency are shown in these figures, respectively. The VSWR value within the operating frequency range was not more than 1.1, and the gain for the investigated RHCP was at least 4 dBi.

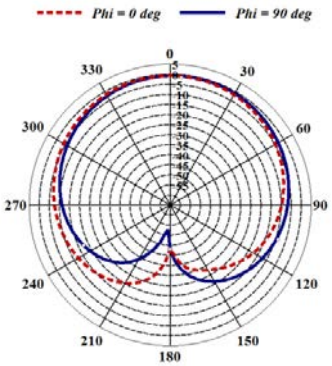

Figure 13 – The radiation patterns of ring antennas, in which the primary line of the directional coupler is located behind the ring strip, in two planes (φ = 0 and φ = 90º)

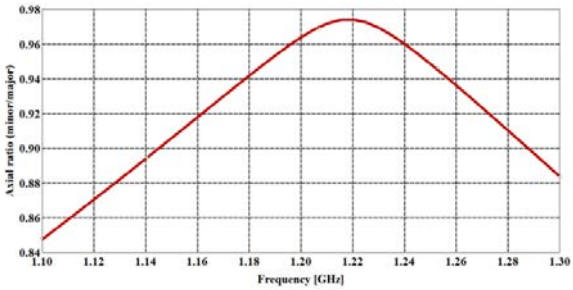

Figure 14 – Dependence of the ellipticity coefficient of ring antennas, in which the primary line of the directional coupler is located behind the ring strip, on the operating frequency in the direction θ = 0

6 DISCUSSION

An analysis of the dependence graphs of the main characteristics of antennas with complex power supply circuits for directional couplers (Figs. 9 and Fig. 10) compared to similar characteristics for simple circuits (Fig. 1 and Fig. 2) showed that the radiation pattern shape in the upper radiation hemisphere became symmetric, especially when using a symmetrical supply of the ring

DOI 10.15588/1607-3274-2023-3-1

with branch-line couplers. Furthermore, the acceptable level of the ellipticity coefficient deviation at – 3dB has been maintained over a broader frequency range.

The branch-line directional coupler has another advantage over the coupler with electromagnetic coupling. This is the supply of the ring emitter with the full power of the power source with an efficiency close to unity. However, unlike the coupler with electromagnetic coupling, the branch-line coupler is more complex to calculate and design, and also occupies a large area on the printed circuit board. Therefore, it is sometimes advisable to use a ring antenna power supply circuit with two directional couplers with electromagnetic coupling, which are located symmetrically with respect to the ring axis.

CONCLUSIONS

The outcomes of the microstrip ring antenna modeling with power supply devices on directional couplers confirm the feasibility of constructing circularly polarized electromagnetic wave emitters that satisfy current technical standards.

The paper discusses factors that can have a detrimental effect on the frequency characteristics of ring antennas and the polarization purity of electromagnetic waves. The study also focuses on the mode of current wave propagation in supply lines. It was found that directional couplers with electromagnetic coupling can be utilized in the construction of receiving ring antennas, which prioritize efficiency over other parameters. Additionally, these antennas can be useful for polarization analysis of radiation fields.

The branch-line directional couplers, by dividing the output powers equally, enable the ring to be supplied with the maximum power from the high-frequency current generator, resulting in a highly efficient power supply for the ring.

The scientific novelty. The study has revealed that using a single-directional coupler in power circuits does not guarantee axial symmetry of the radiation field in the front half-space. The paper elucidates the underlying factors causing this phenomenon. It is demonstrated that symmetrical power supplies and shielding can overcome this issue and enhance the operating frequency range, as determined by the radiation field ellipticity coefficient.

The practical significance. After modelling prototypes of microstrip ring antennas, the results showed that the microstrip power line matched well with the radiating ring. The VSWR did not exceed 1.4 in the operating frequency band in all cases, and the gain for the type of polarization studied (RHCP) was not less than 4 dBi. The cross-polarization component's radiation was not higher than 15 dBi for sophisticated power supply circuits. The radiation pattern in the forward half-space became symmetrical concerning the antenna axis, especially with a symmetrical power supply.

Prospects for further research. Future research will focus on mathematical modeling and experimental study of the utilization of symmetrical branch-line coupler circuits to power ring microstrip antennas for constructing antenna arrays.

REFERENCES

1. Ilnitsky L., Shcherbyna O., Yanovsky F., Zaliskyi M., Holubnychyi O., Ivanets O. Comparison of Circular and Linear Orthogonal Polarization Bases in Electromagnetic Field Parameters Measurement, *International Journal of Image, Graphics and Signal Processing*, 2022, Vol. 14, No. 3, pp. 58–72. DOI: 10.5815/ijigsp.2022.03.06
2. Ilnitsky L. Ya., Savchenko O. Y., Sibruk L. V. Anteny ta prystroyi nadvysokykh chastot: pidruchnyk. Kyiv, Ukrtelecom, 2003, 496 p.
3. Li J., He B., Li L., Zhang A., Liu J., Liu Q. H. Capacitor-loaded circularly polarized annular-ring slotted microstrip patch antenna, *IEEE 11th International Symposium on Antennas, Propagation and EM Theory (ISAPE), China, 18–21 October, 2016: proceedings*. Guilin, 2016, pp. 13–15. DOI: 10.1109/ISAPE.2016.7833897
4. Huang J., Gong X. A Wide-Band Dual-Polarized Frequency Reconfigurable Slot-Ring Antenna Element Using a Diagonal Feeding Method for Array Design, *IEEE International Symposium on Antennas and Propagation and USNC/URSI National Radio Science Meeting, USA, 08–13 July, 2018: proceedings*. Boston, 2018, pp. 477–478. DOI: 10.1109/APUSNCURSINRSM.2018.8608781
5. Huang J., Gong X. A Tri-Band Dual-Polarized Slot-Ring Antenna for Array Design, *IEEE International Symposium on Antennas and Propagation and USNC/URSI National Radio Science Meeting, USA, 07–12 July, 2019: proceedings*. Atlanta, 2019, pp. 1151–1152. DOI: 10.1109/APUSNCURSINRSM.2019.8889188
6. Shirazi M., Huang J., Li T., Gong X. A Switchable-Frequency Slot-Ring Antenna Element for Designing a Reconfigurable Array, *IEEE Antennas and Wireless Propagation Letters*, 2018, Vol. 17, No. 2, pp. 229–233. DOI: 10.1109/LAWP.2017.2781463
7. Chen C., Li C., Zhu Z., Wu W. Wideband and Low Cross-Polarization Planar Annual Ring Slot Antenna, *IEEE Antennas and Wireless Propagation Letters*, 2017, Vol. 16, pp. 3009–3013. DOI: 10.1109/LAWP.2017.2757963
8. Godaymi Al-Tumah W. A., Shaaban R. M., Duffy A. P. Design, simulation, and fabrication of a double annular ring microstrip antenna based on gaps with multiband feature, *Engineering Science and Technology, an International Journal*, 2022, Vol. 29, pp. 1–10. DOI: 10.1016/j.jestch.2021.06.013
9. Phonkitiphan P., Kaewon R., Pancharoen K., Silapan P., Watcharakitchakorn O. Design of Graphene-Based Annular Ring Microstrip Antenna Using Short-Pin Technique for Dual Band Applications, *International Journal of Electrical and Electronic Engineering & Telecommunications*, 2020, Vol. 9, No. 4, pp. 231–236. DOI: 10.18178/ijeetc.9.4.231-236
10. Shcherbyna O., Ilnitsky L., Mykhalchuk I., Kozhokhina O. The Antenna Array with Ring Elements, *Signal Processing Symposium (SPSympo 2017), Poland, 12–14 September, 2017: proceedings*. Jachranka, 2017, pp. 1–4. DOI: 10.1109/SPS.2017.8053700
11. Pozar M. D. Microwave Engineering: 4th edition. New Jersey, John Willey & Sons, 2012. 756 p.
12. Gustrau F. RF and Microwave Engineering: Fundamentals of Wireless Communications. New Jersey, John Willey & Sons, 2012. 368 p.

Received 10.04.2003.
Accepted 22.06.2023.

DOI 10.15588/1607-3274-2023-3-1

УДК 621.396.67

ЖИВЛЕННЯ КІЛЬЦЕВОЇ АНТЕНИ ЗА ДОПОМОГОЮ СПРЯМОВАНИХ ВІДГАЛУЖУВАЧІВ

Ільницький Л. Я. – д-р техн. наук, заслужений діяч науки і техніки України, Національний авіаційний університет, Київ, Україна.

Щербина О. А. – д-р техн. наук, професор кафедри електроніки, робототехніки і технологій моніторингу та інтернету речей, Національний авіаційний університет, Київ, Україна.

Заліський М. Ю. – д-р техн. наук, професор кафедри телекомунікаційних та радіоелектронних систем, Національний авіаційний університет, Київ, Україна.

Mykhalchuk I. I. – канд. техн. наук, асистент кафедри кібербезпеки та захисту інформації, Київський національний університет ім. Тараса Шевченка, Київ, Україна.

Кожохіна О. В. – канд. техн. наук, доцент кафедри авіоніки, Національний авіаційний університет, Київ, Україна.

АНОТАЦІЯ

Актуальність. В різних радіоелектронних системах застосовують радіохвилі з коловою поляризацією. Наприклад, це станції космічного зв'язку, деякі системи радіорелейного зв'язку, радіолокаційні станції, системи передачі даних і т.д. Електромагнітні хвилі, розкладені в коловому ортогональному поляризаційному базисі, використовують у системах радіомоніторингу та радіоконтролю, при дослідженнях особливостей поширення радіохвиль. Серед антен, які створені для приймання і випромінювання електромагнітних хвиль з коловою або обертовою поляризацією, за простотою конструкції та за електродинамічними характеристиками вигідно відрізняється кільцева антена.

Мета роботи – дослідження особливостей побудови та використання мікросмужкових спрямованих відгалужувачів для живлення кільцевих антен.

Метод. Для удосконалення пристроїв живлення мікросмужкових кільцевих антен та покращення їх властивостей розглядаються основні фактори, які викликають звуження робочого діапазону частот антени: частотна залежність параметрів спрямованого відгалужувача, коректність розрахунку схеми спрямованого відгалужувача, випромінювання несиметричних смужкових ліній. Обґрунтування впливу елементів живлення на характеристики кільцевої антени використовується зв'язок між полем випромінювання, аналітично визначене у власній системі координат, і полем випромінювання антени в основній системі координат.

Результати. Аналіз графіків залежностей основних характеристик кільцевих мікросмужкових антен з ускладненими схемами живлення спрямованих відгалужувачів і порівняння з аналогічними характеристиками для простих схем показало, що форма діаграми спрямованості у верхній півсфері випромінювання стала симетричною відносно осі, особливо у випадку симетричного живлення кільця шлейфовими відгалужувачами. Також розширився діапазон частот, у якому відхилення коефіцієнту еліптичності від одиниці знаходиться на допустимому рівні.

Висновки. Результати моделювання мікросмужкових кільцевих антен з лініями живлення на спрямованих відгалужувачах різних типів показали, що збудження кільця за допомогою спрямованого відгалужувача забезпечує випромінювання електромагнітних хвиль колової поляризації. При цьому діапазон робочих частот, у якому залишається на допустимому рівні –3дБ відхилення коефіцієнту еліптичності досить широкий. Живлення кільцевої антени пристроями, побудованими на шлейфових спрямованих відгалужувачах, дає можливість за допомогою однієї кільцевої антени одночасного випромінювання хвиль з правим та лівим напрямом обертання вектора напруженості електричного поля.

КЛЮЧОВІ СЛОВА: мікросмужкова кільцева антена, спрямований мікросмужковий відгалужувач, лінії живлення, коефіцієнт еліптичності, основна система координат, власна система координат.

ЛІТЕРАТУРА

1. Comparison of Circular and Linear Orthogonal Polarization Bases in Electromagnetic Field Parameters Measurement / [L. Ilnitsky, O. Shcherbyna, F. Yanovsky et al.] // International Journal of Image, Graphics and Signal Processing. – 2022. – Vol. 14, No. 3. – P. 58–72. DOI: 10.5815/ijigsp.2022.03.06
2. Ільницький Л. Я. Антени та пристрої надвисоких частот: підручник для ВНЗ / Л. Я. Ільницький, О. Я. Савченко, Л. В. Сібрук. – К. : Укртелеком, 2003. – 496 с.
3. Capacitor-loaded circularly polarized annular-ring slotted microstrip patch antenna / [J. Li, B. He, L. Li et al.] // IEEE 11th International Symposium on Antennas, Propagation and EM Theory (ISAPE), China, 18–21 October, 2016: proceedings. – Guilin, 2016. – P. 13–15. DOI: 10.1109/ISAPE.2016.7833897.
4. Huang J. A Wide-Band Dual-Polarized Frequency Reconfigurable Slot-Ring Antenna Element Using a Diagonal Feeding Method for Array Design / J. Huang, X. Gong // IEEE International Symposium on Antennas and Propagation and USNC/URSI National Radio Science Meeting, USA, 08–13 July, 2018: proceedings. – Boston, 2018. – P. 477–478. DOI: 10.1109/APUSNCURSINRSM.2018.8608781.
5. Huang J. A Tri-Band Dual-Polarized Slot-Ring Antenna for Array Design / J. Huang, X. Gong // IEEE International Symposium on Antennas and Propagation and USNC/URSI National Radio Science Meeting, USA, 07–12 July, 2019: proceedings. – Atlanta, 2019. – P. 1151–1152. DOI: 10.1109/APUSNCURSINRSM.2019.8889188
6. A Switchable-Frequency Slot-Ring Antenna Element for Designing a Reconfigurable Array / [M. Shirazi, J. Huang, T. Li, X. Gong] // IEEE Antennas and Wireless Propagation Letters. – 2018. – Vol. 17, No. 2. – P. 229–233. DOI: 10.1109/LAWP.2017.2781463
7. Wideband and Low Cross-Polarization Planar Annual Ring Slot Antenna / [C. Chen, C. Li, Z. Zhu, W. Wu] // IEEE Antennas and Wireless Propagation Letters. – 2017, Vol. 16. – P. 3009–3013. DOI: 10.1109/LAWP.2017.2757963
8. Godaymi Al-Tumah W. A. Design, simulation, and fabrication of a double annular ring microstrip antenna based on gaps with multiband feature / W. A. Godaymi Al-Tumah, R. M. Shaaban, A. P. Duffy // Engineering Science and Technology, an International Journal. – 2022. – Vol. 29. – P. 1–10. DOI: 10.1016/j.jestch.2021.06.013
9. Design of Graphene-Based Annular Ring Microstrip Antenna Using Short-Pin Technique for Dual Band Applications / [P. Phonkitiphan, R. Kaewon, K. Pancharoen et al.] // International Journal of Electrical and Electronic Engineering & Telecommunications. – 2020. – Vol. 9, No. 4. – P. 231–236. DOI: 10.18178/ijeetc.9.4.231-236
10. The Antenna Array with Ring Elements / [O. Shcherbyna, L. Ilnitsky, I. Mykhalchuk, O. Kozhokhina] // Signal Processing Symposium (SPSympo 2017), Poland, 12–14 September, 2017: proceedings. – Jachranka, 2019. – P. 1–4. DOI: 10.1109/SPS.2017.8053700
11. Pozar M. David. Microwave Engineering: 4th edition / M. David Pozar. – New Jersey : John Willey & Sons, 2012. – 756 p.
12. Gustrau F. RF and Microwave Engineering: Fundamentals of Wireless Communications / F. Gustrau. – New Jersey: John Willey & Sons, 2012. – 368 p.

DOI 10.15588/1607-3274-2023-3-1

UDC 621.396.962

MATHEMATICAL MODEL OF THE CURRENT TIME FOR THREE-FRAGMENT RADAR SIGNAL WITH NON-LINEAR FREQUENCY MODULATION

Kostyria O. O. – Dr. Sc., Senior Research, Leading Research Scientist, Ivan Kozhedub Kharkiv National Air Force University, Kharkiv, Ukraine.

Hryzo A. A. – PhD, Associate Professor, Head of the Research Laboratory, Ivan Kozhedub Kharkiv National Air Force University, Kharkiv, Ukraine.

Dodukh O. M. – PhD, Leading Research Scientist, Ivan Kozhedub Kharkiv National Air Force University, Kharkiv, Ukraine.

Narezhnyi O. P. – PhD, Associate Professor, V. N. Karazin Kharkiv National University, Kharkiv, Ukraine.

Fedorov A. V. – PhD, Research, Ivan Kozhedub Kharkiv National Air Force University, Kharkiv, Ukraine.

ABSTRACT

Context. The authors of the article have developed a new mathematical model that allows taking into account frequency and phase distortions that occur in a three-fragment signal during the transition from one fragment to another, when the rate of frequency modulation of the signal changes. The object of research is the process of formation and processing of radar non-linear frequency modulation signals.

Objective. The purpose of the work is to develop and research a mathematical model of current time for a signal with non-linear frequency modulation, which consists of three linear frequency modulated fragments.

Method. The article provides a theoretical justification of the need to develop a mathematical model in the current time for a three-fragment signal with non-linear frequency modulation, capacity for work of the created model is demonstrated on the example of several radio signals that differ in frequency parameters. With the same signal parameters, the obtained results were compared with the results of the known model, for which known methods of spectral and correlation analysis were used. A distinctive feature of the proposed model is the consideration of jumps in the instantaneous frequency and phase of the signal that occur during the transition from one linear-frequency modulated fragment to the next. Such jump-like changes in frequency and phase in known models of signals with non-linear frequency modulation are not compensated for, which causes distortion of their spectra and an increase the side lobes level of auto-correlation (mutual-correlation) functions.

Results. A comparative check of the developed and known signal models indicates a decrease the side lobes level of the autocorrelation function by 3 dB or more, depending on the given frequency-time parameters.

Conclusions. The application of the proposed mathematical model makes it possible to form and process radar signals, which include three linear-frequency modulated fragments. Compensation of jump-like changes in frequency and phase leads to a decrease in the degree of distortion of the spectrum and, as a result, an increase in its effective width, which ensures a narrowing of the main lobe and a decrease the side lobes level of the auto-correlation function.

KEYWORDS: radar signal; non-linear frequency modulation; autocorrelation function, side lobe level; mathematical model.

ABBREVIATIONS

ACF is a autocorrelation function;
LFM is a linear frequency modulation;
ML is a main lobe;
MM is a mathematical model;
NLFM is a non-linear frequency modulation;
PSD is a power spectral density;
PSLL is a peak side lobe level;
RM is a radar mean;
RFM is a rate of frequency modulation;
RRD is a receiving device;
WP is a weight processing.

NOMENCLATURE

Δf_n is a frequency deviation of the n^{th} signal fragment, Hz;

f_{en} is a final frequency of the n^{th} signal fragment, Hz;

$\dot{U}(t)$ is a complex signal amplitude, V;

$f(t)$ is a instantaneous signal frequency, Hz;

$f_n(t)$ is a neural network model structure;

$\varphi(t)$ is a instantaneous signal phase, rad;

$\varphi_n(t)$ is a instantaneous phase of the n^{th} LFM signal fragment, rad;

$|\dot{U}(t)|$ is a complex signal amplitude module, V;

n is a sequence number of the signal fragment (n=1, 2, 3);

t is a current time, s;

f_0 is a initial signal frequency, Hz;

f_{0n} is a initial frequency of the nth signal fragment, Hz;

δf_{mn} is a frequency jump when moving from the $m = n - 1^{th}$ signal fragment to the n^{th}, Hz;

$\delta\varphi_{mn}$ is a phase jump at the transition from the m^{th} signal fragment to the n^{th}, rad;

Δf_{12} is a total deviation of the frequency of the first and second signal fragments, Hz;

T_s is a total duration of the NLFM signal, s;

DOI 10.15588/1607-3274-2023-3-2

T_{12} is a total duration of the first and second signal fragments, s;

T_n is a duration of the n^{th} signal fragment, s;

$\omega(t)$ is a cyclic frequency of the signal, rad;

β_n RFM of the n^{th} LFM signal fragment, Hz/s.

INTRODUCTION

The widespread use of solid-state (transistor) transmission devices causes certain limitations regarding the peak power of probing signals, the designers are forced to use signals of increased duration, which leads to a deterioration of the range resolution.

In order to overcome the contradiction between the need to increase the duration of probing radio pulses and maintain the necessary resolution of RM, signals with intra-pulse frequency (phase) modulation (manipulation) have become widely used [1–6].

Historically, LFM signals were the first to be used due to the ease of implementation of devices for their formation and processing. However, a significant disadvantage of such signals is the relatively high PSLL of their ACF, which is approximately –13 dB [1, 2], which in some situations requires raising the detection threshold in systems for stabilizing the level of false alarms and, in general, worsens the potentially achievable detection characteristics signals reflected from targets.

One of the most common methods of reducing PSLL is the application of WP in the time or frequency domain (time or spectral windows) [7–9]. It is possible to achieve an even greater reduction of PSLL by using NLFM of the probing signal followed by traditional WP in RRD [2, 10, 11]. In [2, 12, 13], it is proposed to use a signal consisting of three NLFM fragments adjacent to each other in time with a successive increase or decrease in the instantaneous frequency as such an LFM signal. The peculiarity of this signal is that the extreme fragments have a smaller value of the PSD due to the fact that they have a larger RFM β_n, which is determined by the ratio of the deviation of the frequency of the n-th LFM fragment Δf_n to its duration T_n, $\beta_n = \Delta f_n / T_n$. Such a decrease in the PSD at lower and upper frequencies leads to a rounding of the resulting spectrum, as a result of which there is a decrease the PSLL [2, 13] with the expansion the ML of the ACF due to a decrease in its effective width. The expansion the ML leads to a decrease in the resolution of the RM from a distance, which is not always acceptable.

The traditional approach is to choose a compromise solution, that is, to achieve the required PSLL value with a slight permissible deterioration of the specified resolution.

The approach based on the use of different types of signals in accordance with the tasks of the RM has potentially greater advantages.

This work is devoted to the development of a mathematical model of a three-fragment NLFM signal with concoct of three LFM fragments, with the possibility of further implementation of such signals in existing RM and those under development.

The object of study is the process of formation and processing of radar NLFM signals.

The subject of study is mathematical models of NLFM signals.

The purpose of the work is to theoretically substantiate the need to develop and design a MM of an NLFM signal consisting of three LFM fragments, as well as to test its workability.

1 PROBLEM STATEMENT

Among the MMs of three-fragment NLFM signals, the most commonly used are the MMs in which the input values are the current time t, the duration of the fragments T_n, and the deviation of their frequency Δf_n, which is equal to the difference between the final and initial frequencies of the corresponding n-th LFM fragment and is a fixed value. It is determined by the product of the RFM of the n-th LFM signal fragment β_n and its duration T_n.

$$\Delta f_n = f_{en} - f_{0n} = \beta_n T_n .$$

In general, the complex signal amplitude is represented as:

$$\dot{U}(t) = |\dot{U}(t)| \exp\{j\varphi(t)\}. \qquad (1)$$

To simplify the following, we assume $|\dot{U}(t)| = 1$.

The functions of changing the instantaneous frequency and phase of the signal for each n-th fragment are different, the change occurs during the transition from one fragment to the next.

The instantaneous frequency is proportional to the speed of the frequency-modulated n-th fragment and is linearly dependent on time:

$$f_n(t) = \beta_n t ,$$

and the instantaneous phase, in turn, has linear and quadratic components and is determined by the dependence:

$$\varphi_n(t) = 2\pi\left(f_{0n} t + \frac{\beta_n t^2}{2} \right).$$

The total duration of the NLFM signal is defined as the sum of the durations of the LFM fragments:

$$T_s = \sum_{n=1}^{3} T_n ,$$

$T_{12} = T_1 + T_2$ – total duration of the first and second signal fragments.

DOI 10.15588/1607-3274-2023-3-2

Well-known relations interconnect the instantaneous frequency and phase [1–2]:

$$\varphi(t) = \int f(t)dt;$$
$$f(t) = \frac{d\varphi(t)}{dt}.$$

To make the formulas more compact, we introduce the notation of the total frequency deviation of the first and second signal fragments:

$$\Delta f_{12} = \Delta f_1 + \Delta f_2.$$

Further analysis will be carried out by graphically comparing the realizations of signals in the time and frequency domains, their ACF, and the dependence of the instantaneous frequency and phase of signals on time. The signals will be compared by the level of their PSLL at a fixed WP width, or by comparing the degree of WP expansion at a constant level of PSLL.

2 REVIEW OF THE LITERATURE

Many publications have been devoted to the formation and processing of NLFM signals in various fields of application, with the most extensive studies of such signals in the field of air target radar [14–18]. In works [15–16], the potentially achievable PSLL of the ACF is estimated for a three-frame-segment NLFM signal, the range resolution of the RM is analyzed in detail [17], and the effect of the Doppler frequency shift on the characteristics of the ACF is studied [17–18].

Another area related to the use of NLFM signals is meteorological localization, with the peculiarity that the main research direction in this area is to study the problem of reducing the PSLL [19]. A similar problem with respect to RM with a synthesized antenna aperture is discussed in detail in [20–23].

A distinctive feature of papers [14, 24–25] is that to minimize the PSLL, it is proposed to use only NLFM signals, or to combine their use with additional WP in the RDD [2, 17, 19].

Papers [11, 19, 26–27] use mathematical models of NLFM signals of the current time with a smooth (polynomial) change in the frequency modulation law.

The formation of NLFM signals from three LFM fragments was proposed in [2, 12, 13], where the MM is presented, in which the argument (time) changes symmetrically in the middle of the radio pulse. Subsequently, to represent such signals, a mathematical technique is used in which each subsequent fragment starts from a zero time reference (from the zero phase), that is, each time the time is shifted to the zero mark [16, 18, 24, 25, 28–30].

Research has shown that the introduced MM do not fully reflect the peculiarities of the formation of NLFM signals, namely, they do not take into account the phase structure of the signal at the junctions of fragments.

In authors propose to consider the MM of a three-fragment NLFM signal developed by the authors, which is a further development of the MM presented in [2, 12, 13, 31]. Unlike the existing ones, the model more adequately takes into account the phase change at the junctions of LFM signal fragments, preventing the appearance of instantaneous frequency and phase jumps, which allows us to obtain a lower PSLL.

3 MATERIALS AND METHODS

Further analysis is performed using a common MM of a three-fragment NLFM signal introduced in [16, 18, 24, 25, 28–30]. The peculiarity of this MM is that the determination of the instantaneous amplitude (1) for all LFM fragments starts from zero time by shifting the time scale by the duration of the previous signal components. For example, for an NLFM signal consisting of three LFM fragments, the complex signal amplitude is described in accordance with (2).

$$\dot{U}(t) = |\dot{U}(t)| \begin{cases} \exp\left(j\varphi_1(t)\right), & 0 \le t \le T_1; \\ \exp\left(j\varphi_2(t-T_1)\right), & T_1 \le t \le T_{12}; \\ \exp\left(j\varphi_3(t-T_{12})\right), & T_{12} \le t \le T_s. \end{cases} \quad (2)$$

In the future, to record the expressions of the phase and frequency of the NLFM signal fragments, we assume that time intervals similar to (2) are applied to them.

The instantaneous phases of the signal (2) can be found by expressions [16, 18, 24–25, 28–30]:

$$\varphi(t) = 2\pi \begin{cases} f_0 t + \frac{\beta_1 t^2}{2}; \\ (f_0 + \Delta f_1)(t - T_1) + \frac{\beta_2 (t^2 - T_1 t)}{2}; \\ (f_0 + \Delta f_{12})(t - T_{12}) + \frac{\beta_3 (t^2 - T_{12} t)}{2}. \end{cases} \quad (3)$$

By differentiating the expressions of the instantaneous phase (3), the ratios for the instantaneous frequency of the corresponding signal fragments are found [16, 18, 24–25, 28–30]:

$$f(t) = \begin{cases} f_0 + \beta_1 t; \\ f_0 + \Delta f_1 + \beta_2 (t - T_1); \\ f_0 + \Delta f_{12} + \beta_3 (t - T_{12}). \end{cases} \quad (4)$$

A significant drawback of MM (3) – (4) is that due to the shift of the time scale to zero for each subsequent fragment, this model is not sensitive to abrupt changes in instantaneous frequency that occur at the moments of increase or decrease in the RFM (at the junctions of fragments).

The graph of the signal frequency versus time for (4) is shown in Fig. 1.

DOI 10.15588/1607-3274-2023-3-2

From the analysis of Fig. 1 and (4), it follows that the initial frequency of the second LFM fragment has the value of $f_0 + \Delta f_1$, when in fact it is equal to f_{02}. Accordingly, the initial phase of the second fragment has a zero value, while the final phase of the first fragment is equal to $\varphi_{e1} = 2\pi(f_0 + \Delta f_1)T_1$. That is, at the moment $t = T_1$ there is an abrupt change in the instantaneous frequency and instantaneous phase of the signal.

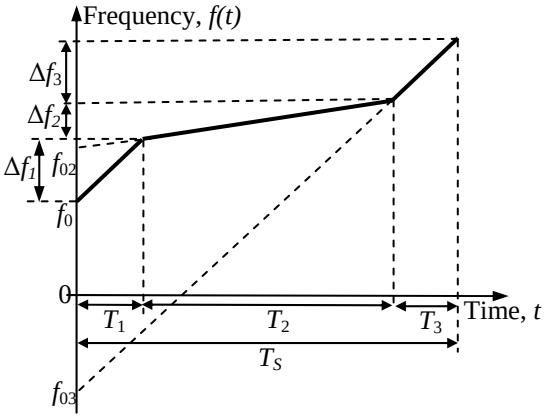

Figure 1 – Graph of changes in the frequency of the NLFM signal consisting of three LFM fragments

The same situation is observed at the junction of the second and third fragments at $t = T_1 + T_2$, the initial frequency of the third fragment is equal to :

$$f_{03} = f_0 + \Delta f_1 + \Delta f_2,$$

and its actual value is f_{03} with a "minus" sign.

For further consideration, we obtain analytical expressions that determine the values of frequency and phase jumps for the time instant $t = T_1$.

The final value of the frequency of the LFM signal of the first fragment at time $t = T_1 - \delta t$, under the condition $\delta t \to 0$ is described by the expression

$$f_{e1} = f_0 + \beta_1 T_1,$$

and the initial frequency value for the second signal fragment at time $t = T_1 + \delta t$ is

$$f_{02} = f_0 + \beta_2 T_1.$$

Thus, the frequency jump at this point in time is equal to their difference:

$$\delta f_{12} = f_{02} - f_{e1} = (\beta_2 - \beta_1)T_1. \quad (5)$$

By integrating, we find the corresponding signal phase jump:

$$\delta\varphi_{12} = \int_0^{T_1} (\beta_2 - \beta_1)T_1 dt = \frac{1}{2}(\beta_2 - \beta_1)T_1^2. \quad (6)$$

The next jump in the frequency-phase parameters of the signal occurs when we move to the third LFM fragment. Let's extend the line segment (Fig. 1), which demonstrates the change in the frequency of this fragment, to the intersection with the abscissa axis and mark the intersection point as f_{03}, i.e., this is the conditional initial frequency of the third fragment. From the analysis of Fig. 1, it turns out that the frequency jump at the moment of transition from the second signal fragment to the third δf_{23}, similar to (5), is:

$$\delta f_{23} = f_0 + \beta_1 T_1 + \beta_2 T_2 - \beta_3 T_{12}.$$

After simplification, we get:

$$\delta f_{23} = (\beta_3 - \beta_1)T_1 + (\beta_3 - \beta_2)T_2. \quad (7)$$

By integrating over the appropriate time intervals, similar to (6), we find the expression for the phase jump:

$$\delta\varphi_{23} = \frac{1}{2}(\beta_3 - \beta_1)T_1^2 + \frac{1}{2}(\beta_3 - \beta_2)T_2^2. \quad (8)$$

Thus, based on (5)–(8), it can be concluded that the process of forming a NLFM signal consisting of three LFM fragments is accompanied by a jump-like change in the instantaneous frequency at the moment of transition from one fragment to the next, which causes a corresponding jump in the instantaneous phase of the signal. In the MM with a time shift (3)–(4), these jumps are not taken into account, which is its essential drawback. For further use, it is proposed to introduce a new MM of the NLFM of a signal in the current time, which takes into account the jumps in instantaneous frequency and phase.

To record the values of the instantaneous phase of a three-fragment NLFM signal in the current time, we use the well-known model of three LFM fragments [16]. The formula uses the same time intervals as in (2):

$$\varphi(t) = 2\pi\begin{cases} f_0 t + \frac{\beta_1 t^2}{2}; \\ (f_0 + \beta_1 T_1)t + \frac{\beta_2 t^2}{2}; \\ (f_0 + \beta_1 T_1 + \beta_2 T_2)t + \frac{\beta_3 t^2}{2}. \end{cases} \quad (9)$$

By differentiating the expressions (9) for the instantaneous frequency, we have the following:

DOI 10.15588/1607-3274-2023-3-2

$$f(t)=\begin{cases} f_0+\beta_1 t; \\ f_0+\beta_1 T_1+\beta_2 t; \\ f_0+\beta_1 T_1+\beta_2 T_2+\beta_3 t. \end{cases} \quad (10)$$

For further consideration, firstly, we obtain an intermediate MM by compensating for the frequency jump taking into account (5) and (7), MM (9) takes the form:

$$\varphi(t)=2\pi\begin{cases} f_0 t+\dfrac{\beta_1 t^2}{2}; \\ \left[f_0-(\beta_2-\beta_1)T_1\right]t+\dfrac{\beta_2 t^2}{2}; \\ \left[f_0-(\beta_3-\beta_1)T_1-(\beta_3-\beta_2)T_2\right]t+\dfrac{\beta_3 t^2}{2}, \end{cases} \quad (11)$$

and the signal frequency changes as:

$$f(t)=\begin{cases} f_0+\beta_1 t; \\ f_0-(\beta_2-\beta_1)T_1+\beta_2 t; \\ f_0-(\beta_3-\beta_1)T_1-(\beta_3-\beta_2)T_2+\beta_3 t. \end{cases} \quad (12)$$

To compensate for phase jumps (6) and (8), we add the corresponding components to (10) and obtain the final MM of the current time for the three-fragment NLFM of the signal:

$$\varphi(t)=2\pi\begin{cases} f_0 t+\dfrac{\beta_1 t^2}{2}; \\ \left[f_0-(\beta_2-\beta_1)T_1\right]t+\dfrac{\beta_2 t^2}{2}+\delta\varphi_{12}; \\ \left[f_0-(\beta_3-\beta_1)T_1-(\beta_3-\beta_2)T_2\right]t+\dfrac{\beta_3 t^2}{2}-\delta\varphi_{23}, \end{cases} \quad (13)$$

whose frequency changes in accordance with (12).

It should be noted that the transition from the first LFM of a fragment to the second is accompanied by a decrease in the RFM, so the additional phase shift has a positive value, and during the next transition the RFM increases, and therefore the phase shift is negative.

To verify the adequacy and reliability of the developed model, simulation modeling was carried out in the MatLab application package.

4 EXPERIMENTS

The MM of the three-fragment NLFM signal was verified for the following LFM parameters of the fragments: $f_0=0$, $\Delta f_1=\Delta f_3=165$ kHz, $\Delta f_2=400$ kHz, $T_1=T_3=20$ μs, $T_2=100$ μs.

The simulation was performed sequentially in accordance with (3) – (4), (9) – (10), (11) – (12), and (13). The simulation results are displayed in the form of graphs of frequency changes and time realizations in the current time, their spectra, and ACF.

5 RESULTS

The results of mathematical modeling using (3)–(4) are shown in Fig. 2. The graph of changes in the frequency of the NLFM signal (Fig. 2a) and its oscilloscope frame $U(t)=|\dot{U}(t)|$ (Fig. 2b) are plotted in the same time interval.

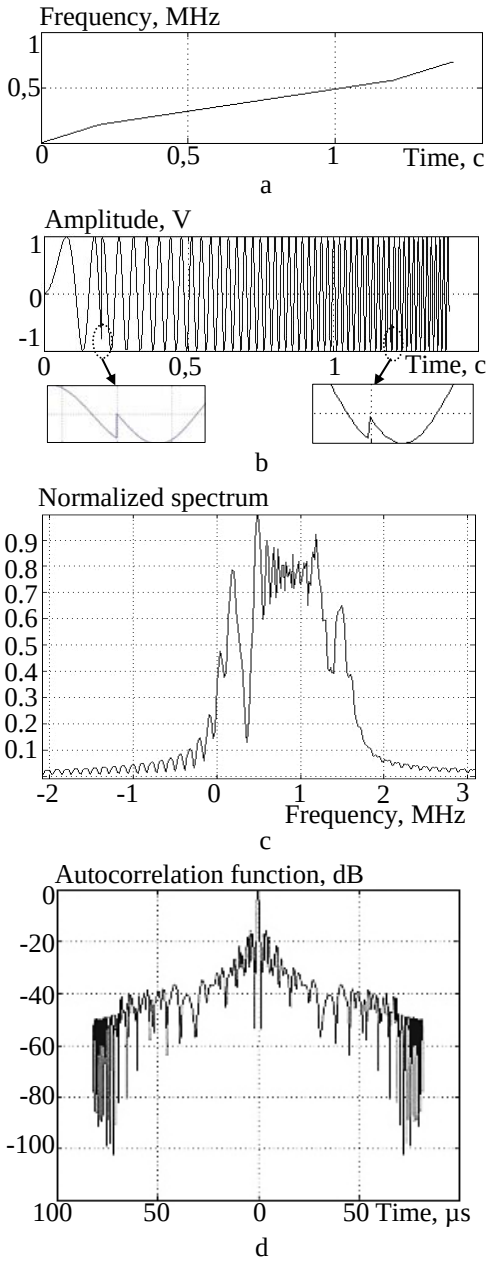

Figure 2 – Graph of instantaneous frequency change (a), oscilloscope (b), spectrum (c), ACF (d) of the NLFM signal with parameters $\Delta f_1=\Delta f_3=165$ kHz, $\Delta f_2=400$ kHz, $T_1=T_3=20$ μs, $T_2=100$ μs

DOI 10.15588/1607-3274-2023-3-2

The analysis of the graphs shows that abrupt changes in the instantaneous phase of the signal (Fig. 2b, the enlarged scale of the phase jumps is shown in the footnotes) occur at the moment of transition to the next LFM fragment (Fig. 2a). The spectrum of the NLFM signal $S(f)$ (Fig. 2c) has dips at the transition frequencies (Fig. 2c), which indicates the presence of phase jumps at these frequencies, as evidenced by the pulsations on the spectrum slopes. The ACF signal $R(\tau)$ is shown in Figure 2d. The PSLL of the ACF is –15.59 dB, the width ML of the ACF is 1.9 μs. There is a sharp change in the PSLL ACF in the time intervals corresponding to the signal region with a higher RFM value, which is also a sign of the presence of phase distortion.

In the course of modeling according to (9)–(10), the results of which are shown in Fig. 3, it was found that the signal frequency change graph in Fig. 3a, in contrast to Fig. 2a demonstrates the presence of instantaneous frequency jumps at the moments of change RFM (Fig. 3a); these moments correspond to jumps in the signal phase (Fig. 3b) with a clear increase in the frequency of oscillations at the beginning of each new fragment.

Due to the frequency jumps between signal fragments, its spectrum (Fig. 3c) has three separate components and clearly expressed pulsations of the steeples. A sharp drop in the PSLL ACF (Fig. 3d) with a sharp change in the frequency and level of the lateral lobe pulsations additionally indicates the presence of significant frequency and phase jumps in the signal.

The ACF parameters for this MM were not evaluated because of the obvious discrepancy between the obtained results and the expected ones. The obtained results prove the validity of (5)–(8) and the need to compensate for frequency and phase jumps during the transition to each new section of the NLFM signal.

The results of the next experiment allow us to compare the work of (3)–(4) and (11)–(12), since (4) and (12) demonstrate a complete coincidence of results, the graph of (12) is not shown.

The results of the modeling according to (11) are shown in Fig. 4. Despite the coincidence of the simulation results according to (4) and (12), the waveform in Fig. 4b shows a different character of the signal phase distortion during changes in the RFM with compared to Fig. 2b. The difference in phase jumps is evident in the spectra of Figs. 2c and Fig. 4c, the PSLL ACF in Fig. 4d is –17.31 dB, and the width of the ML of the ACF is 1.8 μs. Given that (3)–(4) are not sensitive to frequency jumps, and (11)–(12) compensate for frequency jumps, these models demonstrate differences in other signal features.

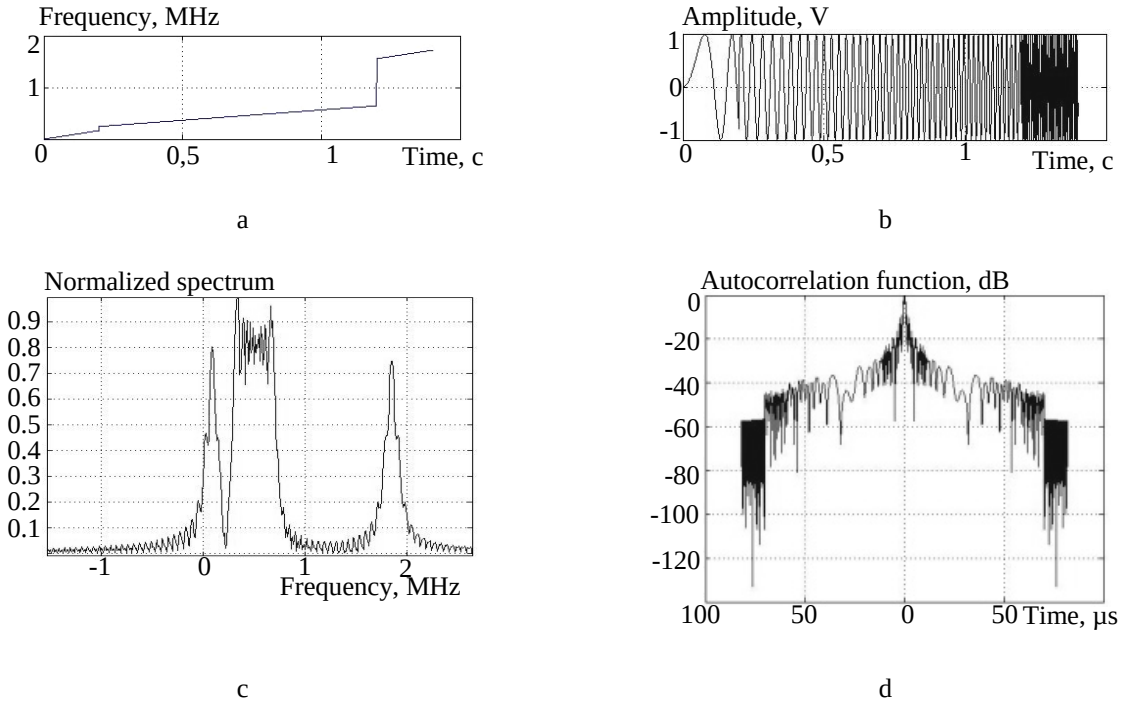

Figure 3 – Graph of instantaneous frequency change (a), oscilloscope (b), spectrum (c), ACF (d) of the NLFM signal without compensation for frequency and phase jumps

DOI 10.15588/1607-3274-2023-3-2

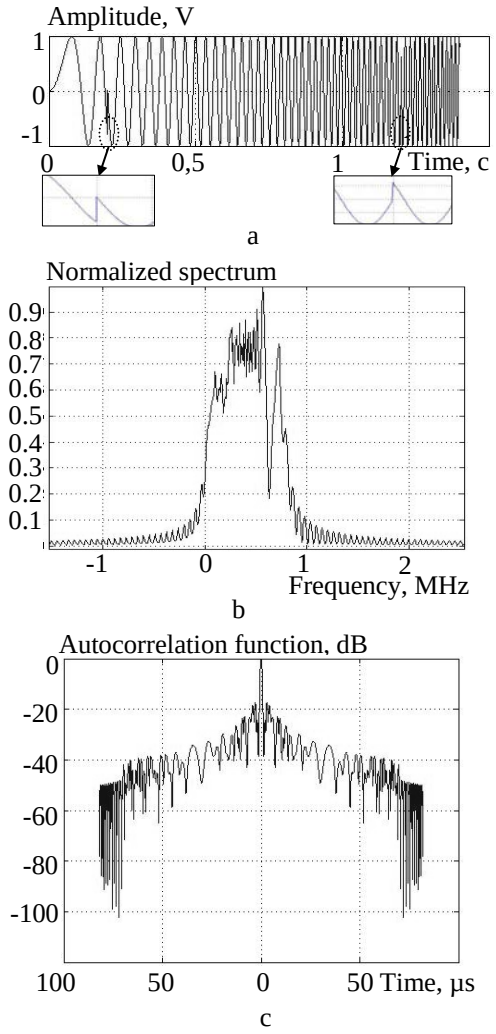

Figure 4 – Waveform (a), spectrum (b), ACF (c) of the NLFM signal with frequency jump compensation

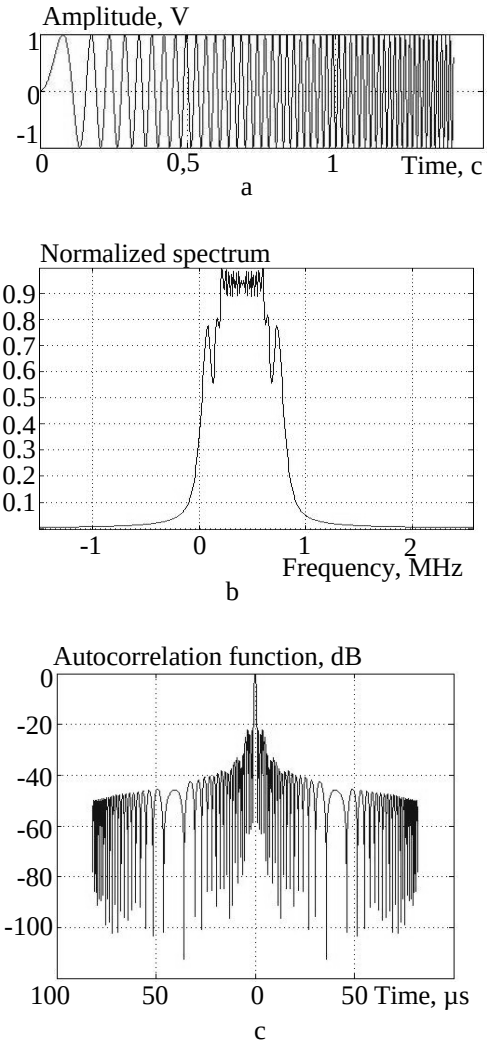

Figure 5 – Waveform (a), spectrum (b), ACF (c) of the NLFM signal with compensation of frequency and phase jumps

Fig. 5 shows the results of modeling only according to (12), since the graph according to (11) is similar to Fig. 2a. In the oscillogram of Fig. 5a, there are no phase distortions at the moments of transitions from one LFM fragment to another, the spectrum of the NLFM signal of Fig. 5b is almost symmetrical, and there are no pulsations on the slopes. The lateral lobes of the ACF of Fig. 5c decay smoothly, the maximum PSLL is –22 dB, and the width of the ML is 1.8 μs.

In comparison with the classical LFM, the PSLL signal decreased by 9 dB, but the price for this is the expansion of the ML of the ACF by almost a third.

6 DISCUSSION

Our studies indicate that the use of the new model (12)–(13) provides compensation for jumps in the instantaneous frequency and phase of the NLFM signal at the moments of transition from one LFM fragment to the next, due to which the resulting spectrum becomes symmetrical, rounded, i.e., acquires the expected shape, and there are no pulsations on its slopes.

As a result of the improved spectrum shape, its effective width has increased, and therefore the ML of the ACF has become narrower compared to MM (3)–(4). The lateral lobes of the ACF decrease smoothly, which is also evidence of the absence of frequency-phase distortions.

In the known works [16, 18, 24–25, 28–30], the spectra of the studied NLFM signals are not given, but the given ACFs demonstrate sharp changes in the level and frequency of the lateral lobes, similar to Figures 2d, 3d, 4c, which indicates the presence of instantaneous frequency and phase jumps. In such circumstances, the reduction of the PSLL can be achieved only in some cases by selecting the values of T_n and Δf_n, which does not ensure the stability and predictability of the final result.

The authors consider it expedient to introduce the three-fragment NLFM signal proposed by the MM into circulation and to continue research in the direction of increasing the number of LFM fragments in order to minimize the PSLL.

DOI 10.15588/1607-3274-2023-3-2

CONCLUSIONS

The scientific novelty of the obtained results is the discovery that frequency and phase jumps during the transition from the first LFM fragment to the second are included as components for determining the magnitude of frequency and phase jumps of the next fragment junction. Based on this, a new MM of the NLFM signal consisting of three LFM fragments is developed. In contrast to the known ones, the proposed model uses the current time instead of the shifted time and compensates for the jumps in the instantaneous frequency and phase of the signal that occur at the moments of transition from one LFM fragment to the next.

The developed model ensures predictability and stability of results when the frequency and time parameters of NLFM signals change.

For the characteristics of the LFM fragments adopted during the modeling, the PSLL of the ACF of the resulting NLFM signal was achieved from –22 dB ($\Delta f_1 = \Delta f_3 = 125$ kHz, $\Delta f_2 = 300$ kHz) to –27 dB ($\Delta f_1 = \Delta f_3 = 55$ kHz, $\Delta f_2 = 100$ kHz), while the duration of the LFM fragments did not change and was $T_1 = T_3 = 20$ μs, $T_2 = 100$ μs.

The practical significance of obtained results consists in the possibility of using the proposed MM to develop devices for the formation and processing of radio signals in various applications, such as radar systems for detecting air targets, aviation and space systems for surveying the earth's surface, meteorology, sonar, ultrasound diagnostics, etc., in which NLFM signals can be used to reduce the PSLL of the ACF independent-ly or in combination with the WP in the receiving device.

Prospects for further research are to improve the developed model to expand the possibilities of changing the initial frequency and time parameters of the NLFM signals, as well as to study the effect of the number of LFM fragments on the level of the PSLL.

ACKNOWLEDGEMENTS

We thank the management of Ivan Kozhedub Kharkiv National Air Force University for the opportunity to conduct scientific research.

REFERENCES

1. Skolnik M. I. Radar Handbook. Editor in Chief. Boston, McGraw-Hill Professional, second edition, 1990, 846 p.
2. Cook C. E., Bernfeld M. Radar Signals: An Introduction to Theory and Application. Boston, Artech House, 1993, 552 p.
3. Barton D. K. Radar System Analysis and Modeling. London, Artech House, 2005, 545 p.
4. Van Trees H. L. Detection, Estimation, and Modulation Theory. New York, John Wiley & Sons, 2004, 716 p.
5. Levanon N., Mozeson E. Radar Signals. New York, John Wiley & Sons, 2004, 403 p.
6. Melvin W. L., Scheer J. A. Principles of modern radar. New York, SciTech Publishing, 2013, 846 p.
7. Doerry A. W. Catalog of Window Taper Functions for Side lobe Control [Electronic resource]. Access mode: https://www.researchgate.net/publication/316281181_Catalog_of_Window_Taper_Functions_for_Sidelobe_Control.
8. Heinzel G., Rüdiger A., Schilling R. Spectrum and spectral density estimation by the Discrete Fourier transform (DFT), including a comprehensive list of window functions and some new flattop windows [Electronic resource]. Access mode: https://pure.mpg.de/rest/items/item_52164_1/component/file_152163/content.
9. Galushko V. G. Performance Analysis of using tapered Windows for Side Lobe Reduction in Chirp-Pulse Compression, *Radio Physics and Radio Astronomy*, 2019, Vol. 24(4), pp. 300–313.
10. Nettem A. V., Daniel E. R., Chandu K. Windows For Reduction Of ACF Side Lobes of Pseudo-NLFM Signal, *International Journal of Scientific & Technology Research*, 2019, Vol. 8, Issue 10, pp. 2155–2161.
11. Ghavamirad R., Sebt M. A. Side Lobe Level Reduction in ACF of NLFM Waveform, *IET Radar, Sonar & Navigation*, 2019, Vol. 13, Issue 1, pp. 74–80.
12. Cook C. E. A class of nonlinear FM pulse compression signals, *Proceedings of the IEEE*, 1964, Vol. 52(11), pp. 1369–1371.
13. Cook C. E., Paolillo J. A pulse compression predistortion function for efficient side lobe reduction in a high-power radar, *Proceedings of the IEEE*, 1964, Vol. 52(4), pp. 377–389.
14. Xu Z., Wang X., Wang Y. Nonlinear Frequency-Modulated Waveforms Modeling and Optimization for Radar Applications, *Mathematics*, 2022, Vol. 10, № 3939.
15. Fan Z., Meng H.-Y. Coded excitation with Nonlinear Frequency Modulation Carrier in Ultrasound Imaging System, *IEEE Far East NDT New Technology & Application Forum (FENDT)*. Kunming, Yunnan province, China, 20–22 November 2020, pp. 31–35.
16. Chukka A., Krishna B. Peak Side Lobe Reduction analysis of NLFM and Improved NLFM Radar signal, *AIUB Journal of Science and Engineering (AJSE)*, 2022, Vol. 21, Issue 2, pp. 125–131.
17. Saleh M., Omar S.-M., E. Grivel et al. A Variable Chirp Rate Stepped Frequency Linear Frequency Modulation Waveform Designed to Approximate Wideband Non-Linear Radar Waveforms, *Digital Signal Processing*, 2021, Vol. 109, № 102884.
18. Nettem A. V., Rani E. Doppler Effect Analysis of NLFM Signals, *International Journal of Scientific & Technology Research*, 2019, Vol. 8, Issue 11, pp. 1817–1821.
19. Kurdzo J. M., Cho John Y. N., Cheong B. L. et al. A Neural Network Approach for Waveform Generation and Selection with Multi-Mission Radar, *IEEE Radar Conference*. Boston, 22–26 April 2019, № 19043446.
20. Zhao Y., Ritchie M., Lu X. et al. Non-continuous piecewise nonlinear frequency modulation pulse with variable subpulse duration in a MIMO SAR Radar System, *Remote Sensing Letters*, 2020, Vol. 11, Issue 3, pp. 283–292.
21. Xu W., Zhang L., Fang C. et al. Staring Spotlight SAR with Nonlinear Frequency Modulation Signal and Azimuth Non-Uniform Sampling for Low Side Lobe Imaging, Sensors, 2021, Vol. 21, Issue 19, № 6487.
22. Song C., Wang Y., Jin G. et al. A Novel Jamming Method against SAR Using Nonlinear Frequency Modulation Waveform with Very High Side Lobes, *Remote Sensing*, 2022, Vol. 14, Issue 21, № 5370.
23. Jin G., Deng Y.-K., Wang R. et al. An Advanced Nonlinear Frequency Modulation Waveform for Radar Imaging With

DOI 10.15588/1607-3274-2023-3-2

Low Side Lobe, *IEEE Transactions on Geoscience and Remote Sensing*, 2019, Vol. 57, Issue 8, pp. 6155–6168.
24. Valli N. A., Rani D. E., Kavitha C. Modified Radar Signal Model using NLFM, *International Journal of Recent Technology and Engineering (IJRTE)*, 2019, Vol. 8, Issue 2S3, pp. 513–516.
25. Adithyavalli N. An Algorithm for Computing Side Lobe Values of a Designed NLFM function, *International Journal of Advanced Trends in Computer Science and Engineering*, 2019, Vol. 8, Issue 4, pp. 1026–1031.
26. Parwana S., Kumar S. Analysis of LFM and NLFM Radar Waveforms and their Performance Analysis, *International Research Journal of Engineering and Technology (IRJET)*, 2015, Vol. 02, Issue 02, pp. 334–339.
27. Bayındır C. A Novel Nonlinear Frequency-Modulated Chirp Signal for Synthetic Aperture Radar and Sonar Imaging, *Journal of Naval Science and Engineering*, 2015, Vol. 11, Issue 1, pp. 68–81.
28. Jeyanthi J. E., Shenbagavalli A., Mani V.R.S. Study of Different Radar Waveform Generation Techniques for Automatic Air Target Recognition, *International Journal of Engineering Technology Science and Research (IJETSR)*, 2017, Vol. 4, Issue 8, pp. 742–747.
29. Widyantara M. R., Suratman F. Y., Widodo S. et al. Analysis of Non Linear Frequency Modulation (NLFM) Waveforms for Pulse Compression Radar, *Journal Electronica dan Telekomunikasi (JET)*, 2018, Vol. 18, №1, pp. 27–34.
30. Valli N. A., Rani D. E., Kavitha C. Performance Analysis of NLFM Signals with Doppler Effect and Back-ground Noise, *International Journal of Engineering and Advanced Technology (IJEAT)*, 2020, Vol. 9, Issue 3, pp. 737–742.
31. Kostyria O. O., Hryzo A. A., Dodukh O. M. et al. Mathematical model of a two-fragment signal with a non-linear frequency modulation in the current period of time, *Visnyk NTUU KPI Seriia – Radiotekhnika Radioaparatobuduvannia*, 2023, Vol. 92, pp. 60–67.

Received 15.06.2023.
Accepted 26.07.2023.

УДК 621.396.962

МАТЕМАТИЧНА МОДЕЛЬ ПОТОЧНОГО ЧАСУ ДЛЯ ТРИФРАГМЕНТНОГО РАДІОЛОКАЦІЙНОГО СИГНАЛУ З НЕЛІНІЙНОЮ ЧАСТОТНОЮ МОДУЛЯЦІЄЮ

Костиря О. О. – д-р техн. наук, старший науковий співробітник, провідний науковий співробітник Харківського національного університету Повітряних Сил імені Івана Кожедуба, Харків, Україна.

Гризо А. А.– канд. техн. наук, доцент, начальник НДЛ Харківського національного університету Повітряних Сил імені Івана Кожедуба, Харків, Україна.

Додух О. М. – канд. техн. наук, провідний науковий співробітник Харківського національного університету Повітряних Сил імені Івана Кожедуба, Харків, Україна.

Нарєжній О. П. – канд. техн. наук, доцент кафедри Харківського національного університету імені В. Н. Каразіна, Харків, Україна.

Федоров А. В. – д-р філос., науковий співробітник Харківського національного університету Повітряних Сил імені Івана Кожедуба, Харків, Україна.

АНОТАЦІЯ

Актуальність. Одним з напрямків удосконалення існуючих та створення нових радіолокаційних засобів є запровадження зондувальних сигналів з модуляцією частоти (фази), так званих складних сигналів, до яких відносяться сигнали з нелінійною частотною модуляцією. Одним з різновидів цих сигналів є такі, що складаються з трьох лінійно-частотно модульованих фрагментів. Однак широке використання трифрагментних сигналів стримується недостатньою проробкою математичного апарату, який достовірно відображає процеси їх формування та обробки. Авторами статті розроблено нову математичну модель, яка дозволяє враховувати частотні та фазові спотворення, що виникають у трифрагментному сигналі при переході від одного фрагменту до іншого, коли відбувається зміна швидкості частотної модуляції сигналу.

Мета роботи – розроблення та дослідження математичної моделі поточного часу для сигналу з нелінійною частотною модуляцією, який складається з трьох лінійно-частотно модульованих фрагментів.

Метод. В статті наведено теоретичне обґрунтування необхідності розроблення математичної моделі у поточному часі для трифрагментного сигналу з нелінійною частотною модуляцією, продемонстровано працездатність створеної моделі на прикладі кількох радіосигналів, які відрізняються за частотними параметрами. За однакових сигнальних параметрів здійснено порівняння отриманих результатів з результатами роботи відомої моделі, для чого використовувалися відомі методи спектрального та кореляційного аналізу. Відмінною особливістю запропонованої моделі є врахування стрибків миттєвої частоти і фази сигналу, які виникають під час переходу від одного лінійно-частотно модульованого фрагменту до наступного. Такі стрибкоподібні зміни частоти та фази в відомих моделях сигналів з нелінійною частотною модуляцією не компенсуються, що спричиняє спотворення їх спектрів та збільшення рівня бічних пелюсток авто-кореляційних (взаємно-кореляційних) функцій.

Результати. Порівняльна перевірка розробленої та відомої моделей сигналів свідчить про зменшення рівня бічних пелюсток автокореляційної функції на 3 дБ і більше в залежності від заданих частотно-часових параметрів.

Висновки. Застосування запропонованої математичної моделі дозволяє формувати та обробляти радіолокаційні сигнали, до складу яких входить три лінійно-частотно модульованих фрагменти. Компенсація стрибкоподібних змін частоти та фази призводить до зменшення ступеня спотворення спектру та, як наслідок, збільшення його ефективної ширини, що забезпечує звуження головної пелюстки та зменшення рівня бічних пелюсток авто-кореляційної функції.

КЛЮЧОВІ СЛОВА: радіолокаційний сигнал; нелінійна частотна модуляція; автокореляційна функція, рівень бічних пелюсток; математична модель.

DOI 10.15588/1607-3274-2023-3-2

ЛІТЕРАТУРА

1. Skolnik M. I. Radar Handbook. Editor in Chief / M. I. Skolnik. – Boston : McGraw-Hill Professional, second edition, 1990. – 846 p.
2. Cook C. E. Radar Signals: An Introduction to Theory and Application / C. E. Cook, M. Bernfeld. – Boston : Artech House, 1993. – 552 p.
3. Barton D. K. Radar System Analysis and Modeling / D. K. Barton. – London: Artech House, 2005. – 545 p.
4. Van Trees H. L. Detection, Estimation, and Modulation Theory / H. L. Van Trees. – Edition, reprint : John Wiley & Sons, 2004. – 716 p.
5. Levanon N. Radar Signals / N. Levanon, E. Mozeson. – Hoboken : John Wiley & Sons, 2004. – 403 p.
6. Melvin W. L. Principles of modern radar / W. L. Melvin, J. A. Scheer. – New York : SciTech Publishing, 2013. – 846 p.
7. Doerry A. W. Catalog of Window Taper Functions for Side lobe Control [Electronic resource] / A. W. Doerry. – Access mode: https://www.researchgate.net/publication/316281181_Catalog_of_Window_Taper_Functions_for_Sidelobe_Control.
8. Heinzel G. Spectrum and spectral density estimation by the Discrete Fourier transform (DFT), including a comprehensive list of window functions and some new flattop windows [Electronic resource] / G. Heinzel, A. Rüdiger, R. Schilling. – Access mode: https://pure.mpg.de/rest/items/item_152164_1/component/file_152163/content.
9. Galushko V. G. Performance Analysis of using tapered Windows for Side Lobe Reduction in Chirp-Pulse Compression / V. G. Galushko // Radio Physics and Radio Astronomy. – 2019. – Vol. 24(4). – P. 300–313.
10. Nettem A. V. Windows For Reduction Of ACF Side Lobes of Pseudo-NLFM Signal / A. V. Nettem, E. R. Daniel, K. Chandu // International Journal of Scientific & Technology Research. – 2019. – Vol. 8, Issue 10. – P. 2155–2161.
11. Ghavamirad R. Side Lobe Level Reduction in ACF of NLFM Waveform / R. Ghavamirad, M. A. Sebt // IET Radar, Sonar & Navigation. – 2019. – Vol. 13, Issue 1. – P. 74–80.
12. Cook C.E. A class of nonlinear FM pulse compression signals / C. E. Cook // Proceedings of the IEEE. – 1964. – Vol. 52(11). – P. 1369–1371.
13. Cook C. E. A pulse compression predistortion function for efficient side lobe reduction in a high-power radar / C. E. Cook, J. Paolillo // Proceedings of the IEEE. – 1964. – Vol. 52(4). – P. 377–389.
14. Xu Z. Nonlinear Frequency-Modulated Waveforms Modeling and Optimization for Radar Applications / Z. Xu, X. Wang, Y. Wang // Mathematics. – 2022. – Vol. 10, № 3939.
15. Fan Z. Coded excitation with Nonlinear Frequency Modulation Carrier in Ultrasound Imaging System / Z. Fan, H.-Y. Meng // IEEE Far East NDT New Technology & Application Forum (FENDT): Kunming, Yunnan province, China, – 20–22 Nov. 2020. – P. 31–35.
16. Chukka A. Peak Side Lobe Reduction analysis of NLFM and Improved NLFM Radar signal / A. Chukka, B. Krishna // AIUB Journal of Science and Engineering (AJSE). – 2022. – Vol. 21, Issue 2. – P. 125–131.
17. A Variable Chirp Rate Stepped Frequency Linear Frequency Modulation Waveform Designed to Approximate Wideband Non-Linear Radar Waveforms / [M. Saleh, S.-M. Omar, E. Grivel et al.] // Digital Signal Processing. – 2021. – Vol. 109. – № 102884.
18. Nettem A. V. Doppler Effect Analysis of NLFM Signals / A. V. Nettem, E. Rani // International Journal of Scientific & Technology Research. – 2019. – Vol. 8, Issue 11. – P. 1817–1821.
19. A Neural Network Approach for Waveform Generation and Selection with Multi-Mission Radar / [J. M. Kurdzo, Y. N. Cho John, B. L. Cheong et al.] // IEEE Radar Conference: Boston – 22–26 April 2019. – № 19043446.
20. Non-continuous piecewise nonlinear frequency modulation pulse with variable sub-pulse duration in a MIMO SAR Radar System / [Y. Zhao, M. Ritchie, X. Lu et al.] // Remote Sensing Letters. – 2020. – Vol. 11, Issue 3. – P. 283–292.
21. Staring Spotlight SAR with Nonlinear Frequency Modulation Signal and Azimuth Non-Uniform Sampling for Low Side Lobe Imaging / [W. Xu, L. Zhang, C. Fang et al.] //Sensors. – 2021. – Vol. 21, Issue 19. – № 6487.
22. A Novel Jamming Method against SAR Using Nonlinear Frequency Modulation Wave-form with Very High Side Lobes / [C. Song, Y. Wang, G. Jin et al.] // Remote Sensing. – 2022. – Vol. 14, Issue 21. – № 5370.
23. An Advanced Nonlinear Frequency Modulation Waveform for Radar Imaging With Low Side Lobe / [G. Jin, Y.-K. Deng, R. Wang et al.] // IEEE Transactions on Geoscience and Remote Sensing. – 2019. – Vol. 57, Issue 8. – P. 6155–6168.
24. Valli N. A. Modified Radar Signal Model using NLFM / N. A. Valli, D. E Rani, C. Kavitha // International Journal of Recent Technology and Engineering (IJRTE). – 2019. – Vol. 8, Issue 2S3. – P. 513–516.
25. Adithyavalli N. An Algorithm for Computing Side Lobe Values of a Designed NLFM function / N. Adithyavalli // International Journal of Advanced Trends in Computer Science and Engineering. – 2019. – Vol. 8, Issue 4. – P. 1026–1031.
26. Parwana S. Analysis of LFM and NLFM Radar Waveforms and their Performance Analysis / S. Parwana, S. Kumar // International Research Journal of Engineering and Technology (IRJET). – 2015. – Vol. 02, Issue 02. – P. 334–339.
27. Bayındır C. A Novel Nonlinear Frequency-Modulated Chirp Signal for Synthetic Aperture Radar and Sonar Imaging / C. Bayındır // Journal of Naval Science and Engineering. – 2015. – Vol 11, Issue 1. – P. 68–81.
28. Jeyanthi J. E. Study of Different Radar Waveform Generation Techniques for Automatic Air Target Recognition / J. E. Jeyanthi, A. Shenbagavalli, V.R.S. Mani // International Journal of Engineering Technology Science and Research (IJETSR). – 2017. – Vol. 4, Issue 8. – P 742–747.
29. Analysis of Non Linear Frequency Modulation (NLFM) Waveforms for Pulse Compression Radar / [M. R. Widyantara, F. Y. Suratman, S. Widodo et al.] //Journal Electronica dan Telekomunikasi (JET). – 2018. – Vol. 18, №1. – P. 27–34.
30. Valli N. A. Performance Analysis of NLFM Signals with Doppler Effect and Back-ground Noise / N. A. Valli, D. E. Rani, C. Kavitha // International Journal of Engineering and Advanced Technology (IJEAT). – 2020. – Vol. 9, Issue 3. – P. 737–742.
31. Mathematical model of a two-fragment signal with a nonlinear frequency modulation in the current period of time / [O. O. Kostyria, A. A. Hryzo, O. M. Dodukh et al.] // Visnyk NTUU KPI Seriia – Radiotekhnika Radioaparatobuduvannia. – 2023. – Vol. 92. – P. 60–67.

DOI 10.15588/1607-3274-2023-3-2

UDC 621.396.946

ENERGY EFFICIENCY RESEARCH OF LPWAN TECHNOLOGIES

Lykov Y. V. – PhD, Associate Professor, Associate Professor of the Department of Computer Radio Engineering and Technical Information Protection Systems, Kharkiv National University of Radio Electronics, Kharkiv, Ukraine.

Gorelov D. Y. – PhD, Associate Professor, Associate Professor of the Department of Computer Radio Engineering and Technical Information Protection Systems, Kharkiv National University of Radio Electronics, Kharkiv, Ukraine.

Lykova A. A. – Senior Lecturer of the Department of Computer Radio Engineering and Technical Information Protection Systems, Kharkiv National University of Radio Electronics, Kharkiv, Ukraine.

Savenko S. O. – Student of the Faculty of Information Radio Technologies and Technical Information Protection, Kharkiv National University of Radio Electronics, Kharkiv, Ukraine.

ABSTRACT

Context. The emergence of the Internet of Things (IoT) has led to the development of various low-power wide area network (LPWAN) technologies that are designed to provide transmission of small data packets over long distances with minimal energy consumption. The two most well-known LPWAN technologies are LoRaWAN and Sigfox. This study aims to compare the energy efficiency of these two technologies to determine their suitability for use in autonomous solutions.

Objective. The objective of this study is to compare the energy efficiency of LoRaWAN and Sigfox technologies for IoT devices. The comparison will help determine which technology is better for autonomous solutions when devices need to operate for extended periods of time without frequent battery replacements.

Method. In this work, taking into account the specifications of the investigated radio technologies, mathematical modeling of the time of data transmission or reception is used depending on the payload, and information on the power supply current is taken from official datasheets for the components of the investigated devices.

Results. The results of the study show that both LoRaWAN and Sigfox are energy-saving technologies, but LoRaWAN is generally more energy-efficient than Sigfox. In addition, LoRaWAN has adaptive modes and significantly more manual settings, which in some cases further reduces the energy per bit of data compared to Sigfox.

Conclusions. LoRaWAN is the best choice for autonomous solutions where energy efficiency is crucial. This study provides valuable information for designers and developers of IoT devices, allowing them to make informed decisions when choosing LPWAN technologies for their autonomous solutions.

KEYWORDS: LoRaWAN, Sigfox, LPWAN, modem, power consumption, autonomy, IoT.

ABBREVIATIONS

IoT is Internet of Things;
LPWAN is Low Power Wide Area Network;
LoRaWAN is Long Range Wide Area Network;
PA is Power Amplifier;
SF is a spreading factor.

NOMENCLATURE

N_p is a payload size;
N_m is a number of uplink messages;
t_sleep_mcu, t_sleep_sensor, t_sleep_modem is a time to sleep of MCU, Sensor, Modem accordingly;
t_meas_sensor is a time to measurement mode of Sensor;
I_mcu_sleep, I_sensor_ sleep, I_modem_sleep is a consumption current to sleep mode of MCU, Sensor, Modem accordingly;
I_mcu_meas, I_sensor_meas, I_modem_meas is a consumption current to measurement mode of MCU, Sensor, Modem accordingly;
*I_mcu_tx, I_sensor_tx, I_modem_t*x is a consumption current to transmit mode of MCU, Sensor, Modem accordingly;
I_mcu_rx, I_sensor_rx, I_modem_rx is a consumption current to receive mode of MCU, Sensor, Modem accordingly;
V_mcu, V_sensor, V_modem is a supply voltage of MCU, Sensor, Modem accordingly;
η is a coefficient that takes into account DC/DC converter efficiency (was taken equal to 1.1)
Power_bat is a power battery (Wh);
α is a battery self-discharge;
P_sum_sleep, P_sum_meas, P_sum_tx, P_sum_rx, is a summary consumption power per day in sleep mode, in measurement mode, in transmit mode, in receive mode accordingly;
P_sum_total_per_day is a total consumption power per day;
T_symbol is a LoRa symbol duration;
BW is a Banwidth;
Number_Characters_in_Pl is a number of characters in the payload;
Payload is a payload size;
IH is a implicit mode;
DE is a low data rate optimization;
CR is a encoding speed;
T_payl_SF is a payload duration;
N_day is a number of day of autonomy.

INTRODUCTION

The IoT is a fast-paced technology. This is a set of sensors that are combined into a single network with analytical and/or control systems. Every day more and more different devices are connecting to the Internet, and this number is constantly growing. When choosing radio technology, one of the main factors that consumers

DOI 10.15588/1607-3274-2023-3-3

consider is the decrease of their maintenance costs, which is mainly determined by energy-saving parameters, or rather, the duration of the device without charging (battery replacement). New types of LPWAN can solve this problem. A technology that was created for wireless data transmission over long distances and for connecting autonomous devices to the global network. Nowadays, there are several popular technologies: LoRa, SIGFOX, NB-IoT, etc. LPWAN systems are a reliable system to transmit information over long distances (2–40km) and at the same time use a minimum of energy costs.

The development of IoT technology has led to an increase in demand for solutions with low power consumption and long-range wireless communication. Among them, LoRaWAN and Sigfox have become popular options due to their ability to support large-scale IoT device networks. However, the choice between these technologies often depends on their energy efficiency, which determines how long devices can operate without battery replacement.

The objective of this comparative study is to compare the energy efficiency of LoRaWAN and Sigfox technologies for IoT. The study aims to determine which technology is better suited for autonomous solutions where devices need to operate for long periods without frequent battery replacement. The study's data will consist of energy consumption data for LoRaWAN and Sigfox technologies, which will be collected from existing literature, previous studies, and other official sources. In addition, the study will use available specifications and technical details of both technologies, such as transmission range, payload size, and transmission frequency.

The desired results of this comparative study are a quantitative comparison of the energy efficiency of LoRaWAN and Sigfox technologies. The comparison will be based on key energy consumption indicators, such as average energy consumption per transmitted data packet, energy consumption per transmitted data packet, and the amount of energy consumed per meter of transmitted data.

This study is limited to comparing the energy efficiency of LoRaWAN and Sigfox technologies for IoT. Other factors that may influence technology selection, such as deployment cost, infrastructure availability, and ease of integration with existing systems, are not considered in this study.

1 PROBLEM STATEMENT

Using the protocol specification of the two LPWAN technologies (LoRaWAN and Sigfox), the message transmission time is calculated with different payload sizes.

Considering the current consumption of individual nodes of a typical IoT device in different modes (in sleep mode: *I_mcu_sleep, I_sensor_sleep, I_modem_sleep;* in measurement mode: *I_mcu_meas, I_sensor_meas, I_modem_meas;* in transmit mode: *I_mcu_tx, I_sensor_tx, I_modem_tx;* in receive mode: *I_mcu_rx, I_sensor_ rx, I_modem_rx*) and battery capacity (*Power_bat*), the battery life of the End Node (*N_day*) is calculated.

The autonomy calculation was performed according to the algorithm shown in Figure 1.

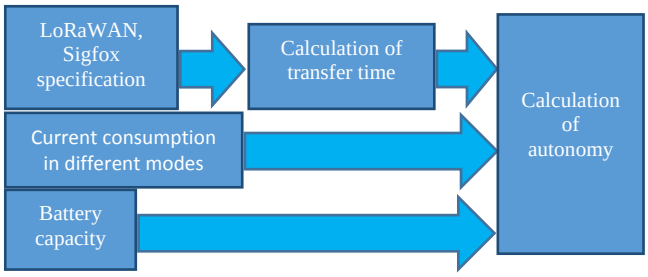

Figure 1 – Algorithm for calculating device autonomy

2 REVIEW OF THE LITERATURE

The growth of IoT technology has led to a surge of interest in low-power wide area networks (LPWANs), which provide communication between IoT devices over long distances. Two popular LPWAN technologies, LoRaWAN and Sigfox, have emerged as leading contenders due to their ability to support large-scale networks of IoT devices. However, the choice between these technologies depends on their energy efficiency, which determines the longevity of the devices and the need for frequent battery replacement.

Several previous studies have compared the energy efficiency of LoRaWAN and Sigfox technologies, but there is a need for a comprehensive comparative study that provides a quantitative comparison of the two technologies. For example, research by Atheer Al Ghamdi (2022) [1] compared the energy efficiency of Sigfox and LoRaWAN for water monitoring and leak detection systems and found that Sigfox is more energy efficient due to lower energy consumption per data packet transmitted. However, this study only considered a specific application scenario. Other scientists also dealt with the topic of energy efficiency [2–5].

An unsolved part of the overall challenge is determining which LPWAN technology is best suited for stand-alone solutions where devices need to operate for long periods of time without frequent battery replacement. This requires a comprehensive benchmarking study that takes into account various factors affecting energy consumption, such as transmission range, payload size, and transmission frequency.

The proposed benchmarking study aims to address this gap by quantitatively comparing the energy efficiency of LoRaWAN and Sigfox technologies for the IoT. The study will use the available specifications and technical details of both technologies to evaluate their energy consumption under different scenarios. The results of the study will help determine which technology is best suited for stand-alone solutions where devices need to operate for long periods of time without frequent battery replacement.

DOI 10.15588/1607-3274-2023-3-3

The creator of LoRaWAN is Semtech. Semtech Corporation is a leading supplier of high-performance analog and mixed-signal semiconductors and advanced algorithms for high-end consumer, enterprise computing, communications, and industrial end-markets. They have nearly 60 years of experience designing and manufacturing proprietary platforms differentiated by innovation, size, efficiency, performance, and reach. Original equipment manufacturers and their suppliers for automotive, broadcast equipment, data centers, passive optical networks, industrial, IoT, LCD TVs, smartphones, tablets, wearables, and wireless infrastructure applications [6] use their balanced portfolio of semiconductor products.

The LoRaWAN network consists of the following elements: end device, gateways, network server, and application server. The end device is designed for the implementation of control or measuring functions. It includes a set of necessary sensors and control elements. A gateway is a device that receives data from end devices using a radio channel and transmits them to a transit network. A network server is created to control the network: setting a schedule, adapting speed, storing, and processing received data. The application server can remotely control the operation of end devices and collect the necessary data from them [7].

LoRa has three classes of subscriber devices:

– Class A: after transmitting something on the air, the device short time waits for a response from the base station, after which it turns off the receiver until the next communication session.

– Class B: the device turns on the receiver according to a predetermined schedule. The base station knows this schedule and can transmit data to the device according to it.

– Class C: the receiver is always on; the base station can transmit data at any time [8].

Table 1 – Specifications of LORAWAN [7]

Parametr	Europe
Frequency range, MHz	863 – 870
Maximum number of channels	35
Spectrum width of radio signal UL, kHz	125/250
DL channel radio spectrum, kHz	125
Modulation	LORA, GFSK, MSK
Transmit power UL, dBm	2–14; 20 (option)
Transmit power UL, mW	1–25; 100 (option)
Transmit power DL, dBm	14
SF	7–12

The most popular LoRa Modem is the Semtech SX1276. Consider the Specifications of Semtech SX1276 [9]:

– 168dB maximum link budget;
– +20dBm – 100 mW constant RF output vs. V supply;
– +14dBm high efficiency PA;
– Programmable bit rate up to 300kbps;
– High sensitivity: down to –148dBm;
– Bullet-proof front end: IIP3 = –11dBm;
– Excellent blocking immunity;
– Low RX current of 9.9mA, 200nA register retention;
– Fully integrated synthesizer with a resolution of 61Hz;
– FSK, GFSK, MSK, GMSK, LoRa and OOK modulation;
– Built-in bit synchronizer for clock recovery;
– Preamble detection;
– 127dB Dynamic Range RSSI;
– Automatic RF Sense and CAD with ultra-fast AFC;
– Packet engine up to 256 bytes with CRC;
– Built-in temperature sensor and low battery indicator.

Physical Layer Frame: At PHY layer, a LoRa frame starts with a preamble. Apart from the synchronization function, the preamble defines the packet modulation scheme, being modulated with the same SF as the rest of the packet. Typically, the preamble duration is 12.25 Ts. The preamble is followed by a PHY Header and a Header CRC that together are 20-bits long and are encoded with the most reliable code rate of, while the rest of the frame is encoded with the code rate specified in the PHY Header. The PHY header also contains such information as payload length and whether the Payload 16-bit CRC is present in the frame. Specifically, in a LoRa network, only uplink frames contain payload CRC. PHY payload contains MAC Frame.

MAC Layer Frame: The packet processed in the MAC layer consists of a MAC Header, a MAC Payload, and a Message Integrity Code (MIC). MAC header defines protocol version and message type, i.e., whether it is a data or a management frame, whether it is transmitted in uplink or downlink, whether it shall be acknowledged. MAC Header can also notify that this is a vendor specific message. In a join procedure for end node activation, the MAC Payload can be replaced by join request or join accept messages. The entire MAC Header and MAC Payload portion is used to compute the MIC value with a network session key (Nwk_SKey). The MIC value is used to prevent the forgery of messages and authenticate the end node (Fig. 1).

Application Layer Packet: The MAC Payload handled by the Application layer consists of a Frame Header, a Frame Port, and a Frame Payload. The Frame Port value is determined depending on the application type. The Frame Payload value is encrypted with an application session key (App_SKey). This encryption is basing on the AES 128 algorithm.

Table 2 – Power consumption specification [9]

Description	Conditions	Typ	Max	Unit
Supply current in Sleep mode		0.2	1	uA
Supply current in Receive mode	LnaBoost Off, band1 LnaBoost On, band1 Bands 2&3	10.8 11.5 12.0	–	mA
Supply current in Transmit mode	RFOP = +13 dBm, on RFO_LF/HF pin	29	–	mA

DOI 10.15588/1607-3274-2023-3-3

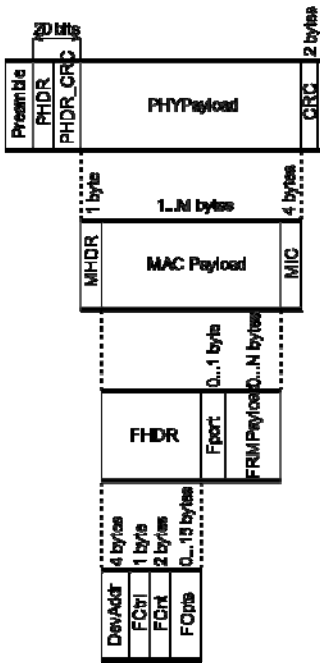

Figure 2 – LoRa Frame Format

Frame Header contains the following information:

– Device address which contains two parts. The first 8 bits identify the network, other bits are assigned dynamically during joining the network and identify the device in a network.

– Frame Control 1 byte for network control information, such as whether to use the data rate specified by the gateway for uplink transmission, whether this message acknowledges the reception of the previous message, whether the gateway has more data for the mote.

– Frame counter for sequence numbering.

Frame options for commands used to change data rate, transmission power and connection validation etc [10].

Now let's move on to Sigfox technology.

Sigfox is a French global network operator founded in 2010 that builds wireless networks to connect low-power objects such as electricity meters and smartwatches. Founders built a global network dedicated to the Internet of Things based on low power, long range and small data that offers an end-to-end connectivity service. From the inception, Sigfox powers a sustainable and connected world, pioneering the next Internet revolution [11].

The network is based on one-hop star topology and requires a mobile operator to carry the generated traffic [12]. The signal can also be used to easily cover large areas and to reach underground objects. The existing standard for Sigfox communications supports up to 140 uplink messages a day, each of which can carry a payload of 12 octets at a data rate of up to 100 bits per second.

Sigfox defines an uplink classification for each radio configuration, which applies to every device and is assessed when passing the Sigfox Ready certification. They indicate the RF radiated performance of a device, which can have a significant impact on the message success rate. They are based on EIRP (effective isotropic radiated power) intervals. Simply put, a U0 device enjoys a much better message reception than a non-U0 device. This means better user feedback and fewer support requests for your team. With a good antenna design, you can lower the device's radiated power on purpose from U0 to U1 or even U2, thus saving energy. These classes are ranked from strongest to weakest: U0, U1, U2, and U3 [13].

Each packet sent can have anywhere between 0–12 bytes of payload data, with a fixed frame of about 12 bytes that contains preamble, device id, and other metadata. In total, each packet sent has between 12–24 bytes, with some extra bits used for authentication parameters [13].

Physical layer. This synthesizes and modules signals using DBPSK in the uplink direction and GFSK in the downlink direction [14].

Table 3 – Structure of Physical Layer

Parametr	Uplink	Downlink
Payload Limit (bytes)	12	8
Throughput (bps)	100	600
Maximum Messages per Day	140	4

MAC layer This adds fields for device identification/authentication (HMAC) and error correcting code (CRC). The Sigfox MAC does not provide any signaling. This implies that devices are not synchronized with the network [14].

Frame Layer: Generates the radio frame from application data and also systematically attaches a sequence number to the frame [14] Sigfox messages can carry a payload (your own data) of 12 bytes. That's maximum, but the payload is flexible: you can send any data size between 1 and 12 bytes. You can even send a payload of 0 bytes, in case you just need a ping message [15].

One of the most popular modems for Sigfox is AX-SIP-SFEU-1-01-TX30 are ultra−low power, ultra−miniature System−in−Package solutions for a node on the Sigfox network with both up and downlink functionality. Specifications of AX-SIP-SFEU-1-01-TX30:

– Maximum output power 13 dBm;
– Power level programmable in 1 dBm steps;
– Supply range 2.1 V − 3.6 V;
– Deep Sleep mode current: 180 nA;
– Sleep mode current: 1.2 mA;
– Standby mode current: 0.55 mA;
– Continuous radio RX − mode at 869.525 MHz:
– 14 mA
– Continuous radio TX − mode at 868.130 MHz:
– 45 mA @ nominal transmitter power (13 dBm).

Receiver

– Carrier frequency of the transmitter 869.525 MHz;
– Data − rate 600 bps FSK;
– Sensitivity −125 dBm @ 600 bps, 869.525 MHz, GFSK 0 dBm maximum input power.

Transmitter

DOI 10.15588/1607-3274-2023-3-3

– Carrier frequency of the transmitter 868.13 MHz;

– Data − rate 100 bps PSK [18].

In effect, the payload bytes have to fit within a certain transmission length, predefined by the Sigfox protocol. The reason for this flexibility is to optimize transmission time and hence save battery consumption at the device level.

Downlink messages have a fixed length too: the payload must be 8 bytes long exactly. Hence, if less information bits are to be transmitted, padding is necessary [13].

Uplink frame construction shows Figure 2.

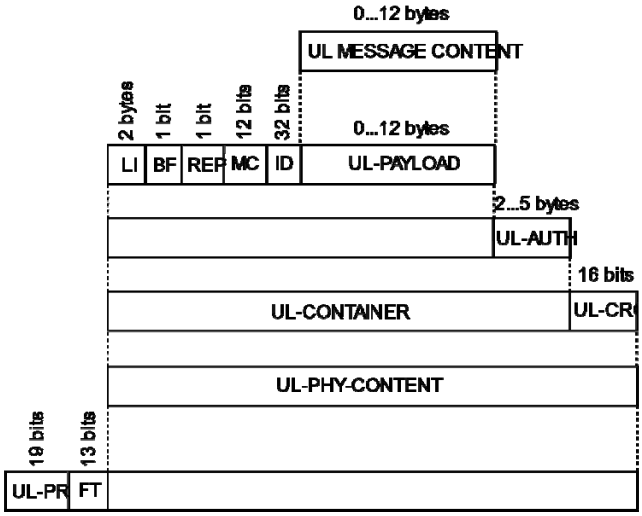

Figure 3 – Sigfox Frame Format

This section deals with formats and functions in uplink, from applicative/control level down to physical level.

Uplink message content The content of the uplink message may be applicative data or control data. The format of an applicative message content is freely defined by the application. LI values and UL-AUTH size in relation with other message parameters (Table 4).

Length Indicator (LI) It is a 2-bit field. EP shall set LI.

Repeated Flag (REP) It is a 1-bit field. EP shall set it to 0x0.

Message Counter (MC) It is a 12-bit field taking values between 0 and (MCmax-1).

Identifier (ID) It is a 32-bit field. EP shall load its EP identifier bytes in reverse order into the ID field.

Uplink Authentication (UL-AUTH) It is a variable length field.

Uplink error detection field (UL-CRC) It is a 16-bit field.

Uplink frame type (FT) It is a 13-bit field.

Uplink preamble (UL-Pr) It is a 19-bit field.

The uplink only procedure (i.e. U-procedure) is initiated by an end-point wishing to send a UL message to the SNW, with no onward downlink message. The end-point chooses the U-procedure on a per message basis.

The content of downlink message is a fixed-length field. It carries applicative data prepared by user's distant application server in response to an uplink message. Format of the DL-PAYLOAD field is user dependent [7].

Table 4 – Uplink Message Component Size

UL message content (bytes)	UL message content	LI value (MSB, LSB)	UL-AUTH size (in bytes)	ULCONTAINER size (in bytes)
empty	empty	00	2	8
0b0	empty	10	2	8
0b1	empty	11	2	8
1	message content	00	2	9
2	message content	10	4	12
3	message content	01	3	12
4	message content	00	2	12
5	message content	11	5	16
6	message content	10	4	16
7	message content	01	3	16
8	message content	00	2	16
9	message content	11	5	20
10	message content	10	4	20
11	message content	01	3	20
12	message content	00	2	20

Thus, the proposed benchmarking study builds on previous studies and the existing specification, providing a comprehensive comparison of the energy efficiency of LoRaWAN and Sigfox technologies for IoT. The research will contribute to the development of LPWAN technology by providing insight into the factors affecting power consumption.

3 MATERIALS AND METHODS

To calculate the battery life, two components are needed – the energy source and the consumer. The source was Li-ion battery (3.7V, 2000mA / h, 19% self-discharge per year). As an energy consumer, a typical solution (use case) was taken consisting of a BME280 sensor (Bosch), an MCU STM32L073, and an SX1276 modem (for LoRa) or AX-SIP-SFEU (for Sigfox).

Operation of components in different modes shown in Figure 4.

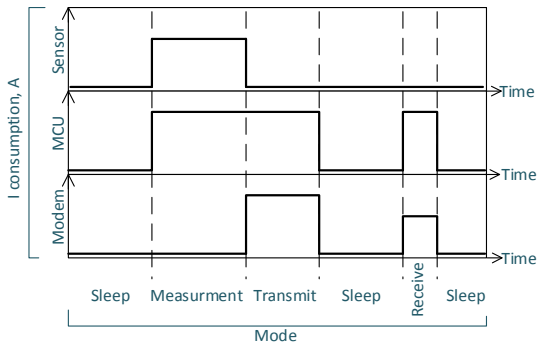

Figure 4 – Operation of devices in different modes

DOI 10.15588/1607-3274-2023-3-3

In the work, the message duration was calculated depending on the payload size. Since the maximum payload size in Sigfox is 12 bytes, then for LoRaWAN this value was taken as the maximum (although according to the protocol it can be 51–222 byte [16].

For our calculations, we will take SF 12 for LoRaWAN technology, since it is the least energy efficient but has the maximum transmission range. In order to put two different technologies (LoRaWAN and Sigfox) in the most identical conditions, as far as possible. SF is an integer, in the standard it is provided from 12 to 7. The higher the SF, the better the noise immunity of the line, but the lower the speed and the longer the transmission takes on the air.

For subsequent studies, it is necessary to calculate the duration of the preamble. First, let's find:

$$T\_symbol = \frac{2^{SF}}{BW}, \quad (1)$$

$$T\_preamble = (4.25 + N\_preamble) \times T\_symbol. \quad (2)$$

AirTime represents the duration required to transmit a message from an end device to a gateway and depends on SF, packet size, coding rate, and other parameters.

$$Number\_Characters\_in\_Pl = 8 + \max[ceil \times \left[\frac{8 \times (Payload - 4) - 4SF + 28 + 16CRC - 20(1 - IH)}{4(SF - DE)}\right] \times (CR), 0]. \quad (3)$$

Next, we calculate the duration of the payload:

$$T\_payl\_SF = Number\_Characters\_in\_Pl \times T\_symbol\_SF. \quad (4)$$

$$AirTime = T\_preamble \times T\_payl\_SF. \quad (5)$$

The calculation of consumption current was carried out for each mode individually Sleep, Measurement, Transmit (Tx), Receive (Rx).

Table 5 – Consumption Current

Mode\ Component	MCU	Sensor	Modem LoRa	Modem Sigfox
Sleep	130	0.1	0.2	0.18
Measurement	230	1.757	0.2	0.18
Transmit	230	0.1	29	45
Receive	230	0.1	10.8	14

End node battery life was calculated using the following formulas:

$$P\_sum\_sleep(N\_p, N\_m) = \frac{I\_mcu\_sleep \times t\_sleep\_mcu(N\_P, N\_m) \times V\_mcu \times \eta \ldots + I\_sensor\_sleep \times t\_sleep\_sensor(N\_m) \times V\_sensor \times \eta \ldots + I\_modem\_sleep \times t\_sleep\_modem(N\_P, N\_m) \times V\_modem}{24 \times 60 \times 60}. \quad (6)$$

$$P\_sum\_meas(N\_p, N\_m) = \frac{N\_m \times [I\_mcu\_sleep \times t\_sleep\_mcu(N\_P, N\_m) \times V\_mcu \times \eta \ldots + I\_sensor\_sleep \times t\_sleep\_sensor(N\_m) \times V\_sensor \times \eta. + I\_modem\_sleep \times t\_sleep\_modem(N\_P, N\_m) \times V\_modem]}{24 \times 60 \times 60}. \quad (7)$$

$$P\_sum\_tx(N\_p, N\_m) = \frac{N\_m \times [I\_mcu\_tx \times t\_tx(N\_p) \times (V\_mcu \times \eta) \ldots + I\_sensor\_tx \times t\_sleep\_sensor(N\_m) \times (V\_sensor \times \eta) + I\_modem\_txt \times t\_tx(N\_p) \times V\_modem]}{24 \times 60 \times 60}. \quad (8)$$

$$P\_sum\_rx(N\_p, N\_m) = \frac{N\_m \times [I\_(mcu\_rx) \times t\_rx \times (V\_mcu \times \eta) \ldots + I\_sensor\_rx \times t\_sleep\_sensor(N\_m) \times (V\_sensor \times \eta) + I\_modem\_rx \times t\_rx \times V\_modem]}{24 \times 60 \times 60}. \quad (9)$$

$$P\_sum\_total\_per\_day(N\_p, N\_m) = P\_sum\_sleep(N\_p, N\_m) + P\_sum\_meas(N\_p, N\_m) + P\_sum\_tx(N\_p, N\_m) + P\_sum\_rx(N\_p, N\_m). \quad (10)$$

$$N\_day(N\_p, N\_m) = \frac{\frac{Power\_bat}{24} \times (1 - \frac{\alpha}{100})}{P\_sum\_total\_per\_day(N\_p, N\_m)}. \quad (11)$$

4 RESULTS

Figure 6 shows the time on air which shows the number of bytes transmitted per second for each SF.

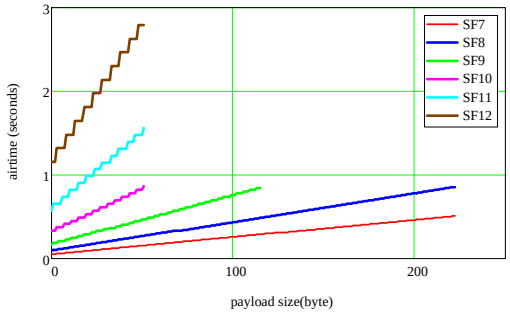

Figure 5 – Airtime for each SF

The results of calculating the power consumption for different modes are given in Table 6.

The paper shows the dependence of the number of days of autonomy on the number of messages per day (Fig. 6).

Table 6 – Power Consumption Per Day

Parametr	LoRaWAN		Sigfox	
	1 mess/day	140 mess/day	1 mess/day	140 mess/day
P_sum_sleep, W	$1.725 \cdot 10^{-4}$	$1.721 \cdot 10^{-4}$	$1.725 \cdot 10^{-4}$	$1.72 \cdot 10^{-4}$
P_sum_meas, W	$2.53 \cdot 10^{-11}$	$3.541 \cdot 10^{-9}$	$2.529 \cdot 10^{-11}$	$3.54 \cdot 10^{-9}$
P_sum_tx, W	$2.216 \cdot 10^{-6}$	$3.103 \cdot 10^{-4}$	$4.214 \cdot 10^{-6}$	$5.9 \cdot 10^{-4}$
P_sum_rx, W	0 (downlink only mode)			
P_sum_total_per_day, W	$1.748 \cdot 10^{-4}$	$4.824 \cdot 10^{-4}$	$1.767 \cdot 10^{-4}$	$7.62 \cdot 10^{-4}$
Self-discharge per day, W	$1.644 \cdot 10^{-4}$			

DOI 10.15588/1607-3274-2023-3-3

In Fig. 6 shows that for any payload from 1 bit to 12 bytes, LoRaWAN radio technology is more energy efficient for any number of messages per day. At the same time, the minimum difference of 5 days of autonomy between the considered protocols is observed with 1 single-bit message per day. And the maximum difference was 234 days for 140 12-byte messages per day.

Figure 7 displays two elements: total power in Sleep mode (taking into account battery self-discharge) and total power in transmission mode (for minimum and maximum payload). For LoRaWAN technology the number of messages per day at which these two components are equal is in the region of 85 +/–10 messages per day.

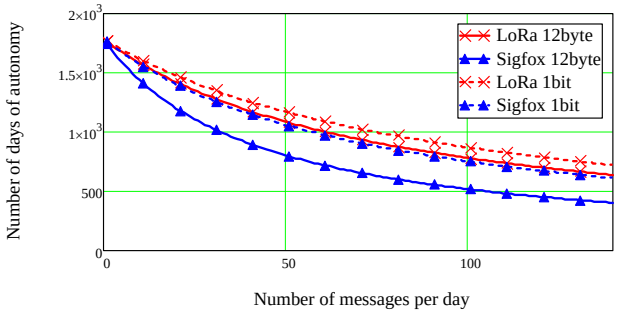

Figure 6 – Dependence of number of days of autonomy on the number of Uplink messages per day

Therefore, to increase the autonomy of the device with a small number of messages less frequently (75 messages per day), it is necessary to optimize power consumption in Sleep mode, in particular, the MCU current, which is two to three orders of magnitude higher than other nodes in this mode. Consumption in Sleep mode is practically independent of the number of messages per day (within 12 Bytes).

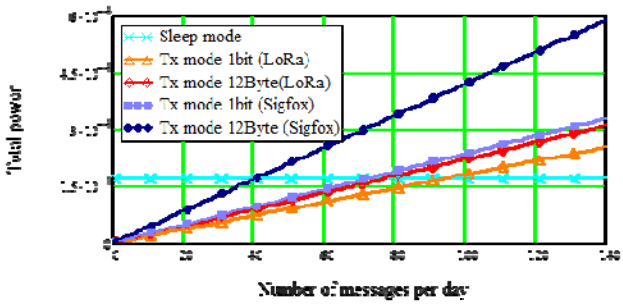

Figure 7 – Endnode power consumption in Sleep mode and in Tx mode for LoRaWAN and Sigfox

For Sigfox technology, the number of messages per day, when these two components are equal, is in the range of about 58 messages per day (+/– 16 messages).

Moreover, as can be seen from Table 6, the self-discharge of the battery is proportional to the consumption in sleep mode. So, one of the ways to increase autonomy is to use a battery with a low self-discharge and ensure the optimal operating mode (temperature, humidity).

In Figure 8 shows the results of the dependence of the number of days of autonomy on the size of the payload (from 1 bit to 12 bytes) at 1 and 140 messages per.

From Figure 8, it can be seen that for LoRaWAN, in the case of sending 1 message per day, when the payload increases, the autonomy time almost does not change (it decreases by only 4 days). When transmitting 140 messages with an increased payload, the battery life will decrease by about 85 days (with payload changes ranging from 1 bit to 12 bytes). Similarly, for Sigfox, which sends 1 message per day, the battery life decreases by 18.5 days as the payload increases. If you transmit 140 messages, it will decrease by about 209 days. In general, it can be seen that LoRaWAN maintains autonomy longer than Sigfox.

When sending 1 message, the autonomy of LoRaWAN and Sigfox is almost the same (in Sigfox, only 5 days less autonomy), but with increasing payload, the autonomy of Sigfox is significantly reduced.

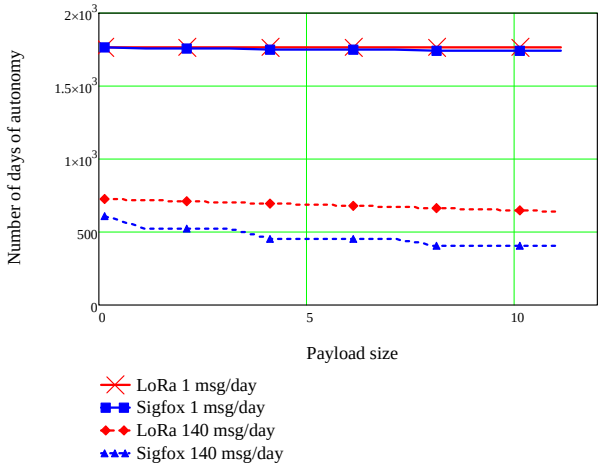

Figure 8 – Dependence of a number of days of autonomy on ther number of payloads at 1 and 140 messages per day

It should be said that previous results for Sigfox were obtained for transmission of each message without repetitions (Nrep = 1). In order to increase the reliability of message delivery from the end node to the base station, the Sigfox standard provides a mode for repeating the same message three times. In this case, the autonomy of the device will be even lower (Figure 9).

As can be seen from Figure 9, the reduction in the number of autonomous days can reach up to 60% in the case of sending 140 12-byte messages per day, and is not significant when the number of messages is less than 5 per day.

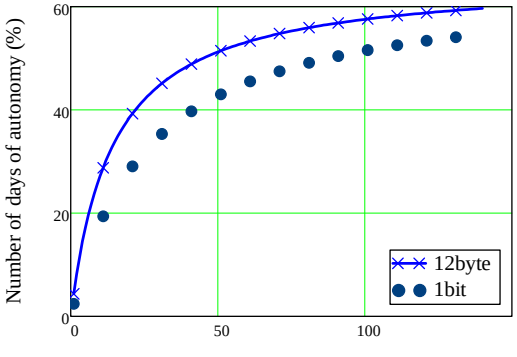

Figure 9 – Downtime reduction for Sigfox device when using Nrep = 3 instead of Nrep = 1 from number of messages per day for different payload sizes

DOI 10.15588/1607-3274-2023-3-3

5 DISCUSSION

The results of this comparative study show that LoRaWAN technology outperforms Sigfox in terms of energy efficiency for IoT. The comparison was based on the energy consumption of each technology during the transmission and reception of data packets.

However, it should be noted that the energy efficiency of LPWAN technologies can be influenced by various factors, such as the number of devices in the network, the distance between devices and gateways, the type of data transmitted, and environmental conditions. Therefore, the results of this study should be interpreted cautiously, and their generalization should be limited to specific conditions and scenarios in which the tests were conducted.

The practical significance of the obtained results is essential, especially for IoT, where there is a requirement for end devices to work for a long time without frequent battery replacement. Our results show that LoRaWAN is the best choice for such applications, as it can extend the battery life of devices and reduce network maintenance costs. In addition, the feasibility of further research into energy-efficient LPWAN technologies is justified by the growing demand for IoT solutions in various industries, including smart cities, healthcare, and logistics.

Finally, this comparative study demonstrated the energy efficiency of LoRaWAN and Sigfox technologies for IoT applications. Although LoRaWAN was found to be more energy efficient than Sigfox, the results should be interpreted in the context of specific settings and scenarios in which the tests were conducted. The study provides valuable information for researchers, practitioners, and decision-makers in choosing the most appropriate LPWAN technology for their IoT applications.

CONCLUSIONS

This benchmarking study aimed to compare the energy efficiency of LoRaWAN and Sigfox IoT technologies to determine which technology is best suited for autonomous solutions requiring long battery life. The study showed that the main sources of energy consumption were sleep mode and transmission mode. In addition, losses from self-discharge of lithium-ion batteries were equal to energy consumption in these modes. The advantage of sending one large message over multiple small messages of the same overall size has also been highlighted in terms of energy efficiency.

The results showed that LoRaWAN outperforms Sigfox in terms of energy efficiency. In particular, the size of any payload of LoRaWAN radio technology from 1 bit to 12 bytes was more energy efficient. Moreover, LoRaWAN provided additional energy optimization mechanisms such as data rate variation, including adaptive data rate, class B and C end node capability, and a much larger maximum payload size. The obtained simulation results agree with the experimental results published in [19].

It should be noted that, in addition to energy efficiency, properties such as immunity to interference, maximum network bandwidth, and price policy of communication operators are also important for consumers.

Thus, the study found that LoRaWAN is the best LPWAN technology for IoT applications requiring long battery life. The results of the study can be used in the selection of LPWAN technologies for such applications. The scientific novelty of the results lies in the comprehensive and comparative analysis of the energy efficiency of two LPWAN technologies for autonomous IoT solutions.

The practical significance of the results lies in the possibility of saving costs and increasing the productivity of IoT devices using LPWAN technologies. The results can be used to select and optimize LPWAN technologies for autonomous IoT applications.

Further research can be conducted to examine the trade-offs between energy efficiency, network bandwidth, and immunity to interference in LPWAN technologies. Additionally, future research could explore the integration of multiple LPWAN technologies to improve performance in complex IoT applications.

ACKNOWLEDGEMENTS

The authors express their gratitude to the EKTOS-Ukraine for consultations on the experience in the development of IoT devices and for the access to equipment for experimental research.

REFERENCES

1. Atheer M. Alghamdi. LoRaWAN Performance Analysis for a Water Monitoring and Leakage Detection System in a Housing Complex. Removed from: https://www.mdpi.com/1424-8220/22/19/7188
2. Husam R., Tibor C., Taoufik B. Evaluation of Energy Consumption of LPWAN Technologies. Removed from: https://www.researchgate.net/publication/350641637_Evaluation_of_Energy_Consumption_of_LPWAN_Technologies
3. Ritesh kumar S., Priyesh P. Energy Consumption Analysis of LPWAN Technologies and Lifetime Estimation for IoT Application. Removed from: https://www.researchgate.net/publication/343871606_Energy_Consumption_Analysis_of_LPWAN_Technologies_and_Lifetime_Estimation_for_IoT_Application
4. Lam-Thanh T., Abbas B. Energy Efficiency Analysis of LoRa Networks. Removed from: https://hal.science/hal-02977258/document
5. Rúni E., Energy Consumption of Low Power Wide Area Network Node Devices in the Industrial, *Scientific and Medical Band.* Removed from: https://www.diva-portal.org/smash/get/diva2:1351642/FULLTEXT01.pdf
6. Company Semtech Corporation, Removed from: https://www.semtech.com/company.
7. Обзор технологии LoRa. Removed from: https://itechinfo.ru/content/%D0%BE%D0%B1%D0%B7%D0%BE%D1%80-%D1%82%D0%B5%D1%85%D0%BD%D0%BE%D0%BB%D0%BE%D0%B3%D0%B8%D0%B8-lora.

DOI 10.15588/1607-3274-2023-3-3

8. Связь в интернете вещей: LoRa против UNB Removed from: https://habr.com/ru/company/unwds/blog/372645/.
9. Semtech. LoRa. SX1276/77/78/79. Removed from: https://semtech.my.salesforce.com/sfc/p/#E0000000JelG/a/2R0000001OKs/Bs97dmPXeatnbdoJNVMIDaKDlQz8q1N_gxDcgqi7g2o [Accessed: 2020, june 17].
10. LoRa-(Long Range) Network and Protocol Architecture with Its Frame Structure. Removed from: http://www.techplayon.com/lora-long-range-network-architecture-protocol-architecture-and-frame-formats
11. SIGFOX. Removed from: https://www.sigidwiki.com/wiki/SIGFOX
12. ОБЗОР И СРАВНИТЕЛЬНЫЙ АНАЛИЗ ТЕХНОЛОГИЙ LPWAN СЕТЕЙ. Removed from: https://www.sut.ru/doci/nauka/review/20164/33-48.pdf
13. Sigfox connected objects: Radio specifications. Removed from: https://storage.sbg.cloud.ovh.net/v1/AUTH_669d7dfced0b44518cb186841d7cbd75/prod_medias/b2be6c79-4841-4811-b9ee-61060512ecf8.pdf
14. Internet of Things for Architects. Removed from: https://cutt.ly/cuFDW2B
15. Sigfox Platform Information. Removed from: https://build.sigfox.com/payload
16. LoRa best practices Packet Optimisation Parametrs Removed from: https://lora-developers.semtech.com/library/tech-papers-and-guides/the-book/packet-size-considerations/
17. ST Microelectronics. Removed from: https://midatronics.com/development-boards/breakout-sharky-i/
18. AX-SIP-SFEU. Removed from: https://www.onsemi.com/pub/Collateral/AX-SIP-SFEU-D.PDF
19. Singh R. K., Puluckul P. P., Berkvens R., Weyn M. Energy Consumption Analysis of LPWAN Technologies and Lifetime Estimation for IoT Application Sensors 2020 Removed from: https://doi.org/10.3390/s20174794

Received 23.07.2023.
Accepted 04.09.2023.

УДК 621.396.946

ДОСЛІДЖЕННЯ ЕНЕРГОЕФЕКТИВНОСІ ТЕХНОЛОГІЙ LPWAN

Ликов Ю. В. – канд. техн. наук, доцент, доцент кафедри комп'ютерної радіотехніки та систем технічного захисту інформації Харківського національного університету радіоелектроніки, м. Харків, Україна.

Горелов Д. Ю. – канд. техн. наук, доцент, доцент кафедри комп'ютерної радіотехніки та систем технічного захисту інформації Харківського національного університету радіоелектроніки, м. Харків, Україна.

Ликова Г. О. – старший викладач кафедри комп'ютерної радіотехніки та систем технічного захисту інформації Харківського національного університету радіоелектроніки, м. Харків, Україна.

Савенко С. О. – студент факультету інформаційних радіотехнологій та технічного захисту інформації Харківського національного університету радіоелектроніки, м. Харків, Україна.

АНОТАЦІЯ

Актуальність. Поява Інтернету речей (IoT) спричинила розробку різних технологій глобальної мережі з низьким енергоспоживанням (LPWAN), які призначені для забезпечення передачі невеликих пакетів даних на великі відстані при мінімальному споживанні енергії. Двома найбільш відомими технологіями LPWAN є LoRaWAN та Sigfox. Це дослідження спрямоване на порівняння енергоефективності цих двох технологій, щоб визначити їхню придатність для використання в автономних рішеннях.

Мета. Метою цього дослідження є порівняння енергоефективності технологій LoRaWAN та Sigfox для пристроїв IoT. Порівняння допоможе визначити, яка технологія краща для автономних рішень, коли пристрої повинні працювати протягом тривалого часу без частої заміни батареї.

Метод. У роботі враховуючи специфікації досліджуємих радіотехнологій використовується математичне моделювання часу передачі або прийому даних в залежності від корисного навантаження, інформацію про струми споживання взято з офіційних специфікацій на компоненти досліджуваних пристроїв.

Результати. Результати дослідження показують, що і LoRaWAN, і Sigfox є енергозберігаючими технологіями, але LoRaWAN загалом енергоефективний, ніж Sigfox. Крім того, LoRaWAN має адаптивні режими та значно більше ручних налаштувань, що в деяких випадках ще додатково зменшить енергію на біт даних в порівняні з Sigfox.

Висновки. LoRaWAN є найкращим вибором для автономних рішень, де енергоефективність має вирішальне значення. Це дослідження дає цінну інформацію проектувальникам і розробникам пристроїв IoT, дозволяючи їм приймати обгрунтовані рішення при виборі технологій LPWAN для своїх автономних рішень.

КЛЮЧОВІ СЛОВА: LoRaWAN, Sigfox, LPWAN, модем, енергоспоживання, автономність, IoT.

ЛІТЕРАТУРА

1. Atheer M. Alghamdi. LoRaWAN Performance Analysis for a Water Monitoring and Leakage Detection System in a Housing Complex / M. Atheer. – Removed from: https://www.mdpi.com/1424-8220/22/19/7188
2. Husam R. Evaluation of Energy Consumption of LPWAN Technologies / R. Husam, C. Tibor, B. Taoufik. – Removed from: https://www.researchgate.net/publication/350641637_Evaluation_of_Energy_Consumption_of_LPWAN_Technologies
3. Ritesh kumar S. Energy Consumption Analysis of LPWAN Technologies and Lifetime Estimation for IoT Application / S. Ritesh kumar, P. Priyesh. – Removed from: https://www.researchgate.net/publication/343871606_Energy_Consumption_Analysis_of_LPWAN_Technologies_and_Lifetime_Estimation_for_IoT_Application

DOI 10.15588/1607-3274-2023-3-3

4. Lam-Thanh T., Abbas B. Energy Efficiency Analysis of LoRa Networks / T. Lam-Thanh, B. Abbas. – Removed from: https://hal.science/hal-02977258/document
5. Rúni E., Energy Consumption of Low Power Wide Area Network Node Devices in the Industrial / E. Rúni // Scientific and Medical Band. Removed from: https://www.diva-portal.org/smash/get/diva2:1351642/FULLTEXT01.pdf
6. Company Semtech Corporation, Removed from: https://www.semtech.com/company.
7. Обзор технологии LoRa. Removed from: https://itechinfo.ru/content/%D0%BE%D0%B1%D0%B7%D0%BE%D1%80-%D1%82%D0%B5%D1%85%D0%BD%D0%BE%D0%BB%D0%BE%D0%B3%D0%B8%D0%B8-lora.
8. Связь в интернете вещей: LoRa против UNB Removed from: https://habr.com/ru/company/unwds/blog/372645/.
9. Semtech. LoRa. SX1276/77/78/79. Removed from: https://semtech.my.salesforce.com/sfc/p/#E0000000JelG/a/2R0000001OKs/Bs97dmPXeatnbdoJNVMIDaKDlQz8q1N_gxDcgqi7g2o.
10. LoRa-(Long Range) Network and Protocol Architecture with Its Frame Structure. Removed from: http://www.techplayon.com/lora-long-range-network-architecture-protocol-architecture-and-frame-formats
11. SIGFOX. Removed from: https://www.sigidwiki.com/wiki/SIGFOX
12. ОБЗОР И СРАВНИТЕЛЬНЫЙ АНАЛИЗ ТЕХНОЛОГИЙ LPWAN СЕТЕЙ. Removed from: https://www.sut.ru/doci/nauka/review/20164/33-48.pdf
13. Sigfox connected objects: Radio specifications. Removed from: https://storage.sbg.cloud.ovh.net/v1/AUTH_669d7dfced0b44518cb186841d7cbd75/prod_medias/b2be6c79-4841-4811-b9ee-61060512ecf8.pdf
14. Internet of Things for Architects. Removed from: https://cutt.ly/cuFDW2B
15. Sigfox Platform Information. Removed from: https://build.sigfox.com/payload
16. LoRa best practices Packet Optimisation Parametrs Removed from: https://lora-developers.semtech.com/library/tech-papers-and-guides/the-book/packet-size-considerations/
17. ST Microelectronics. Removed from: https://midatronics.com/development-boards/breakout-sharky-i/
18. AX-SIP-SFEU. Removed from: https://www.onsemi.com/pub/Collateral/AX-SIP-SFEU-D.PDF
19. Energy Consumption Analysis of LPWAN Technologies and Lifetime Estimation for IoT Application Sensors / [R. K. Singh, P. P. Puluckul, R. Berkvens, M. Weyn], 2020 Removed from: https://doi.org/10.3390/s20174794

DOI 10.15588/1607-3274-2023-3-3

УДК 621.391.17

МЕТОД СИНТЕЗУ РАДІОТЕХНІЧНИХ СЛІДКУВАЛЬНИХ СИСТЕМ ВИСОКОЇ ТОЧНОСТІ З РОЗДІЛЕНИМИ ПРОЦЕДУРАМИ УПРАВЛІННЯ І ФІЛЬТРАЦІЇ

Ревенко В. Б. – канд. техн. наук, доцент, доцент кафедри електротехніки і електроніки Житомирського військового інституту імені С. П. Корольова, Житомир, Україна.

Каращук Н. М. – канд. техн. наук, доцент, старший викладач кафедри телекомунікацій та радіотехніки Житомирського військового інституту імені С. П. Корольова, Житомир, Україна.

АНОТАЦІЯ

Актуальність. У комбінованих системах автоматичного управління (САУ) з принципом керування за збуренням виникають труднощі контролю збурень у деяких об’єктах радіотехнічних систем та дещо менша точність. Це особливо помітно, коли на об’єкт діє кілька рівноцінних збурень, врахування яких потребує підвищення складності і зменшення надійності САУ. А нехтування різко знижує точність системи. Тому є необхідність у розробці методу синтезу радіотехнічних слідкувальних систем, який усуває вказані недоліки.

Мета. Розробка методу синтезу автоматичних слідкувальних систем високої точності із розділеними процедурами управління та фільтрації в умовах, коли величина, яка управляється, не вимірюється (вхідний корисний вплив), при наявності збурень для побудови слідкувальних систем (особливо радіотехнічних, де вхідна корисна дія не вимірюється, а тому комбіноване управління не можливе).

Метод. Для досягнення мети дослідження використовувалися методи теорії автоматичного управління.

Результати. Показано, що в слідкувальних САУ, які працюють за відхиленням існує протиріччя між умовами роздільного синтезу фільтра оцінювання (зглажування) і фільтра (регулятора) управління.

Запропоновано рішення задачі управління і оцінювання в рамках двоконтурних систем, еквівалентних комбінованим системам. Другий контур можна представити добутком зворотної передаточної функції за помилкою першого контуру на передаточну функцію регулятора, охопленого позитивним зворотнім зв’язком, а також на зворотну передаточну функцію об’єкту управління без інтегруючих ланок. Запропоновано замість розімкнутого регулятора застосувати фільтр оцінювання з передаточною функцією замкнутого фільтра для отримання оцінки.

Характеристичний поліном двоконтурної системи автоматичного управління виключає вплив стійкого фільтра оцінювання другого контуру на стійкість всієї САУ. Поліном чисельника передаточної функції за помилкою повинен мати різницю поліномів, що забезпечує досягнення інваріантності.

Двоконтурна САУ являється еквівалентною комбінованій, так як в ній забезпечується: інваріантність помилки відносно задавальної дії без безпосереднього її вимірювання; стійкість першого контуру при стійкому другому контурі.

Синтезована двоконтурна САУ, еквівалентна комбінованій. Розрахований та побудований фільтр оцінювання, проведений аналіз впливу цього фільтра на астатизм САУ (тобто на її точність).

Висновки. Наукова новизна розробленого методу синтезу автоматичних слідкувальних систем високої точності із розділеними процедурами управління та фільтрації в умовах, коли величина, яка управляється, не вимірюється при наявності збурень полягає в тому, що еквівалентність комбінованим системам, на відміну від методів диференціальних зв’язків, досягається не трьома, а двома контурами управління. Практична значущість полягає в тому, що запропонований метод доцільно застосовувати для побудови слідкувальних радіотехнічних систем, де вхідна корисна дія не вимірюється при наявності зовнішніх впливів та збурень, в системах управління літальними апаратами.

КЛЮЧОВІ СЛОВА: радіотехнічні слідкувальні системи; висока точність; метод синтезу; системи автоматичного управління; передаточна функція; інваріантність; пристрій управління; об’єкт управління; фільтр оцінювання; контур; регулятор.

АБРЕВІАТУРИ

САУ – система автоматичного управління;

ПФ – передаточна функція.

НОМЕНКЛАТУРА

$A(p)$ – поліном, який впливає на управління;

$A_1(p)$ – поліном чисельника ПФ за помилкою одноконтурної системи (рис. 2) [14];

$A_к(p)$ – поліном чисельника ПФ еквівалентної комбінованій САУ за помилкою цієї ж системи;

$B(p)$ – поліном, який впливає на оцінювання;

$B_{рег2}(p)$ – поліном ПФ регулятора 2 (рис. 2) [14];

$C(p)$ – характеристичний поліном замкнутої слідкувальної САУ;

$C_1(p)$ – поліном знаменника ПФ одноконтурної системи (рис. 2) [14] ;

$C_к(p)$ – характеристичний поліном системи, еквівалентної комбінованій САУ;

$C_{рег2}(p)$ – поліном ПФ регулятора 2 (рис. 2) [14];

$F(t)$ – невідома функція часу;

$g(t)$ – адитивна суміш задавального впливу $x(t)$ та збурення $f(t)$;

I – одинична матриця;

DOI 10.15588/1607-3274-2023-3-4

$P_{11}(t), P_{21}(t)$ – елементи кореляційної матриці помилки фільтрації, які визначаються із відомого рівняння Рикатті [6];

$[PI - A]^{-1}$ – зворотна характеристична матриця стану, яка виражається через під'єднану матрицю $[PI - A]^{\wedge}$;

$\tilde{u}(t)$ – нев'язка управління;

$W_{\text{ОУ}}(p)$ – передаточна функція об'єкту управління;

$W_{\text{per}}(p)$ – передаточна функція регулятора;

$W_{\text{ф}}(p)$ – передаточна функція фільтра;

$\hat{x}(t)$ – оцінка задавального впливу;

σ_f^2 – дисперсія збурення $f(t)$.

ВСТУП

Підвищення точності автоматичних систем є однією із основних проблем теорії автоматичного управління. Найбільш перспективними в цьому відношенні є клас комбінованих систем, в яких одночасно реалізовані принципи управління за відхиленням та за задавальною дією. Значні можливості підвищення точності відтворення в цих системах пояснюються відсутністю протиріччя між умовами інваріантності та стійкості. Математичною основою побудови високоякісних комбінованих САУ, в яких можливо досягнути незалежності (інваріантності) управляємої величини від збурення та точного відтворення задавальної дії, є теорія інваріантності. Тому досягнення інваріантності без порушення стійкості дозволяє підвищити точність відтворення [3, 4, 9, 18].

Досягнення інваріантності (високої точності) без порушення стійкості систем автоматичного управління розглядається в значній кількості робіт, наприклад [1–3, 5, 7, 11–13, 15, 17–35]. Проблема адаптивного нейронного управління із слідкуванням за зворотним зв'язком за виходом для класу невизначених нелінійних систем, які не перемикаються в структурі нестрогого зворотного зв'язку з середнім часом затримки, досліджується в [22]. В [23] розглянуто проблему адаптивного нейронного управління стійкого до відмов для класу нелінійних систем з невизначеною комутацією і нестрогим зворотним зв'язком із динамікою та станами, які не моделюються та не вимірюються. Адаптивні стратегії навчання нейронних мереж на основі консенсусних стратегій управління запропоновані в [26].

Адаптивне управління потребує вхідного впливу, який вимірюється. Також підвищується складність реалізації для отримання високої точності. У випадку, коли вхідний вплив не вимірюється (невідомий) адаптивні алгоритми не завжди доцільні.

Краще всього подібні задачі розв'язуються в класі комбінованих автоматичних систем, що працюють за помилкою і задавальним (збурюючим) впливом за наявності перешкод [4, 16, 31–35]. Комбінований алгоритм управління стендом для випробовування мікрогравітаційного середовища літального апарату може ефективно скоротити час маневру із збереженням високоточного управління, враховуючи вимоги маневру під великим кутом, запропоновано в [21].

У слідкувальних САУ, які працюють за відхиленням, існують протиріччя між умовами роздільного синтезу фільтрів оцінювання та управління [11–14].

В умовах, якщо зовнішні впливи (задавальний та збурюючий) не вимірюються, доцільно використовувати теорію САУ, які еквівалентні комбінованим автоматичним системам (з точки зору інваріантності та стійкості) та реалізують метод диференціальних зв'язків, або оцінювання змінних станів розширеного об'єкту.

Об'єктом дослідження є автоматичні слідкувальні системи з непрямим вимірюванням зовнішніх дій.

Предметом дослідження – принципи та методи теорії автоматичного управління і обробки інформації.

Метою статті є розробка методу синтезу автоматичних слідкувальних систем високої точності із розділеними процедурами управління та фільтрації в умовах, коли величина, яка управляється, не вимірюється (вхідний корисний вплив), при наявності збурень для побудови слідкувальних систем (особливо радіотехнічних, де вхідна корисна дія не вимірюється, а тому комбіноване управління не можливе).

1 ПОСТАНОВКА ЗАВДАННЯ

У [14] отримано умови інваріантності одноконтурної САУ (рис. 1). Зокрема передаточну функцію за помилкою управління (1) та (2), умову інваріантності (3), характеристичне рівняння (4) [14]. Показано за допомогою виразів (3), (4), що умова інваріантності входить в характеристичне рівняння, тому досягнення умов інваріантності пов'язане із зміною характеристичного рівняння, тобто із зміною коренів на комплексній площині p [14]. Тому в одноконтурній САУ не можливо досягти інваріантності без зміни стійкості системи.

Відомо, що задача синтезу слідкувальних САУ часто ставиться як задача оцінювання. Це пояснюється наступним чином:

– на вході слідкувальної САУ разом із задавальним (корисним) впливом присутні збурення та перешкоди, які необхідно відфільтрувати від задавального впливу;

– враховуючи, що в слідкувальних САУ задавальний вплив часто безпосередньо не вимірюється, необхідно даний фільтр ставити в замкнутий контур управління та синтезувати його за всіма правилами теорії оцінювання [6].

Структурна схема одноконтурної слідкувальної САУ з фільтром оцінювання всередині контуру управління показана на рис. 1.

DOI 10.15588/1607-3274-2023-3-4

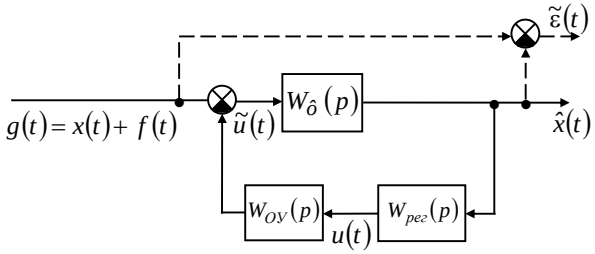

Рисунок 1 – Структурна схема одноконтурної слідкувальної САУ з фільтром оцінювання всередині контуру

Покажемо, що в слідкувальних САУ, які працюють за відхиленням, існує протиріччя між умовами роздільного синтезу фільтра оцінювання (згладжування) і фільтра (регулятора) управління.

Для цього введемо нев'язку оцінювання

$$\tilde{\varepsilon}(t)=g(t)-\hat{x}(t). \qquad (1)$$

Відношення нев'язки управління $\tilde{u}(t)$ до вхідного впливу $g(t)$ визначимо у вигляді передаточної функції за помилкою, тобто

$$\frac{\tilde{u}(t)}{g(t)}=\frac{A(p)}{C(p)},\ p\equiv\frac{d}{dt}. \qquad (2)$$

Відношення нев'язки оцінювання $\tilde{\varepsilon}(t)$ до вхідного впливу $g(t)$ визначимо аналогічно, тобто

$$\frac{\tilde{\varepsilon}(t)}{g(t)}=\frac{B(p)}{C(p)},\ p\equiv\frac{d}{dt}. \qquad (3)$$

Із (1) маємо наступний вираз для оцінки

$$\hat{x}(t)=g(t)-\tilde{\varepsilon}(t) \qquad (4)$$

яка повинна (відповідно до рис. 1) формуватися за нев'язкою управління $\tilde{u}(t)$.

Необхідний процес для отримання $g(t)$ із нев'язки $\tilde{u}(t)$ маємо із (2)

$$g(t)=\frac{C(p)}{A(p)}\tilde{u}(t),\ p\equiv\frac{d}{dt}, \qquad (5)$$

а аналогічний необхідний процес для $\tilde{\varepsilon}(t)$ – із (3) з урахуванням (5), тобто

$$\tilde{\varepsilon}(t)=\frac{B(p)}{A(p)}\tilde{u}(t),\ p\equiv\frac{d}{dt}. \qquad (6)$$

Підставляючи праві частини (5) і (6) в (4), маємо

$$\hat{x}(t)=\frac{C(p)-B(p)}{A(p)}\tilde{u}(t),\ p\equiv\frac{d}{dt}, \qquad (7)$$

звідки передаточна функція фільтру оцінювання наступна

$$W_{\text{ф}}(p)=\frac{C(p)-B(p)}{A(p)}. \qquad (8)$$

З іншого боку, передаточна функція за помилкою (нев'язкою управління) буде

$$\frac{A(p)}{C(p)}=\frac{1}{1+W_{\text{ф}}(p)W_{\text{рег}}(p)W_{OУ}(p)}. \qquad (9)$$

Звідки

$$A(p)+A(p)W_{\text{ф}}(p)W_{\text{рег}}(p)W_{\text{ОУ}}(p)=C(p),$$

$$W_{\text{рег}}(p)=\frac{C(p)-A(p)}{A(p)W_{\text{ф}}(p)W_{\text{ОУ}}(p)}. \qquad (10)$$

Підставляючи в (10) вираз (8) для передаточної функції фільтра, маємо

$$W_{\text{рег}}(p)=\frac{C(p)-A(p)}{[C(p)-A(p)]W_{\text{ОУ}}(p)}. \qquad (11)$$

Із аналізу виразів (8) для фільтра та (11) для регулятора видно, що всі три поліноми $A(p)$, $B(p)$, $C(p)$ входять в ці структури, що не дозволяє отримати роздільний синтез як фільтра оцінювання, так і фільтра (регулятора) управління.

Навіть якщо при синтезі регулятора будуть задіяні тільки два поліноми $A(p)$ та $C(p)$. то для синтезу фільтра оцінювання буде залишатися вільним тільки поліном $B(p)$, що недостатньо для побудови оптимального фільтра оцінювання [6]. Тому в слідкувальних САУ, які працюють за відхиленням, існує протиріччя між умовами роздільного синтезу фільтрів оцінювання та управління.

2 ОГЛЯД ЛІТЕРАТУРИ

Відомо ряд робіт про методи синтезу регуляторів комбінованих САУ та їх місце розташування в розімкнутих каналах (у зв'язках за задавальним та збурюючим впливами).

Так, наприклад, задача синтезу систем, яка дозволяє компенсувати дію збурень, сформована Г. В. Щипановим. В. С. Кулебакиним та Б. Г. Петровим вказані шляхи практичної реалізації компенсації [1, 7–9].

Методи синтезу регуляторів при компенсації зовнішніх збурень та відновленні задавальних впливів із умов досягнення інваріантності помилки відносно даних впливів розглянуті А. Г. Івахненко, Г. Ф. Зайцевим, Б. М. Менским для комбінованих САУ, а та-

DOI 10.15588/1607-3274-2023-3-4

кож для САУ еквівалентних комбінованим автоматичним системам (з точки зору стійкості).

Застосування величини, яка управляється (виходу системи) для побудови систем, еквівалентних комбінованим потребує додаткових апаратурних затрат та вносить додаткові помилки вимірювання величини, яка управляється.

3 МАТЕРІАЛИ І МЕТОДИ

Відомо, що слідкувальна система – автоматична система, мета якої полягає у формуванні величини, яка управляється згідно з невідомою вхідною функцією часу:

$$x(t)=F(t),\ \varepsilon_{\text{ст}}=x(t)-y(t)\le\varepsilon_{\text{доп}},$$

де $F(t)$ – невідома функція часу.

У слідкувальній системі величина, що управляється, повинна слідкувати за задавальною дією, яка плавно змінюється, але є невідомою функцією часу.

В САУ для організації управління найчастіше вхідний сигнал $x(t)$ порівнюється із сигналом зворотного зв'язку $y_{\text{зз}}(t)$. Як правило, в слідкувальних системах реалізований принцип управління за відхиленням.

Сучасні системи автоматичного управління високої точності будуються на основі принципу комбінованого управління, тобто сполучення принципів за відхиленням та задавальною дією, за відхиленням та за збуренням, за відхиленням та задавальною дією та за збуренням та ін.

При цьому точність роботи комбінованих систем, як правило, вища, ніж у системах, де реалізується один принцип управління.

Якщо вхідна корисна дія не вимірюється (невідома), то комбіноване управління, сполучення принципів за відхиленням (похибкою) та задавальною дією, не можливе [4, 5, 14, 18].

Відомо, що для отримання комбінованого управління $u_{\text{к}}$ необхідно мати дві складові [4, 16, 18]

$$u_{\text{к}}=u_1(\varepsilon)+u_2(x),$$

де складова u_1 залежить від похибки ε (перший контур), а u_2 – від задавального впливу x (другий контур).

Враховуючи, що в системах еквівалентних комбінованим задавальний вплив безпосередньо не вимірюється, то зробимо наступним чином. Задавальний вплив X можна отримати із сигналу похибки $\varepsilon_{\text{к}}$ системи, еквівалентної комбінованій САУ [10].

Використовуючи відношення

$$\frac{\varepsilon_{\text{к}}(p)}{X(p)}=\frac{A_{\text{к}}(p)}{C_{\text{к}}(p)},$$

отримаємо

$$X(p)=\frac{C_{\kappa}(p)}{A_{\kappa}(p)}\varepsilon_{\kappa}(p) \qquad (12)$$

У [14] розв'язання задачі управління розглянуто в рамках двоконтурних систем, еквівалентних комбінованим системам (рис. 2), в яких перший блок другого контуру здійснює операцію виведення x із ε_{κ} за виразом (12).

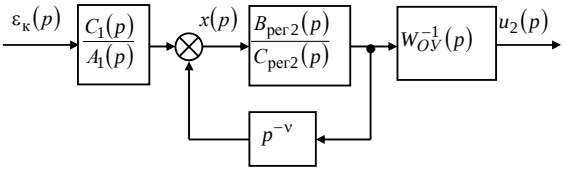

Рисунок 2 – Структурна схема розімкнутого другого контуру із замкнутим регулятором

Передаточну функцію другого регулятора (другий блок другого контуру) задано наступним виразом

$$W_{\text{per}2}(p)=\frac{B_{\text{per}2}(p)}{C_{\text{per}2}(p)}. \qquad (13)$$

Третій блок здійснює інверсію передаточної функції об'єкту управління $W_{\text{OY}}(p)$.

Отримано інваріантність без порушення стійкості першого контуру (рис. 2) [14].

Характеристичний поліном $C_{\text{к}}(p)$ двоконтурної САУ має вид

$$C_{\kappa}(p)=C_1(p)C_{\text{per}2}(p). \qquad (14)$$

Це усуває вплив другого контуру на стійкість першого.

Розглянута двоконтурна САУ в [14] еквівалентна комбінованій САУ, оскільки в ній забезпечуються:

інваріантність помилки відносно задавального впливу без безпосереднього його вимірювання;

стійкість першого контуру за умовою стійкого другого контуру.

До структурної схеми розімкнутого другого контуру (рис. 2) [14] з урахуванням (13), (14) та (15) відноситься добуток наступних передаточних функцій (без урахування $W_{OY}^{-1}(p)$):

$$\frac{C_{\text{к}}(p)}{A_{\text{к}}(p)}W_{\text{per}2}(p)=\frac{C_1(p)C_{\text{per}2}(p)}{A_1(p)\left[C_{\text{per}2}(p)-B_{\text{per}2}(p)p^{-\nu}\right]}\frac{B_{\text{per}2}(p)}{C_{\text{per}2}(p)}.$$

Після ділення чисельника та знаменника на $C_{\text{per}2}^2(p)$ отримаємо:

DOI 10.15588/1607-3274-2023-3-4

$$\frac{C_к(p)}{A_к(p)}W_{per\,2}(p)=\frac{C_1(p)}{A_1(p)}\times$$
$$\times\frac{B_{per\,2}(p)/C_{per\,2}(p)}{1-B_{per\,2}(p)p^{-\nu}/C_{per\,2}(p)}.$$

Другий співмножник представляє собою регулятор 2, охоплений позитивним зворотнім зв'язком з інтегруючою ланкою ν -го порядку (рис. 2).

Відповідно, другий контур представляє собою добуток зворотної передаточної функції за помилкою першого контуру на передаточну функцію регулятора 2, охопленого позитивним зворотнім зв'язком із оператором $p^{-\nu}$, а також на зворотну передаточну функцію об'єкту управління без інтегруючих ланок.

У реальних умовах роботи часто на задавальний вплив $x(t)$ накладається збурення, тому необхідна процедура його фільтрації (рис. 2) [14] та подальшого формування управління $u_2(t)$ на основі оцінки $\hat{x}(t)$.

Нехай структурна схема одноконтурної САУ має вид (рис. 3).

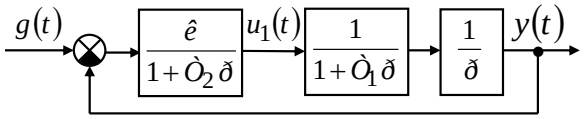

Рисунок 3 – Структурна схема одноконтурної САУ

Вхідний вплив $g(t)$ представляє собою адитивну суміш лінійного задавального впливу $x(t)$ та збурення $f(t)$ з нормальним законом розподілу, тобто

$$g(t)=x(t)+f(t),\ x(t)=vt,\ f(t):N\left(0,\sigma_f^2\right). \qquad (15)$$

Необхідно розробити структурну схему двоконтурної САУ, еквівалентну комбінованій.

За даними спостереження за процесом $\varepsilon(t)$, розрахувати та побудувати фільтр оцінювання процесу $x(t)$. Крім того, необхідно також провести аналіз впливу цього фільтру на астатизм САУ (тобто на її точність).

4 ЕКСПЕРИМЕНТИ

Виходячи із поставленого завдання, виберемо двоконтурну САУ, рис. 1 та рис. 2 [14], в якій:

– замість задавального впливу $x(t)$ має місце вхідний вплив $g(t)$ (15);

– замість розімкненого регулятора [14], охопленого позитивним зворотнім зв'язком за інтегратором (рис. 2), необхідно використати фільтр оцінювання із передаточною функцією замкнутого фільтра $W_{ЗФ}(p,t)$.

Перетворена схема (рис. 2) [14] для розв'язання задачі оцінювання задавального впливу $x(t)$ приведена на рис. 4.

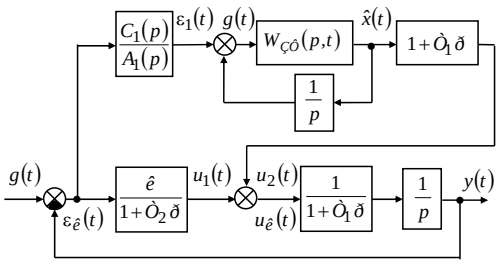

Рисунок 4 – Структурна схема двоконтурної САУ, еквівалентної комбінованій, із замкненим фільтром оцінювання у другому контурі

В якості фільтра оцінювання виберемо векторно-матричний безперервний фільтр Р. Калмана, зображений на рис. 5.

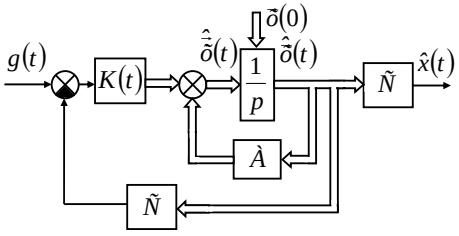

Рисунок 5 – Структурна схема безперервного фільтра Р. Калмана із скалярним виходом $\tilde{x}(t)$

Матриці стану A, спостереження C та ваги $K(t)$ для вхідної моделі (15) мають вид

$$A=\begin{vmatrix}0 & 1\\ 0 & 0\end{vmatrix},\ C=\begin{vmatrix}1 & 0\end{vmatrix},\ K(t)=\begin{vmatrix}P_{11}(t)/\sigma_f^2\\ P_{21}(t)/\sigma_f^2\end{vmatrix}, \qquad (16)$$

$$\dot{P}(t)=P(t)A+A^TP(t)-$$
$$-P(t)C^TR^{-1}CP(t)+B(t)Q(t)B^T(t), \qquad (17)$$
$$P(0)=P_0.$$

За відсутності збурюючого впливу на вектор стану $\vec{x}(t)$, матриці $Q(t)$ та $B(t)$ дорівнюють нулю.

Із рис. 5 видно, що відношення зображення оцінки $\hat{x}(p)$ до зображення вхідного процесу $g(p)$ утворюють передаточну функцію замкнутого фільтра

DOI 10.15588/1607-3274-2023-3-4

$$W_{3\Phi}(p,t)=\frac{C\frac{\frac{1}{p}}{1-A\frac{1}{p}}K(t)}{\left[1+C\frac{\frac{1}{p}}{1-A\frac{1}{p}}K(t)\right]}= \tag{18}$$

$$=\frac{C[PI-A]^{-1}K(t)}{\left[1+C[PI-A]^{-1}K(t)\right]},$$

$$[PI-A]^{-1}=\frac{[PI-A]^{\wedge}}{\Delta}. \tag{19}$$

Замінивши зворотну характеристичну матрицю стану у виразі (18) на праву частину виразу (19), отримаємо

$$W_{3\Phi}(p,t)=\frac{C[PI-A]^{\wedge}K(t)}{\Delta+C[PI-A]^{\wedge}K(t)} \tag{20}$$

де чисельник

$$C[PI-A]^{\wedge}K(t)=B_{\Phi}(p,t) \tag{21}$$

– поліном чисельника оптимального фільтра, а знаменник

$$\Delta+C[PI-A]^{\wedge}K(t)=C_{\Phi}(p,t) \tag{22}$$

– поліном знаменника оптимального фільтра.

Тоді різниця між поліномами фільтра

$$C_{\Phi}(p,t)-B_{\Phi}(p,t)p^{\nu}= \tag{23}$$
$$=\Delta+C[PI-A]^{\wedge}K(t)-C[PI-A]^{\wedge}K(t)p^{\nu}.$$

Із аналізу виразу (23) випливає, що якщо б астатизм першого контуру дорівнював нулю ($\nu=0$), то вказана різниця дорівнювала Δ.

Для випадку, який розглядається

$$\Delta=\det[PI-A]=\det\begin{bmatrix}p & -1\\ 0 & p\end{bmatrix}=p^2. \tag{24}$$

Тоді поліном чисельника передаточної функції двоконтурної системи за помилкою

$$A_{\kappa}(p)=A_1(p)p^2. \tag{25}$$

При цьому астатизм підвищується на два порядки ($\Delta\nu=2$), тобто двоконтурна САУ рис. 4. крім розв'язання задачі оцінювання задавального впливу приводить до підвищення астатизму на два порядки, якщо б в першому контурі не було астатизму. При цьому сам фільтр стійкий і не впливає на стійкість першого контуру. В чому легко переконатися, якщо знайти поліном $C_{\Phi}(p,t)$ за виразом (22).

Послідовність визначення приєднаної матриці наступна:

$$[PI-A]^{T}=\begin{bmatrix}p & 0\\ -1 & p\end{bmatrix}\Rightarrow[PI-A]^{\wedge}=\begin{bmatrix}p & 1\\ 0 & p\end{bmatrix}. \tag{26}$$

Тоді відповідно до (22), (16), (24) та (26)

$$C_{\Phi}(p,t)=p^2+K_{11}(t)p+K_{21}(t), \tag{27}$$

де

$$K_{11}(t)=\frac{P_{11}(t)}{\sigma_f^2},\quad K_{21}(t)=\frac{P_{21}(t)}{\sigma_f^2}. \tag{28}$$

елементи вагової матриці $K(t)$.

Характеристичний поліном двоконтурної САУ має вид

$$C_{\kappa}(p,t)=C_1(p)C_{\Phi}(p,t), \tag{29}$$

що виключає вплив стійкого фільтра оцінювання на стійкість всієї САУ.

Відповідно до поставленої задачі розглянемо вплив фільтра на точність САУ при наявності в першому контурі астатизму першого порядку ($\nu=1$).

Аналіз лівої частини виразу (23) показує, що при $\nu=1$ необхідно в поліномі $B_{\Phi}(p,t)$ мати множник p. Це стає можливим, якщо передаточну функцію замкнутого фільтра помножити на похідну, яка фізично реалізується

$$\frac{\tau p}{1+\tau p}, \tag{30}$$

тобто

$$W_{3\Phi}(p,t)=\frac{B_{\phi}(p,t)}{C_{\phi}(p,t)}\frac{\tau p}{1+\tau p}, \tag{31}$$

де $C_{\Phi}(p,t)$ визначається виразом (27), а вираз для $B_{\Phi}(p,t)$ на основі (21) прийме вигляд

$$B_{\phi}(p,t)=K_{11}(t)p+K_{21}(t). \tag{32}$$

Тоді структурна схема розімкненого другого контуру в САУ рис. 4. прийме вигляд. рис. 6.

DOI 10.15588/1607-3274-2023-3-4

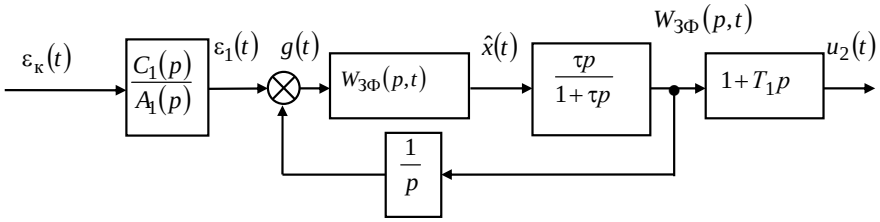

Рисунок 6 – Структурна схема розімкненого другого контуру із похідною, яка фізично реалізується

Складемо добуток наступних поліномів:

$$B_Ф(p,t)\tau p = K_{11}(t)\tau p^2 + K_{21}(t)\tau p = \\ = B_{per\,2}(p,t),$$

$$C_Ф(p,t)(1+\tau p) = \\ = \left[p^2 + K_{11}(t)p + K_{21}(t)\right](1+\tau p) = \\ = \tau p^3 + (1+\tau K_{11}(t))p^2 + (K_{11}(t)+\tau K_{21}(t))p + \\ + K_{21}(t) = C_{per\,2}(p,t).$$

Знову складемо перетворену різницю між поліномами фільтра (як ліва частина виразу (23)):

$$C_{per\,2}(p,t) - B_{per\,2}(p,t)p^{-1} = \\ = \tau p^3 + (1+\tau K_{11}(t))p^2 + (K_{11}(t)+\tau K_{21}(t))p + \\ + K_{21}(t) - K_{11}(t)\tau p - K_{21}(t)\tau. \qquad (33)$$

Якщо $\tau = 1$ із (33) маємо

$$C_{per\,2}(p,t) - B_{per\,2}(p,t)p^{-1} = \\ = p\left[p^2 + (1+K_{11}(t))p + K_{21}(t)\right].$$

Через наявність вільного множника p, поліном чисельника передаточної функції двоконтурної системи за помилкою має вигляд

$$A_к(p) = A_1(p)\times \\ \times p\left[p^2 + (1+K_{11}(t))p + K_{21}(t)\right], \qquad (34)$$

що свідчить про підвищення порядку астатизму на одиницю ($\Delta\nu = 1$). При цьому характеристичний поліном двоконтурної САУ

$$C_к(p,t) = C_1(p)C_Ф(p,t)(1+\tau p), \qquad (35)$$

звідки видно, що порівняно із виразом (29), в системі з'являється один новий стійкий корінь – $1/\tau$, який не впливає на стійкість двоконтурної САУ.

Таким чином, запропонований метод доцільно застосовувати для побудови радіотехнічних систем (в системах управління трафіком високошвидкісних мультисервісних мереж зв'язку), у системах управління літальними апаратами різного призначення (безпілотними літальними апаратами, квадрокоптерами, штучними супутниками Землі, літаками різного призначення).

5 РЕЗУЛЬТАТИ

Синтезована двоконтурна САУ, еквівалентна комбінованій. Розрахований та побудований фільтр оцінювання (рис. 5), проведений аналіз впливу цього фільтра на астатизм САУ (тобто на її точність). Поліноми $B_Ф(p,t)$, $C_Ф(p,t)$, $A_к(p,t)$, $C_к(p,t)$ при різних значеннях астатизму першого контуру наведено в таблиці 1.

Таблиця 1 – Поліноми передаточних функцій САУ

ν	0	1
$B_Ф(p,t)$	$K_{11}(t)p + K_{21}(t)$	$\left[K_{11}(t)p + K_{21}(t)\right]\tau p$
$C_Ф(p,t)$	$p^2 + K_{11}(t)p + K_{21}(t)$	$\left[p^2 + K_{11}(t)p + K_{21}(t)\right]\times$ $\times(1+\tau p)$
$A_к(p,t)$	$A_1(p)p^2$	$A_1(p)p\left[p^2 + (1+K_{11}(t)\times\right.$ $\left.\times\, p + K_{21}(t)\right]$
$C_к(p,t)$	$C_1(p)C_Ф(p,t)$	$C_1(p)C_Ф(p,t)(1+\tau p)$

Порівняльна оцінка ефективності синтезованої системи з існуючою проведена аналітичним методом [23, 31–35] та методом математичного моделювання, при подачі на вхід одиничного перепаду швидкості (стрибок за швидкістю). На рис. 7 наведені графіки перехідних процесів: 1 – для існуючої системи; 2 – для системи, синтезованої за даним методом.

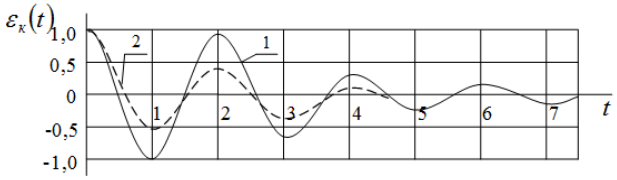

Рисунок 7 – Графіки перехідних процесів

Порівняльний аналіз показує, що при однакових умовах роботи показники якості перехідного процесу синтезованої системи вищі.

Результати моделювання слідкувальних систем з фільтрами (регуляторами) управління та оцінювання показали їх значну ефективність.

DOI 10.15588/1607-3274-2023-3-4

При застосуванні синтезованої двохконтурної САУ підвищується також точність супроводження, особливо маневруючих об'єктів, і тому зменшується можливість зриву супроводження.

6 ОБГОВОРЕННЯ

1. Запропонований метод синтезу двоконтурних систем, еквівалентних комбінованим, з розділеними процедурами управління та фільтрації, в умовах наявності одночасно як вхідного (задавального) впливу, так і зовнішніх впливів та збурень.

2. Розроблений метод дозволяє синтезувати слідкувальні САУ високої точності, еквівалентні комбінованим, в умовах, якщо управляюча величина не вимірюється (вхідна корисна дія).

3. В даному апараті побудови САУ, еквівалентність комбінованим системам, на відміну від методу диференціальних зв'язків, досягається не трьома, а двома контурами управління.

4. Розроблений метод дозволяє здійснити роздільний синтез фільтрів оцінювання у двоконтурних слідкувальних САУ, еквівалентних комбінованим.

5. Синтезована двоконтурна САУ, еквівалентна комбінованій. Розрахований та побудований фільтр оцінювання, здійснений аналіз впливу цього фільтру на астатизм САУ (тобто на її точність).

ВИСНОВКИ

Наукова новизна отриманих результатів проведеного дослідження полягає в розробленні методу синтезу слідкувальних САУ високої точності, еквівалентних комбінованим, в умовах, якщо управляюча величина не вимірюється (вхідна корисна дія). Еквівалентність комбінованим системам, на відміну від методу диференціальних зв'язків, досягається не трьома, а двома контурами управління. Розроблений метод дозволяє здійснити роздільний синтез фільтрів оцінювання у двоконтурних слідкувальних САУ, еквівалентних комбінованим.

Запропонований метод доцільно застосовувати для побудови слідкувальних систем (особливо радіотехнічних, де вхідна корисна дія не вимірюється при наявності зовнішніх впливів та збурень, а тому і комбіноване управління не можливе), а також в системах управління літальними апаратами різного призначення.

Перспективи подальших досліджень в даному напрямку полягають у застосуванні запропонованого методу синтезу для дискретних САУ та при розробці систем управління літальними апаратами різного призначення.

ЛІТЕРАТУРА

1. Гайдук А. Р. К условиям существования абсолютно инвариантных к неизмеряемым воздействиям систем / А. Р. Гайдук // Автомат. и телемех. – 2010. – № 8 – С. 3–12.
2. Жуков В. П. О существовании инвариантных простых контуров в инвариантных множествах нелинейных динамических систем второго порядка / В. П. Жуков // Автомат. и телемех. – 2002. – № 3 – С. 36–49.
3. Зайцев Г. Ф. Синтез дискретных систем на основе условий инвариантности по каналам оценивания и управления / Г. Ф Зайцев, Ю. А. Пушкарев // Теория инвариантности, теория чувствительности и их применение. Тез. док. VII Всесоюзное совещ. – Москва : Институт проблем управления, 1987. – 162 с.
4. Зайцев Г. Ф. Комбинированные следящие системы / Г. Ф. Зайцев. – Київ : Техника, 1978. – 262 с.
5. Методы современной теории автоматического управления / Под общей ред. К. А. Пупкова. – Москва : МГУ им. Н. Э. Баумана, 2000. – 747 с.
6. Медич Дж. Статистические оптимальные линейные оценки и управление / Дж. Медич. – Москва : Энергия, 1973. – 439 с.
7. Петров Б. Н. Теория автоматического управления: Избранные труды. Т. 1. / Б. Н. Петров. – Москва : Наука, 1983. – 429 с.
8. Петров Б. Н. Управление авиационными и космическими аппаратами: Избранные труды. Т. 2. / Б. Н. Петров. – Москва : Наука, 1983. – 328 с.
9. Петров Б. Н. Принцип инвариантности в измерительной технике / Б. Н. Петров, В. А. Викторов, Б. В. Лункин. – Москва: Наука, 1976. – 239 с.
10. Пушкарев Ю. А. Анализ и синтез дискретных систем оценивания / Ю. А. Пушкарев. – Москва : МО СССР, 1989. – 350 с.
11. Пушкарев Ю. А. Новые эффективные цифровые фильтры второго и третьего порядка / Ю. А. Пушкарев, В. Б. Ревенко // Изв. вузов. Радиоэлектроника. – 1994. – Т. 37, № 4.– С. 54–61.
12. Пушкарев Ю. А. Новый структурный метод синтеза эффективных цифровых фильтров обработки информации для автоматических следящих систем / Ю. А. Пушкарев, В. Б. Ревенко // Институт кибернетики УССР им. акад. В. М. Глушкова. Проблемы управления и информатики. – 1995. – № 1. – С. 138–148.
13. Пушкарев Ю. А. Метод конструирования следящей системы с цифровым фильтром внутри контура слежения и повышенной точностью управления / Ю. А. Пушкарев, В. Б. Ревенко // Изв. вузов. Радиоэлектроника. – 2005. – Т.48, № 10. – С. 29–37.
14. Ревенко В. Б. Метод синтеза следящих систем автоматического управления высокой точности / В. Б. Ревенко, Н. Н. Каращук // Вісник НТУУ «КПІ». Серія Радіотехніка, Радіоапаратобудування. – Київ, 2021. – Вип. № 87. – С. 30–38. https://doi.org/10.20535/RADAP.2021.87.30-38.
15. Синтез регуляторов и теория оптимизации систем автоматического управления / Под общей редакцией К. А. Пупкова. – Москва : МГТУ им. Н. Э. Баумана, 2000. – 735 с.
16. Солнечный Э. М. Инвариантность и астатизм в системах без измерения возмущения / Э. М. Солнечный // Автомат. и телемех. – 2008. – № 12. – С. 76–85.
17. Уткин В. А. Инвариантность и автономность в системах с разделяемыми движениями / В. А. Уткин // Автомат. и телемех. – 2001. – Вып. 11. – С. 73–94.
18. Теория управления. Терминология. Вып. 107. – Москва: Наука, 1988. – 56 с.
19. Davison E. J. The output control of linear time-invariant systems with unmesurable arbitrary disturbances / E. J. Davison // IEEE. Trans. – 1972. – Vol. 17, No. 5. – P. 621–630.

DOI 10.15588/1607-3274-2023-3-4

20. Linear Matrix Inequalities in System and Control Theory / [S. Boyd, L. Ghaoui, E. Feron, V. Balakrishnan]. – Philadelphia : STAM, 1994. – 193 p.
21. Zhiming Chen. Research on High-Precision Attitude Control of Joint Actuator of Three-Axis Air-Bearing Test Bed / [Chen Zhiming, Luo Zhouhuai, Wu Yunhua et al.] // Journal of Control Science and Engineering. – 2021. – Vol. 1. – P. 11. doi.org/10.1155/2021/5582541.
22. Neural network-based adaptive tracking control for switched nonlinear systems with prescribed performance: an average dwell time switching approach / [Y. Wang, B. Niu, H. Wang et al.] // Neurocomputing. – 2021. – Vol. 435. – P. 295–306. doi.org/10.1016/j.neucom.2020.10.023.
23. Ma L. Small-gain technique-based adaptive neural output-feedback faulttolerant control of switched nonlinear systems with unmodeled dynamics / [L. Ma, N. Xu, X. Zhao et al.] // IEEE Transactions on Systems, Man, and Cybernetics: Systems. – 2020. – Vol. 49. – P. 1–12. doi.org: 10.1109/TSMC.2020.2964822.
24. Nonfragile fault-tolerant control of suspension systems subject to input quantization and actuator fault / [J. Xiong, X. Chang, J. H. Park et al.] // International Journal of Robust and Nonlinear Control. – 2020. – Vol. 30. – P. 6720–6743. doi.org/10.1002/rnc.5135.
25. Yuan W. Adaptive backstepping sliding mode control of the hybrid conveying mechanism with mismatched disturbances via nonlinear disturbance observers / W. Yuan, G. Gao, and J. Li // Journal of Control Science and Engi-neering. – 2020. – Vol. 2020. – 13 p. Article ID 7376503. doi.org/10.1155/2020/7376503.
26. Jin X. Adaptive fault-tolerant consensus for a class of leader-following systems using neural network learningstrategy / [X. Jin, X. Zhao, J. Yu et al.] // Neural Netw. – 2020. – Vol. 121. – P. 474–483. doi.org/10.1016/j.neunet.2019.09.028.
27. Yao X. Disturbance-observer-based fault tolerant control of high-speed trains: a Markovian jump system model approach / X. Yao, L. Wu, L. Guo // IEEE Trans Syst Man Cybernet Syst. – 2020. – Vol. 50(4). – P. 1476–1485. doi.org/10.1109/TSMC.2018.2866618.38.
28. Observer-based fixed-time continuous nonsingular terminal sliding mode control of quadrotor aircraft under uncertainties and disturbances for robust trajectory tracking: Theory and experiment / [Omar Mechaliab, Limei Xu, Ya Huang et al.] // Control Engineering Practice. – 2021. – Vol. 111. article 104806. doi.org/10.1016/j.conengprac.2021.104806.
29. Sharma Manmohan. Control of a quadrotor with network induced time delay / Manmohan Sharma, Indrani Kar // ISA Transactions. – 2021. – Vol. 111. – P. 132–143. doi.org/10.1016/j.isatra.2020.11.008.
30. Benjamin Kuo C. Automatic Control Systems / Kuo C. Benjamin. – Technology and Engineering, 1995. – 928 p. ISBN: 9788120309685, 9788120309685.
31. Dorf Richard C. Modern Control Systems, Global Edition. 13th Edition / Richard C. Dorf, Robert H. Bishop. – Pearson (Intl), 2019. – 1032 p.
32. Ageev S. A. An Adaptive Method for Assessing Traffic Characteristics in High-Speed Multiservice Communication Networks Based on a Fuzzy Control Procedure / S. A. Ageev, A. A. Privalov, A. A. Butsanets // Intellectual control systems. – 2021. – Vol. 82. – P. 1222–1232. doi.org/10.1134/S0005117921070067.
33. Bazhenov S. G. Stability Analysis of an Airplane with MIMO Control System Based on Frequency Methods / S. G. Bazhenov, A. N. Kozyaichev, V. S. Korolev // Control sciences. – 2021. – Vol. 82. – P. 1271–1280. doi.org/10.1134/S0005117921070109.
34. Alexandrov V. A. Optimization of the Altitude and Speed Profile of the Aircraft Cruise with Fixed Arrival Time / V. A. Alexandrov, E. Yu. Zybin, M. V. Khlebnikov // Automation and Remote Control. – 2021. – Vol. 82. – P. 1169–1182. doi.org/10.1134/S0005117921070031.
35. Hien N. van. An object-oriented systems engineering point of view to develop controllers of quadrotor unmanned aerial vehicles / N. van Hien, V.-T. Truong, and N.-T. Bui // International Journal of Aerospace Engineering. – 2020. – Vol. 2020. Article ID 8862864. – 17 p. doi.org/10.1155/2020/8862864.

Стаття надійшла до редакції 07.04.2023.
Після доробки 26.06.2023.

UDC 621.391.17

A METHOD FOR SYNTHESIS OF HIGH PRECISION RADIO TRACKING SYSTEMS WITH SPLIT CONTROL AND FILTERING PROCEDURES

Revenko V. B. – PhD, Associate Professor, Associate Professor of the Chair of Electrical Engineering and Electronics of S. P. Korolev Military Institute of Zhytomyr, Zhytomyr, Ukraine.

Karashchuk N. N. – PhD, Associate Professor, Senior Instructor of the Chair of Telecommunication and Radiomachinery of S. P. Korolev Military Institute of Zhytomyr, Zhytomyr, Ukraine.

ABSTRACT

Context. In combined automatic control systems (ACS) with the principle of control by disturbance, there are difficulties in controlling disturbances in some objects of radio engineering systems and somewhat lower accuracy. This is especially noticeable when the object is affected by several equal disturbances. Taking them into account requires increasing the complexity and reducing the reliability of the ACS. And neglect sharply reduces the accuracy of the system. Therefore, there is a need to develop a method of synthesis of radio technical tracking systems that eliminates the indicated shortcomings.

Objective. The article presents a synthesis method for high precision radio tracking systems, which are equivalent to combined systems with split control and filtering procedures when the entry useful (preset) action, which is not measured and external disturbances and interferences are present simultaneously.

Method. Methods of automatic control theory were used to achieve the goal of the research.

Results. It has been demonstrated that there is a conflict between the conditions for split synthesis of the evaluation (smoothing) filter and the control filter (regulator) in automatic tracking control systems operating with deviation.

The article offers a solution to the problem of control and evaluation in the framework of two-circuit systems, which are equivalent to combined systems. The second circuit can be presented as a product of a reverse transfer function with an error in the first

DOI 10.15588/1607-3274-2023-3-4

circuit to the transfer function of Controller, which has a positive feedback from the operator, as well as the reverse transfer function of the control object without integrating links. It is proposed to use for evaluation an evaluation filter with closed filter transfer function instead of an open regulator.

The characteristic polynomial of a two-circuit automatic control system (ACS) excludes the influence of the stable second-circuit evaluation filter on the stability of the entire ACS. The polynomial of the numerator of the transfer function must have the difference of polynomials by error, which ensures the achievement of invariance.

A double-circuit ACS is equivalent to a combined one, since it provides the following: invariance of the error with respect to the preset action without directly measuring it; stability of the first circuit with a stable second circuit.

The synthesized double-circuit ACS is equivalent to a combined one. The author has calculated and constructed the evaluation filter, the influence of this filter on ACS astatism (i. e., on its accuracy) has been analyzed.

Conclusions. The scientific novelty of the developed method of synthesis of high-precision automatic tracking systems with separate control and filtering procedures in conditions where the controlled value is not measured in the presence of disturbances is as follows. Equivalence to combined systems, in contrast to the methods of differential connections, is achieved not by three, but by two control loops. The practical significance lies in the fact that the proposed method is advisable to use for the construction of surveillance radio engineering systems, where the input useful effect is not measured in the presence of external influences and disturbances. In aircraft control systems.

KEYWORDS: radio tracking systems; high precision; synthesis method; automatic control systems; transfer function; invariance; control device; control object; evaluation filter; contour; regulator.

REFERENCES

1. Gaiduk A. R. To the conditions for the existence of systems absolutely invariant to unmeasured influences, *Automation and telemechanics*, 2010, Iss. 8, pp. 3–12. (in Russian).
2. Zhukov V. P. On the existence of invariant simple contours in invariant sets of second-order nonlinear dynamical systems, *Automation and telemechanics*, 2002, Iss. 3, pp. 36–49. (in Russian).
3. Zaitsev G. F. and Pushkarev Yu. A. Sintez diskretnykh sistem na osnove uslovii invariantnosti po kanalam otsenivaniya i upravleniya, *Teoriya invariantnosti, teoriya chuvstvitel'nosti i ikh primenenie. Tez. dok. VII Vsesoyuznoe soveshch.* Moscow, Institut problem upravleniya, 1987, 162 p. (in Russian).
4. Zaitsev G. F. Kombinirovannye sledyashchie sistemy. Kyiv, Equipment Publ., 1978, 262 p. (in Russian).
5. Pupkov K. A. Metody sovremennoi teorii avtomaticheskogo upravleniya. Moscow, State University N. E. Bauman, 2000, 747 p. (in Russian).
6. Medich Dzh. Statisticheskiye optimalnyye lineynyye otsenki i upravleniye. Moscow, Energiya, 1973, 439 p. (in Russian).
7. Petrov B. N. Teoriya avtomaticheskogo upravleniya: Izbrannye trudy. Vol.1. Moscow, Nauka, 1983, 429 p. (in Russian).
8. Petrov B. N. Upravlenie aviatsionnymi i kosmicheskimi apparatami: Izbrannye trudy, Vol. 1. Moscow, Nauka, 1983, 328 p. (in Russian).
9. Petrov B. N., Viktorov V. A. and Lunkin B. V. Printsip invariantnosti v izmeritel'noi tekhnike. Moscow, Nauka, 1976, 239 p. (in Russian).
10. Pushkarev Yu. A. Analiz i sintez diskretnykh sistem otsenivaniya. MO SSSR, 1989, 350 p. (in Russian).
11. Pushkarev Yu. A. and Revenko V. B. New efficient digital filters of the second and third order, *Izv. universities. Radioelectronics*, 1994, Vol. 37, Iss. 4. (in Russian).
12. Pushkarev Yu. A. and Revenko V. B. A new structural method for the synthesis of effective digital filters for information processing for automatic tracking systems. Institute of Cybernetics of the Ukrainian SSR named after acad. V.M. Glushkova. Problems of management and informatics, 1995, Iss. 1, pp. 138–148. (in Russian).
13. Pushkarev Yu. A. and Revenko V. B. () Tracking system design method with a digital filter inside the tracking loop and increased control accuracy. *Izv. universities. Radioelectronics*, 2005, Vol. 48, Iss. 10, pp. 29–37. (in Russian).
14. Revenko V. B. and Karashchuk N. N. () Method for Synthesis of High Precision Servo Systems, *Bulletin of NTUU KPI Radio Engineering Series. Radioequipment construction.* Kyiv, 2021, Iss. 87, pp. 30–38. https://doi.org/10.20535/RADAP.2021.87.30-38. (in Ukraine).
15. Punkova K. A. () Sintez regulyatorov i teoriya optimizatsii sistem avtomaticheskogo upravleniya. Moscow, State University N. E. Bauman, 2000, 735 p. (in Russian).
16. Solnechnyi E. M. Invariance and astitism in systems without disturbance measurement, *Automation and telemechanics*, 2008, Iss. 12, pp. 76–85. (in Russian).
17. Utkin V. A. () Invariance and autonomy in systems with shared motions, *Automation and telemechanics*, 2001, Iss. 11, pp. 73–94. (in Russian).
18. Teoriya upravleniya, *Terminologiya.* Moscow, Nauka, 1988Vol. 107, 56 p. (in Russian).
19. Davison E. J. () The output control of linear time-invariant systems with unmesurable arbitrary disturbances, *IEEE. Trans*., 1972, Vol. 17, Iss. 5, pp. 621–630. (in English).
20. Boyd S., Ghaoui L., Feron E. and Balakrishnan V. Linear Matrix Inequalities in System and Control Theory. Philadelphia, STAM, 1994, 193 p. (in English).
21. Zhiming Chen, Zhouhuai Luo, Yunhua Wu, Wei Xue, Wenxing Li Research on High-Precision Attitude Control of Joint Actuator of Three-Axis Air-Bearing Test Bed. Journal of Control Science and Engineering, 2021, Vol. 1, P. 11. (in India). doi.org/10.1155/2021/5582541.
22. Wang Y., Niu B., Wang H. et al. Neural network-based adaptive tracking control for switched nonlinear systems with prescribed performance: an average dwell time switching approach. Neurocomputing, 2021, Vol. 435, pp. 295–306. (in China). doi.org/10.1016/j.neucom.2020.10.023.
23. Ma L., Xu N., Zhao X., Zong G., and Huo X. (2020) Small-gain technique-based adaptive neural output-feedback fault-tolerant control of switched nonlinear systems with unmodeled dynamics, *IEEE Transactions on Systems, Man, and Cybernetics: Systems*, Vol. 49, pp. 1–12. (international). doi.org: 10.1109/TSMC.2020.2964822.
24. Xiong J., Chang X., Park J. H. et al. () Nonfragile fault-tolerant control of suspension systems subject to input quantization and actuator fault, *International Journal of Robust and Nonlinear Control*, 2020, Vol. 30, pp. 6720–6743. (international). doi.org/10.1002/rnc.5135.
25. Yuan W., Gao G., and Li J. Adaptive backstepping sliding mode control of the hybrid conveying mechanism with mismatched disturbances via nonlinear disturbance observ-

DOI 10.15588/1607-3274-2023-3-4

ers. Journal of Control Science and Engineering, 2020, Vol. 2020, 13 pages, Article ID 7376503. (in India). doi.org/10.1155/2020/7376503.
26. Jin X., Zhao X., Yu J., Wu X., Chi J. Adaptive fault-tolerant consensus for a class of leader-following systems using neural network learningstrategy, *Neural Netw*, 2020, Vol. 121. pp. 474–483. (international). doi.org/10.1016/j.neunet. 2019.09.028.
27. Yao X., Wu L., Guo L. (2020) Disturbance-observer-based fault tolerant control of high-speed trains: a Markovian jump system model approach. IEEE Trans Syst Man Cybernet Syst. Vol. 50 (4). pp. 1476–1485. doi.org/10.1109/TSMC.2018.2866618.38.
28. Mechaliab Omar, Xu Limei, Huang Ya, Shi Mengji, Xie Xiaomei Observer-based fixed-time continuous nonsingular terminal sliding mode control of quadrotor aircraft under uncertainties and disturbances for robust trajectory tracking: Theory and experiment, *Control Engineering Practice*. 2021, Vol. 111. article 104806. (in-ternational IFAC) doi.org/10.1016/j.conengprac.2021.104806.
29. Sharma Manmohan, Indrani Kar Control of a quadrotor with network induced time delay, *ISA Transactions*, 2021, Vol. 111, pp. 132–143. (in USA). doi.org/10.1016/j.isatra.2020.11.008.
30. Benjamin Kuo C. Automatic Control Systems. Published by PHI LEARNING PVT LTD: Technology and Engineering, 928 p. ISBN: 9788120309685, 9788120309685. (in China).
31. Richard C. Dorf, Robert H. Bishop Modern Control Systems, Global Edition. 13th Edition. Pearson (Intl), 2019, 1032 p. (in USA).
32. Ageev S. A., Privalov A. A., Butsanets A. A. An Adaptive Method for Assessing Traffic Characteristics in High-Speed Multiservice Communication Networks Based on a Fuzzy Control Procedure. Intellectual control systems, 2021, Vol. 82, pp. 1222–1232. (in Russian). doi.org/10.1134 /S0005117921070067.
33. Bazhenov S. G., Kozyaichev A. N., Korolev V. S. () Stability Analysis of an Airplane with MIMO Control System Based on Frequency Methods, *Control sciences*, 2021, Vol. 82, pp. 1271–1280. (in Russian). doi.org/10.1134/ S0005117921070109.
34. Alexandrov V. A., Zybin E. Yu., Khlebnikov M. V. (2021) Optimization of the Altitude and Speed Profile of the Aircraft Cruise with Fixed Arrival Time. Automation and Remote Control. Vol. 82. pp. 1169–1182. (in Russian). doi.org/10.1134/S0005117921070031.
35. Hien N. van, Truong V.-T. and Bui N.-T. An object-oriented systems engineering point of view to develop controllers of quadrotor unmanned aerial vehicles. International Journal of Aerospace Engineering, 2020, Vol. 2020. Article ID 8862864. 17 p. (international). doi.org/10.1155/2020/8862864.

DOI 10.15588/1607-3274-2023-3-4

МАТЕМАТИЧНЕ ТА КОМП'ЮТЕРНЕ МОДЕЛЮВАННЯ

MATHEMATICAL AND COMPUTER MODELING

UDC 51–74, 517.968.21

GENERALIZED FRACTIONAL GAUSSIAN NOISE PREDICTION BASED ON THE WALSH FUNCTIONS

Gorev V. N. – PhD, Associate Professor, Head of the Department of Physics, Dnipro University of Technology, Dnipro, Ukraine.

Gusev A. Yu. – PhD, Associate Professor, Professor of the Department of Information Security and Telecommunications, Dnipro University of Technology, Dnipro, Ukraine.

Korniienko V. I. – Dr. Sc., Professor, Head of the Department of Information Security and Telecommunications, Dnipro University of Technology, Dnipro, Ukraine.

Shedlovska Y. I. – PhD, Associate Professor of Department of Information Technology and Computer Engineering, Dnipro University of Technology, Dnipro, Ukraine.

ABSTRACT

Context. Some of the authors' recent papers were devoted to the Kolmogorov-Wiener filter for telecommunication traffic prediction in some stationary models, such as the fractional Gaussian noise model, the power-law structure function model, and the GFSD (Gaussian fractional sum-difference) model. Recently, the so-called generalized fractional Gaussian noise model was proposed for stationary telecommunication traffic description in some cases. So, in this paper the theoretical fundamentals of the continuous Kolmogorov-Wiener filter used for the prediction of the generalized fractional Gaussian noise are investigated.

Objective. The aim of the work is to obtain the filter weight function as an approximate solution of the corresponding Wiener–Hopf integral equation with the kernel equal to the generalized fractional Gaussian noise correlation function.

Method. A truncated Walsh function expansion is proposed in order to obtain the corresponding solution. This expansion is a special case of the Galerkin method, in the framework of which the unknown function is sought as a truncated series in orthogonal functions. The integral brackets and the results for the mean absolute percentage errors, which are a measure of discrepancy between the left-hand side and the right-hand side of the Wiener-Hopf integral equation, are calculated numerically on the basis of the Wolfram Mathematica package.

Results. The investigation is made for approximations up to sixty four Walsh functions. Different model parameters are investigated. It is shown that for different model parameters the proposed method is convergent and leads to small mean absolute percentage errors for approximations of rather large numbers of Walsh functions.

Conclusions. The paper is devoted to a theoretical construction of the continuous Kolmogorov-Wiener filter weight function for the prediction of a stationary random process described by the generalized fractional Gaussian noise model. As is known, this model may give a good description of some actual telecommunication traffic data in systems with packet data transfer. The corresponding weight function is sought on the basis of the truncated Walsh function expansion method. The corresponding discrepancy errors are small and the method is convergent.

KEYWORDS: continuous Kolmogorov-Wiener filter, weight function, Galerkin method, Walsh functions, generalized fractional Gaussian noise, telecommunication traffic.

ABBREVIATIONS

GFGN is a generalized fractional Gaussian noise;
FGN is a fractional Gaussian noise;
GFSD is Gaussian fractional sum-difference;
MAPE is a mean absolute percentage error.

NOMENCLATURE

T is a time interval on which the input process data are observed;

z is a time interval for which the forecast should be made;

$h(t)$ is the Kolmogorov-Wiener filter weight function;

H is the Hurst exponent;

$R(t)$ is a traffic correlation function in the GFGN model;

$a \in (0,1]$ is a GFGN model parameter;

σ is a traffic standard deviation;

n is a number of Walsh functions in the corresponding approximations;

g_s are coefficients multiplying the Walsh functions;

DOI 10.15588/1607-3274-2023-3-5

$\text{wal}_s(t)$ are the Walsh functions in the Walsh numeration orthogonal on $t \in [0,T]$;

Left(t) is the left-hand side of the Wiener-Hopf integral equation;

Right(t) is the right-hand side of the Wiener-Hopf integral equation;

G_{ks} are integral brackets;

B_k are free terms in the linear system of algebraic equations in g_s;

$W_{ls}^{(n)}$ are values of the Walsh functions in corresponding points;

V_{ls}, Q_s are auxiliary integrals.

INTRODUCTION

The problem of traffic prediction is very important for telecommunications, see the corresponding description in [1, 2].

Our recent papers were devoted to such a simple approach as the Kolmogorov-Wiener filter for stationary traffic prediction. For example, in our recent paper [3] it is shown that both the continuous and the discrete Kolmogorov-Wiener filter may be applicable to the prediction of smoothed heavy-tail data similar to FGN which may describe telecommunication traffic in systems with data packet transfer.

Recently Ming Li proposed a GFGN model for stationary traffic description [4]. The theoretical fundamentals of the Kolmogorov-Winer filter construction for traffic in the GFGN model are still to be investigated, so this paper is devoted to the corresponding investigation.

The object of study is the Kolmogorov-Wiener filter for the prediction of continuous stationary telecommunication traffic in the GFGN model.

The subject of study is the weight function of the corresponding filter.

The aim of the work is to obtain the weight function on the basis of the truncated Walsh function expansion method.

1 PROBLEM STATEMENT

The weight function under consideration obeys the following Wiener-Hopf integral equation, see, for example, [5]:

$$\int_0^T d\tau h(\tau) R(t-\tau) = R(t+z) \qquad (1)$$

where the traffic correlation function in the GFGN model is as follows [4]:

$$R(t) = \frac{\sigma^2}{2}\left(\left(|t|^a + 1\right)^{2H} + \left||t|^a - 1\right|^{2H} - 2|t|^{2aH}\right). \qquad (2)$$

It should be stressed that in the case where $a = 1$ the GFGN model coincides with the FGN model.

The problem statement is as follows: to obtain the unknown filter weight function as an approximate solution of equation (1) with the correlation function (2) on the basis of the truncated Walsh function expansion method.

2 REVIEW OF THE LITERATURE

There are a variety of different and rather sophisticated approaches to traffic prediction, see, for example, [6–8]. Our recent papers were devoted to the Kolmogorov-Wiener filter approach. For example, the theoretical fundamentals of the weigh function construction were investigated for the power-law structure function model [9], for the FGN model [10], and for the GFSD model [11]. Telecommunication traffic in the systems with data packet transfer nowadays is treated as a heavy-tail random process, see, for example, [12–14] and references therein. In [3], the applicability of the Kolmogorov-Wiener filter to the prediction of smoothed heavy-tail data is shown.

In [4], the so-called GFGN model for traffic description is proposed. For example, in [4] it is stressed that such a model gives a good description of the experimental traffic data recorded by the Bellcore in 1989, recorded by the Digital Equipment Corporation in 1995, and recorded by the Measurement and Analysis on the Working Group Traffic Archive in 2019.

Any theoretical construction of the continuous Kolmogorov-Wiener filter for the prediction of a process described by the GFGN model is still to be done. So, the aim of this paper is to obtain the corresponding filter weight function.

The corresponding investigation is made in the framework of the Galerkin method [15] on the basis of a Walsh function expansion. The Walsh functions in the Walsh numeration are used, see [16].

3 MATERIALS AND METHODS

The unknown weight function is sought in the form

$$h(\tau) = \sum_{s=1}^{n} g_s \text{wal}_s(\tau), \qquad (3)$$

which on substitution into (1) followed by integration leads to the following matrix expression for the unknown coefficients g_s (see similar expressions, for example, in [11]):

$$\begin{pmatrix} g_1 \\ g_2 \\ \vdots \\ g_n \end{pmatrix} = \begin{pmatrix} G_{11} & G_{12} & \cdots & G_{1n} \\ G_{21} & G_{22} & \cdots & G_{2n} \\ \vdots & \vdots & \ddots & \vdots \\ G_{n1} & G_{n2} & \cdots & G_{nn} \end{pmatrix}^{-1} \cdot \begin{pmatrix} B_1 \\ B_2 \\ \vdots \\ B_n \end{pmatrix}, \qquad (4)$$

where

DOI 10.15588/1607-3274-2023-3-5

$$G_{ks} = \int_0^T \int_0^T d\tau dt \mathrm{wal}_k(t)\,\mathrm{wal}_s(\tau) R(t-\tau),$$
$$B_k = \int_0^T dt \mathrm{wal}_k(t) R(t+z). \quad (5)$$

Similarly to [16], it may be shown that

$$G_{jk} = \sum_{l,s=1}^{n} W_{jl}^{(n)} W_{ks}^{(n)} V_{ls} \quad (6)$$

where

$$W_{jl}^{(n)} = \mathrm{wal}_j\left(\frac{(2l-1)T}{2n}\right),$$
$$V_{ls} = \int_{\frac{(l-1)T}{n}}^{\frac{lT}{n}} \int_{\frac{(s-1)T}{n}}^{\frac{sT}{n}} dt d\tau R(t-\tau). \quad (7)$$

Similarly to [16], it may be shown that

$$V_{ls} = V_{l+1,s+1},\ V_{ls} = V_{sl},\ G_{jk} = G_{kj}, \quad (8)$$

so only the quantities V_{1l}, $l = \overline{1,n}$ should be calculated on the basis of the integration (7), while all the other quantities V_{ls} may be calculated on the basis of (8) with account for calculated results for V_{1l}. The corresponding analytical calculation may meet difficulties, so the following approximate expressions were used:

$$V_{1l} = \int_0^{\frac{T}{n}} \int_{\frac{(l-1)T}{n}}^{\frac{lT}{n}} dt d\tau R(t-\tau) \approx \sum_{i,j} R(i-j)\cdot 10^{-3}\cdot 10^{-3},$$
$$i = 0.1\cdot 10^{-3}, 2\cdot 10^{-3}, \ldots, \text{ and so on while } i < T/n,$$
$$j = \frac{(l-1)T}{n}, \frac{(l-1)T}{n} + 1\cdot 10^{-3}, \frac{(l-1)T}{n} + 2\cdot 10^{-3}, \ldots,$$
$$\text{and so on while } j < lT/n. \quad (9)$$

The idea of (9) is that the square region $\tau \in [0, T/n]$, $t \in [(l-1)T/n, lT/n]$ is divided into small squares with a side equal to 10^{-3}. Of course, such a calculation is valid only if $T/n \gg 10^{-3}$, but this inequality holds in the framework of the numerical calculations made in this paper.

Similarly to [16], it may be shown that

$$B_k = \sum_{s=1}^{n} W_{ks}^{(n)} Q_s \quad (10)$$

where

$$Q_s = \int_{(s-1)T/n}^{sT/n} dt R(t+z). \quad (11)$$

The integrals Q_s are calculated in the Wolfram Mathematica package by direct integral calculation.

So, the quantities V_{1l} are calculated on the basis of (9), all the other quantities V_{ls} are calculated from V_{1l} on the basis of (8), and the corresponding integral brackets G_{jk} are calculated on the basis of (6) with account for (7) and (8). The coefficients B_k are calculated on the basis of (10) with account for (11). Then the unknown coefficients g_s are calculated on the basis of (4), and the unknown weight function is obtained on the basis of (3).

4 EXPERIMENTS

The following values of the parameters are investigated:

$$T = 100,\ z = 3,\ H = 0.75. \quad (12)$$

The following values of the model parameters are investigated: $a = 0.8$, $a = 0.4$, and $a = 0.08$. The quality of the obtained solution for the weight function is checked by the calculation of the corresponding MAPE error, which is a measure of discrepancy between the left-hand side and the right-hand side of equation (1):

$$\mathrm{MAPE} = \frac{1}{T}\int_0^T \left|\frac{\mathrm{Left}(t) - \mathrm{Right}(t)}{\mathrm{Right}(t)}\right| dt \cdot 100\% \quad (13)$$

where

$$\mathrm{Left}(t) = \int_0^T d\tau h(\tau) R(t-\tau),\ \mathrm{Right}(t) = R(t+z). \quad (14)$$

The method of trapezoids is used for an approximate numerical calculation of the function Left(t):

$$\mathrm{Left}(t) \approx \sum_j \left(\frac{T}{10^3}\cdot\frac{1}{2}\cdot\left(h(j)R(t-j) + h\left(j+\frac{T}{10^3}\right)R\left(t-j-\frac{T}{10^3}\right)\right)\right),$$
$$j = 0, 1\cdot\frac{T}{10^3}, 2\cdot\frac{T}{10^3}, \ldots, \left(10^3-1\right)\cdot\frac{T}{10^3}. \quad (15)$$

The MAPE is roughly estimated as

DOI 10.15588/1607-3274-2023-3-5

$$\mathrm{MAPE} = \frac{1}{10^2}\cdot\sum_j \left|\frac{\mathrm{Left}(j)-\mathrm{Right}(j)}{\mathrm{Right}(j)}\right|\cdot 100\%, \quad (16)$$
$$j = 0{,}1\cdot\frac{T}{10^2}, 2\cdot\frac{T}{10^2}, ..., \left(10^2-1\right)\cdot\frac{T}{10^2}.$$

Numerical results for the MAPE are given in the next section.

5 RESULTS

The obtained results for the MAPE are given in Table 1.

Table 1 – MAPE values (in %, rounded off to 2 significant digits) for the approximation of n Walsh functions for different values of the parameter a

	$a = 0.08$	$a = 0.4$	$a = 0.8$
$n = 2$	1.9	7.6	15
$n = 4$	0.93	3.4	6.7
$n = 8$	0.66	1.7	3.0
$n = 16$	0.44	0.92	1.5
$n = 32$	0.30	0.40	0.62
$n = 64$	0.23	0.37	0.50

Comparison graphs for the approximations of 64 Walsh functions are given in Fig. 1 – Fig. 3.

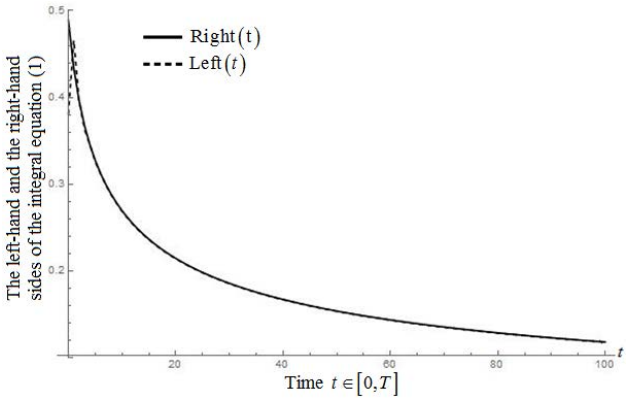

Figure 1 – Graphs of Left(t) and Right(t) for the approximation of 64 Walsh functions; $a = 0.8$

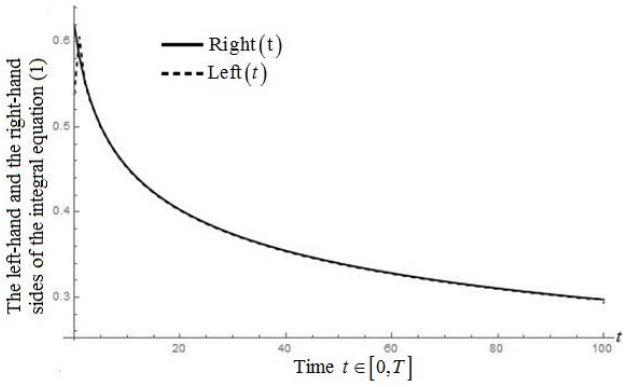

Figure 2 – Graphs of Left(t) and Right(t) for the approximation of 64 Walsh functions; $a = 0.4$

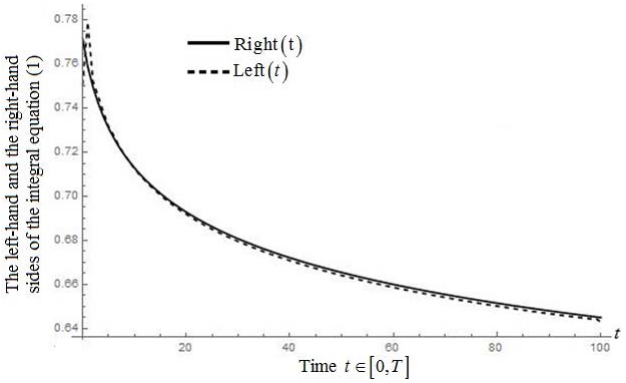

Figure 3 – Graphs of Left(t) and Right(t) for the approximation of 64 Walsh functions; $a = 0.08$

As can be seen, the left-hand side and the right-hand side of (1) are rather close.

6 DISCUSSION

As can be seen, the approximations of rather great numbers of the Walsh functions are accurate enough. The accuracy increases with the number of the Walsh functions. Thus, the proposed method of solving the integral equation (1) is convergent for the correlation function (2).

It should also be stressed that the corresponding approximations are rather accurate for all the three considered values of the parameter a, thus indicating that the proposed method works well. Of course, the estimation of the MAPE on the basis of (16) is rather rough, but it is adequate in order of magnitude. As can be seen from the obtained graphs, the left-hand side of the integral equation (1) is indeed rather close to the corresponding right-hand side for the approximation of 64 Walsh functions.

The paper is devoted to a theoretical construction of the continuous Kolmogorov-Wiener filter weight function for the prediction of a stationary random process described by the GFGN model. As indicated in [4], that model may give a good description of some actual telecommunication traffic data.

The corresponding weight function is the solution of the Wiener-Hopf integral equation (1). This equation is solved on the basis of the Galerkin method with the help of a truncated expansion in the Walsh functions. The Walsh functions in the Walsh numeration are used. The algorithm of the weight function derivation is described in detail. The quality of agreement between the left-hand side and the right-hand side of the integral equation is estimated by the MAPE parameter. It is shown that for a rather large number of Walsh functions the agreement is good enough, and the corresponding MAPE values are rather small. Graph comparisons are given to illustrate the fact that the corresponding left-hand side is indeed close to the corresponding right-hand side for the obtained solutions. It is shown that the MAPE decreases with the number of Walsh functions, which justifies the convergence of the method. The approximations of up to 64 Walsh functions are investigated. The calculations are made with the help of the Wolfram Mathematica package.

DOI 10.15588/1607-3274-2023-3-5

The use of a Walsh function expansion is known not only for integral equations, but also for variational calculus, see [17, 18]. As is known, variational calculus is widely used in optimal control problems, see, for example, [19, 20]. Paper [20] is devoted to a practical electrical engineering problem, so the mathematics of this paper may be applicable in part to, for example, electrical engineering problems.

CONCLUSIONS

The Kolmogorov-Wiener filter weight function for the prediction of continuous stationary telecommunication traffic in the GFGN model is calculated on the basis of the truncated Walsh function expansion method. Approximations up to 64 Walsh functions are investigated. The convergence of the method is illustrated.

The results of this paper may be useful for the practical prediction of stationary telecommunication traffic in systems with data packet transfer.

The scientific novelty of the paper is the fact that for the first time the Kolmogorov-Wiener filter weight function is calculated for the prediction of telecommunication traffic in the GFGN model.

The practical significance is that the obtained results may be applied to the practical prediction of telecommunication traffic in systems with data packet transfer.

Prospects for further research are to investigate the Galerkin method for other orthogonal systems of functions, for example, polynomial or trigonometric ones, and to compare the obtained MAPE results with the results based on the Walsh functions. Another plan for the future is to generate simulated data described by the GFGN model and to investigate the corresponding prediction for them.

ACKNOWLEDGEMENTS

The work was made in the framework of the Project “Research of methods of increase of efficiency of the automated control of thermal work of units of high power of industrial and household function” (State Registration No. 0122U002601) of the Dnipro University of Technology.

REFERENCES

1. Jacob S., Y. Qiao, Y. Ye et al.] Anomalous distributed traffic: Detecting cyber security attacks amongst micro-services using graph convolutional networks, *Computers & Security*. 2022, Vol. 118, 102728 (13 pages). DOI: 10.1016/j.cose.2022.102728.
2. Alqahtani H. Learning and prediction of cyber-attack based on correlation mapping in classical optical networks, *Optical and Quantum Electronics*, 2022, Vol. 54, 776. DOI: 10.1007/s11082-022-04176-8.
3. Gorev V., Gusev A., Korniienko V. et al. On the use of the Kolmogorov-Wiener filter for heavy-tail process prediction, *Journal of Cyber Security and Mobility*, 2023, Vol. 12, № 3, pp. 315–338. DOI: 10.13052/jcsm2245-1439.123.4.
4. Li M. Direct Generalized fractional Gaussian noise and its application to traffic modeling, *Physica A*, 2021, Vol. 579, 126138 (22 pages). DOI: 10.1016/j.physa.2021.126138
5. Miller S., Childers D. Probability and Random Processes With Applications to Signal Processing and Communications. Second edition. Amsterdam, Academic Press, 2012, 598 p. DOI: 10.1016/B978-0-12-386981-4.50001-1
6. Alghamdi VT., Mostafi S., Abdelkader G. et al. A Comparative Study on Traffic Modeling Techniques for Predicting and Simulating Traffic Behavior, *Future Internet*, 2022, Vol. 14, 294 (21 pages). DOI: 10.3390/fi14100294.
7. Dogra A. K., Kaur J. Oving towards smart transportation with machine learning and Internet of Things (IoT): a review, *Journal of Smart Environments and Green Computing*, 2022, Vol. 2, pp. 3–18. DOI: 10.20517/jsegc.2021.09.
8. Saha S., Haque A., Sidebottom G. An Empirical Study on Internet Traffic Prediction Using Statistical Rolling Model, *2022 International Wireless Communications and Mobile Computing (IWCMC)*, Dubrovnik, 30 May – 03 June, 2022 : proceedings. Los Alamitos, IEEE, 2022, pp. 1058–1063. DOI: 10.1109/IWCMC55113.2022.9825059.
9. Gorev V. N., Gusev A. Yu., Korniienko V. I. Polynomial solutions for the Kolmogorov-Wiener filter weight function for fractal processes, *Radio Electronics, Computer Science, Control*, 2019, № 2, pp. 44–52. DOI: 10.15588/1607-3274-2019-2-5.
10. Gorev V. N., Gusev A. Yu., Korniienko V. I. Approximate solutions for the Kolmogorov-Wiener filter weight function for continuous fractional Gaussian noise, *Radio Electronics, Computer Science, Control*, 2021, № 1, pp. 29–35. DOI: 10.15588/1607-3274-2021-1-3.
11. Gorev V. N., Gusev A. Yu., Korniienko V. I. Kolmogorov-Wiener filter for continuous traffic prediction in the GFSD model, *Radio Electronics, Computer Science, Control*, 2022. № 3, pp. 31–37. DOI: 10.15588/1607-3274-2022-3-3.
12. Kawaminami I., Estrada A., Elsakkary Y. et al. Large Scale Enrichment and Statistical Cyber Characterization of Network Traffic, *2022 IEEE High Performance Extreme Computing Conference, Massachusetts, September 19–23, 2022 : proceedings*. Los Alamitos, IEEE, 2022, pp. 1–7. DOI: 10.1109/HPEC55821.2022.9926397.
13. Wu H., Liu Y., Cheng G. et al. Real-time Identification of VPN Traffic based on Counting Bloom Filter and Chained Hash Table from Sampled Data in High-speed Networks, The ICC 2022 – IEEE International Conference on Communications, Seoul, Republic of Korea, 16–20 May 2022 : proceedings. Los Alamitos, IEEE, 2022, pp. 5070–5075. DOI: 10.1109/ICC45855.2022.9839256.
14. Popoola J., Popoola O. J., Olaniran O. R. Modelling Internet Traffic Streams with Ga/M/1/K Queuing Systems under Self-similarity, *Tanzania Journal of Science*, 2022, Vol. 28, pp. 394–401. DOI: 10.4314/tjs.v48i2.14.
15. Polyanin A. D., Manzhirov A. V.. Handbook of integral equations. Second edition. New York, Chapman and Hall, 2008, 1144 p. DOI: 10.1201/9781420010558.
16. Gorev V., Gusev A., Korniienko V. Fractional Gaussian Noise Traffic Prediction Based on the Walsh Functions, *CEUR Workshop proceedings*, 2021, Vol. 2853, pp. 389–400.
17. Chen C. F., Hsiao C. H. A walsh series direct method for solving variational problems, *Journal of the Franklin Institute*, 1975, Vol. 300, № 4, pp. 265–280. DOI: 10.1016/0016-0032(75)90199-4

DOI 10.15588/1607-3274-2023-3-5

18. Ordokhani Y. Direct Walsh-Hybrid Method for Variational Problems, *International Journal of Nonlinear Science*, 2011, Vol. 11, № 1, pp. 114–120.
19. Kupenko O. P, Manzo R. Approximation of an optimal control problem in coefficient for variational inequality with anisotropic p-laplacian, *Nonlinear Differential Equations and Applications*, 2016, Vol. 23, № 3, 35 (18 pages). DOI: 10.1007/s00030-016-0387-9
20. Diachenko G., Aziukovskyi O., Rogoza M. et al. Optimal Field-Oriented Control of an Induction Motor for Loss Minimization in Dynamic Operation, *2019 IEEE International Conference on Modern Electrical and Energy Systems (MEES), Kremenchuk, 23–25 September 2019, proceedings*. Los Alamitos, IEEE, 2019, pp. 94–97. DOI: 10.1109/MEES.2019.8896455.

Received 05.06.2023.
Accepted 26.08.2023.

УДК 51–74, 517.968.21

ПРОГНОЗУВАННЯ УЗАГАЛЬНЕНОГО ФРАКТАЛЬНОГО ГАУСІВСЬКОГО ШУМУ НА ОСНОВІ ФУНКЦІЙ ВОЛША

Горєв В. М. – канд. фіз.-мат. наук, доцент, завідувач кафедри фізики, Національний технічний університет «Дніпровська Політехніка», Дніпро, Україна.

Гусєв О. Ю. – канд.фіз.-мат. наук, доцент, професор кафедри безпеки інформації та телекомунікацій, Національний технічний університет «Дніпровська Політехніка», Дніпро, Україна.

Корнієнко В. І. – д-р техн. наук, професор, завідувач кафедри безпеки інформації та телекомунікацій, Національний технічний університет «Дніпровська Політехніка», Дніпро, Україна.

Шедлоська Я. І. – канд. техн. наук, доцент кафедри інформаційних технологій та комп'ютерної інженерії, Національний технічний університет «Дніпровська Політехніка», Дніпро, Україна.

АНОТАЦІЯ

Актуальність. Деякі з нещодавніх статей авторів присвячені фільтру Колмогорова-Вінера для прогнозування телекомунікаційного трафіку в деяких стаціонарних моделях, таких як модель фрактального гаусівського шуму, модель степеневої структурної функції та GFSD (Gaussian fractional sum-difference) модель. Нещодавно так звана модель узагальненого фрактального гаусівського шуму була запропонована для опису стаціонарного телекомунікаційного трафіку в деяких випадках. Тож в цій статті досліджено теоретичні основи неперервного фільтра Колмогорова-Вінера, застосовного для прогнозування узагальненого фрактального гаусівського шуму.

Мета роботи. Метою роботи є отримати вагову функцію фільтра як наближений розв'язок відповідного інтегрального рівняння Вінера-Хопфа з ядром, що дорівнює кореляційній функції узагальненого фрактального гаусівського шуму.

Метод. Метод обірваних розвинень за функціями Волша запропоновано для отримання відповідного розв'язку. Таке розвинення є частинним випадком методу Галеркіна, в рамках якого невідома функція шукається у вигляді обірваного розвинення за ортогональними функціями. Інтегральні дужки та результати для середньої абсолютної відсоткової помилки відхилу лівої частини інтегрального рівняння Вінера-Хопфа від правої обчислені чисельно на основі пакету Wolfram Mathematica.

Результати. Дослідження зроблене для наближень включно до наближення шістдесяти чотирьох функцій Волша. Досліджено різні параметри моделі. Показано, що для різних параметрів моделі запропонований метод є збіжним та призводить до малих середніх абсолютних відсоткових помилок для наближень доволі великої кількості функцій Волша.

Висновки. Статтю присвячено теоретичній побудові вагової функції неперервного фільтра Колмогорова-Вінера для прогнозування стаціонарного випадкового процесу, що описується моделлю узагальненого фрактального гаусівського шуму. Як відомо, така модель може добре описувати певні експериментальні дані в системах з пакетною передачею даних. Відповідна вагова функція шукається на основі обірваного розвинення за функціями Волша. Відповідні помилки відхилу є малими та метод є збіжним.

КЛЮЧОВІ СЛОВА: неперервний фільтр Колмогорова-Вінера, вагова функція, метод Галеркіна, функції Волша, узагальнений фрактальний гаусівський шум, телекомунікаційний трафік.

ЛІТЕРАТУРА

1. Anomalous distributed traffic: Detecting cyber security attacks amongst micro-services using graph convolutional networks / [S. Jacob, Y. Qiao, Y. Ye et al.] // Computers & Security. – 2022. – Vol. 118. – 102728 (13 pages). DOI: 10.1016/j.cose.2022.102728.
2. Alqahtani H. Learning and prediction of cyber-attack based on correlation mapping in classical optical networks / H. Alqahtani // Optical and Quantum Electronics. – 2022. – Vol. 54. – 776. DOI: 10.1007/s11082-022-04176-8.
3. On the use of the Kolmogorov-Wiener filter for heavy-tail process prediction / [V. Gorev, A. Gusev, V. Korniienko et al.] // Journal of Cyber Security and Mobility. – 2023. – Vol. 12, № 3. – P. 315–338. DOI: 10.13052/jcsm2245-1439.123.4.
4. Li M. Direct Generalized fractional Gaussian noise and its application to traffic modeling / M. Li // Physica A. – 2021. – Vol. 579. – 126138 (22 pages). DOI: 10.1016/j.physa.2021.126138
5. Miller S. Probability and Random Processes With Applications to Signal Processing and Communications. Second edition / S. Miller, D. Childers. – Amsterdam: Academic Press, 2012. – 598 p. DOI: 10.1016/B978-0-12-386981-4.50001-1
6. A Comparative Study on Traffic Modeling Techniques for Predicting and Simulating Traffic Behavior / [VT. Alghamdi, S. Mostafi, G. Abdelkader et al.] // Future Internet. – 2022. – Vol. 14. – 294 (21 pages). DOI: 10.3390/fi14100294.
7. Dogra A. K. oving towards smart transportation with machine learning and Internet of Things (IoT): a review / A. K. Dogra, J. Kaur // Journal of Smart Environments and Green Computing. – 2022. – Vol. 2. – P. 3–18. DOI: 10.20517/jsegc.2021.09.
8. Saha S. An Empirical Study on Internet Traffic Prediction Using Statistical Rolling Model / S. Saha, A. Haque,

DOI 10.15588/1607-3274-2023-3-5

G. Sidebottom // 2022 International Wireless Communications and Mobile Computing (IWCMC), Dubrovnik, 30 May – 03 June, 2022 : proceedings. Los Alamitos: IEEE, 2022. – P. 1058–1063. DOI: 10.1109/IWCMC55113.2022.9825059.

9. Gorev V. N. Polynomial solutions for the Kolmogorov-Wiener filter weight function for fractal processes / V. N. Gorev, A. Yu. Gusev, V. I. Korniienko // Radio Electronics, Computer Science, Control. – 2019. – № 2. – P. 44–52. DOI: 10.15588/1607-3274-2019-2-5.
10. Gorev V. N. Approximate solutions for the Kolmogorov-Wiener filter weight function for continuous fractional Gaussian noise / V. N. Gorev, A. Yu. Gusev, V. I. Korniienko // Radio Electronics, Computer Science, Control. – 2021. – № 1. – P. 29–35. DOI: 10.15588/1607-3274-2021-1-3.
11. Gorev V. N. Kolmogorov-Wiener filter for continuous traffic prediction in the GFSD model / V. N. Gorev, A. Yu. Gusev, V. I. Korniienko // Radio Electronics, Computer Science, Control. – 2022. – № 3. – P. 31–37. DOI: 10.15588/1607-3274-2022-3-3.
12. Large Scale Enrichment and Statistical Cyber Characterization of Network Traffic / [I. Kawaminami, A. Estrada, Y. Elsakkary et al.] // 2022 IEEE High Performance Extreme Computing Conference, Massachusetts, September 19–23, 2022 : proceedings. Los Alamitos: IEEE, 2022. – P. 1–7. DOI: 10.1109/HPEC55821.2022.9926397.
13. Real-time Identification of VPN Traffic based on Counting Bloom Filter and Chained Hash Table from Sampled Data in High-speed Networks / [H. Wu, Y. Liu, G. Cheng et al.] // The ICC 2022 – IEEE International Conference on Communications, Seoul, Republic of Korea, 16–20 May 2022 : proceedings. Los Alamitos: IEEE, 2022. – P. 5070–5075. DOI: 10.1109/ICC45855.2022.9839256.
14. Popoola J. Modelling Internet Traffic Streams with Ga/M/1/K Queuing Systems under Self-similarity / J. Popoola, O. J. Popoola, O. R. Olaniran // Tanzania Journal of Science. – 2022. – Vol. 28. – P. 394–401. DOI: 10.4314/tjs.v48i2.14.
15. Polyanin A. D. Handbook of integral equations. Second edition / A. D. Polyanin, A. V. Manzhirov. – New York : Chapman and Hall, 2008. – 1144 p. DOI: 10.1201/9781420010558.
16. Gorev V. Fractional Gaussian Noise Traffic Prediction Based on the Walsh Functions / V. Gorev, A. Gusev, V. Korniienko // CEUR Workshop proceedings. – 2021. – Vol. 2853. – P. 389–400.
17. Chen C. F. A walsh series direct method for solving variational problems / C.F. Chen, C.H. Hsiao // Journal of the Franklin Institute. – 1975. – Vol. 300, № 4. – P. 265–280. DOI: 10.1016/0016-0032(75)90199-4
18. Ordokhani Y. Direct Walsh-Hybrid Method for Variational Problems / Y. Ordokhani // International Journal of Nonlinear Science. – 2011. – Vol. 11, №1. – P. 114–120.
19. Kupenko O. P. Approximation of an optimal control problem in coefficient for variational inequality with anisotropic p-laplacian / O. P. Kupenko, R. Manzo // Nonlinear Differential Equations and Applications. – 2016. – Vol. 23, № 3. – 35 (18 pages). DOI: 10.1007/s00030-016-0387-9
20. Optimal Field-Oriented Control of an Induction Motor for Loss Minimization in Dynamic Operation / [G. Diachenko, O. Aziukovskyi, M. Rogoza et al.] // 2019 IEEE International Conference on Modern Electrical and Energy Systems (MEES), Kremenchuk, 23–25 September 2019 : proceedings. Los Alamitos : IEEE, 2019. – P. 94–97. DOI: 10.1109/MEES.2019.8896455.

DOI 10.15588/1607-3274-2023-3-5

UDC 519.24

GROWING TREE METHOD FOR OPTIMISATION OF MULTIFACTORIAL EXPERIMENTS

Koshovyi M. D. – Dr. Sc., Professor, Professor of the Department of Intelligent Measuring Systems and Quality Engineering, National Aerospace University M. E. Zhukovsky "Kharkiv Aviation Institute", Kharkiv, Ukraine.

Pylypenko O. T. – Post-graduate student of the Department of Intelligent Measuring Systems and Quality Engineering, National Aerospace University M. E. Zhukovsky "Kharkiv Aviation Institute", Kharkiv, Ukraine.

Ilyina I. V. – PhD, Associate Professor, Associate Professor of the Department of Electronic Computing, Kharkiv National University of Radio Electronics, Kharkiv, Ukraine.

Tokarev V. V. – PhD, Associate Professor, Associate Professor of the Department of Electronic Computing, Kharkiv National University of Radio Electronics, Kharkiv, Ukraine.

ABSTRACT

Context. The task of planning multifactorial experiments is important in science and industrial production. In the context of competition, rising costs, and increasing efficiency, it is necessary to optimize plans for multifactorial experiments in terms of cost and time. To solve this problem, there are a number of approaches and methods, the choice of which for a competitive technical task is an important and difficult task. In this regard, there is a need to develop new methods for optimizing the cost (time) of multifactorial experiment plans, compare them with existing methods, and give recommendations for practical application in the study of real objects.

Objective. The purpose of the study is to develop and test the method of growing trees, to evaluate its effectiveness in comparison with other methods. The following tasks has been solved to achieve this goal: the proposed method of growing trees has been implemented in the form of software; the method has been used to optimize plans for multifactorial experiments in the study of real objects; its effectiveness has been evaluated in comparison with other methods; recommendations for its use were given.

Method. The proposed method of growing trees is based on the application of graph theory. The advantage of the method is the reduction of time for solving optimization problems related to the construction of optimal plans for multifactorial experiments in terms of cost (time) expenses. Another characteristic feature is the high accuracy of solving optimization problems.

Results. The results of experiments and comparisons with other optimization methods confirm the efficiency and effectiveness of the proposed method and allow us to recommend it for the study of objects with the number of significant factors $k \leq 7$. It is promising to further expand the range of scientific and industrial objects for their study using this method.

Conclusions. A growing tree method has been developed for the optimization of multifactorial experimental plans in terms of cost and time expenditures, along with software that implements it using the Angular framework and the TypeScript programming language.

The effectiveness of the growing tree method is shown in comparison with the following methods: complete and limited enumeration, monkey search, modified Gray code application, and bacterial optimization. The growing tree method is faster than complete enumeration and can be applied to optimize multifactorial experimental plans in terms of cost (time) expenses for objects with a number of factors $k \leq 7$. In solving optimization problems, the method of growing trees gives better results compared to monkey search, limited enumeration and bacterial optimization.

KEYWORDS: growing tree method, algorithm, multifactorial experiment, software, comparison.

NOMENCLATURE

X_{IE} is a matrix of the initial plan of the multifactorial experiment;

X_i^j is a value of the *i*-th factor of the process under study in the j-th experiment;

k is a number of factors of the research object;

N is a number of experiments in the experiment planning matrix;

S_{tl} is a matrix of transition costs of factor levels;

$S^i_{(+1)(-1)}, S^i_{(-1)(+1)}$ is a value of the cost of level transitions for the *i*-th factor;

t_{tl} – matrix of transition durations of factor levels;

$t^i_{(+1)(-1)}, t^i_{(-1)(+1)}$ is a value of the duration of level transitions for the *i*-th factor;

X_{opt} is a matrix of the optimal or near-optimal experiment plan;

S_t is a total cost of the experiment;

$S_{i,j}$ is a cost of installing the *i*-th factor in the *j*-th experiment;

t_t is total time of the experiment;

$t_{i,j}$ is a duration of the installation of the *i*-th factor in the *j*-th experiment.

INTRODUCTION

Saving resources and time is an important issue in industrial production and scientific research. Due to global inflation, the cost of resources is increasing, which leads to the need to optimize technological processes, production, etc. By optimizing, a company reduces the amount of raw materials required, shortens production time, and increases its potential and efficiency. Therefore, the issue of optimizing plans for multifactorial experiments in terms of cost and time is relevant.

The object of study: the process of optimizing plans for multifactorial experiments in terms of cost and time.

DOI 10.15588/1607-3274-2023-3-6

The subject of study: the method of growing trees for optimization of multifactorial experimental plans in terms of cost and time and the software that implements it.

The purpose of the work: development of the growing tree method and the software that implements it; application of the method to optimize the plans of multifactorial experiments; comparison with other optimization methods and evaluation of its effectiveness.

1 PROBLEM STATEMENT

For a given matrix X_{IE} of the initial plan of a multifactorial experiment

$$X_{IE} = \begin{vmatrix} X_1^1 & X_2^1 & \dots & X_i^1 & \dots & X_k^1 \\ X_2^1 & X_2^2 & \dots & X_i^2 & \dots & X_k^2 \\ \dots & \dots & \dots & \dots & \dots & \dots \\ X_1^j & X_2^j & \dots & X_i^j & \dots & X_k^j \\ X_1^N & X_2^N & \dots & X_k^N & \dots & X_k^N \end{vmatrix} \quad (1)$$

and a matrix of transition costs of factor levels S_{tl}, or a matrix of transition durations of factor levels ttl

$$S_{tl} = \begin{vmatrix} S^1_{(+1)(-1)} & S^1_{(-1)(-1)} \\ S^2_{(+1)(-1)} & S^2_{(-1)(+1)} \\ \dots \dots & \dots \dots \\ S^i_{(+1)(-1)} & S^i_{(-1)(+1)} \\ \dots \dots & \dots \dots \\ S^k_{(+1)(-1)} & S^k_{(-1)(+1)} \end{vmatrix},$$

$$t_{tl} = \begin{vmatrix} t^1_{(+1)(-1)} & t^1_{(-1)(-1)} \\ t^2_{(+1)(-1)} & t^2_{(-1)(+1)} \\ \dots \dots & \dots \dots \\ t^i_{(+1)(-1)} & t^i_{(-1)(+1)} \\ \dots \dots & \dots \dots \\ t^k_{(+1)(-1)} & t^k_{(-1)(+1)} \end{vmatrix} \quad (2)$$

it is necessary to find the optimal or near-optimal experiment plan X_{opt}, for which the total cost or duration of the experiment is minimized, i. e.

$$S_t = \sum_{j=2}^{N}\sum_{i=1}^{k} S_{i,j} \to \min;$$

$$t_t = \sum_{j=2}^{N}\sum_{i=1}^{k} t_{i,j} \to \min. \quad (3)$$

2 REVIEW OF THE LITERATURE

The following optimization methods can be applied to solve the problem of constructing optimal plans for multifactorial experiments in terms of cost (time) expenses: lion [1], black hole [2], grey wolf [3], artificial algae algorithm [4], firefly algorithm [5], hunting search [6], water cycle algorithm [7], bat algorithm [8], binary dragonfly algorithm [9], binary butterfly algorithm [10], cat swarm optimization [11], cuckoo search [12], dolphin echolocation algorithm [13], flower pollination algorithm [14], honey bee mating optimization [15], fish migration optimization [16], immune algorithm [17], tumbleweed algorithm [18], ant lion optimization [19].

Currently, the following methods have been developed and tested to optimize experimental plans in terms of cost (time): permutation analysis [20], complete enumeration [20, 21], particle swarm [20, 22, 23], genetic algorithm [20, 24], jumping frogs [20, 25], application of Gray code [20, 26], branch and bound [20, 21], monkey search [20, 27], fish school search [20, 28], ant algorithm [20], sequential approximation [20], greedy algorithm [20], nearest neighbor [20], tabu search [20, 23], simulated annealing [20, 29], nested partitions [20], combinatorial graph [20], based on serial sequences [20, 21], and simplex method [20].

Each of them has its own advantages and disadvantages [20]. When studying a variety of objects, each task of constructing optimal experimental plans has a technical task with its own priorities and conditions. Some objects require high optimization accuracy, while others require fast calculation. There are also difficulties with the fact that when using the method, you need to calculate many steps that are irrational, which leads to a large time spent on finding the optimal experiment plan. Therefore, the usefulness of a particular optimization method depends on the specific technical task.

In this regard, there is a need to develop and investigate the method of growing trees for optimizing multifactorial experimental plans in terms of cost (time) in order to assess its effectiveness.

3 MATERIALS AND METHODS

The growing tree optimization method is based on the use of tree graphs.

A tree is a connected acyclic graph in which one vertex has a zero in-degree and the other vertices have an in-degree of 1. The vertex with zero in-degree is called the root of the tree, and the vertices with zero out-degree are referred to as terminal vertices or leaves [30]. Figure 1 shows the standard representation of a tree graph, illustrating that there is only one path between any pair of vertices.

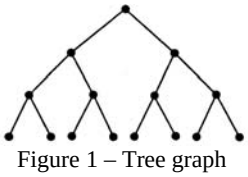

Figure 1 – Tree graph

The application of graph theory for analyzing plans of multifactorial experiment is considered on the example of the study of non-contact direct current and density meters [21]. Table 1 shows an experiment plan for the study of such meters.

DOI 10.15588/1607-3274-2023-3-6

Table 1 – Experimental plan for the study of non-contact direct current and density meters

Number	X_1	X_2
1	–1	–1
2	–1	+1
3	+1	–1
4	+1	+1

The cost of changing factor levels is shown in Table 2.

Table 2 – Cost of changing factors

Changing factors	X_1	X_2
From “–1” to “+1”	0.48	0.40
from “+1” to “–1”	0.50	0.42

After analyzing the experiment plan. we have four initial vertices for graph construction.

We optimized the experiment plan in terms of cost by constructing graphs for each of the four initial vertices (Fig. 2).

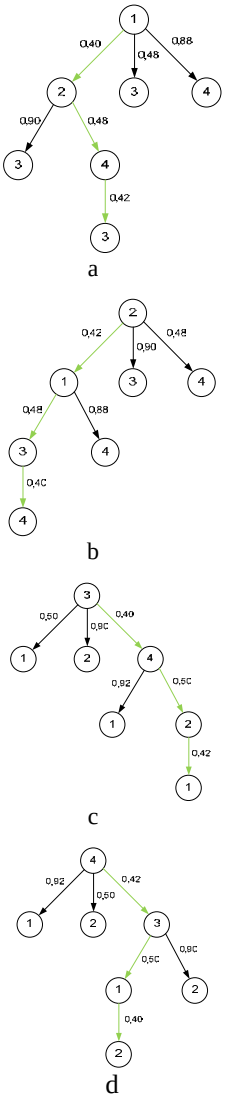

Figure 2 – Graph construction for each of the *i*-th vertices: a – *i* = 1; b – *i* = 2; c – *i* = 3; d – *i* = 4

After constructing the graphs for each of the possible vertices. we calculate the costs of implementing the experiment plans. which are shown in Table 3.

Table 3 – Cost of implementing the experimental plans

Vertex	Cost
1	1.30
2	1.30
3	1.32
4	1.32

Based on the calculation. we can conclude that the best performance is achieved with experiment plans represented by graphs with initial vertices 1 and 2. with a cost of 1.30 u. m.. compared to the initial plan’s cost of 1.70 u. m.

Thus. the gain in the cost of implementing the optimal plans compared to the initial plan is 1.31 times.

The algorithm for optimizing the cost (time) of a multifactorial experiment plan using the growing tree method is as follows.

Step 1. Select the number of factors.

Step 2. Input the transition costs values for each factor.

Step 3.1. Generate the initial plan matrix based on the number of factors.

Step 3.2. Determining the sequence of matrix calculations.

Step 4. Calculate the cost of the initial matrix.

Step 5.1. Inserting a row at the beginning of the matrix.

Step 5.1.1. Calculate the cost of the transition between the selected row and the next.

Step 5.1.2. Search for the minimum difference in the transition cost between the selected row and the row that has not yet been used in the matrix.

Step 5.1.3. All rows in the matrix have been used.

Step 5.1.4. Replace the initial row of the matrix with the next unused. and perform the calculation.

Step 5.2. All rows of the matrix have been substituted at its beginning and calculations have been performed according to the above scheme.

Step 6.1. Calculate the costs of all obtained matrices.

Step 6.2. Compare the costs of the obtained matrices.

Step 7. Select the matrix with the minimum total cost Based on the results.

Step 8. Compare and analyze the initial matrix with the optimal one calculated using the growing trees method.

Step 9. Display the results on the screen.

The algorithm diagram implementing the method of growing trees is presented in Figure 3.

The software implementation of the algorithm was performed using the Angular framework in the TypeScript development language [31]. which is an add-on to the JavaScript programming language. The advantage of using Angular is that it is built on the basic principles of object-oriented programming (OOP). OOP includes three main principles: encapsulation. inheritance. and polymorphism. These principles enable the creation of more modular and scalable programs that are easier to maintain and evolve. As a result. the number of input factors can be increased seamlessly.

DOI 10.15588/1607-3274-2023-3-6

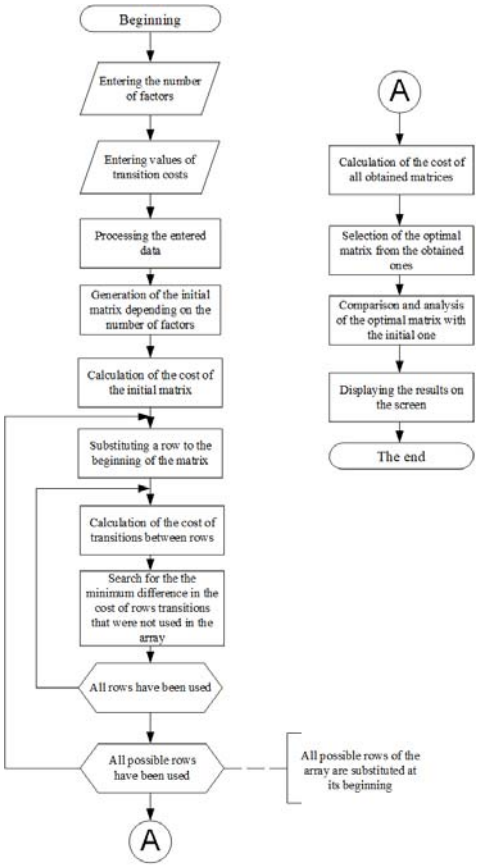

Figure 3 – Diagram of the algorithm for implementing the growing trees method

4 EXPERIMENTS

Optimization of multifactorial experiment plans was carried out using the method of growing trees. and a comparative analysis of the obtained experimental plans was performed with plans obtained using the following methods: monkey search. complete enumeration. limited enumeration. modified Gray code. bacterial optimization.

Optimization based on the cost expenses of the experiment plan has been conducted for the investigation of the technological process of welding thin plates. The factors considered: X_1 – capacitor capacity. μF; X_2 – conversion coefficient. X_3 – electrode force. N. The cost of changing the values of the factor levels is presented in Table 4.

The initial and optimal plans for conducting a multifactorial experiment for the investigation of the technological process of welding thin plates are provided in Tables 5 and 6 respectively.

Table 4 – Cost of changing the values of the factor levels

Factor	Costs of changes in the values of factor levels. u. m.	
	from “–1” to “+1”	from “+1” to “–1”
X_1	2.5	3
X_2	2	2.5
X_3	1.5	2

Table 5 – Initial plan of a multifactorial experiment

Experiment number	Factors		
	X_1	X_2	X_3
1	–1	–1	–1
2	+1	–1	–1
3	–1	+1	–1
4	+1	+1	–1
5	–1	–1	+1
6	+1	–1	+1
7	–1	+1	+1
8	+1	+1	+1

Table 6 – Optimal plan of a multifactorial experiment obtained by the growing tree method

Experiment number	Factors		
	X_1	X_2	X_3
1	–1	–1	–1
2	–1	–1	+1
3	–1	+1	+1
4	–1	+1	–1
5	+1	+1	–1
6	+1	+1	+1
7	+1	–1	+1
8	+1	–1	–1

The cost of the initial experiment plan is 27 u. m.. and the cost of the plans obtained by the growing tree method and full search is 14 u. m. The cost of the plan obtained by the monkey search method is 14.5 u. m. [32].

During the investigation of the accuracy of a device for measuring material humidity. the following factors were selected as dominant: X_1 – power supply voltage;

DOI 10.15588/1607-3274-2023-3-6

X_2 – resistance value connected to the output of the operational amplifier; X_3 – number of turns W in the main winding of the magnetostrictive transducer; X_4 – number of turns W1 in the additional winding 3 or 4 [21]. The cost of changing the levels of factor values is presented in Table 7.

The initial plan of a full factorial experiment for studying the accuracy of the material moisture meter is presented in Table 8.

As a result of applying the growing tree method. an optimal plan for a multifactorial experiment was obtained. as shown in Table 9.

Table 7 – Costs of changing factor level values

Factor	Costs of changing factor level values. u. m.	
	from “–1” to “+1”	from “+1” to “–1”
X_1	0.52	0.51
X_2	0.72	0.71
X_3	5.5	1.4
X_4	6.7	2.4

Table 8 – Initial plan of a multifactorial experiment

Experiment number	Factors			
	X_1	X_2	X_3	X_4
1	–1	–1	–1	–1
2	+1	–1	–1	–1
3	–1	+1	–1	–1
4	+1	+1	–1	–1
5	–1	–1	+1	–1
6	+1	–1	+1	–1
7	–1	+1	+1	–1
8	+1	+1	+1	–1
9	–1	–1	–1	+1
10	+1	–1	–1	+1
11	–1	+1	–1	+1
12	+1	+1	–1	+1
13	–1	–1	+1	+1
14	+1	–1	+1	+1
15	–1	+1	+1	+1
16	+1	+1	+1	+1

Table 9 – Initial plan of a multifactor experiment

Experiment number	Factors			
	X_1	X_2	X_3	X_4
1	+1	+1	+1	+1
2	–1	+1	+1	+1
3	–1	–1	+1	+1
4	+1	–1	+1	+1
5	+1	–1	–1	+1
6	–1	–1	–1	+1
7	–1	+1	–1	+1
8	+1	+1	–1	+1
9	+1	+1	–1	–1
10	–1	+1	–1	–1
11	–1	–1	–1	–1
12	+1	–1	–1	–1
13	+1	–1	+1	–1
14	–1	–1	+1	–1
15	–1	+1	+1	–1
16	+1	+1	+1	–1

The cost of the initial experiment plan is 31.84 u. m.. the cost of the plans obtained by the growing trees method and the method based on the use of the modified Gray code [33] is 16.28 u. m.

When investigating a section of the machine-building workshop [21]. the overall working time of computer numerically controlled (CNC) machines was chosen as the optimization criterion. The dominant factors affecting this metric were selected as follows: X_1 – maintenance time t_m. hours; X_2 – number of CNC machines y_m; X_3 – machine working time within a day t_d. hours; X_4 – maintenance periodicity t_0. The time for changing the levels of these factors is presented in Table 10. The initial and optimal plans for conducting the experiment on the CNC machine section are provided in Tables 11 and 12. respectively.

Table 10 – Time changes in factor levels

Factor	Time changes in factor levels. hours.	
	from “–1” to “+1”	from “+1” to “–1”
X_1	7	3
X_2	6	2
X_3	16	12
X_4	100	50

Table 11 – Initial pan of a multifactorial experiment

Experiment number	Factors			
	X_1	X_2	X_3	X_4
1	–1	–1	–1	–1
2	+1	–1	–1	–1
3	–1	+1	–1	–1
4	+1	+1	–1	–1
5	–1	–1	+1	–1
6	+1	–1	+1	–1
7	–1	+1	+1	–1
8	+1	+1	+1	–1
9	–1	–1	–1	+1
10	+1	–1	–1	+1
11	–1	+1	–1	+1
12	+1	+1	–1	+1
13	–1	–1	+1	+1
14	+1	–1	+1	+1
15	–1	+1	+1	+1
16	+1	+1	+1	+1

Table 12 – Optimal plan of a multifactor experiment obtained by the growing trees method

Experiment number	Factors			
	X_1	X_2	X_3	X_4
1	–1	+1	–1	+1
2	–1	–1	–1	+1
3	+1	–1	–1	+1
4	+1	+1	–1	+1
5	+1	+1	+1	+1
6	+1	–1	+1	+1
7	–1	–1	+1	+1
8	–1	+1	+1	+1
9	–1	+1	+1	–1
10	–1	–1	+1	–1
11	+1	–1	+1	–1
12	+1	+1	+1	–1
13	+1	+1	–1	–1
14	+1	–1	–1	–1
15	–1	–1	–1	–1
16	–1	+1	–1	–1

The time required to implement the initial experiment plan is 251 hours [21]. while the optimal plan takes 130 hours.

DOI 10.15588/1607-3274-2023-3-6

5 RESULTS

The results of the conducted experiment. presented in Table 13. demonstrate gains in the implementation of experiment plans obtained using the recalculated methods compared to the cost of conducting the initial plan for the study of the technological process of welding thin plates.

Table 13 – Comparison of costs for implementing experimental plans for the investigation of the technological process of welding thin plates

Optimization method	Cost. standard u. m.	Gain
Method of constructing the initial plan	27	1
Complete enumeration	14	1.93
Monkey search method	14.5	1.86
Growing tree method	14	1.93

Table 14 presents the gains in implementing the experimental plans obtained using mentioned methods compared to the cost of the initial plan for the study of the accuracy of the humidity meter for materials.

Table 14 – Comparison of implementation costs for experimental plans investigating the accuracy of the moisture meter

Optimization method	Cost. u. m.	Gain
Method of constructing the initial plan	31.84	1
Modified Gray code	16.28	1.96
Growing trees method	16.28	1.96

The time expenditures for implementing the experiment plans obtained by different methods [32]. along with the time savings compared to the time of conducting the initial plan for the study of the numerical program-controlled machine shop area. are presented in Table 15.

Table 15 – Comparison of optimization methods for experiment plans in the study of the machining workshop with numerical program control

Optimization method	Plan implementation time. hours	Gain
Method of constructing the initial plan	251	1
Monkey search method	180	1.39
Limited enumeration method	214.5	1.17
Bacterial method	181	1.39
Growing trees method	130	1.93

6 DISCUSSION

Based on the comparison of methods. the following conclusions can be drawn. When optimizing plans for multifactorial experiments in the study of technological processes using the growing trees method. we obtain plans with cost expenditures that coincide with those obtained through complete enumeration and the application of modified Gray code. This confirms the effectiveness and efficiency of the growing tree method.

In comparison to methods such as monkey search. limited enumeration. and bacterial optimization. the growing tree method yields better results.

The growing tree method has faster performance than complete enumeration and can be applied for optimizing plans of multifactorial experiments in terms of cost (time) expenditures for objects with up to $k \leq 7$ factors.

CONCLUSIONS

The growing tree method has been developed for optimizing plans of multifactorial experiments in terms of cost and time expenditures. along with the corresponding software implementation.

The scientific novelty of the obtained results lies in the development of the growing tree method that allows for obtaining optimal or near-optimal plans of multifactor experiments with high speed in terms of cost and time expenditures.

The practical value of the research results is that the developed software. implementing the growing tree method. enables the generation of optimal or near-optimal plans of multifactor experiments for a wide range of objects with up to $k \leq 7$ factors.

The prospects for further research lie in the application of the growing tree method to a wide range of scientific and industrial objects. such as capacitance moisture meters [34].

REFERENCES

1. Yazdani M., Jolai F. Lion optimization algorithm (loa): a nature-inspired metaheuristic algorithm, *Journal of computational design and engineering*, 2016, Vol. 3, №1, pp. 24–36. DOI: 10.1016/j.jcde.2015.06.003.
2. Hatamlou A. Black hole: A new heuristic optimization approach for data clustering, *Information sciences*, 2013, Vol. 222, pp. 175–184. DOI: 10.1016/j.ins.2012.08.023.
3. Mirjalili S., Mirjalili S. M., Lewis A. Grey wolf optimizer, *Advances in engineering software*, 2014, Vol. 69, pp. 46–61. DOI: 10.1016/j.advengsoft.2013.12.007.
4. Uymaz S. A., Tezel G., Yel E. Artificial algae algorithm (aaa) for nonlinear global optimization, *Applied Soft Computing*, 2015, Vol. 31, pp. 153–171. DOI: 10.1016/j.asoc.2015.03.003.
5. Gandomi A. H., Yang X. S., Talatahari S., Alav A. H. Firefly algorithm with chaos, *Communications in Nonlinear Science and Numerical Simulation*, 2013, Vol. 18, No. 1, pp. 89–98. DOI: 10.5815/ijitcs.2014.06.03.
6. Oftadeh R., Mahjoob M. A new meta-heuristic optimization algorithm: Hunting search, *Soft Computing. Computing with Words and Perceptions in System Analysis. Decision and Control: ICSCCW 2009: Fifth International Conference on. IEEE*, 2009, pp. 1–5. DOI: 10.1109/ICSCCW.2009.5379451
7. Sadollah A., Eskandar H., Bahreininejad A., Kim J. H. Water cycle algorithm with evaporation rate for solving constrained and unconstrained optimization problems, *Applied Soft Computing*, 2015, Vol. 30, pp. 58–71. DOI: 10.1016/j.asoc.2015.01.050.
8. Yang X. S. A new metaheuristic bat-inspired algorithm, *Nature inspired cooperative strategies for optimization*, 2010, pp. 65–74. DOI: 10.1007/978-3-642-12538-6_6.
9. Mafarja M. M., Eleyan D., Jaber I. et al. Binary dragonfly algorithm for feature selection, *International Conference on*

DOI 10.15588/1607-3274-2023-3-6

New Trends in Computing Sciences (ICTCS): 11–13 October 2017: proceedings. Amman, IEEE, 2017, pp. 12–17. DOI: 10.1109/ICTCS.2017.43.
10. Arora S., Anand P. Binary butterfly optimization approaches for feature selection, *Expert Systems with Applications*, 2019, Vol. 116, pp. 147–160. DOI: 10.1016/j.eswa.2018.08.051.
11. Chu S. C., Tsai P. W., Pan J. S. Cat swarm optimization, *Pacific Rim International Conference on Artificial Intelligence, 7–11 August 2006, proceedings.* Guilin, China, 2006, pp. 854–858. DOI:10.1007/11801603_94.
12. Yang X. S., Deb S. Cuckoo search via Lévy flights / X. S. Yang. // *World congress on nature & biologically inspired computing. NaBIC*, 2009, pp. 210–214. DOI: 10.1109/NABIC.2009.5393690.
13. Kaveh A. A new optimization method: Dolphin echolocation / A. Kaveh. N. Farhoudi // Advances in Engineering Software. – 2013. – Vol. 59. – P. 53-70. DOI: 10.1016/j.advengsoft.2013.03.004.
14. Yang X. S. Flower pollination algorithm for global optimization, *International Conference on Unconventional Computing and Natural Computation, 3–7 September 2012, proceedings.* Orléans, pp. 240–249. DOI: 10.1007/978-3-642-32894-7_27.
15. Chang H. S. Converging Marriage in Honey-Bees Optimization and Application to Stochastic Dynamic Programming, *Journal of Global Optimization*, 2006, № 35, pp. 423–441. DOI: 10.1007/s10898-005-5608-4.
16. Pan J. S., Tsai P. W., Liao Y. B. Fish migration optimization based on the fishy biology, *2010 Fourth International Conference on Genetic and Evolutionary Computing, 13–15 December 2010, proceedings*. Washington, IEEE, 2010, pp. 783–786. DOI: 10.1109/ICGEC.2010.198.
17. De Castro L. N., Von Zuben F. J. Learning and optimization using the clonal selection principle, *IEEE Transactions Evolutionary Computation*, 2002, Vol. 6, № 3, pp. 239–251. DOI: 10.1109/TEVC.2002.1011539.
18. Yang Q., Chu S. C., Liang A. et al. Tumbleweed Algorithm and Its Application for Solving Location Problem of Logistics Distribution Center, *International Conference on Genetic and Evolutionary Computing, 10–14 July 2021, proceedings*, 2021, pp. 641–652. DOI: 10.1007/978-981-16-8430-2_58.
19. Mirjalili S. The ant lion optimizer, *Advances in Engineering Software*, 2015, Vol. 83, pp. 90–98. DOI: 10.1016/j.advengsoft.2015.01.010.
20. Koshovyj M. D., Burljejev O. L., Pampuha A. I. Analiz metodiv optymal'nogo planuvannja bagatofaktornogo eksperymentu za vartisnymy ta chasovymy pokaznykamy, *Zbirnyk naukovyh prac' Vijs'kovogo instytutu Kyi'vs'kogo nacional'nogo universytetu imeni Tarasa Shevchenka*, 2022, №75, pp. 94-107. DOI: 10.17721/2519-481X/2022/75-10.
21. Koshevoj N. D., Kostenko E. M., Pavlik A. V. i dr. Metodologija optimal'nogo po stoimostnym i vremennym zatratam planirovanija jeksperimenta: monografija. Poltava, Poltavskaja gosudarstvennaja agrarnaja akademija, 2017, 232 p.
22. Kennedy J., Eberhart R. Particle swarm optimization, *International Conference on Neural Networks : 27 November – 01 December 1995 : proceedings*. Perth, IEEE, 2002, Vol. 4, pp. 1942–1948. DOI: 10.1109/ICNN.1995.488968.
23. Koshevoy N. D., Kostenko E. M., Beliaieva A. A. Comparative analysis of optimization methods in the investigation of weigh-measuring system and thermoregulator, *Radio Electronics. Computer Science, Control, 2018*, № 4, pp. 179–187. DOI: 10.15588/1607-3274-2018-4-17.
24. Holland J., Goldberg D. Genetic algorithms in search. optimization and machine learning. Massachusetts, Addison-Wesley, 1989, P. 414.
25. Koshevoy N. D., Muratov V. V., Kirichenko A. L. et al. Application of the "Jumping frogs" algorithm for research and optimization of the technological process, *Radio Electronics. Computer Science, Control*, 2021, №1, pp. 57–65. DOI: https://doi.org/10.15588/1607-3274-2021-1-6.
26. [Koshevoy N. D., Dergachov V. A., Pavlyk A. V. et al. The method of building plans of multifactorial experiments with minimal number of factor levels measurements and optimal by cost(time) expenses, *Radio Electronics. Computer Science, Control*, 2020, №4, pp. 55–64. DOI: 10.15588/1607-3274-2020-4-6.
27. Koshevoy N. D., Kostenko E. M., Muratov V. V. et al. Comparative analysis of optimization methods by cost (time) costs of full factor experiment plans, 2020, № 1, pp. 54–62. DOI: 10.15588/1607-3274-2020-1-6.
28. Koshevoy N. D., Kostenko E. M., Muratov V. V. Application of the fish search method for optimization plans of the full factor experiment, *Radio Electronics. Computer Science, Control*, 2020, № 2, pp. 44–50. DOI: 10.15588/1607-3274-2020-2-5.
29. Rutenbar R. A. Simulated annealing algorithms: An overview, *IEEE Circuits and Devices Magazine*, 1989, № 5, pp. 19–26. DOI: 10.1109/101.17235.
30. Harari F. Teorija grafov. Moscow, Mir, 1973, pp. 48-59.
31. Vvedenie v typescript [Jelektronnyj resurs], 2021. URL: https://metanit.com/web/typescript.
32. Muratov V. V. Udoskonalennja doslidzhennja tehnologichnyh procesiv. prystroi'v i system na osnovi planuvannja eksperymentu : dys. … doktor filosofii' : 11.21.21. Kharkiv, Nacional'nyj aerokosmichnyj universytet im. M. Je. Zhukovs'kogo "Kharkivs'kyj aviacijnyj instytut", 2021, 230 p.
33. Koshova I. I. Metody ta zasoby optymal'nogo planuvannja eksperymentiv dlja doslidzhennja tehnologichnyh procesiv. prystroi'v i system : dys. … doktor filosofii' : 03.12.20. Kharkiv, Nacional'nyj aerokosmichnyj universytet im. M. Je. Zhukovs'kogo "Kharkivs'kyj aviacijnyj instytut", 2020, 209 p.
34. Zabolotnyi O., Koshevoy N. An effective method of bulk materials moisture measurement using capacitive sensors, *Journal of Stored Products Research*, 2020, Vol. 89. doi.org/10.1016/j.jspr.2020.101733.

Received 19.06.2023.
Accepted 25.08.2023.

DOI 10.15588/1607-3274-2023-3-6

УДК 519.24

МЕТОД ЗРОСТАЮЧИХ ДЕРЕВ ДЛЯ ОПТИМІЗАЦІЇ ПЛАНІВ БАГАТОФАКТОРНИХ ЕКСПЕРИМЕНТІВ

Кошовий М. Д. – д-р техн. наук. професор. професор кафедри інтелектуальних вимірювальних систем та інженерії якості. Національний аерокосмічний університет ім. М. Є. Жуковського «Харківський авіаційний інститут». Харків. Україна.

Пилипенко О. Т. – аспірант кафедри інтелектуальних вимірювальних систем та інженерії якості. Національний аерокосмічний університет ім. М. Є. Жуковського «Харківський авіаційний інститут». Харків. Україна.

Ільїна І. В. – канд. техн. наук. доцент. доцент кафедри електронних обчислювальних машин. Харківський національний університет радіоелектроніки. Харків. Україна.

Токарєв В. В. – канд. техн. наук. доцент. доцент кафедри електронних обчислювальних машин. Харківський національний університет радіоелектроніки. Харків. Україна.

АНОТАЦІЯ

Актуальність. Задача планування багатофакторних експериментів займає важливе місце в науці та промисловому виробництві. При цьому в умовах конкуренції. зростання витрат. підвищення ефективності необхідна оптимізація планів багатофакторних експериментів за вартісними та часовими витратами. Для вирішення цієї задачі існує ряд підходів та методів. вибір яких для конкретного технічного завдання є важливою та складною задачею. У зв'язку з цим виникає необхідність в розробці нових методів оптимізації за вартісними (часовими) витратами планів багатофакторних експериментів. порівнянні їх з уже існуючими методами та видачі рекомендацій по практичному застосуванні при дослідженні реальних об'єктів.

Мета. Мета роботи полягає у розробці та апробації методу зростаючих дерев. оцінки його ефективності у порівнянні з іншими методами. При цьому для дослідження мети вирішені наступні завдання: запропонований метод зростаючих дерев реалізований у вигляді програмного забезпечення; метод застосований для оптимізації планів багатофакторних експериментів при дослідженні реальних об'єктів; проведена оцінка його ефективності у порівнянні з іншими методами; видані рекомендації по його використанню.

Метод. Запропонований метод зростаючих дерев заснований на застосуванні теорії графів. Перевагою методу є скорочення часу вирішення оптимізаційних задач. пов'язаних з побудовою оптимальних за вартісними (часовими) витратами планів багатофакторних експериментів. Характерною рисою є також висока точність вирішення оптимізаційних задач.

Результати. Результати експериментів та порівняння з іншими методами оптимізації підтверджують працездатність та ефективність запропонованого методу та дозволяють рекомендувати його для дослідження об'єктів із числом суттєвих факторів $k \leq 7$. Перспективним є подальше розширення кола об'єктів наукового та промислового призначення для їх дослідження цим методом.

Висновки. Розроблено метод зростаючих дерев для оптимізації за вартісними та часовими витратами планів багатофакторних експериментів та програмне забезпечення. що його реалізує за допомогою framework Angular на мові розробки TypeScript.

Показана ефективність методу зростаючих дерев у порівнянні з наступними методами: повний та обмежений перебір. мавпячий пошук. застосування модифікованого коду Грея. бактеріальна оптимізація. Метод зростаючих дерев має більшу швидкодію ніж повний перебір та може застосовуватися для оптимізації планів багатофакторних експериментів за вартісними (часовими) витратами для об'єктів з кількістю факторів $k \leq 7$. При рішенні оптимізаційних задач метод зростаючих дерев дає кращі результати у порівнянні з мавпячим пошуком. обмеженим перебором та бактеріальною оптимізацією.

КЛЮЧОВІ СЛОВА: метод зростаючих дерев, алгоритм, багатофакторний експеримент, програмне забезпечення, порівняння.

ЛІТЕРАТУРА

1. Yazdani M. Lion optimization algorithm (loa): a nature-inspired metaheuristic algorithm / M. Yazdani. F. Jolai // Journal of computational design and engineering. – 2016. – Vol. 3, № 1. – P. 24–36. DOI: 10.1016/j.jcde.2015.06.003.
2. Hatamlou A. Black hole: A new heuristic optimization approach for data clustering / A. Hatamlou // Information sciences. – 2013. – Vol. 222. – P. 175–184. DOI: 10.1016/j.ins.2012.08.023.
3. Mirjalili S. Grey wolf optimizer / S. Mirjalili, S. M. Mirjalili. A. Lewis // Advances in engineering software. – 2014. – Vol. 69. – P. 46–61. DOI: 10.1016/j.advengsoft.2013.12.007.
4. Uymaz S. A. Artificial algae algorithm (aaa) for nonlinear global optimization / S. A. Uymaz, G. Tezel, E. Yel // Applied Soft Computing. – 2015. – Vol. 31. – P. 153–171. DOI: 10.1016/j.asoc.2015.03.003.
5. Firefly algorithm with chaos / [A. H. Gandomi, X. S. Yang, S. Talatahari, A. H. Alav] // Communications in Nonlinear Science and Numerical Simulation. – 2013. – Vol. 18, № 1. – P. 89–98. DOI: 10.5815/ijitcs.2014.06.03.
6. Oftadeh R. A new meta-heuristic optimization algorithm: Hunting search / R. Oftadeh. M. Mahjoob // Soft Computing. Computing with Words and Perceptions in System Analysis. Decision and Control: ICSCCW 2009: Fifth International Conference on. IEEE: 2009. – P. 1–5. DOI: 10.1109/ICSCCW.2009.5379451
7. Water cycle algorithm with evaporation rate for solving constrained and unconstrained optimization problems / [A. Sadollah, H. Eskandar, A. Bahreininejad, J. H. Kim] // Applied Soft Computing. – 2015. – Vol. 30. – P. 58–71. DOI: 10.1016/j.asoc.2015.01.050.
8. Yang X. S. A new metaheuristic bat-inspired algorithm / X. S. Yang // Nature inspired cooperative strategies for

DOI 10.15588/1607-3274-2023-3-6

optimization. – 2010. – P. 65–74. DOI: 10.1007/978-3-642-12538-6_6.
9. Binary dragonfly algorithm for feature selection / [M. M. Mafarja, D. Eleyan, I. Jaber et al.] // International Conference on New Trends in Computing Sciences (ICTCS): 11–13 October 2017: proceedings. – Amman : IEEE. 2017. – P. 12–17. DOI: 10.1109/ICTCS.2017.43.
10. Arora S. Binary butterfly optimization approaches for feature selection / S. Arora, P. Anand // Expert Systems with Applications. – 2019. – Vol. 116. – P. 147–160. DOI: 10.1016/j.eswa.2018.08.051.
11. Chu S. C. Cat swarm optimization / S. C. Chu, P. W. Tsai, J. S. Pan // Pacific Rim International Conference on Artificial Intelligence: 7–11 August 2006: proceedings. – Guilin, China, 2006. – P. 854–858. DOI:10.1007/11801603_94.
12. Yang X. S. Cuckoo search via Lévy flights / X. S. Yang. S. Deb // World congress on nature & biologically inspired computing. NaBIC. – 2009. – P. 210–214. DOI: 10.1109/NABIC.2009.5393690.
13. Kaveh A. A new optimization method: Dolphin echolocation / A. Kaveh, N. Farhoudi // Advances in Engineering Software. – 2013. – Vol. 59. – P. 53–70. DOI: 10.1016/j.advengsoft.2013.03.004.
14. Yang X. S. Flower pollination algorithm for global optimization / X. S. Yang // International Conference on Unconventional Computing and Natural Computation : 3–7 September 2012 : proceedings. – Orléans. – P. 240–249. DOI: 10.1007/978-3-642-32894-7_27.
15. Chang H. S. Converging Marriage in Honey-Bees Optimization and Application to Stochastic Dynamic Programming / H. S. Chang // Journal of Global Optimization. – 2006. – № 35. – P. 423–441. DOI: 10.1007/s10898-005-5608-4.
16. Pan J. S. Fish migration optimization based on the fishy biology / J. S. Pan, P. W. Tsai, Y. B. Liao // 2010 Fourth International Conference on Genetic and Evolutionary Computing : 13–15 December 2010 : proceedings. – Washington: IEEE, 2010. – P. 783–786. DOI: 10.1109/ICGEC.2010.198.
17. De Castro L. N. Learning and optimization using the clonal selection principle / L. N. De Castro, F. J. Von Zuben // IEEE Transactions Evolutionary Computation. – 2002. – Vol. 6. – №3. – P. 239-251. DOI: 10.1109/TEVC.2002.1011539.
18. Tumbleweed Algorithm and Its Application for Solving Location Problem of Logistics Distribution Center / [Q. Yang. S. C. Chu. A. Liang et al.] // International Conference on Genetic and Evolutionary Computing : 10–14 July 2021 : proceedings. – 2021. – P. 641–652. DOI: 10.1007/978-981-16-8430-2_58.
19. Mirjalili S. The ant lion optimizer / S. Mirjalili // Advances in Engineering Software. – 2015. – Vol. 83. – P. 90–98. DOI: 10.1016/j.advengsoft.2015.01.010.
20. Кошовий М. Д. Аналіз методів оптимального планування багатофакторного експерименту за вартісними та часовими показниками / М. Д. Кошовий. О. Л. Бурлєєв. А. І. Пампуха // Збірник наукових праць Військового інституту Київського національного університету імені Тараса Шевченка. – 2022. – № 75. – P. 94–107. DOI: 10.17721/2519-481X/2022/75-10.
21. Методология оптимального по стоимостным и временным затратам планирования эксперимента: монография / [Н. Д. Кошевой, Е. М. Костенко, А. В. Павлик и др.]. – Полтава : Полтавская государственная аграрная академия. 2017. – 232 с.
22. Kennedy J. Particle swarm optimization / J. Kennedy. R. Eberhart // International Conference on Neural Networks : 27 November – 01 December 1995 : proceedings. – Perth : IEEE. 2002. – Vol. 4. – P. 1942–1948. DOI: 10.1109/ICNN.1995.488968.
23. Koshevoy N. D. Comparative analysis of optimization methods in the investigation of weigh-measuring system and thermoregulator / N. D. Koshevoy, E. M. Kostenko. A. A. Beliaieva // Radio Electronics, Computer Science, Control. – 2018. – № 4. – P. 179–187. DOI: 10.15588/1607-3274-2018-4-17.
24. Holland J. Genetic algorithms in search. optimization and machine learning / J. Holland, D. Goldberg. – Massachusetts : Addison-Wesley. 1989. – P. 414.
25. Application of the “Jumping frogs” algorithm for research and optimization of the technological process / [N. D. Koshevoy, V. V. Muratov, A. L. Kirichenko et al.] // Radio Electronics., Computer Science, Control. – 2021. – № 1. – P. 57–65. DOI: https://doi.org/10.15588/1607-3274-2021-1-6.
26. The method of building plans of multifactorial experiments with minimal number of factor levels measurements and optimal by cost(time) expenses / [N. D. Koshevoy. V. A. Dergachov. A. V. Pavlyk et al.] // Radio Electronics, Computer Science, Control. – 2020. – № 4. – P. 55–64. DOI: 10.15588/1607-3274-2020-4-6.
27. Comparative analysis of optimization methods by cost (time) costs of full factor experiment plans / [N. D. Koshevoy. E. M. Kostenko. V. V. Muratov et al.]. – 2020. – №1. – P. 54-62. DOI: 10.15588/1607-3274-2020-1-6.
28. Koshevoy N. D. Application of the fish search method for optimization plans of the full factor experiment / N. D. Koshevoy. E. M. Kostenko. V. V. Muratov // Radio Electronics, Computer Science, Control. – 2020. – № 2. – P. 44–50. DOI: 10.15588/1607-3274-2020-2-5.
29. Rutenbar R. A. Simulated annealing algorithms: An overview / R. A. Rutenbar // IEEE Circuits and Devices Magazine. – 1989. – № 5. – P. 19–26. DOI: 10.1109/101.17235.
30. Харари Ф. Теория графов / Ф. Харари. – М. : Мир, 1973. – С. 48–59.
31. Введение в typescript [Электронный ресурс]. – 2021. URL: https://metanit.com/web/typescript.
32. Муратов В. В. Удосконалення дослідження технологічних процесів. пристроїв і систем на основі планування експерименту : дис. … доктор філософії : 11.11.21 / Муратов Віктор Володимирович. – Харків : Національний аерокосмічний університет ім. М. Є. Жуковського «Харківський авіаційний інститут», 2021. – 230 с.
33. Кошова І. І. Методи та засоби оптимального планування експериментів для дослідження технологічних процесів. пристроїв і систем : дис. … доктор філософії : 03.12.20 / Кошова Ірина Іванівна. – Харків : Національний аерокосмічний університет ім. М. Є. Жуковського «Харківський авіаційний інститут». 2020. – 209 с.
34. Zabolotnyi O. An effective method of bulk materials moisture measurement using capacitive sensors / O. Zabolotnyi. N. Koshevoy // Journal of Stored Products Research. – 2020. – Vol. 89. doi.org/10.1016/j.jspr.2020.101733.

DOI 10.15588/1607-3274-2023-3-6

UDC 519.2:004.94

POLYNOMIAL ESTIMATION OF DATA MODEL PARAMETERS WITH NEGATIVE KURTOSIS

Chepynoha V. V. – Postgraduate student of the Department of Computer Science and System Analysis, Cherkasy State Technological University, Cherkasy, Ukraine.

Chepynoha A. V. – PhD, Associate Professor, Dean of the Faculty of Information Technologies and Systems, Cherkasy State Technological University, Cherkasy, Ukraine.

Palahin V. V. – Dr. Sc., Professor, Head of the Department of Robotics and Telecommunication Systems and Cyber Security, Cherkasy State Technological University, Cherkasy, Ukraine.

ABSTRACT

Context. The paper focuses on the problem of estimating the center of distribution of the random component of experimental data for density models with a negative kurtosis.

Objective. The goal of this research is to develop methods to improve the efficiency of polynomial estimation of parameters of experimental data with a negative kurtosis coefficient.

Method. The study applies a relatively new approach to obtaining estimates for the center of the probability distribution from the results of experimental data with a stochastic component. This approach is based on polynomial estimation methods that rely on the mathematical apparatus of Kunchenko's stochastic polynomials and the description of random variables by higher-order statistics (moments or cumulants). A number of probability density distributions with a negative kurtosis coefficient are used as models of the random component.

As a measure of efficiency, the ratio of variance of the estimates for the center of the distribution found using polynomial and classical methods based on the parameter of amount of information obtained is used.

The relative accuracy of polynomial estimates in comparison with the estimates of the mean, median and quantile estimates (center of curvature) is researched using the Monte Carlo method for multiple tests.

Results. Polynomial methods for estimating the distribution center parameter for data models of probability distribution density with a negative kurtosis coefficient have been constructed.

Conclusions. The research carried out in this paper confirms the potentially high efficiency of polynomial estimates of the coordinates of the center of the experimental data, which are adequately described by model distributions with a negative kurtosis. Statistical modeling has confirmed the effectiveness of the obtained estimates in comparison with the known non-parametric estimates based on the statistics of the mean, median, and quantile, even with small sample sizes.

KEYWORDS: data sampling, estimation, stochastic polynomial, cumulants, negative kurtosis.

ABBREVIATIONS

PMM – polynomial maximization method;

NOMENCLATURE

$a_i(\theta) = E\{x_i\}$ are mathematical expectations that depend on the parameter being estimated;

$g_{(\theta)mean}$ is a coefficient of variance reduction relative to the method of moments;

$h_1 - h_3$ are weighting coefficients;

$J_{rn}(\theta)$ is an amount of obtained information;

N is a number of experiments to obtain a predetermined accuracy;

n is a sample volume;

r is a predefined order of the polynomial;

x is a sample value;

$\vec{x}$ is a sample of equally distributed random variables;

$\hat{\alpha}_i$ are sample statistical initial moments;

γ_3 and γ_6 are cumulant coefficients;

θ is an informative parameter;

$\hat{\theta}$ is an estimation of informative parameter;

ξ is a random component of sample data;

$\sigma^2_{(\theta)r}$ is a theoretical variance of the parameter estimated by the PMM;

$\hat{\sigma}^2_{(\theta)mean}$ is an empirical value of the variance of the mean estimates;

$\hat{\sigma}^2_{(\theta)med}$ is an empirical value of the variance of the median estimates;

$\hat{\sigma}^2_{(\theta)qvant}$ is an empirical value of the variance of the quantile estimates;

$\hat{\sigma}^2_{(\theta)PMM3}$ is an empirical value of the variance of the PMM estimates ($r = 3$);

χ_2 is a second-order cumulant;

INTRODUCTION

Statistical estimation methods are the usually core mathematical tool for many tasks where the analysis of experimental data is required, such as interpretation of scientific experiments, stochastic signal processing, product quality assurance, non-destructive testing of structures, network intrusion detection systems, theoretical fundamental metrology etc. The need to use them is predetermined by the impact of various noises and interferences, random errors or errors of measuring instruments on the experimental data. In such cases, a typical ap-

DOI 10.15588/1607-3274-2023-3-7

proach is to present the data model as an additive interaction of informative parameter and a stochastic component [1, 2].

There are several tasks in which a stochastic component of the experimental data symmetrical in nature, and under the following condition, the center of the probability distribution of this stochastic component can be determined as center of symmetry, and its coordinate will be the actual value of the informative parameter [3].

Quite often, in practice, simple averaging is used to calculate an estimate of the coordinate the center of the stochastic experimental data distribution. However, the application of arithmetic mean to estimate the parameters of random series is actually optimal only for models with a Gaussian probability distribution density. But in fact, it is impossible to represent all the variety of real probability distributions of the random component with this law alone. Therefore, some tasks require the use of other distribution laws, sometimes significantly different from the normal one [2–5].

The object of study is the process of estimating the parameters of random variable models with the moment-cumulant description.

The subject of study is models of experimental data with negative kurtosis and methods of polynomial estimation of their parameters.

The purpose of the work is to increase the efficiency of polynomial estimation of parameters of experimental data with a negative kurtosis coefficient when creating methods and tools for mathematical and computer modelling based on the application of the polynomial maximization method and moment-cumulant description of random variables to improve the quality of the estimates obtained by increasing their accuracy in the functioning of data processing systems of the corresponding class.

1 PROBLEM STATEMENT

It is necessary to estimate the value of the informative parameter θ based on statistical processing of the vector $\vec{x} = \{x_1, x_2, ...x_n\}$ of sample values $x = \theta + \xi$, which are statistically independent and identically distributed and obtained by conducting multiple experiments.

It is assumed that the mathematical model of the random component of the data ξ is adequately described by the distribution laws shown in Table 1.

The research is supposed to obtain estimates of the center of the distribution, analytical expressions describing the variances of the PMM estimates, and, using Monte Carlo statistical modelling, to check the actual efficiency of the estimates compared to the ones obtained by other methods, depending on the amount of sample data and the distribution with a negative kurtosis.

2 REVIEW OF THE LITERATURE

In a number of tasks of processing experimental data of various origins, it turns out that the random component in them has a distribution with a negative kurtosis, and the type of distribution itself is concave (bimodal). Models of such distributions are used in information and measurement systems [2, 7], in determining electromagnetic compatibility [8–10], in sociology [11], evolutionary biology [12], hydrology [13], and other fields.

Among such probability density models, according to which the random component of the experimental data is distributed, the following can be distinguished: U-quadratic distribution, arcsine distribution, V-shaped distribution and symmetrical Kumaraswamy distribution. These distributions are symmetric, have a negative kurtosis, and have another property: they are defined on a limited interval. A graphical representation of their probability density is shown in Figure 1. Table 1 shows the mathematical expressions for the probability density function of the corresponding laws:

Table 1 – Mathematical representation of probability distribution

№	Type of distribution	Distribution parameters	
a)	$p(x) = \alpha(x-\beta)^2$	$\alpha = \frac{12}{(b-a)^3}$	$\beta = \frac{b+a}{2}$
b)	$p(x) = \frac{1}{\pi\sqrt{w^2-(x-h)^2}}$	$w = \frac{b-a}{2}$	$w = \frac{b+a}{2}$
c)	$p(x) = \frac{\lvert x-a\rvert}{b^2}$	$a = 0$	$b = 1$
d)	$p(x) = a \cdot b \cdot x^{a-1}\left(1-x^a\right)^{b-1}$	$a = 0.5$	$b = 0.5$

DOI 10.15588/1607-3274-2023-3-7

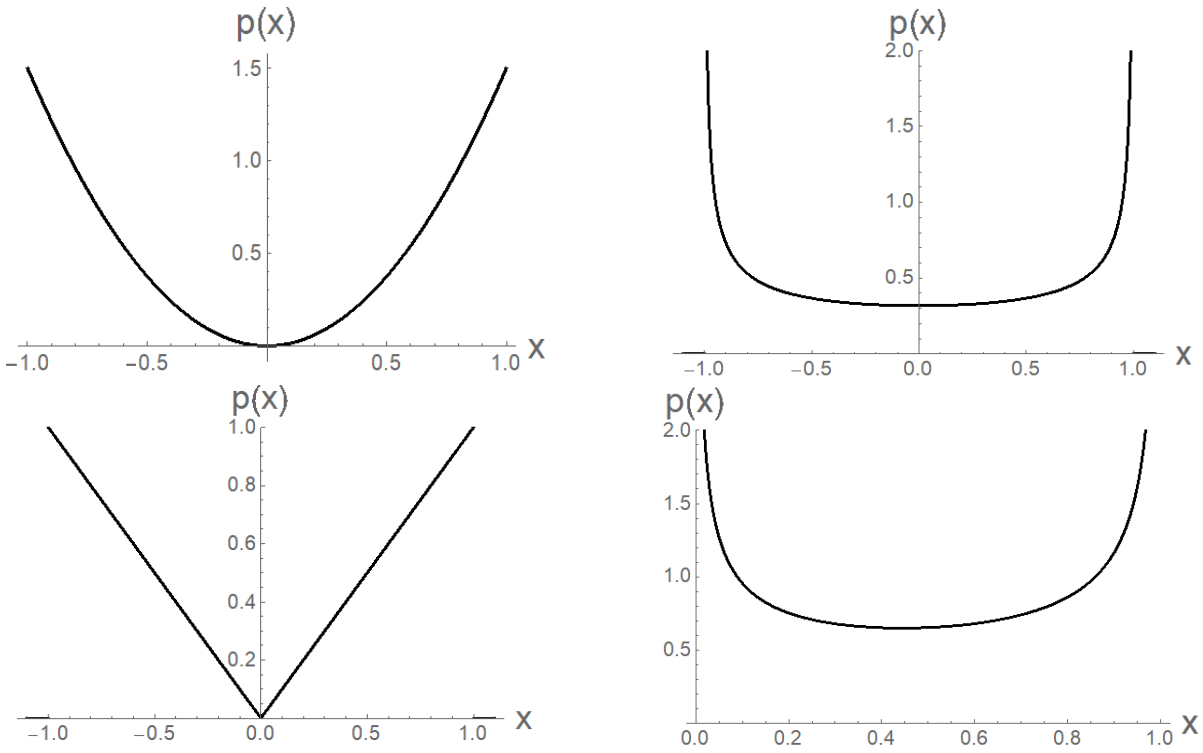

Figure 1 – Symmetric distributions with negative kurtosis: a – U-quadratic distribution, b – arcsine distribution, c – V-shaped distribution, d – symmetrical Kumaraswamy distribution

It is well known that the application of mathematical models of the random component of experimental data with any probability distribution requires the use of certain mathematical procedures for statistical processing. The existing fundamental approaches to finding estimates of the parameters of such models are based on the method of moments and the method of maximum likelihood or its modifications, respectively. The first one has a relatively low accuracy, but is notable for its simple calculation. The other requires the implementation of rather complex algorithms and the availability of as large a sample size as possible, which characterizes it as asymptotically efficient [13–15]. In addition to these methods, other statistics can also be used to obtain an estimate: median, quantile (center of curvature) or rank estimates [5, 16].

3 MATERIALS AND METHODS

In general, finding estimates of an unknown scalar parameter θ by the polynomial maximization method over a sample of equally distributed random variables $\vec{x} = \{x_1, x_2, ...x_n\}$ involves solving a polynomial equation of the form:

$$\sum_{i=1}^{r} h_i(\theta)\left[\frac{1}{n}\sum_{v=1}^{n}\left(x_v^i - \alpha_i(\theta)\right)\right]\Bigg|_{\theta=\hat{\theta}} = 0, \qquad (1)$$

where r – predefined order of the polynomial, $a_i(\theta) = E\{x_i\}$ – mathematical expectations that depend on the parameter being estimated. The weighting coefficients $h_i(\theta)$ of equation (1) can be found under the condition of ensuring the minimum variance of the estimates of the parameter θ when using a polynomial of power r [17]. These coefficients are found from solving a system of linear algebraic equations of the form:

$$\sum_{i=1}^{r} h_i(\theta) F_{i,j}(\theta) = \frac{d}{d\theta}\alpha_j(\theta), \quad j = \overline{1,r}, \qquad (2)$$

where the centered correlants $F_{i,j}(\theta) = \alpha_{i+j}(\theta) - \alpha_i(\theta)\alpha_j(\theta)$, $i, j = \overline{1,r}$. When forming a stochastic polynomial of power r for equation (2), it is necessary to have a partial probability description in the form of a set of moments up to the $2r$-th order.

It is known from [17–19] that when using power transforms as basis functions, polynomial estimates obtained with the powers of the polynomial $r = 1,2$ are equivalent to estimates of the mean for any symmetric distribution law of random variables. Therefore, in order to obtain estimates of the PMM that can prevail in accuracy, it is necessary to use a stochastic polynomial of power $r = 3$. To form the polynomial equation (1) with the unknown parameter θ, the relations for the first 6 initial moments were calculated. They will depend on the desired parameter θ, the second-order cumulant χ_2, and the cumulant coefficients γ_4 and γ_6:

DOI 10.15588/1607-3274-2023-3-7

$$\begin{aligned}\alpha_1(\theta)=\theta,\ \alpha_2(\theta)=\theta^2+\chi_2,\ \alpha_3(\theta)=\theta^3+3\theta\chi_2,\\ \alpha_4(\theta)=\theta^4+6\theta^2\chi_2+(3+\gamma_4)\chi_2^2,\\ \alpha_5(\theta)=\theta^5+10\theta^3\chi_2+5\theta(3+\gamma_4)\chi_2^2,\\ \alpha_6(\theta)=\theta^6+15\theta^4\chi_2+15\theta^2(3+\gamma_4)\chi_2^2+\\ +(15(1+\gamma_4)+\gamma_6)\chi_2^3.\end{aligned} \quad (3)$$

To find the weighting coefficients that minimize the variance of the PMM estimates of the distribution center parameter, the necessary expressions for the derivatives of the first 3 moments are as follows:

$$\frac{d}{d\theta}\alpha_1(\theta)=1,\frac{d}{d\theta}\alpha_2(\theta)=2\theta,\frac{d}{d\theta}\alpha_3(\theta)=3(\theta^2+\chi_2). \quad (4)$$

If we use a polynomial of power $r=3$, then the equation for finding the PMM estimates $\hat{\theta}$ for the case of a symmetrically distributed random component of the experimental data can be written as follows:

$$\begin{aligned}h_1\sum_{v=1}^{n}[x_v-\theta]+h_2\sum_{v=1}^{n}\left[x_v^2-(\theta^2+\chi_2)\right]+\\ +h_3\sum_{v=1}^{n}\left[x_v^3-(\theta^3+3\theta\chi_2)\right]\Big|_{\theta=\hat{\theta}}\end{aligned} \quad (5)$$

where h_1-h_3 – are the weighting coefficients obtained from the analytical solution of the system of equations (2) by the Kramer method, and taking into account expressions (3) and (4), and are as follows:

$$\begin{aligned}h_1&=\frac{3\theta^2\gamma_4-(6+12\gamma_4+\gamma_6)\chi_2}{((\gamma_4-9)\gamma_4-6-\gamma_6)\chi_2^2},\\ h_2&=\frac{-3\theta\gamma_4}{((\gamma_4-9)\gamma_4-6-\gamma_6)\chi_2^2},\\ h_3&=\frac{\gamma_4}{((\gamma_4-9)\gamma_4-6-\gamma_6)\chi_2^2}.\end{aligned} \quad (6)$$

If the found coefficients (6) are substituted into the into the PMM equation (5), then a polynomial equation of the third power with respect to the parameter θ is obtained:

$$P_1\theta^3+P_2\theta^2+P_3\theta+P_4\Big|_{\theta=\hat{\theta}}=0, \quad (7)$$

where the coefficients P_1-P_4 depend on the second-order cumulant χ_2 and the cumulant coefficients γ_4 and γ_6. They can be found by using sample statistical initial moments $\hat{\alpha}_i=\frac{1}{n}\sum_{v=1}^{n}x_v^i$, $i=\overline{1,6}$.

It is known [16, 19] that the solution of the cubic equation of the form (7) is obtained analytically on the basis of Cardano's formulas. However, there are alternative methods for obtaining an analytical solution, for example, the general cubic formula, Viete`s substitution, trigonometric and hyperbolic solutions, and the Lagrange method [20]. The effectiveness of these methods depends on the type of roots of the cubic equation. It is known that the correct solution of a PMM is a real root, which in general can be more than one, which requires additional verification by the criterion of minimum variance.

In [18], it was proposed to use numerical iterative algorithms for solving nonlinear equations. As an initial approximation for finding the root of equation (7), it is proposed to use a linear estimate of the desired parameter in the form of a sample mean $\hat{\alpha}_1$. The condition for stopping iterations is set based on the standard deviation of the estimates.

It is known that the Newton-Raphson method is most commonly used to solve nonlinear equations and their systems, but the method of simple iteration, the method of fastest descent, etc. can also be applied.

So, in fact, the question of using mathematical methods to solve a polynomial maximization equation requires a more thorough study, comparing analytical and numerical methods, the speed of algorithms, and the types of roots obtained.

It was proved in [17] that the estimates obtained as a result of solving the PMM equation are valid and asymptotically unbiased. It is also important that there is an analytical solution for the variance of such estimates. It is based on the concept of the amount of information obtained about the estimated parameter θ and is calculated using a well-known formula:

$$J_{rn(\theta)}=n\sum_{i=1}^{r}h_i(\theta)\frac{d}{d\theta}\alpha_i(\theta). \quad (8)$$

The previously found values of the moments and weighting coefficients are used here. The inverse of the amount of obtained information in the asymptotic case tends to the variance of the estimated parameter, namely:

$$\sigma^2_{(\theta)r}=\lim_{n\to\infty}J^{-1}_{rn(\theta)}. \quad (9)$$

Analogous to [16–17], for a comparative analysis of the relative accuracy of estimates, it is advisable to introduce the concept of the coefficient of variance reduction:

$$g_{(\theta)mean}=\frac{\sigma^2_{(\theta)PMM3}}{\sigma^2_{(\theta)mean}}. \quad (10)$$

DOI 10.15588/1607-3274-2023-3-7

This coefficient indicates the ratio of the variance of the PMM estimates of the parameter θ obtained from the r-order polynomial equation to the variance of the PMM estimates when $r=1$ or to the variance of the method of moments estimates.

The variance $\sigma^2_{(\theta)mean}$ of the estimates of the parameter θ, found by the method of moments, does not depend on the value of this parameter. It is uniquely determined by the ratio of the second-order cumulant χ_2 to the volume of the sample n [17]:

$$\sigma^2_{(\theta)mean} = \frac{\chi_2}{n}. \qquad (11)$$

If substituting the values of the obtained weighting coefficients (6) and the derivatives of the moments (4) into expression (8), then in the asymptotic case (at $n \to \infty$), it is possible to determine the variance of the PMM estimates of the order of the polynomial $r=3$ through the value of the cumulant coefficients:

$$\sigma^2_{(\theta)PMM3} = \frac{\chi_2}{n}\left[1 - \frac{\gamma_4^2}{6+9\gamma_4+\gamma_6}\right]. \qquad (12)$$

In this case, the coefficient of variance reduction (10) will depend on the cumulant coefficients characterizing the kurtosis of the random variable and has the form:

$$g_{(\theta)mean} = 1 - \frac{\gamma_4^2}{6+9\gamma_4+\gamma_6}. \qquad (13)$$

As a result of the research, theoretical coefficients for reducing the variance of estimates of the center of distributions with a negative kurtosis coefficient were calculated, as shown in Table 2. Since the selected distribution models have constant cumulant coefficients characterizing the kurtosis, the values obtained are numerical:

Table 2 – Theoretical coefficients of variance reduction

№	Вид розподілу	$g_{(\theta)mean}$	γ_4	γ_6
a)	U-quadratic distribution	0,037	–1,81	13,69
b)	Arcsine distribution	0,1	–1,5	10
c)	V-shaped distribution	0,074	–1,67	12
d)	Symmetrical Kumaraswamy distribution	0,058	–1,46	9,42

As shown in Table 2, all distributions are non-Gaussian, but it is the coefficient γ_4 that is negative. The results obtained do not contradict the domain of permissible values of cumulant coefficients shown in [17], and they cannot take on arbitrary values.

Based on the results of the research on the use of the PMM to estimate the parameter θ, it is possible to say that such estimates are superior in accuracy to the classical average method for distributions with a negative kurtosis. Thus, when the order of the stochastic polynomial is $r=3$, the efficiency advantage of the PMM estimates of the distribution center is more than 10 times. Although, of course, in solving certain practical problems, the efficiency advantage of such estimates using the PMM may be somewhat less.

4 EXPERIMENTS

Usually, it is quite problematic to check and prove the effectiveness of both methods and algorithms in practice due to the limited amount of data obtained through a real-world experiment. A way out of this situation may be the use of simulation modeling methods, among which the most common is the Monte Carlo method, which is based on obtaining a large number of random data realizations that have stochastic properties of the real process being reproduced.

In this work, a software implementation of a series of repeated experiments was developed in Mathematica to compare the accuracy of the PMM estimates of the polynomial order $r=3$ with other classical estimates. For this purpose, the experiment was supplemented with the calculation of median and quantile estimates (center of curve), which are also used to determine the center of the distribution.

As shown above, expression (10) can serve as a precise criterion of efficiency, but for experimental data it will contain empirical values of the variance reduction coefficients of the corresponding estimates:

$$\hat{g}_{(\theta)mean} = \frac{\hat{\sigma}^2_{(\theta)PMM3}}{\hat{\sigma}^2_{(\theta)mean}},\ \hat{g}_{(\theta)med} = \frac{\hat{\sigma}^2_{(\theta)PMM3}}{\hat{\sigma}^2_{(\theta)med}},\ \hat{g}_{(\theta)qvan} = \frac{\hat{\sigma}^2_{(\theta)PMM3}}{\hat{\sigma}^2_{(\theta)qvan}}, \qquad (14)$$

where $\hat{\sigma}^2_{(\theta)mean}$, $\hat{\sigma}^2_{(\theta)med}$, $\hat{\sigma}^2_{(\theta)qvan}$, $\hat{\sigma}^2_{(\theta)PMM3}$ – average values of the variance of estimates for N experiments, obtained using the mean, median, quantile estimate, and PMM ($r=3$), respectively.

In the implementation of the experiment, the estimates of the sample initial moments for substitution into the stochastic polynomial equation were obtained using the known formula:

$$\hat{\alpha}_i = \frac{1}{n}\sum_{v=1}^{n} x_v^i,\ i=\overline{1,6}. \qquad (15)$$

DOI 10.15588/1607-3274-2023-3-7

When analyzing expressions (11) and (12), we can talk about the asymptotic efficiency of the methods, i.e., to obtain valid results, the sample of one experiment should be as large as possible. As for averaging the variance of the estimates, it is also necessary to have a certain number of experiments to ensure a predetermined accuracy and statistical stability of the modeling results. This calculation is performed using confidence intervals [21].

If a parameter $\hat{\theta}$ with mathematical expectation θ is estimated from a sample and has a mean $M(X)$, then there exists a value ε such that $|\theta - M(X)| < \varepsilon$, which will be the accuracy of the estimate. The probability of fulfillment of this inequality is its reliability $P(|\theta - M(X)| < \varepsilon) = E$.

Since the scheme of independent statistical tests with a relative frequency of occurrence of the required event m/N is considered, for sufficiently large N, a distribution close to normal will be obtained. Therefore, for each value of reliability E, the value of the function $\Phi(t) = E$ can be selected from the probability integral tables for such a value t_E that the accuracy ε is equal:

$$\varepsilon = t_E \sqrt{D(m/N)} = t_E \sqrt{D(X)/N}\,. \qquad (16)$$

Thus, the number of experiments to obtain a given accuracy will be found as follows:

$$N = t_E^2 D(X)/\varepsilon^2\,. \qquad (17)$$

If a number of random variables are evaluated during one experiment, then $\max D_i(X)$ is usually chosen to calculate the number of experiments N.

Typically, the reliability is set at $E = 0.95$, so the table value found is $t_E = 1.96$. The accuracy of calculating the variance and the coefficient of variance reduction will be adequate when the number has two decimal places, i.e. $\varepsilon = 0.01$. Calculating the variance values for the given probability distribution models with constant parameters, it is obtained $\max D_i(X) = 0.6$. Thus, the required number of experiments to get a given accuracy is as follows:

$$N = \frac{t_E^2 D(X)}{\varepsilon^2} = 23000\,. \qquad (18)$$

5 RESULTS

The results of statistical modeling by the Monte Carlo method for the various distributions considered in the research and the volume of experimental sample values $n = 20 \div 200$ obtained at the number of experiments $N = 23 \cdot 10^3$ are presented in Table 3.

For a more visual representation and comparison, the coefficients of variance reduction obtained as a result of Monte Carlo simulation relative to the method of moments and their theoretical values were plotted, since they were calculated analytically. Figure 2 shows them depending on the volume of the sample n.

6 DISCUSSION

Usually, methods that perform nonlinear processing of any data, especially stochastic data, lead to the complication of mathematical and computational algorithms. The polynomial estimation of the parameters of the experimental data proposed in this study is no exception. Moreover, it is known that increasing the order of the stochastic polynomial r does not lead to a linear dependence of the increase in the accuracy of the obtained estimates. This fact somewhat reduces the application of the method in practice and forces a compromise between increasing accuracy or complexity. That is why in this study it was decided to choose the order $r = 3$ of the stochastic polynomial.

The analysis of the results of theoretical (Table 2) and experimental (Table 3) studies of variance reduction coefficients shows their significant correlation. This is especially evident when the sample size n increases, and also indicates the correctness of the statistical modeling. Such results fully confirm the asymptotic efficiency of polynomial estimation based on the property of the amount of obtained information (8).

Table 3 – Coefficients of variance reduction of estimates

Вид розподілу	$g_{(\theta)3}$	Результати статистичного моделювання											
		$\hat{g}_{(\theta)mean}$				$\hat{g}_{(\theta)med}$				$\hat{g}_{(\theta)qvan}$			
		n											
		20	50	100	200	20	50	100	200	20	50	100	200
U-quadratic distribution	0,037	0.16	0.044	0.038	0.035	0.018	0.002	0.001	0.001	0.284	0.161	0.151	0.153
Arcsine distribution	0,1	0.305	0.138	0.114	0.102	0.077	0.031	0.024	0.021	0.236	0.108	0.088	0.082
V-shaped distribution	0,074	0.25	0.097	0.08	0.071	0.039	0.009	0.005	0.003	0.319	0.17	0.154	0.14
Symmetrical Kumaraswamy distribution	0,058	0.196	0.093	0.068	0,061	0.109	0.044	0.031	0.026	0.284	0.138	0.108	0.094

DOI 10.15588/1607-3274-2023-3-7

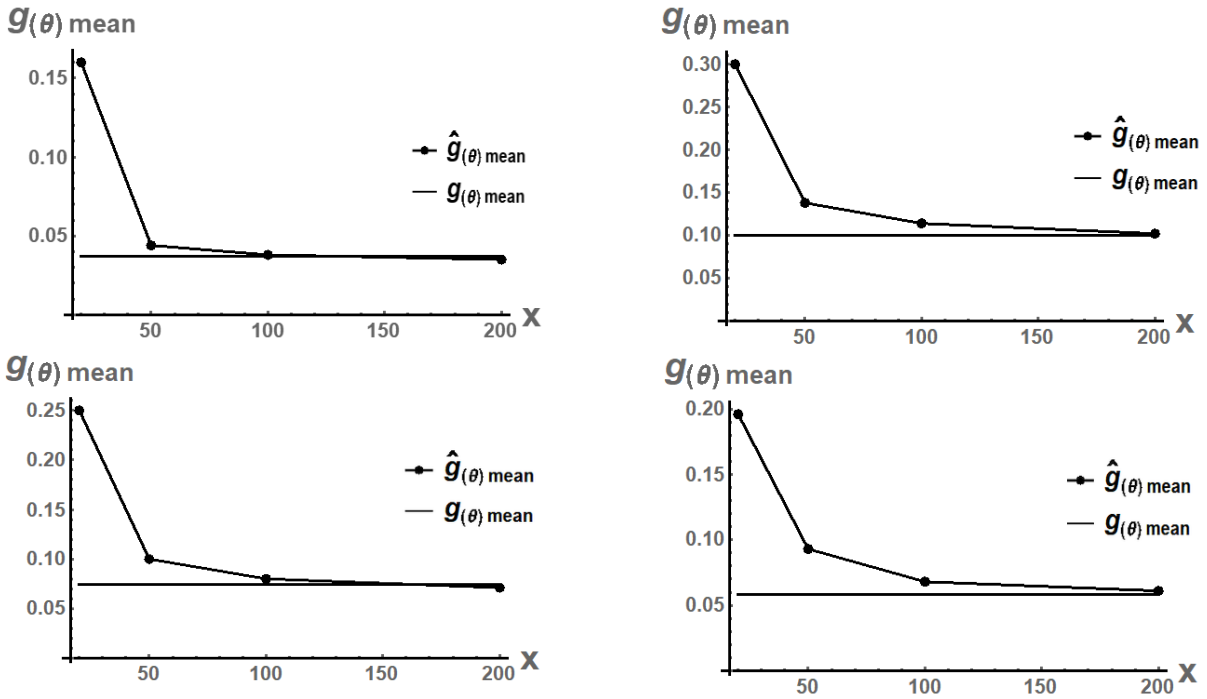

Figure 2 – Comparison of the efficiency of methods for finding center coordinate estimates depending on the volume of the sample: a – U-quadratic distribution, b – arcsine distribution,
c – V-shaped distribution, d – symmetrical Kumaraswamy distribution

A general analysis of the results of comparing different estimation methods with the PMM shows its high efficiency. It is demonstrated by the fact that the PMM has an average 3-5 times higher accuracy of estimates than classical methods, as shown in Figure 2. This is also true for small (20 values) sample volumes, which is important for limited experiments, although the smallest reduction in the variance of the estimate in such cases is observed compared to the method of quantile estimates. As for the median estimate, the PMM has the greatest advantage over it in terms of accuracy for models with a gentler curve.

As the sample volume increases, the coefficient of variance reduction tends to its theoretical value, as it should be, which is confirmed by the results of statistical modeling. This trend can be observed both in the numerical results (Table 3) and in the graphical interpretation (Figure 2), which shows a comparison of the experimental value and the theoretical one. Although the coefficient of variance reduction increases with decreasing non-Gaussianity of the experimental data (the advantage in accuracy decreases), the advantage of polynomial estimates remains significant.

CONCLUSIONS

The research conducted in this paper confirms the potentially high efficiency of the polynomial maximization method in determining estimates of the coordinates of the center of distribution of experimental data that are adequately described by models of probability distributions with a negative kurtosis. An important and essential feature of this approach is the fact that it does not require any prior information about the type and parameters of the distributions. However, for the purpose of demonstration, the necessary well-known models were used, which are adequate to the task at hand. The paper shows that the algorithm for finding the PMM estimates of an informative parameter using the polynomial order $r = 3$ can be reduced to solving a cubic equation. For this purpose, both explicit and numerical methods can be used. The coefficients of this equation are obtained from the calculation of a posteriori estimates of the initial moments up to the 6-th order of the stochastic component of the experimental data.

The basis for finding the coefficient of variance reduction in this paper is the concept of the amount of information extracted, which is identical to Fisher's information for the Maximum Likelihood Estimation. However, the amount of information extracted was calculated based on sample statistical characteristics, such as moments and cumulants. The result is an analytical expression that, for each model distribution, when substituting the numerical values of the interval on which it is defined, gives a number in the final case.

Statistical modeling has confirmed the effectiveness of the PMM estimates compared to known nonparametric estimates based on the mean, median, and quantile statistics, even with small sample sizes. The simulation results show that the accuracy of the proposed approach is sometimes significantly (more than 3 times) higher than classical nonparametric estimates.

ACKNOWLEDGEMENTS

The work is supported by the registered research project of Cherkasy State Technological University «Models, methods and tools of joint signal detection and parameter

DOI 10.15588/1607-3274-2023-3-7

estimation in non-Gaussian noise» (state registration number 0122U201835).

REFERENCES

1. International Vocabulary of Metrology Fourth edition – Committee Draft (VIM4 CD). [Effective from 2021-01-11]. JCGM, 2021, 55 p.
2. Dorozhovets M. Opratsiuvannia rezultativ vymiriuvan: Navch. posibnyk. Lviv, Vydavnytstvo Natsionalnoho universytetu «Lvivska politekhnika», 2007, 624 p.
3. Dikhtiievskyi O. V., Kvasnikov V. P., Vozniakovskyi A. O. Otsinka systematychnoi ta vypadkovoi skladovykh pokhybky vymiriuvannia tsylindrychnykh zubchastykh kolis, *Perspektyvni tekhnolohii ta prylady*, 2019, № 14, pp. 62–66. DOI: 10.36910/6775-2313-5352-2019-14-10
4. Nevyznachenist vymiriuvan. Chastyna 3. Nastanova shchodo podannia nevyznachenosti u vymiriuvanni (GUM:1995): DSTU ISO/IEC Guide 98-3:2018 (ISO/IEC Guide 98-3:2008, IDT). [Chynnyi vid 2018-12-18]. Kyiv, DP «UkrNDNTs», 2019, 272 p. (Natsionalnyi standart Ukrainy)
5. Zakharov Y. P., Shtefan N. V. Opredelenye эffektyvnыkh otsenok tsentra raspredelenyia pry statystycheskoi obrabotke rezultatov nabliudenyi, *Radioe'lektronika i informatika*,, 2002, Vyp. 3, S. 97–99
6. Dodge Y. The Concise Encyclopedia of Statistics. NY,: Springer New York, 2008, 612 p. DOI: 10.1007/978-0-387-32833-1
7. Ribeiro A. S., Sousa J. A., Castro M. P. Some remarks on the use of U-shape probability distribution functions in Monte Carlo simulation, *Advances of Measurement Science 2004: 10th IMEKO TC7 Symposium, Saint-Petersburg, 30 June – 2 July 2004: proceedings*. NY, IMEKO-International Measurement Federation Secretariat, 2004, pp. 124–130.
8. Ceekala M. Stochastic ADC with random U-quadratic distributed reference voltages to uniformly distribute comparators trip point : thesis … Master of Applied Science. Nova Scotia, Dalhousie University, 2013, 91 p.
9. Carpenter D. A demystification of the U-shaped probability distribution, *Electromagnetic Compatibility: 2003 IEEE Symposium, Boston, 18–22 August 2003: proceedings*. Los Alamitos, IEEE, 2003, Vol. 2, pp. 521–525, DOI: 10.1109/ISEMC.2003.1236656.
10. Harris I. A., Warner F. L. Re-examination of mismatch uncertainty when measuring microwave power and attenuation *IEE Proceedings H: Microwaves Optics and Antennas*, 1981, Vol. 128, Issue 1, pp. 35–41, DOI: 10.1049/ip-h-1.1981.0007
11. Badircea R. M., Florea N. M., Manta A. G. et al. Comparison between Romania and Sweden based on three dimensions: Environmental performance, green taxation and economic growth, *Sustainability*, 2020, Vol. 12, Issue 9, pp. 3817–3834, DOI: 10.3390/su12093817
12. Sella G., Hirsh A. E. The application of statistical physics to evolutionary biology, *Proceedings of the National Academy of Sciences of the United States of America*, 2005, Vol. 102, Issue 27, pp. 9541–9546. DOI: 10.1073/pnas.0501865102
13. Javanshir Z., Habibi Rad A., Arghami N. R. Exp-Kumaraswamy distributions: some properties and applications, *Journal of Sciences, Islamic Republic of Iran*, 2015, Vol. 26, Issue 1, pp. 57–69.
14. Emam W., Tashkandy Y. The arcsine Kumaraswamy-generalized family: Bayesian and classical estimates and application, *Symmetry*, 2022, Vol. 14, Issue 11, pp. 2311–2330. DOI: 10.3390/sym14112311
15. Muhammad M., Rano S., Sani R. et al. Parameter estimation of exponentiated U-quadratic distribution: alternative maximum likelihood and percentile methods, *Asian Research Journal of Mathematics*, 2018, Vol. 9, Issue 2, pp. 1–10., DOI: 10.9734/ARJOM/2018/39446
16. Zabolotnii S. V., Kucheruk V. Yu., Warsza Z. L. et al. Polynomial estimates of measurand parameters for data bimodal mixtures of exponential distributions, *Bulletin of the Karaganda University*, 2018, Vol. 2, Issue 90, pp. 71–80.
17. Kunchenko Y. P. Polynomial parameter estimation of close to Gaussian random variables. Aachen, Shaker Verlag, 2002, 396 p.
18. Zabolotnii S. V., Chepynoha A. V., Bondarenko Yu. Yu. et al. Polynomial parameter estimation of exponential power distribution data, *Visnyk NTUU KPI Seriia – Radiotekhnika Radioaparatobuduvannia*, 2018, Vol. 75, pp. 40–47. DOI: 10.20535/RADAP.2018.75.40-47
19. Warsza Z. L., Zabolotnii S. W. A Polynomial Estimation of Measurand Parameters for Samples of Non-Gaussian Symmetrically Distributed Data, *Advances in Intelligent Systems and Computing*, 2017, Vol. 550, pp. 468–480, DOI: 10.1007/978-3-319-54042-9_45
20. Cooke R. Classical Algebra: Its Nature, Origins, and Uses. New Jersey, John Wiley & Sons, 2008, 224 p. DOI:10.1002/9780470277980
21. Tomashevskyi V. M. Modeliuvannia system. Kyiv, Vydavnycha hrupa BHV, 2005, 352 p.

Received 12.06.2023.
Accepted 25.08.2023.

УДК 519.2:004.94

ПОЛІНОМІАЛЬНЕ ОЦІНЮВАННЯ ПАРАМЕТРІВ МОДЕЛЕЙ ДАНИХ З ВІД'ЄМНИМ КОЕФІЦІЄНТОМ ЕКСЦЕСУ

Чепинога В. В. – аспірант кафедри комп'ютерних наук та системного аналізу, Черкаський державний технологічний університет, Черкаси, Україна.

Чепинога А. В. – канд. техн. наук, доцент, декан факультету інформаційних технологій та систем, Черкаський державний технологічний університет, Черкаси, Україна.

Палагін В. В. – д-р техн. наук, професор, завідувач кафедри робототехнічних і телекомунікаційних систем та кібербезпеки, Черкаський державний технологічний університет, Черкаси, Україна.

АНОТАЦІЯ

Актуальність. В роботі розглянуто задачу оцінювання центру розподілу випадкової складової експериментальних даних для моделей щільності з від'ємним коефіцієнтом ексцесу.

Мета. Метою роботи є отримання методів підвищенні ефективності поліноміального оцінювання параметрів експериментальних даних з від'ємним коефіцієнтом ексцесу.

Метод. В дослідженні застосовано відносно новий підхід для отримання оцінок центру розподілу імовірності з результатів експериментальних даних, що мають стохастичну складову. Цей підхід засновано на поліноміальних методах оціню-

DOI 10.15588/1607-3274-2023-3-7

вання, котрі спираються на математичний апарат стохастичних поліномів Кунченка та опис випадкових величин статистиками вищих порядків (моментами чи кумулянтами). В якості моделей випадкової складової в роботі використано ряд розподілів щільності імовірності з від'ємним коефіцієнтом ексцесу.

В якості міри ефективності оцінок було використано відношення дисперсії оцінки центру розподілу, знайденої з використанням поліноміальних та класичних методів, виходячи із параметра кількості добутої інформації.

Досліджено, із застосуванням методу Монте-Карло для багаторазових випробувань, відносну точність поліноміальних оцінок у порівнянні з оцінками середнього, медіани та квантильних оцінок (центру перегину).

Результати. Побудовано поліноміальні методи оцінювання параметра центру розподілу для моделей даних щільності розподілу імовірності з від'ємним коефіцієнтом ексцесу.

Висновки. Дослідження, що були проведені в даній роботі, підтверджують потенційно високу ефективність поліноміальних оцінок координати центру експериментальних даних, що адекватно описуються модельними розподілами з від'ємним коефіцієнтом ексцесу. Статистичне моделювання підтвердило ефективність отриманих оцінок в порівнянні із відомими непараметричними оцінками, на основі статистик середнього, медіани і квантильної оцінки, причому навіть при малих об'ємах вибірки.

КЛЮЧОВІ СЛОВА: вибірка даних, оцінювання, стохастичний поліном, кумулянти, від'ємний ексцес.

REFERENCES

1. International Vocabulary of Metrology Fourth edition – Committee Draft (VIM4 CD). – [Effective from 2021-01-11]. – JCGM, 2021. – 55 p.
2. Дорожовець М. Опрацювання результатів вимірювань: Навч. посібник / М. Дорожовець. – Львів : Видавництво Національного університету «Львівська політехніка», 2007. – 624 с.
3. Діхтієвський О. В. Оцінка систематичної та випадкової складових похибки вимірювання циліндричних зубчастих коліс / О. В. Діхтієвський, В. П. Квасніков, А. О. Возняковський // Перспективні технології та прилади. – 2019. – № 14. – С. 62-66 DOI: 10.36910/6775-2313-5352-2019-14-10
4. Невизначеність вимірювань. Частина 3. Настанова щодо подання невизначеності у вимірюванні (GUM:1995): ДСТУ ISO/IEC Guide 98-3:2018 (ISO/IEC Guide 98-3:2008, IDT). – [Чинний від 2018-12-18]. – К.: ДП «УкрНДНЦ», 2019. – 272 с. – (Національний стандарт України)
5. Захаров И. П. Определение эффективных оценок центра распределения при статистической обработке результатов наблюдений / И. П. Захаров, Н. В. Штефан //, Радиоэлектроника и информатика. – 2002. – Вып. 3. – С. 97–99
6. Dodge Y. The Concise Encyclopedia of Statistics / Y. Dodge – NY: Springer New York, 2008. – 612 p., DOI: 10.1007/978-0-387-32833-1
7. Ribeiro A. S. Some remarks on the use of U-shape probability distribution functions in Monte Carlo simulation / A. S. Ribeiro, J. A. Sousa, M. P. Castro // Advances of Measurement Science 2004: 10th IMEKO TC7 Symposium, Saint-Petersburg, 30 June – 2 July 2004: proceedings. – NY: IMEKO-International Measurement Federation Secretariat, 2004. – P. 124–130
8. Ceekala M. Stochastic ADC with random U-quadratic distributed reference voltages to uniformly distribute comparators trip point : thesis … Master of Applied Science / Mithun Ceekala. – Nova Scotia: Dalhousie University, 2013. – 91 p.
9. Carpenter D. A demystification of the U-shaped probability distribution / D. Carpenter // Electromagnetic Compatibility: 2003 IEEE Symposium, Boston, 18–22 August 2003: proceedings. – Los Alamitos: IEEE, 2003. – Vol. 2 – P. 521–525. DOI: 10.1109/ISEMC.2003.1236656.
10. Harris I. A. Re-examination of mismatch uncertainty when measuring microwave power and attenuation / I. A. Harris, F. L. Warner // IEE Proceedings H: Microwaves Optics and Antennas. – 1981. – Vol. 128, Issue 1. – P. 35–41. DOI: 10.1049/ip-h-1.1981.0007
11. Comparison between Romania and Sweden based on three dimensions: Environmental performance, green taxation and economic growth / [R. M. Badircea, N. M. Florea, A. G. Manta et al.] // Sustainability. – 2020. – Vol. 12, Issue 9. – P. 3817–3834, DOI: 10.3390/su12093817
12. Sella G. The application of statistical physics to evolutionary biology / G. Sella, A. E. Hirsh // Proceedings of the National Academy of Sciences of the United States of America. – 2005. – Vol. 102, Issue 27. – P. 9541–9546., DOI: 10.1073/pnas.0501865102
13. Javanshir Z. Exp-Kumaraswamy distributions: some properties and applications / Z. Javanshiri, A. Habibi Rad, N.R. Arghami // Journal of Sciences, Islamic Republic of Iran. – 2015. – Vol. 26, Issue 1. – P. 57–69.
14. Emam W. The arcsine Kumaraswamy-generalized family: Bayesian and classical estimates and application / W. Emam, Y. Tashkandy // Symmetry. – 2022. – Vol. 14, Issue 11. – P. 2311–2330., DOI: 10.3390/sym14112311
15. Parameter estimation of exponentiated U-quadratic distribution: alternative maximum likelihood and percentile methods / [M. Muhammad, S. Rano, R. Sani et al.] // Asian Research Journal of Mathematics. – 2018. – Vol. 9, Issue 2. – P. 1–10., DOI: 10.9734/ARJOM/2018/39446
16. Polynomial estimates of measurand parameters for data bimodal mixtures of exponential distributions / [S. V. Zabolotnii, V. Yu. Kucheruk, Z. L. Warsza et al.] // Bulletin of the Karaganda University. – 2018. – Vol. 2, Issue 90. – P. 71–80.
17. Kunchenko Y. P. Polynomial parameter estimation of close to Gaussian random variables / Y. P. Kunchenko. – Aachen: Shaker Verlag, 2002. – 396 p.
18. Поліноміальні оцінки параметрів для даних з експоненційним степеневим розподілом / [С. В. Заболотній, А. В. Чепинога, Ю. Ю. Бондаренко та ін.] // Вісник НТУУ «КПІ». Серія: Радіотехніка. Радіоапаратобудування. – 2018. – Вип. 75. – С. 40–47. DOI: 10.20535/RADAP.2018.75.40-47
19. Warsza Z. L. A Polynomial Estimation of Measurand Parameters for Samples of Non-Gaussian Symmetrically Distributed Data / Z. L. Warsza, S. W. Zabolotnii // Advances in Intelligent Systems and Computing, – 2017. – Vol. 550. – P. 468–480, DOI: 10.1007/978-3-319-54042-9_45
20. Cooke R. Classical Algebra: Its Nature, Origins, and Uses / R. Cooke. – New Jersey: John Wiley & Sons, 2008. – 224 p. DOI:10.1002/9780470277980
21. Томашевський В.М. Моделювання систем / В. М. Томашевський – К. : Видавнича група BHV, 2005. – 352 с.

DOI 10.15588/1607-3274-2023-3-7

НЕЙРОІНФОРМАТИКА ТА ІНТЕЛЕКТУАЛЬНІ СИСТЕМИ

NEUROINFORMATICS AND INTELLIGENT SYSTEMS

UDC 621.391:004.93

RECOGNITION OF REFERENCE SIGNALS AND DETERMINATION OF THEIR WEIGHTING COEFFICIENTS IF AN ADDITIVE INTERFERENCE PRESENTS

Avramenko V. V. – Associate Professor of the Department of Computer Science, Sumy State University, Sumy, Ukraine.

Bondarenko M. O. – Post-graduate student of the Department of Computer Science, Sumy State University, Sumy, Ukraine.

ABSTRACT

Context. The subject matter of the article is the recognition of a reference signal in the presence of additive interference.

Objective. The recognition of the reference signal by the obtained value of its weighting factor in conditions where additive interference is imposed on the spectrum of the reference signal at unknown random frequencies. The task is the development of a method for recognizing a reference signal for the case when the interference consists of an unknown periodic signal that can be represented by a finite sum of basis functions. In addition, interference may also include deterministic signals from a given set with unknown weighting coefficients, which are simultaneously transmitted over the communication channel with the reference signal.

Method. The method of approximating the unknown periodic component of the interference by the sum of basis functions is used. The current number of values of the signal that enters the recognition system depends on the number of basis functions. This signal is the sum of the basis functions and the reference signal with unknown weighting coefficients. To obtain the values of these coefficients, the method based on the properties of the disproportion functions is used. The recognition process is reduced to the calculation of the weight coefficient of the reference signal. If it is zero, it indicates that the reference signal is not part of the signal being analyzed. The recognition system is multi-level. The number of levels depends on the number of basis functions.

Results. The obtained results show that, provided that the reference signal differs by at least one component from the given set of basis functions, the recognition is successful. The given examples show that the system recognizes the reference signal even in conditions where the weighting coefficient of the interference is almost 1000 times greater than the coefficient for the reference signal. The recognition system also works successfully in conditions where the interference includes the sum of deterministic signals from a given set, which are simultaneously transmitted over the communication channel.

Conclusions. The scientific novelty of the obtained results is that a method for recognizing the reference signal has been developed in conditions where only an upper estimate of its maximum frequency is known for the periodic component of the interference. Also, recognition occurs when, in addition to unknown periodic interference, the signals from a given set with unknown weighting coefficients are superimposed on the reference signal. In the process of recognition, in addition to the weighting factor for the reference signal, the factors for the interference components are also obtained.

KEYWORDS: recognition of reference signals, additive interference, weighting coefficients, disproportion functions, basis functions, interference spectrum, Fourier series.

NOMENCLATURE

t is a time;

$y(t)$ is a signal received at the input of the recognition system;

$g(t)$ is a reference signal;

$\eta(t)$ is an interference;

M is a number of basis functions

$f_i(t)$ is a set of given basis functions, i=1, 2,...M;

e_i is a set of unknown coefficients;

k_1 is a weight of the reference signal;

k_2 is a weight of the interference signal;

d is a derivative;

@ is a symbol for calculating disproportion;

h is a step of calculation;

c_i is an unknown coefficient;

N is a number of consecutive measurements;

l is a level;

n is a sequence number of calculating the disproportion at this level;

$D_{l,n}(j)$ is a disproportion;

ω is a circular frequency;

DOI 10.15588/1607-3274-2023-3-8

$@d_x^{(1)}y$ is a disproportion over the 1-th order derivative of y with respect to x. Read as: “at d one y with respect to x”.

INTRODUCTION

Recognition of reference signals and estimation of their weighting coefficients occurs when solving many problems. In particular, it is necessary for the recognition of radar signals [1], phonemes in a voice signal [2], modulation for the analysis of an intercepted signal [3], emotions in the creation of intelligent systems [4] in medicine [5, 6], in prosthetics [7], radio monitoring [8, 9], etc. Most of the works are devoted to the detection and recognition of the reference signals if interference is random noise. In particular, it can be a random quasi-stationary periodic process with an unknown current spectral characteristic, about which only an upper estimate of the possible maximum frequency is known. In addition, simultaneously with the periodic process, other deterministic signals from a given set with unknown weighting coefficients can be transmitted over the communication channel.

The cited circumstances testify to the urgency of developing new methods of signal recognition.

The object of research is the process of recognizing a reference signal in the presence of additive interference.

The subject of research is the method and algorithm for recognizing reference signals under the influence of listed types of interference.

The purpose of this work is to develop a method for accurately identifying a reference signal by determining its weighting factor in the presence of additive interference. The primary goal is to address the challenge of recognizing reference signals when the interference consists of an unknown periodic signal and deterministic signals from a given set with unknown weighting coefficients. The research aims to propose a reliable approach based on the use of disproportion functions and the approximation of the unknown periodic component of the interference by a sum of basis functions.

1 LITERATURE REVIEW

Many works are devoted to the detection, recognition, and estimation of parameters of reference signals. Thus, in [8], radio monitoring of radio frequency ranges is carried out to find unoccupied frequency channels in cognitive radio networks. At the same time, signals are detected and recognized under conditions of a priori uncertainty. The noise in the frequency channel is given by the training sample of realizations. The decision rule is implemented in the spectral domain using the discrete Fourier transform. Recognition of phonendoscopy signals in the space of autocorrelation functions and linear prediction coefficients is considered in [5].

In [10], the apparatus of fuzzy sets is used to increase the reliability of positional-binary recognition of signals. Recognition of cyclic signals is carried out by comparing their fuzzy interpretations with the corresponding fuzzy interpretations of reference signals reflecting the temporal arrangement of positional-binary components.

In [11], discrete orthogonal transformation is used for signal recognition. When the investigated signal coincides with the sample, the spectrum of such a transformation contains only one non-zero transformation. It should be noted that the application of the normal transformation to evaluate the similarity of signals based on the obtained coefficients makes it possible to introduce a numerical measure of the evaluation of such similarity. In radio communication, an important task is the recognition of signal modulation. To improve its recognition, a fusion of multimodal features is proposed in [3]. Various functions in the time and frequency domains are obtained as inputs to the network at the signal preprocessing stage. Deep neural convolutional networks are built to obtain spatial features that interact with temporal features.

In [8], to quickly obtain complete information about the characteristics of pulse signals, time and frequency characteristics are obtained. They are mixed in a convolutional neural network for final classification and recognition. Recognition of signals with a time-varying spectrum is considered in [12]. A new radar emitter signal recognition method based on a one-dimensional deep residual shrinkage network is proposed in [1]. In [13], recognition of periodic signals in the presence of additive periodic interference occurs using the first-order derivative disproportionality function.

2 PROBLEM STATEMENT

It is necessary to develop a method for recognizing reference signals and estimating their weighting coefficients when additive interference is imposed on them at unknown frequencies. The interference consists of two parts. The first part is an unknown periodic signal with a random spectrum. We will assume that it meets the requirements for its approximation by a finite sum of basis functions. For example, it can be represented by a finite Fourier series. The second part is the sum of deterministic signals from a given set that can be transmitted over a communication channel simultaneously with a reference signal with unknown coefficients.

First, consider the case where the interference is a random periodic signal that can be decomposed into a finite sum of basis functions. A signal is received at the input of the recognition system:

$$y(t) = k_1 g(t) + k_2 \eta(t). \quad (1)$$

The interference is quasi-stationary with an unknown current spectrum superimposed on the spectrum of the reference signal at unknown frequencies. Coefficients k_1 and k_2 in (1) characterize the weight of the reference signal and interference, respectively. The values of k_1 and k_2 are unknown.

DOI 10.15588/1607-3274-2023-3-8

$$\eta(t) = \sum_{i=1}^{M} e_i f_i(t). \quad (2)$$

After substituting (2) into (1), we get:

$$y(t) = k_1 g(t) + k_2 \sum_{i=1}^{M} e_i f_i(t). \quad (3)$$

It is necessary to find the unknown value of the coefficient k_1 at the reference signal $g(t)$ using the given functions $f_i(t)$ and the current values $y(t)$. The inequality of this coefficient to zero indicates that the reference signal $g(t)$ is recognized in $y(t)$. Its value is the weight of the reference signal. Conversely, if $k_1 = 0$, the reference signal is absent. To solve the problem, it is necessary to specify a set of basis functions. Their number M should not be less than what is needed to approximate the interference. The case when deterministic signals from a given set are added to $\eta(t)$, which are simultaneously transmitted over the communication channel with the reference signal, is easily reduced to the previous one. For this, the list of functions for the decomposition of interference is expanded. $f_{M+2}(t)$, $f_{M+3}(t)$, ... $f_{M+r}(t)$ are added to it, where r is the number of signals superimposed on the reference signal.

3 MATERIALS AND METHODS

Disproportion functions are used to solve the problem [13, 14]. There are the disproportion functions by derivatives, by values, and relative disproportions.

In particular, the disproportion with respect to the first-order derivative of the function $w(t)$ with respect to $x(t)$, where t is a parameter, has the form:

$$z(t) = @\, d_x^{(1)} y = \frac{w(t)}{x(t)} - \frac{dw(t)/dt}{dx(t)/dt}. \quad (4)$$

In case $w(t)$ can be represented by the sum of known functions $r_1(t)$, $r_2(t)$, … $r_M(t)$ with unknown coefficients $q_1, q_2, \ldots q_M$.

$$w(t) = q_1 r_1(t) + q_2 r_2(t) + ... + q_M r_M(t), \quad (5)$$

sequential calculation of disproportion (4) allows the finding of unknown coefficients in (5) [13]. In order to use this property to solve the problem, it is necessary to reduce $y(t)$ (3) to the form (5). For this, we will introduce new notations in (3): $c_i = k_2 e_i$

$$f_{M+1}(t) = g(t), \quad (6)$$

$$c_{M+1} = k_1. \quad (7)$$

Substituting (6) and (7) into (3), we get:

$$y(t) = \sum_{i=1}^{M+1} c_i f_i(t). \quad (8)$$

Thus, the problem is reduced to the application of disproportion (4) according to the algorithm given in [13] to calculate the unknown coefficient c_{M+1} in (8). For this, the current values of $y(t)$ are used. At the same time the coefficients c_1, c_2, ... c_M, which determine the interference $\eta(t)$, are also calculated.

In contrast to [13], the case where $y(t)$ is measured discretely in time with a step h and is represented by the array $y_j = y(jh)$ is considered below. Here $j = 0, 1, 2, ...N–1$. The value of N is determined by the total number of functions involved in the recognition system. In addition to M, the reference function $f_{M+1}(t)$ and $y(t)$ should be taken into account. In this case

$$N \geq (M + 1 + 1) + 1. \quad (9)$$

The discrete functions are not differentiable, therefore, instead of disproportion (4), an integral disproportion of the first order should be used [15]. For $w(j)$ and $x(j)$ measured with the same step h, this disproportion has the form:

$$I(j) = @\, I_x^{(1)} w = \frac{w(j-1+w(j)}{w(j-1)+x(j)} - \frac{w(j)}{x(j)}. \quad (10)$$

Let's present (8) in discrete form, where $f(i, j) = f_i(jh)$, $j = 0, 1, \ldots N–1$:

$$y(j) = \sum_{i=1}^{M+1} c_i f(i, j). \quad (11)$$

To describe the algorithm, it is advisable to consider the simplified case when $M = 4$, i.e., the interference is represented by the sum of only four functions in (11), calculated with step h. Now $f(5,j)$ is the reference function that must be recognized. And it is necessary to determine the coefficient c_5. In this case, the signal (11) has the form:

$$y(j) = c_1 f(1, j) + c_2 f(2, j) + c_3 f(3, j) + c_4 f(4, j) + c_5 f(5, j). \quad (12)$$

The algorithm for calculating the coefficients c_i in (12) consists of $(M+1)$ levels. The disproportions (10) $D_{l,n}(j)$ are calculated on each of them.

At the first level, let's calculate the disproportion (10) $y(j)$ with respect to any function from the right-hand side of (12). Let it be $f(1,j)$:

DOI 10.15588/1607-3274-2023-3-8

$$D_{1,1}(j) = @\, I^{(1)}_{f_i} y = \frac{y(j-1)+y(j)}{f(1,j-1)+f(1,j)} - \frac{y(i)}{f(1,j)} =$$
$$= c_1\left[\frac{f(1,j-1)+f(1,j)}{f(1,j-1)+f(1,j)} - \frac{f(1,j)}{f(1,j)}\right] +$$
$$+ c_2\left[\frac{f(2,j-1)+f(2,j)}{f(1,j-1)+f(1,j)} - \frac{f(2,j)}{f(1,j)}\right] + \cdots \qquad (13)$$
$$= c_{m+1}\left[\begin{array}{l}\dfrac{f(M+1,j-1)+f(M+1,j)}{f(1,j-1)+f(1,j)} \\ -\dfrac{f(M+1,j)}{f(1,j)}\end{array}\right].$$

We will also calculate the disproportions of other functions $f(r, j)$ from (12) with respect to $f(1, j)$:

$$D_{1,r}(j) = @\, I^{(1)}_{f_1} f_r =$$
$$= \frac{f(r,j-1)+f(r,j)}{f(1,j-1)+f(1,j)} - \frac{f(r,j)}{f(1,j)}, \qquad (14)$$

where $j = 0, 1, \ldots N–1$; $r = 2, 3, 4, 5$.

Substitute (14) into (13) and take into account that the first component in (13) is zero. As a result, we get:

$$D_{1,1}(j) = c_2 D_{1,2}(j) + c_3 D_{1,3}(j) +$$
$$+ c_4 D_{1,4}(j) + c_5 D_{1,5}(j). \qquad (15)$$

At the second level, in (15), we choose, for example, $D_{1,2}(j)$ and calculate the disproportion (10) of $D_{1,1}(j)$ with respect to $D_{1,2}(j)$:

$$D_{2,1}(j) = @\, I^{(1)}_{D_{1,2}} D_{1,1} =$$
$$= \frac{D_{1,1}(j-1)+D_{1,1}(j)}{D_{1,2}(j-1)+D_{1,2}(j)} - \frac{D_{1,1}(j)}{D_{1,2}(j)} =$$
$$= c_2\left[\frac{D_{1,2}(j-1)+D_{1,2}(j)}{D_{1,2}(j-1)+D_{1,2}(j)} - \frac{D_{1,2}(j)}{D_{1,2}(j)}\right] +$$
$$+ c_3\left[\frac{D_{1,3}(j-1)+D_{1,3}(j)}{D_{1,2}(j-1)+D_{1,2}(j)} - \frac{D_{1,3}(j)}{D_{1,2}(j)}\right] + \qquad (16)$$
$$+ c_4\left[\frac{D_{1,4}(j-1)+D_{1,4}(j)}{D_{1,2}(j-1)+D_{1,2}(j)} - \frac{D_{1,4}(j)}{D_{1,2}(j)}\right] +$$
$$+ c_5\left[\frac{D_{1,5}(j-1)+D_{1,5}(j)}{D_{1,2}(j-1)+D_{1,2}(j)} - \frac{D_{1,5}(j)}{D_{1,2}(j)}\right].$$

Let's also calculate

$$D_{2,r}(j) = @\, I^{(1)}_{D_{1,2}} D_{1,r} =$$
$$= \frac{D_{1,r}(j-1)+D_{1,r}(j)}{D_{1,2}(j-1)+D_{1,2}(j)} - \frac{D_{1,r}(j)}{D_{1,2}(j)}, \qquad (17)$$

where $j = 0, 1, \ldots N–1$; $r = 3, 4, 5$.

After substituting (17) into (16), taking into account that the first term is zero, we obtain:

$$D_{2,1}(j) = c_3 D_{2,3}(j) + c_4 D_{2,4}(j) + c_5 D_{2,5}(j). \qquad (18)$$

Again, we choose any of the components in (18), for example, $D_{2,3}(j)$. Let's calculate the disproportion (10) of $D_{2,1}(j)$ with respect to $D_{2,3}(j)$:

$$D_{3,1}(j) = @\, I^{(1)}_{D_{2,3}} D_{2,1} =$$
$$= \frac{D_{2,1}(j-1)+D_{2,1}(j)}{D_{2,3}(j-1)+D_{2,3}(j)} - \frac{D_{2,1}(j)}{D_{2,3}(j)} =$$
$$= c_3\left[\frac{D_{2,3}(j-1)+D_{2,3}(j)}{D_{2,3}(j-1)+D_{2,3}(j)} - \frac{D_{2,3}(j)}{D_{2,3}(j)}\right] + \qquad (19)$$
$$+ c_4\left[\frac{D_{2,4}(j-1)+D_{2,4}(j)}{D_{2,3}(j-1)+D_{2,3}(j)} - \frac{D_{2,4}(j)}{D_{2,3}(j)}\right] +$$
$$+ c_5\left[\frac{D_{2,5}(j-1)+D_{2,5}(j)}{D_{2,3}(j-1)+D_{2,3}(j)} - \frac{D_{2,5}(j)}{D_{2,3}(j)}\right].$$

Let's also calculate

$$D_{3,r}(j) = @\, I^{(1)}_{D_{2,3}} D_{2,r} =$$
$$= \frac{D_{2,r}(j-1)+D_{2,r}(j)}{D_{2,3}(j-1)+D_{2,3}(j)} - \frac{D_{2,r}(j)}{D_{2,3}(j)}, \qquad (20)$$

where $j = 0, 1, \ldots N–1$; $r = 4, 5$.

Substituting (20) into (19) gives:

$$D_{3,1}(j) = c_4 D_{3,2}(j) + c_5 D_{3,3}(j). \qquad (21)$$

We choose $D_{3,2}(j)$ in (21) and calculate the disproportions (10) with respect to it:

$$D_{4,1}(j) = @\, I^{(1)}_{D_{3,2}} D_{3,1} =$$
$$= \frac{D_{3,1}(j-1)+D_{3,1}(j)}{D_{3,2}(j-1)+D_{3,2}(j)} - \frac{D_{3,1}(j)}{D_{3,2}(j)} =$$
$$= c_4\left[\frac{D_{3,2}(j-1)+D_{3,2}(j)}{D_{3,2}(j-1)+D_{3,2}(j)} - \frac{D_{3,2}(j)}{D_{3,2}(j)}\right] + \qquad (22)$$
$$+ c_5\left[\frac{D_{3,3}(j-1)+D_{3,3}(j)}{D_{3,2}(j-1)+D_{3,2}(j)} - \frac{D_{3,3}(j)}{D_{3,2}(j)}\right],$$

$$D_{4,2}(j) = @\, I^{(1)}_{D_{3,2}} D_{3,3} =$$
$$= \frac{D_{3,3}(j-1)+D_{3,3}(j)}{D_{3,2}(j-1)+D_{3,2}(j)} - \frac{D_{3,3}(j)}{D_{3,2}(j)}, \qquad (23)$$

DOI 10.15588/1607-3274-2023-3-8

After substituting (23) into (22), we get:

$$D_{4,1}(j) = c_5 D_{4,2}(j). \quad (24)$$

Let's calculate the disproportion (10) of $D_{4,1}(j)$ with respect to $D_{4,2}(j)$:

$$D_{5,1}(j) = @\, I^{(1)}_{D_{4,2}} D_{4,1} = \\ = \frac{D_{4,1}(j-1) + D_{4,1}(j)}{D_{4,2}(j-1) + D_{4,2}(j)} - \frac{D_{4,1}(j)}{D_{4,2}(j)} = \\ = c_5 \left[\frac{D_{4,2}(j-1) + D_{4,2}(j)}{D_{4,2}(j-1) + D_{4,2}(j)} - \frac{D_{4,2}(j)}{D_{4,2}(j)} \right] = 0. \quad (25)$$

The equality of $D_{5,1}(j)$ to zero is explained by the presence of a proportional relationship between $D_{4,1}(j)$ and $D_{4,2}(j)$, as can be seen from (24). The unknown coefficient c_5 is calculated from this equation.

$$c_5 = \frac{D_{4,1}(j)}{D_{4,2}(j)}. \quad (26)$$

At the same time, the values of the other coefficients in (12) can be obtained to obtain additional information about the interference and the structure of the signal $y(t)$. This information is necessary to verify compliance with the conditions under which the obtained value of the coefficient c_5 can be considered reliable.

Let's continue the calculation of the coefficients in (12). From (21, 18, 15, 12) we find c_4, c_3, c_2, c_1:

$$c_4 = \frac{D_{3,1}(j) - c_5 D_{3,3}(j)}{D_{3,2}(j)}, \quad (27)$$

$$c_3 = \frac{D_{2,1}(j) - c_4 D_{2,4}(j) - c_5 D_{2,5}(j)}{D_{2,3}(j)}, \quad (28)$$

$$c_2 = \frac{D_{1,1}(j) - c_3 D_{1,3}(j) - c_4 D_{1,4}(j) - c_5 D_{1,5}(j)}{D_{1,2}(j)}, \quad (29)$$

$$c_1 = \frac{y(j) - c_2 f(2,j) - c_3 f(3,j) - c_4 f(4,j) - c_5 f(5,j)}{f(1,j)}. \quad (30)$$

4 EXPERIMENTS

Let's consider the case when the interference consists only of a periodic signal with a frequency limited from above. In (8), it is represented by the sum of harmonic functions:

$$y(t) = c_1 \cos \omega t + c_2 \sin \omega t + c_3 \cos 2\omega t + \\ + c_4 \sin 2\omega t + \cdots + c_{M-1} \cos \frac{M}{2} \omega t + \\ + c_M \sin \frac{M}{2} \omega t + c_{M+1} f_{M+1}(t). \quad (31)$$

In this case, the coefficients c_1 and c_2 represent the first harmonic, c_3 and c_4 – the second, etc.

To be able to present a periodic interference, one must know its period and, at least approximately, the maximum frequency component. This will allow us to determine the frequency of the first and highest harmonic with the number $M/2$ in (31).

At the same time, the frequency of the highest harmonic with the number $M/2$ can be both equal to the maximum frequency with which the interference is controlled and greater than it.

Let's consider example №1. When solving the problem, it is assumed that the interference $\eta(t)$ has the form (2). It is necessary to make sure that for known functions $f_i(t)$ the proposed algorithm allows obtaining the correct values of coefficients c_i i = 1, 2, ...M in (2). For this, we take $y(t)$ (31) and set the c_{M+1} coefficient to zero at the reference function $f_{M+1}(t)$. As a result, we get:

$$\eta(t) = 0.5\cos(t) - 7.25\cos(2t) + \\ + 1.25\sin(2t) - 2.5\sin(5t) + \\ + 0.12\cos(7t) + 2\cos(9t) + \\ + 0.625\sin(10t) - 3\sin(11t) + \\ + 6.75\cos(20t) - 10\sin(20t) = \\ = 0.5 f_1(t) - 7.25 f_3(t) + \\ + 1.25 f_4(t) - 2.5 f_{10}(t) + \\ + 0.12 f_{13}(t) + 2 f_{17}(t) + \\ + 0.625 f_{20}(t) - 3 f_{22}(t) + \\ + 6.75 f_{39}(t) - 10 f_{40}(t). \quad (33)$$

The frequency band in which the interference is included is approximately known to us. Therefore, it is assumed that its highest harmonic is equal to 25, although, in reality, it is equal to only 20. Thus, the number of functions that determine the interference is M = 50. The total number of functions used to determine the coefficients in (33), taking into account $y(t)$, is 51. According to (9), taking into account the absence of a reference function, the number of elements in the discrete representations of the functions is $N \geq (M + 1) + 1 = 52$. Let's take N = 52. The step of changing the argument h = 1. The results are given in Table 1.

The obtained values of coefficients are following: c_1 = 0.5; c_3 = –7.25; c_4 = 1.25; c_{10} = –2.5; c_{13} = 0.12; c_{17} = 2; c_{22} = –3; c_{40} = –10. All other coefficients are equal to zero. It is obvious that the obtained results coincide with the values of the corresponding coefficients in (33). The algorithm works correctly.

DOI 10.15588/1607-3274-2023-3-8

Table 1 – Example 1

i	c_i	i	c_i
1	0.5	26	–1.20E–12
2	8.18E–12	27	4.86E–12
3	–7.25	28	1.04E–12
4	1.25	29	4.14E–12
5	2.28E–12	30	2.35E–12
6	2.05E–12	31	–1.98E–12
7	7.18E–12	32	–3.30E–12
8	8.20E–12	33	1.34E–12
9	–1.14E–12	34	–4.15E–12
10	–2.5	35	3.09E–12
11	1.45E–13	36	–1.71E–12
12	–1.00E–14	37	2.38E–12
13	0.12	38	–9.99E–12
14	3.98E–12	39	6.75
15	–6.86E–12	40	–10
16	2.59E–13	41	6.36E–11
17	2	42	–5.45E–11
18	–1.01E–11	43	5.52E–12
19	1.29E–11	44	–3.16E–11
20	6.25E–01	45	–3.70E–11
21	2.57E–12	46	–7.89E–11
22	–3	47	1.21E–11
23	–4.11E–13	48	–2.46E–11
24	1.93E–13	49	1.39E–12
25	8.18E–14	50	–9.09E–12

For comparison, the interference $\eta(t)$ (33) was also decomposed into a Fourier series of 26 harmonics and N = 52. The step of changing the argument $h = 2\pi/N = 0.12083$. As expected, the cosine components for each harmonic coincided with the coefficients for the odd-numbered functions in (33), and the sine components for the even-numbered ones. That is, in this case, the proposed algorithm can be used to decompose the function into harmonics. It should be noted that in the proposed method, $h = 1$ does not depend on N.

In example №2 the case where the frequency range in which the interference is located is incorrectly determined is being investigated. For example, when $\cos(27t)$ is added to the expression (33), which defines the interference:

$$\begin{aligned}\eta(t) = 0.5\cos(t) - 7.25\cos(2t)\\ +1.25\sin(2t) - 2.5\sin(5t)\\ +0.12\cos(7t) + 2\cos(9t)\\ +0.625\sin(10t)\\ -3\sin(11t) + 6.75\cos(20t)\\ -10\sin(20t) + \cos(27t).\end{aligned} \quad (34)$$

As can be seen from Table 2, all coefficients are not equal to zero and differ from the values in (34). That is, in this case, the algorithm does not work.

Let's consider the example #3. The decomposition of the sum of the reference function $g(t)$ and the interference $\eta(t)$ is considered:

$$y(t) = g(t) + \eta(t), \quad (35)$$

Table 2 – Example 2

i	c_i	i	c_i
1	0.5218	26	–0.00255814
2	–0.0135554	27	–0.00866345
3	–7.47506	28	–0.0321576
4	1.18038	29	–0.0195644
5	–0.0234714	30	0.0329743
6	–0.0409719	31	–0.0267472
7	0.0184056	32	0.00830763
8	–0.083213	33	0.84833
9	–0.0356034	34	0.419396
10	–2.47883	35	0.00274051
11	–0.0093848	36	0.0116143
12	–0.00439558	37	–0.0428529
13	0.119222	38	0.0417336
14	–0.00837845	39	6.49839
15	0.0635089	40	–10.0569
16	–0.0605521	41	0.460666
17	1.97527	42	0.815869
18	–0.000225677	43	–0.0841818
19	–0.0203486	44	0.361305
20	0.606359	45	–0.81944
21	0.0018544	46	0.558422
22	–2.95846	47	0.243344
23	–0.00546663	48	0.0592147
24	0.00449403	49	0.0183457
25	–0.00684171	50	0.0526963

where the interference $\eta(t)$ has the form (33), and the reference function is described by the expression:

$$\begin{aligned}g(t) = 1.5\cos(t) + 3\sin(5t) +\\ +4.75\sin(2t) - 2.5\sin(5t) +\\ +10\cos(7t) + 2.15\sin(10t) +\\ +3.5\cos(15t) + 4\cos(20t) -\\ -10\sin(25t) =\\ = 1.5 f_1(t) + 3 f_2(t) + 4.75 f_4(t) -\\ -2.5 f_{10}(t) + 10 f_{13}(t) + 2.15 f_{20}(t) +\\ +3.5 f_{29}(t) + 4 f_{39}(t) - 10 f_{50}(t).\end{aligned} \quad (36)$$

In this example, the reference function (36) and the interference are in the same frequency range. There are six common basis functions in $g(t)$ as well as in $\eta(t)$. The reference signal can be represented by a finite sum of the same basis functions $f_1(t)$, …, $f_{50}(t)$ that represent the interference. In fact, the sum of the interference and the reference function (36) is decomposed by means of 51 functions, since $f_{M+1}(t)$ must also be taken into account.

Including $y(t)$, a total of 52 functions are involved in recognition. Therefore, according to (9), N = 53 is taken. The results are shown in Table 3. Instead of $c_{51} = 1$, $c_{51} = -0.49484$ was obtained. That is, in this case, the method does not work.

Two important conditions follow from the three examples given:

1. The finite number of basis functions must be sufficient to represent the interference.

2. The basis functions that define the interference should not be sufficient to represent the reference signal. That is, the reference signal must differ by at least one component from the given set of basis functions.

DOI 10.15588/1607-3274-2023-3-8

Table 3 – Example 3

i	c_i	i	c_i
1	2.74225	27	2.80E–11
2	4.48451	28	–8.87E–11
3	–7.25	29	5.23
4	8.35047	30	–1.11E–10
5	–7.28E–11	31	6.45E–11
6	1.84E–10	32	2.51E–11
7	–2.61E–10	33	1.57E–11
8	–2.00E–10	34	1.53E–10
9	6.49E–11	35	3.38E–11
10	–6.23709	36	–6.31E–11
11	1.07E–11	37	6.87E–11
12	–3.48E–12	38	–3.31E–11
13	15.0684	39	–3.31E–11
14	7.12E–11	40	–10
15	2.37E–10	41	–2.02E–09
16	–1.13E–10	42	3.96E–10
17	2	43	2.11E–10
18	3.16E–10	44	–7.62E–10
19	–3.55E–10	45	1.67E–09
20	–3.55E–10	46	1.26E–09
21	8.31E–11	47	1.67E–10
22	–3	48	–1.08E–09
23	–1.33E–11	49	–4.05E–11
24	–1.62E–11	50	–14.9484
25	1.97E–11	51	–0.49484
26	6.26E–12	52	–

Based on this, consider the following examples. In example #4, the interference has the form (33). The reference function differs from (36) due to the addition of cos(30*t*) and thus satisfies the second condition:

$$g(t) = 1.5\cos(t) + 3\sin(t) + 4.75\sin(2t) - \\ - 2.5\sin(5t) + 10\cos(7t) + 2.15\sin(10t) + \\ + 3.5\cos(15t) + 4\cos(20t) - 10\sin(25t) + \\ + 5\cos(30t). \quad (37)$$

Let

$$y(t) = -1.256g(t) + 1000\eta(t). \quad (38)$$

The results are given in Table 4.

That is, it is necessary to find the weighting coefficient for the reference signal, which is almost 1000 times smaller than the coefficient for interference. As in the previous case, 52 functions and $N = 53$ take part in the recognition process.

It should be noted that the decomposition of the interference took place. Therefore, the table shows its coefficients from (33), multiplied by 1000. The reference signal was not decomposed.

The coefficient $c_{M+1}(t) = c_{51}(t) = -1.256$ coincides with the coefficient for $g(t)$ in (38). Thus, it was established that $y(t)$ includes the reference signal $g(t)$ with the coefficient –1.256. So, the signal was recognized in the presence of additive interference and its weighting coefficient was determined.

In example #5 consider the case when the signal $g_1(t)$ is added to the periodic interference (33):

$$g_1(t) = 5\sin(6t) - 2.5\exp(-t) + 4.5. \quad (39)$$

Table 4 – Example 4

i	c_i	i	c_i
1	500	27	–1.94E–08
2	–4.54E–09	28	–1.61E–08
3	–7250	29	–1.67E–08
4	1250	30	3.56E–09
5	7.61E–09	31	–1.09E–09
6	–1.47E–08	32	3.24E–09
7	1.64E–08	33	6.85E–10
8	1.44E–08	34	–4.37E–09
9	8.18E–09	35	5.73E–09
10	–2500	36	–5.41E–09
11	3.81E–09	37	1.83E–08
12	2.97E–09	38	–2.65E–08
13	120	39	6750
14	4.66E–09	40	–10000
15	–9.62E–09	41	1.07E–07
16	–4.24E–09	42	–4.83E–08
17	2000	43	–1.51E–08
18	–2.30E–08	44	6.28E–08
19	2.67E–08	45	–7.63E–08
20	625	46	–8.78E–08
21	8.39E–10	47	3.71E–09
22	–3000	48	–1.04E–07
23	3.02E–09	49	–5.06E–09
24	–4.15E–10	50	3.30E–08
25	3.44E–09	51	–1.256
26	–7.02E–10	52	–

It contains a permanent component. The spectrum of the signal $g_1(t)$ goes beyond the frequency band in which the interference is located. Let

$$y(t) = -1.256g(t) + 1000\eta(t) + 0.725g_1(t). \quad (40)$$

In addition to the given 50 functions and $y(t)$, two more functions are added. Therefore, according to (9), $N = 54$ is taken. The results are shown in Table 5.

Table 5 – Example 5

i	c_i	i	c_i
1	500	27	–3.73E–07
2	–2.24E–07	28	–1.92E–07
3	–7250	29	–3.08E–07
4	1250	30	–1.26E–09
5	9.74E–09	31	1.31E–08
6	8.01E–09	32	–3.65E–09
7	–7.16E–09	33	5.96E–09
8	8.69E–09	34	1.33E–08
9	9.16E–08	35	1.75E–08
10	–2500	36	–1.13E–08
11	–1.47E–08	37	–3.11E–07
12	–2.63E–08	38	–3.44E–07
13	120	39	6750
14	5.40E–09	40	–10000
15	–6.14E–09	41	–9.08E–08
16	–1.88E–08	42	–2.88E–08
17	2000	43	1.86E–08
18	6.30E–09	44	–6.19E–08
19	3.51E–09	45	1.03E–07
20	625	46	1.60E–08
21	–3.10E–08	47	–1.02E–07
22	–3000	48	–3.90E–07
23	1.13E–08	49	4.58E–07
24	9.07E–09	50	7.11E–07
25	9.65E–09	51	–1.256
26	–1.71E–08	52	0.725

For interference, the same results as in the previous case are obtained. Accordingly, the coefficients are

DOI 10.15588/1607-3274-2023-3-8

obtained for $g(t)$ and $g_1(t)$. c_{51}= –1.256 and c_{52}=0.725, which coincide with the coefficients in (40). The recognition of the reference signal $g(t)$, the calculation of its weighting coefficient, and the signal coefficient, which is added to the periodic component of the interference, took place. At the same time, the interference practically has a weight 1000 times greater compared to the reference signal.

Example #6 differs from the previous one only in the absence of $g(t)$ in the composition of $y(t)$:

$$y(t) = 1000\eta(t) + 0.725g_1(t). \quad (41)$$

As can be seen from Table 6, the coefficient at $g(t)$ c_{51} = 0, which indicates the absence of the reference signal in the composition of $y(t)$.

It is also known that $g_1(t)$ with the coefficient c_{52} = 0.725 is part of the interference.

Table 6 – Example 6

i	c_i	i	c_i
1	500	27	8.90E–07
2	5.42E–07	28	4.48E–07
3	–7250	29	7.35E–07
4	1250	30	3.11E–08
5	1.33E–08	31	–8.37E–09
6	–2.31E–08	32	–1.07E–08
7	6.26E–08	33	–2.16E–08
8	–1.27E–08	34	–5.11E–08
9	–2.18E–07	35	–3.30E–08
10	–2500	36	1.98E–08
11	4.57E–08	37	8.62E–07
12	7.40E–08	38	8.72E–07
13	120	39	6750
14	–1.81E–09	40	–10000
15	–2.65E–08	41	5.03E–07
16	4.52E–08	42	1.65E–07
17	2000	43	–3.67E–08
18	–2.41E–08	44	1.50E–07
19	4.24E–08	45	–5.27E–07
20	625	46	–7.45E–08
21	6.40E–08	47	2.75E–07
22	–3000	48	8.61E–07
23	–2.58E–08	49	–1.23E–06
24	–2.47E–08	50	–1.66E–06
25	–1.89E–08	51	–2.08E–07
26	4.44E–08	52	0.725

The results obtained for examples 5 and 6 show that the proposed method allows you to recognize the reference signal and determine its weighting coefficient in the presence of combined additive interference.

CONCLUSIONS

The actual problem of recognizing a reference signal in the presence of additive interference is being solved.

The scientific novelty lies in the introduction of a new method of recognizing reference signals and determining their weighting coefficients in the presence of additive interference when the overlapping of the spectrum occurs at unknown frequencies. The interference can include both the random periodic signal and the sum of other deterministic signals from a given set with unknown weighting coefficients. The periodic random component of the interference must meet the conditions for its approximation by a finite sum of basis functions. In particular, it can be represented by a finite Fourier series. To solve the problem, it is necessary to specify a set of basis functions. Their number should not be less than what is needed to determine the interference. At the same time, the reference signal must include at least one component that is not included in this set. In particular, it can be a harmonic that is absent among those specified for decomposition of the periodic component of the interference or a constant component.

The practical significance of this research is evident in its potential application in operational signal recognition systems. Research results indicate that the method works even in conditions where the interference has a weighting coefficient almost 1000 times greater than that of the reference signal. Accurately identifying reference signals amidst additive interference improves signal processing and analysis in various domains.

Prospects for further research involve improving the proposed method in order to identify signs of violation of the conditions necessary for the successful recognition of the reference signal.

ACKNOWLEDGEMENTS

The work is supported by the state budget scientific research project of Sumy State University “Methods, mathematical models and information technologies for analysis and synthesis of infocommunication systems” (№ DR 0118U006971)

REFERENCES

1. Zhang S., Pan J., Han Z. et al. Recognition of noisy radar emitter signals using a one-dimensional deep residual shrinkage network, *Sensors*, 2021, Vol. 21, № 23. DOI: 10.3390/s22176539
2. Wang Y., Cai W., Gu T. et al. Secure your voice: an oral airflow-based continuous liveness detection for voice assistants, *Proceedings of the ACM on Interactive, Mobile, Wearable and Ubiquitous Technologies*, 2019, Vol. 3, № 4. pp. 1–28. DOI: 10.1145/3369811
3. Zhang X., Tianyun L., Gong P. et al. Modulation recognition of communication signals based on multimodal feature fusion, *Sensors*, 2022, Vol. 22, № 17. DOI: 10.3390/s22176539
4. Fathalla R. S., Alshehri W. S. Emotions recognition and signal classification, *International Journal of Synthetic Emotions*, 2020, Vol. 11, № 1, pp. 1–16. DOI: 10.4018/ijse.2020010101
5. Sabut S., Pandey O., Mishra B. S. P. et al. Detection of ventricular arrhythmia using hybrid time–frequency-based features and deep neural network, *Physical and Engineering Sciences in Medicine*, 2021, Vol. 44, № 1, pp. 135–145. DOI: 10.1007/s13246-020-00964-2
6. Chen H., Guo C., Wang Z. et al. Research on recognition and classification of pulse signal features based on EPNCC, *Scientific Reports*, 2022, Vol. 12, № 6731. DOI: 10.1038/s41598-022-10808-6

DOI 10.15588/1607-3274-2023-3-8

7. Dovbysh A. S., Piatachenko V. Y., Simonovskiy J. V. et al. Information-extreme hierarchical machine learning of the hand brush prosthesis control system with a non-invasive bio signal reading system, *Radio Electronics, Computer Science, Control*, 2020, № 4, pp. 178–187. DOI: 10.15588/1607-3274-2020-4-17
8. Jondral F. K. Software-defined radio – basics and evolution to cognitive radio, *EURASIP Journal on Wireless Communications and Networking*, 2005, Vol. 2005, No. 3, pp. 652784. DOI: 10.1155/WCN.2005.275
9. Jondral F. K., Blaschke V. Evolution of digital radios. *Cognitive Wireless Networks*. Dordrecht, Springer Netherlands, 2007, pp. 635–655. DOI: 10.1007/978-1-4020-5979-7_33
10. Nusratov O., Almasov A., Mammadova A. Positional-binary recognition of cyclic signals by fuzzy analyses of their informative attributes, *Procedia Computer Science*, 2017, Vol. 120, pp. 446–453. DOI: 10.1016/j.procs.2017.11.262
11. Nizhebetska Y. Kh. Classification of signals by using normal orthogonal transformation ,*Visnyk NTUU KPI Seriia – Radiotekhnika Radioaparatobuduvannia*, 2011, Vol. 0, № 47, P. 58–70. DOI: 10.20535/RADAP.2011.47.58-70
12. Swiercz E. Recognition of signals with time-varying spectrum using time-frequency transformation with non-uniform sampling, *MIKON 2018 – 22nd International Microwave and Radar Conference: proceedings.* Poznan, 2018, pp. 140–144. DOI: 10.23919/MIKON.2018.8405158
13. Avramenko V. V., Prohnenko Y. I. Raspoznavanie periodicheskix e'talonnyx signalov pri nalozhenii periodicheskix pomex, *Eastern-European Journal of Enterprise Technologies*, 2012, Vol. 6/4, № 60, pp. 64–67. Access mode: https://cyberleninka.ru/article/n/raspoznavanie-periodicheskih-etalonnyh-signalov-pri-nalozhenii-periodicheskih-pomeh
14. Avramenko V. V., Demianenko V. M. Serial encryption using the functions of real variable, *Radioelectronic and computer systems*, 2021, №21, pp. 39–50. DOI: 10.32620/reks.2021.2.04
15. Karpenko A. P. Integral'nye xarakteristiki nepraporcional'nosti chislovyx funkcij i ix primenenie v diagnostike, *Visnyk of the Sumy State University. Series: Technical Sciences*, Vol. 16, № 2000, pp. 20–25. Access mode: https://essuir.sumdu.edu.ua/bitstream-download/123456789/10931/1/4_Karpenko.pdf

Received 11.05.2023.
Accepted 02.08.2023.

УДК 621.391:004.93

РОЗПІЗНАВАННЯ ЕТАЛОННИХ СИГНАЛІВ ТА ВИЗНАЧЕННЯ ЇХНІХ ВАГОВИХ КОЕФІЦІЄНТІВ ПРИ НАЯВНОСТІ АДИТИВНОЇ ЗАВАДИ

Авраменко В. В. – канд. техн. наук, доцент кафедри комп'ютерних наук, Сумський державний університет, Суми, Україна.
Бондаренко М. О. – аспірант кафедри комп'ютерних наук, Сумський державний університет, Суми, Україна.

АНОТАЦІЯ

Актуальність. Розв'язана актуальна задача є розпізнавання еталонного сигналу при наявності адитивної завади.
Мета. Розпізнавання еталонного сигналу по отриманому значенню його вагового коефіцієнту, коли адитивна завада накладається на спектр еталонного сигналу на невідомих випадкових частотах. Завдання: розробити метод розпізнавання еталонного сигналу для випадку, коли завада складається із невідомого періодичного сигналу, який може бути представлений кінцевою сумою базисних функцій. В заваду можуть також входити детерміновані сигнали із заданої множини з невідомими ваговими коефіцієнтами, які одночасно із еталонним передаються по каналу зв'язку. Для розв'язання задачі застосовується метод апроксимації невідомої періодичної складової завади сумою базисних функцій. Поточна кількість значень сигналу, що поступає на систему розпізнавання залежить від кількості базисних функцій. Цей сигнал є сумою базисних функцій і еталонного сигналу із невідомими ваговими коефіцієнтами.
Метод. Для отримання їх значень вагових коефіцієнтів використовується метод, що базується на властивостях функцій непропорційності. Процес розпізнавання зводиться до обчислення вагового коефіцієнта еталонного сигналу і порівняння його з нулем. Система розпізнавання багаторівнева. Кількість рівнів залежить від кількості базисних функцій.
Результати. Отримані результати свідчать, що якщо еталонний сигнал відрізнятися хоча б на одну складову від заданої множини базисних функцій, розпізнавання відбувається успішно. Приведені приклади свідчать, що система розпізнає еталонний сигнал навіть в умовах, коли ваговий коефіцієнт завади майже в 1000 раз перевершує коефіцієнт при еталонному сигналові. Система розпізнавання працює успішно також в умовах, коли завада включає суму детермінованих сигналів із заданої множини, які одночасно передаються по каналу зв'язку.
Висновки. Наукова новизна отриманих результатів в тому, що розроблено метод розпізнавання еталонного сигналу в умовах, коли для періодичної складової завади відома лише оцінка зверху її максимальної частоти. Також розпізнавання відбувається, коли крім невідомої періодичної завади на корисний еталонний сигнал накладаються сигнали із заданої множини з невідомими ваговими коефіцієнтами. В процесі розпізнавання крім вагового коефіцієнту для корисного еталонного сигналу також отримуються коефіцієнти для складових завади.
КЛЮЧОВІ СЛОВА: еталонний сигнал, завада, розпізнавання сигналу, ваговий коефіцієнт, функції непропорційності, базисні функції, конечний ряд Фур'є.

DOI 10.15588/1607-3274-2023-3-8

ЛІТЕРАТУРА

1. Recognition of noisy radar emitter signals using a one-dimensional deep residual shrinkage network / [S. Zhang, J. Pan, Z. Han et al.] // Sensors. – 2021. – Vol. 21, № 23. DOI: 10.3390/s22176539
2. Secure your voice: an oral airflow-based continuous liveness detection for voice assistants / [Y. Wang, W. Cai, T. Gu et al.] // Proceedings of the ACM on Interactive, Mobile, Wearable and Ubiquitous Technologies. – 2019. – Vol. 3, № 4. – P. 1–28. DOI: 10.1145/3369811
3. Modulation recognition of communication signals based on multimodal feature fusion / [X. Zhang, L. Tianyun, P. Gong et al.] // Sensors. – 2022. – Vol. 22, № 17. DOI: 10.3390/s22176539
4. Fathalla R. S. Emotions recognition and signal classification / R. S. Fathalla, W. S. Alshehri // International Journal of Synthetic Emotions. – 2020. – Vol. 11, № 1. – P. 1–16. DOI: 10.4018/ijse.2020010101
5. Detection of ventricular arrhythmia using hybrid time–frequency-based features and deep neural network / [S. Sabut, O. Pandey, B. S. P. Mishra et al.] // Physical and Engineering Sciences in Medicine. – 2021. – Vol. 44, № 1. – P. 135–145. DOI: 10.1007/s13246-020-00964-2
6. Research on recognition and classification of pulse signal features based on EPNCC / [H. Chen, C. Guo, Z. Wang et al.] // Scientific Reports. – 2022. – Vol. 12, № 6731. DOI: 10.1038/s41598-022-10808-6
7. Information-extreme hierarchical machine learning of the hand brush prosthesis control system with a non-invasive bio signal reading system / [A. S. Dovbysh, V. Y. Piatachenko, J. V. Simonovskiy et al.] // Radio Electronics, Computer Science, Control. – 2020. – № 4. – P. 178–187. DOI: 10.15588/1607-3274-2020-4-17
8. Jondral F. K. Software-defined radio – basics and evolution to cognitive radio / F. K. Jondral // EURASIP Journal on Wireless Communications and Networking. – 2005. – Vol. 2005, No. 3. – P. 652784. DOI: 10.1155/WCN.2005.275
9. Jondral F. K. Evolution of digital radios / F. K. Jondral, V. Blaschke // Cognitive Wireless Networks – Dordrecht : Springer Netherlands, 2007. – P. 635–655. DOI: 10.1007/978-1-4020-5979-7_33
10. Nusratov O. Positional-binary recognition of cyclic signals by fuzzy analyses of their informative attributes / O. Nusratov, A. Almasov, A. Mammadova. // Procedia Computer Science. – 2017. – Vol. 120. – P. 446–453. DOI: 10.1016/j.procs.2017.11.262
11. Nizhebetska Y. Kh. Classification of signals by using normal orthogonal transformation / Y. Kh. Nizhebetska // Visnyk NTUU KPI Seriia – Radiotekhnika Radioaparatobuduvannia. – 2011. – Vol. 0, № 47. – P. 58–70. DOI: 10.20535/RADAP.2011.47.58-70
12. Swiercz E. Recognition of signals with time-varying spectrum using time-frequency transformation with non-uniform sampling / E. Swiercz // MIKON 2018 – 22nd International Microwave and Radar Conference : proceedings. – Poznan : 2018. – P. 140–144. DOI: 10.23919/MIKON.2018.8405158
13. Авраменко В. В. Распознавание периодических эталонных сигналов при наложении периодических помех / В. В. Авраменко, Ю. И. Прохненко // Восточно-Европейский Журнал Передовых Технологий. – 2012. – Т. 6/4, № 60. – С. 64–67. – Режим доступа: https://cyberleninka.ru/article/n/raspoznavanie-periodicheskih-etalonnyh-signalov-pri-nalozhenii-periodicheskih-pomeh
14. Avramenko V. V. Serial encryption using the functions of real variable. / V. V. Avramenko, V. M. Demianenko. // Radioelectronic and computer systems. – 2021. – № 21. – P. 39–50. DOI: 10.32620/reks.2021.2.04
15. Карпенко А. П. Интегральные характеристики непропорциональности числовых функций и их применение в диагностике / А. П. Карпенко // Вісник Сумського державного університету. Серія: Технічні науки. – Т. 16, № 2000. – С. 20–25. – Режим доступу: https://essuir.sumdu.edu.ua/bitstream-download/123456789/10931/1/4_Karpenko.pdf

DOI 10.15588/1607-3274-2023-3-8

UDC 004.021

K-NN'S NEAREST NEIGHBORS METHOD FOR CLASSIFYING TEXT DOCUMENTS BY THEIR TOPICS

Boyko N. I. – Candidate of Economics, Associate Professor, Associate Professor of the Department of Artificial Intelligence Systems, Lviv Polytechnic National University, Lviv, Ukraine.

Mykhailyshyn V. Yu. – Assistant Professor, Department of Artificial Intelligence Systems, Lviv Polytechnic National University, Lviv, Ukraine.

ABSTRACT

Context. Optimization of the method of nearest neighbors *k*-NN for the classification of text documents by their topics and experimentally solving the problem based on the method.

Objective. The study aims to study the method of nearest neighbors *k*-NN for classifying text documents by their topics. The task of the study is to classify text documents by their topics based on a dataset for the optimal time and with high accuracy.

Method. The *k*-nearest neighbors (*k*-NN) method is a metric algorithm for automatic object classification or regression. The *k*-NN algorithm stores all existing data and categorizes the new point based on the distance between the new point and all points in the training set. For this, a certain distance metric, such as Euclidean distance, is used. In the learning process, *k*-NN stores all the data from the training set, so it belongs to the "lazy" algorithms since learning takes place at the time of classification. The algorithm makes no assumptions about the distribution of data and it is nonparametric. The task of the *k*-NN algorithm is to assign a certain category to the test document *x* based on the categories *k* of the nearest neighbors from the training dataset. The similarity between the test document *x* and each of the closest neighbors is scored by the category to which the neighbor belongs. If several of *k*'s closest neighbors belong to the same category, then the similarity score of that category for the test document *x* is calculated as the sum of the category scores for each of these closest neighbors. After that, the categories are ranked by score, and the test document is assigned to the category with the highest score.

Results. The *k*-NN method for classifying text documents has been successfully implemented. Experiments have been conducted with various methods that affect the efficiency of *k*-NN, such as the choice of algorithm and metrics. The results of the experiments showed that the use of certain methods can improve the accuracy of classification and the efficiency of the model.

Conclusions. Displaying the results on different metrics and algorithms showed that choosing a particular algorithm and metric can have a significant impact on the accuracy of predictions. The application of the ball tree algorithm, as well as the use of different metrics, such as Manhattan or Euclidean distance, can lead to improved results. Using clustering before applying *k*-NN has been shown to have a positive effect on results and allows for better grouping of data and reduces the impact of noise or misclassified points, which leads to improved accuracy and class distribution.

KEYWORDS: method, cluster, classification, text document, subject, ball tree algorithm, metric.

ABBREVIATIONS

k-NN is a *k*-nearest neighbor method;

kd-tree is a *k*-dimensional tree;

*L*1 – distance is a Manhattan metric;

TF-IDF is a *TF* – term frequency, *IDF* – inverse document frequency;

CSV is a comma-separated value.

NOMENCLATURE

di is a text document;

CI is a appropriate classification of the document;

$f(x)$ is a label intended for the test document x;

Score (x,C_j) is a score assigned to a category based on the points of category K of the nearest neighbors to the test document X;

sim (x,d_i) is a similarities between X and the training document D;

$y(d_i, C_j) \in \{0,1\}$ is a binary value of the category for the educational document regarding d_iC_j;

$w_{c_i^0}^{j+1}(t)$ is a denotes the new weight of the word t in the cluster C_i^0;

$w_{c_i^0}^{j}$ is a weight of the word t in the cluster C_i^0;

$w(t)_p$ is a weight of the word t in the text p;

$C_i^0$is a number of texts contained in the cluster C_i^0;

ClusterScore(x,C_j) is a score assigned to a category based on category points to test the document C_jX;

sim(x,C_i^0) is a similarity between X and cluster in model $C_i^0m_0$;

$y(C_i^0, C_j) \in \{0,1\}$ is a cluster relative to $C_i^0C_j$;

N is a total number of signs;

count(c_i, C) is a number of votes for the class c_i in the set C;

argmax is a function that returns the index of the maximum value.

INTRODUCTION

In today's world, a large amount of information is created and accumulated daily in various formats. As the volume of textual information grows in various fields, effective methods of processing and analysis are increasingly needed. Therefore, it is important to be able to analyze and classify this information effectively.

Classification of documents on their topics can be useful for many tasks, for example, selecting documents that meet certain criteria, building recommender systems, analyzing text data in social networks, etc.

DOI 10.15588/1607-3274-2023-3-9

The importance of the task of classifying text documents by the method of nearest neighbors will reduce the dimension of the data, save information about the classification and increase its accuracy. It is also quite easy to use and does not require a lot of computing power, which makes it popular in many areas [1, 3].

This method does not require pre-modeling, which allows it to be used for online classification and for the classification of text documents with a small data set, which is a fairly common situation in natural language processing. In addition, *k*-NN can be applied to the classification of documents without regard to their contents, only based on information about the topics. In addition, *k*-NN is a fairly flexible algorithm, since it is possible to use different distance metrics and distinguish the weight of each sample depending on its significance for classification [5, 6].

The task of the nearest neighbors method is to classify new data based on their similarity with known data (training data set). The problem of the nearest neighbors method is guided by the concept that if points in the data space are close to each other, then the probability that they belong to the same class is high, therefore, it is solved accordingly according to the principle such that in the variant *k*-NN each feature belongs to the predominant class of nearest neighbors, where *k* is the method parameter. The basis of the *k*-NN method is the fact that, according to the compactness hypothesis, it is expected that the test feature *d* will have the same label as the learning features in the local region surrounding the sign *d* [2, 4].

In the case of researching the use of the nearest neighbors method *k*-NN to classify text documents according to their topics, the novelty is that it offers the use of a method that is quite simple and effective to solve the complex problem of classifying text documents by their topics. The study proposes the use of clustering and dimensionality reduction to improve the quality of text classification. In addition, the study compares the efficiency of different types of term oscillation and different *k* values in the *k*-NN method for classifying text documents. Thus, the study expands our understanding of how the *k*-NN nearest neighbors method can be applied to classify text documents by their topics and helps to improve methods for classifying texts.

The aim of the study is to train the method of *k*-NN's nearest neighbors to classify text documents by their topics.

The subject of research is the creation and optimization of the method of nearest neighbors *k*-NN for the classification of text documents by their topics, as well as the solution of the problem based on the method experimentally.

The main objectives of the study are:

– General overview of the *k*-NN nearest neighbors method for creating a software solution for classifying text documents by their topics.

– Development of a system that can automatically classify text documents by their topics.

– Reducing classification errors to improve system accuracy.

– Research on the effectiveness of *k*-NNs in classifying documents with different numbers of categories and developing methods to improve efficiency in such cases.

1 PROBLEM STATEMENT

The purpose of the study is to build a model that can automatically assign a category to a new text document.

Suppose we have a set of text documents $D = \{d_1, d_2, ..., d_n\}$, where each document is represented as a sequence of words or tokens. Each d_i document belongs to one of the predefined classes or categories $C = \{c_1, c_2, ..., c_k\}$.

To build a model, we have a training dataset consisting of pre-classified documents and corresponding classes.

Mathematically, the problem of classification of text documents can be formulated as follows:

Given: Training dataset $D\_train = \{(d_1, c_1), (d_2, c_2), ..., (d_m, c_m)\}$, where d_i is a text document and c_i is its corresponding classification.

Find: *Function* $f:D\_test \rightarrow C$ which can categorize a new text document from test set *D_test* into one of *C* classes.

2 LITERATURE REVIEW

A special role for research is the methods of classification and clustering of text data. In the study [1, 3], the authors provide an introduction to the *k*-NN nearest neighborhood method and consider its application to the classification of text documents. They describe how the *k*-NN method can be used to classify texts and provide examples of how this method can be applied to data from various fields, including biology, medicine, and e-commerce.

This paper [7] is an important source for studying the basics of textual information processing and data retrieval. The book covers a wide range of topicss from the field of information retrieval, including index building, weighted estimation methods, vector models, thematic modeling, ranking, and more.

The paper [8] describes a wide range of methods of machine learning and statistical data analysis. It is useful for researchers working with the *k*-NN closest neighbor method to classify text documents by their topics.

The book [10] contains a lot of material about probabilistic models, multivariate data analysis, teaching methods, and graphical models. These techniques can be useful for improving the accuracy of classification using the *k*-NN closest neighbor method. In addition, the book contains numerous examples that demonstrate how different machine-learning methods can be applied to solve real-world problems.

The study [13] describes in detail the theoretical and practical aspects of working with text, including topicss

DOI 10.15588/1607-3274-2023-3-9

such as statistical models of language, thematic modeling, tone analysis, machine translation, and others.

The book discusses various methods of vector representation of text that can be used to build a model for the *k*-NN method and also discusses other machine-learning methods for classifying text documents, such as the naïve Bayesian classifier and the support vector method.

In particular, the authors [14] describe in detail the use of bag-of-words models and address the construction of a dataset for training and testing the model, as well as the choice of model parameters, such as the number of nearest neighbors to be used to classify documents.

The research [15] is devoted to the analysis of text data and methods of their processing, in particular the problems of classification and clustering of documents. It describes various methods, including the *k*-NN nearest neighbor method.

The book [12] discusses the following problems:

– Training, statistical methods, and association rules in the field of text mining, which describe different approaches to analyzing text data, including machine techniques.

– Building machine learning models used to classify and cluster documents, in particular the *k*-NN closest neighbor method.

– Preparing data for text analysis, including feature selection and data dimensionality reduction. The book describes in detail how to select the most significant features from the text that will improve the results of data analysis. The book also discusses methods for reducing the dimensionality of data, such as the principal component method and clustering method.

– The book contains many examples of applications of text mining techniques, including text tone analysis, document classification, and email spam detection.

Thus, the analysis of text documents is quite an important topics in our time, since the number of their application in various fields is increasing every day. Accordingly, consideration is relevant for this study and will help in improving the accuracy of the model.

3 MATERIALS AND METHODS

The *k*-nearest neighbor method is a metric algorithm for automatically classifying objects or regression. The *k*-NN algorithm stores all existing data and classifies the new point based on the distance between the new point and all points in the training set. To do this, use a specific distance metric, such as Euclidean distance. In the process of learning, *k*-NN stores all the data from the training set, so it belongs to the "lazy" algorithms since learning takes place at the time of classification. The algorithm makes no assumptions about the distribution of data and it is nonparametric [1, 11].

For the classification of text documents on the topics, the *k*-nearest neighbors method was chosen because of several reasons: simplicity and ease of implementation, high accuracy, and the ability to take into account the importance of each feature:

The *k*-NN method also has some disadvantages, in particular, it can be sensitive to noise and a large number of features and may require a significant amount of memory and computing resources when processing large amounts of data. Therefore, before proceeding with the classification of text documents, you can apply actions that can improve the quality and performance of the algorithm and its accuracy, namely [13]:

– Apply noise or unnecessary signs to data before using the *k*-NN method, which can reduce their impact on forecasting and help make the algorithm more efficient.

– Use distributed computing systems to handle large amounts of data, which can reduce the load on memory and computing resources. You can also use the approach of reducing the dimensionality of the data, which allows you to reduce the number of features and simplify the data space.

– Weights can be assigned to each sign depending on its importance for forecasting. This can help reduce the impact of less important features on forecasting and increase accuracy.

The task of the *k*-NN algorithm is to assign a test document x a certain category based on the categories k of closest neighbors from the training dataset. The similarity between the test document x and each of the closest neighbors is scored by the category to which the neighbor belongs. If several of k's closest neighbors belong to the same category, then the similarity score of that category for the test document x is calculated as the sum of the category points for each of these closest neighbors. After that, the categories are ranked by score, and the test document is assigned to the category with the highest score. The decision rule for *k*-NN can be written as follows (Formula 1):

$$f(x) = \arg\max Score(x, C_j) = \\ = \sum_{d_i \in kNN} sim(x, d_i) y(d_i, C_j), \quad (1)$$

This approach is effective, nonparametric and easy to implement. However, the classification time is very long, and accuracy is seriously impaired by the presence of noise training documents [9].

To improve the accuracy of the *k*-NN algorithm for text data classification in the study, a number of actions will be performed, such as:

1. Representation of documents/text as a vector space model, where each document/text is represented as a vector in an *n*-dimensional word space where each word is represented as coordinates. The more often a certain term appears in a document, the greater its significance in this document and the greater its coordinate in the vector representation of the document. Accordingly, this will speed up the work and classification of the *k*-NN method. The weight of each word in a document is calculated by weighing how often that word is used in the document and throughout the document collection. If the word is

DOI 10.15588/1607-3274-2023-3-9

used often in a document, but rarely in other documents, then its weight will be high.

2. Create a classification model based on clustering. For this, one-pass clustering algorithm with constraints should be used. This algorithm provides incremental clustering with time complexity close to linear.

3. During the clustering process, each cluster is represented as a cluster vector according to the centroid vector for each cluster [14, 20]. The change in word weight of each cluster is calculated by the formula 2:

$$w_{c_i^0}^{j+1}(t) = \frac{w_{C_i^0}^{j}(t) \times w(t)_p}{\left|C_i^0\right| + 1}. \quad (2)$$

According to the applied changes, the decision-making formula for *k*-NN will look like this (Formula 3):

$$f(x) = \arg\max ClusterScore(x, C_j) = \\ = \sum_{C_i^0 \in kNN} sim(x, C_i^0) y(C_i^0, C_j). \quad (3)$$

Suppose we have a training set of text documents with known classes that match their topicss. Each text document is represented as a feature vector $X = [x_1, x_2, ..., x_N]$, where x_i is a sign (for example, word, term) for the i-th document, and N is the total number of signs. Using a certain similarity metric, such as cosine similarity, we calculate the similarity between the feature vectors of two documents. Let $sim(x, y)$ denotes similarities between documents x and y. Accordingly, we find k documents from the training kit that have the greatest similarity with the new document. Denote these documents as $S = \{s_1, s_2, ..., s_k\}$, where s_i is the i-th closest neighbor. Hence we determine the class of the new document, by voting or by majority among k nearest neighbors. Let $C = \{c_1, c_2, ..., c_k\}$ – document classes $s_1, s_2, ..., s_k$.. The class of the new document will be the class with the most votes among these k closest neighbors.

Thus, the definition of the class of a new document, based on the vote of the nearest neighbors, can be written as follows (Formula 4):

$$argmax_i(count(c_i, C)), i = 1 \rightarrow k. \quad (4)$$

In the context of *k*-nearest neighbors (*k*-NN), hyperparameters are used to tune the algorithm itself, not to train a model with data. Hyperparameters determine the behavior of *k*-NN and its characteristics. The main hyperparameters include [17, 19]:

1. *k*: This is the main *k*-NN hyperparameter that determines the number of nearest neighbors to be used for decision-making.

2. Neighbor search algorithm: *k*-NN can use different neighbor search algorithms, such as “ball tree”, “kd tree” and others.

3. Distance or metric: *k*-NN uses distance or metric to determine how close points are to each other. For example, Euclidean distance, Manhattan distance, or cosine similarity.

In our context, we will apply them to analyze their impact on *k*-NN and, through them, try to improve the accuracy of the method.

The following Neighbor search algorithms are considered in the study:

1. The Ball Tree algorithm is one of the methods of constructing a data structure for the efficient execution of operations of the nearest neighbor in classification and clustering problems. It is based on the idea of partitioning a data space into minimally convex balls, known as “balls”. The basic principle of constructing a Ball Tree is to recursively partition data into subsets by calculating the center point (center of the “ball”) and the radius of the ball that best covers the data. The Ball Tree method allows you to quickly find *k*-nearest neighbors, reducing the number of comparisons between points and speeding up searches. It is especially useful for large data sets or when the distances between points have a large difference.

2. A *kd*-tree is a data structure used in the *k*-NN algorithm to quickly find the nearest neighbors. It divides a data space as a binary tree, where each node represents a point in space and divides that space into two subdomains. A key feature of the *kd*-tree is the way data is divided in space using hyperplanes parallel to the coordinate axes. The *kd*-tree significantly reduces the number of comparisons operations required to find the nearest neighbors, which makes it an effective method for *k*-NN. It is especially useful in problems with a large number of points in the data space.

The Minkow metric is a general term for a family of metrics that include Manhattan distance and Euclidean distance as partial cases of them. It is used to calculate the distance between two points in *n*-dimensional space. Formally, the Minkov metric is defined as follows for two points $P(p_1, p_2,\ldots,p_n)$ and $Q(q_1, q_2,\ldots,q_n)$ in *n*-dimensional space (Formula 5):

$$d = (|p_1 - q_1|^p + |p_2 - q_2|^p + \ldots + |p_n - q_n|^p). \quad (5)$$

In this formula, p is a parameter that controls the shape of the metric. Depending on the value of p, the Minkov metric can vary from Manhattan distance ($p = 1$) to Euclidean distance ($p = 2$). Using the p parameter, the Minkow metric can simulate various types of distances, including $L1$ distance (Manhattan), $L2$ distance (Euclidean), and others [16, 18].

The Minkowi metric is a popular choice in the *k*-NN algorithm. It allows you to determine the distance between objects and take into account their location in space. Depending on the type of data and the nature of the task, it is advantageous to use different values of the pa-

DOI 10.15588/1607-3274-2023-3-9

rameter p for optimal results. Minkowian metrics can be computationally efficient, especially for large datasets.

The choice of the Reuters dataset to classify text documents by their subject using *k*-nearest neighbors is the most optimal for several reasons:

– Variety of topicss: The Reuters-21578 dataset contains a wide range of topicss, covering news from various fields such as finance, technology, sports, politics, and others. This ensures representativeness and diversity of data, which is important for the classification of texts.

– Data volume: The Reuters-21578 dataset contains a significant number of documents on various topicss. Most classification algorithms, including *k*-NN, require enough data to achieve reliable results. Therefore, the presence of a large amount of data in the Reuters-21578 dataset makes it attractive for *k*-NN applications.

– The similarity of text documents: The *k*-NN algorithm is based on the hypothesis that similar data have similar classes. The Reuters-21578 dataset contains news articles that may have similar characteristics depending on the topics. This supports the *k*-NN hypothesis and contributes to its effectiveness in classifying these texts.

In total, the Reuters-21578 dataset contains about 21,578 news documents written in English. Each document includes a title, date, text table of contents, and category labels assigned to it (Table 1). The documents in the dataset are classified into 135 different categories, such as “foreign news”, “sports”, “politics”, etc. Each document can have many categories to which it belongs.

Table 1 – Data Set fields

Field name	Type	Description
Title	String	Contains text data represented as a character string.
Date	String	Represents the date of publication of the article.
Topicss	Sequence	Represents categories or topicss related to the article. It is stored as a set or list of lines, where each line represents a topics or category label.
Places	Sequence	Represents the geographical locations mentioned in the article. It is stored as a set or list of rows, where each row represents a place label.
People	Sequence	Contains the names of persons mentioned in the article. It is stored as a set or list of strings.
Orgs	Sequence	Contains the names of organizations mentioned in the article. It is stored as a set or list of strings.
Exchanges	Sequence	Represents mentions of stock exchanges or financial markets in an article. It is usually stored as a set or list of strings.
Text	String	Contains the main text of the news article and is presented as a string of characters.

Since the dataset Reuters-21578 may contain data or their type, which may worsen the results of the study, it must carry out preliminary processing of the data.

First, we need to balance the text and process it further. Some documents may contain symbols, punctuation, or numbers that do not carry essential information for text analysis. Data pre-processing allows you to remove these unnecessary elements and focus on essential aspects of the text. We also need to reduce everything to lowercase to ensure uniformity. Breaking the text into separate tokens or words is also an important step for further analysis. Tokenization helps to understand the structure of a text and divide it into separate units, which facilitates further processing and use. To improve your workout results, you need to remove stop words, which will reduce noise. Stop words are common words that do not carry essential information for text analysis, for example, “the”, “and”, “is”, etc. Another very important step is that it is necessary to reduce words to their basic form (lemmatization). This reduces the number of unique words in the text and makes it easier to recognize the semantic relationship between them. For example, given that we have texts in English, words like “running”, “run” and “ran” will be reduced to the lemma “run”.

Secondly, we need to convert the words’ text to vector format. Vectorization is the process of converting text data into numerical vectors that can be used to further analyze or train machine learning models. This is achieved using methods such as bag-of-words or TF-IDF (Term Frequency-Inverse Document Frequency) in our case, where each word or term is represented by a numeric value. This allows textual data to be treated as numerical features that can be used in machine learning models for classification, clustering, or other analysis.

Therefore, these steps will help prepare data from the Reuters-21578 dataset for further application of machine learning and text analysis models, since data preprocessing helps to improve data quality and representativeness, reduce noise, etc.

4 EXPERIMENTS

The next step is to study the effectiveness of the *k*-NN closest neighbors method for classifying text documents by their topics. Therefore, we will show in more detail the influence of the parameter *k* and the choice of distance metric and other factors.

To begin with, we display the number of articles belonging to a certain category (Fig. 1):

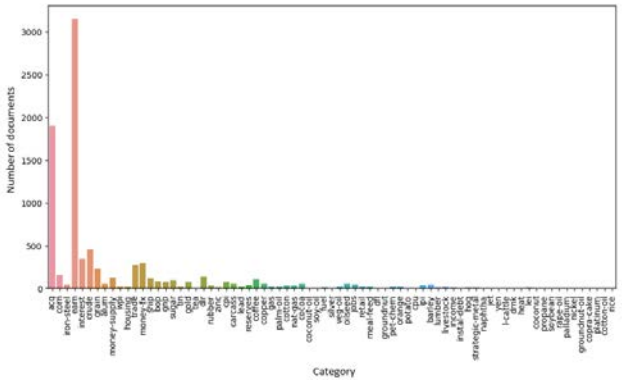

Figure 1 – A bar chart showing the categorization

We divide the experiments, the purpose of which is to improve the accuracy of classification, into:

1. Effect of parameter *k*: Experiments will be performed with different values of the parameter *k* (number

DOI 10.15588/1607-3274-2023-3-9

of neighbors) and the accuracy of the model on the test set will be measured.

2. Clustering Impact: Experiments will be conducted with the generated clustering-based classification model and its impact on the accuracy of the *k*-NN model on the test set.

3. Choosing a distance metric and *k*-NN hyperparameters: Experiments will be conducted with different distance metrics and with different *k*-NN hyperparameters, namely an algorithm such as “ball_tree” (partitioning the data space into minimally convex balls) and a *k*-distance tree and metrics (such as the Manhattan metric and Euclidean distance), and the accuracy will be measured on the test set.

To assess the quality of the classification model, we will use metrics. Here is a brief explanation of each metric:

1. Accuracy: Measures the ratio of the number of correctly classified documents to the total number of documents. The higher the value, the better the model.

2. Precision: Measures the ratio of the number of correctly positively classified documents to the total number of positively classified documents. This indicates how accurately the model identifies positive documents.

3. Recall: Measures the ratio of the number of correctly positively classified documents to the total number of documents belonging to the positive class (correctly classified positive documents plus false negative documents). This indicates how fully the model defines positive documents.

4. F1 score: This is the harmonic average between accuracy and completeness. It is used as a compromise metric that combines information about accuracy and completeness. It takes into account both the accuracy and completeness of the model and uses its harmonic average to calculate the final value.

To estimate the error of our model, we will build a histogram comparing real and predicted data, where count represents the number of cases or frequency of each category in the data set, and category respectively the category itself. We will also build a prediction matrix. The prediction matrix reflects the correspondence between actual and predicted classes and allows quantitative analysis of classification results. It consists of rows and columns, where the rows represent the actual classes, and the columns represent the provided classes. Each cell in the matrix shows the number of samples that belong to a certain actual class and have been mistakenly classified into a specific predicted class. For both options, we will take the top 15 values to see the result better.

These studies will allow us to understand under what parameters and characteristics *k*-NN shows itself best.

The purpose of the experiment №1 is to study the influence of the number of neighbors (parameter *k*) on the results of a particular operation or algorithm.

We will conduct a study on the parameters k = 1, 5, 10, 15, 20 where k is the number of neighbors. We calculate the assessment of the quality of the classification model at k = 1 (Fig. 2).

```
Accuracy:0.79935125115848
Precision:0.8054679150341048
Recall:0.79935125115848
F1 score:0.7980253922562135
```

Figure 2 – Evaluation of the quality of the classification model

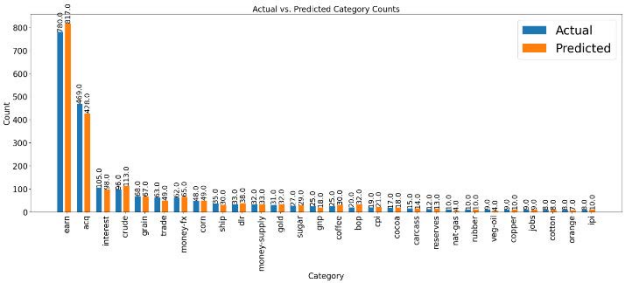

Figure 3 – Histogram comparison number of predicted and real data for k=1

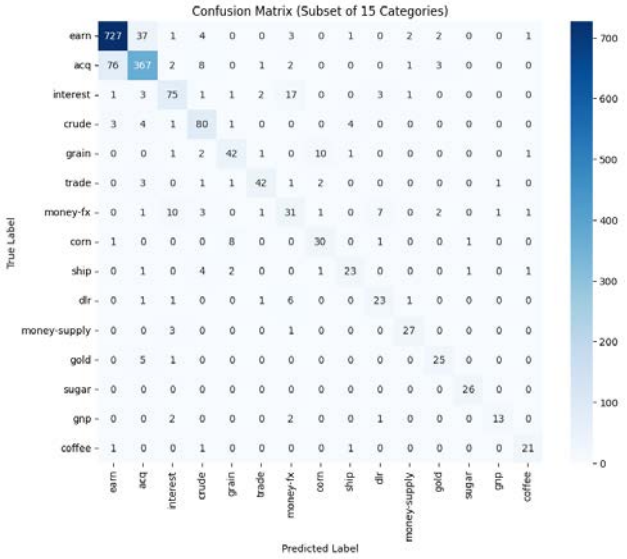

Figure 4 – Prediction matrix for k=1

As we can see from the Fig. 2, the results are satisfactory, but they should be improved. In Fig. 3 shows that the largest error belongs to the EARN category. From the matrix of predictions in Fig. 4 we can also see that most often the algorithm was wrong in determining the category of EARN and ACQ.

We calculate the assessment of the quality of the classification model at k = 5 (Fig. 5).

```
Accuracy:0.8178869323447636
Precision:0.8153930325993035
Recall:0.8178869323447636
F1 score:0.8101419178618491
```

Figure 5 – Evaluation of the quality of the classification model

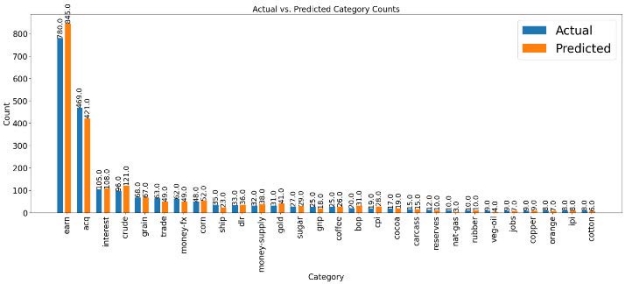

Figure 6 – Histogram comparison number of predicted and real data for k=5

DOI 10.15588/1607-3274-2023-3-9

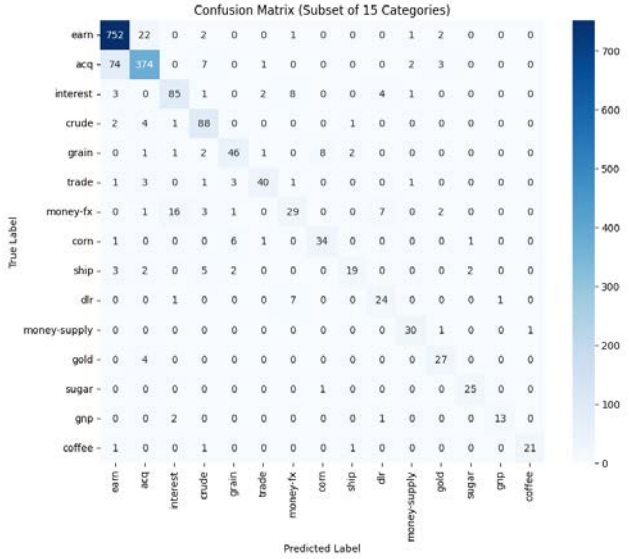

Figure 7 – Prediction matrix for k=5

As we can see from the Fig. 5, the results improved compared to the results in Fig. 2, but they should be improved. In Fig. 6 it can be seen that again the greatest error belongs to the prediction of data in EARN, but compared to the results achieved at k = 1, the error has increased. Following the matrix of predictions in Fig. 7 we can also see that most often the algorithm was wrong in determining the category EARN and ACQ, but for ACQ, it decreased compared to the results at k = 1. However, the number of correct distributions has increased.

We calculate the assessment of the quality of the classification model at k = 10 (Fig. 8).

```
Accuracy:0.8341056533827618
Precision:0.8317522368556206
Recall:0.8341056533827618
F1 score:0.8252637674684895
```

Figure 8 – Evaluation of the quality of the classification model

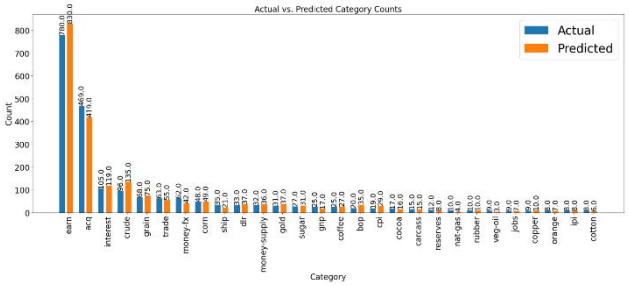

Figure 9 – Histogram comparison number of predicted and real data for k=10

As we can see from Fig. 8, the results improved compared to the results in Fig. 5 which makes them quite accurate. In Fig. 9 it can be seen that again the greatest error belongs to the prediction of data in EARN, but compared to the results achieved at k = 5, the error has decreased. Following the matrix of predictions in Fig. 10 we can also see that the algorithm was most often wrong in determining the categories of EARN and CRUDE, instead of ACQ. However, the number of correct distributions has increased.

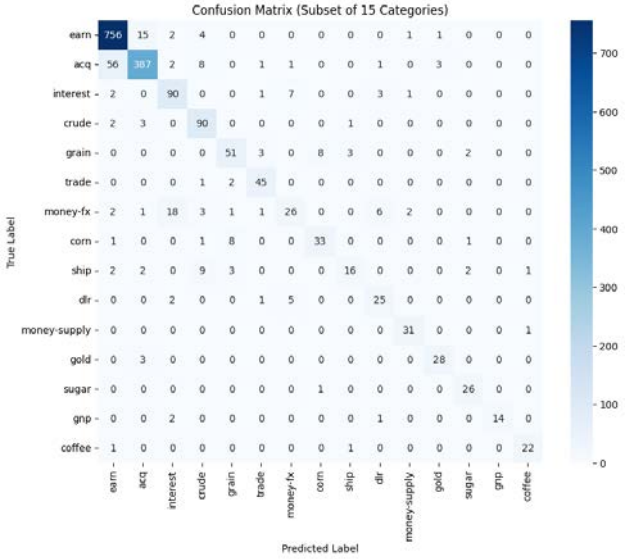

Figure 10 – Prediction matrix for k=10

We calculate the quality assessment of the classification model at k = 15 (Fig. 11).

```
Accuracy:0.8387395736793327
Precision:0.8352195686724123
Recall:0.8387395736793327
F1 score:0.8290827008957881
```

Figure 11 – Evaluation of the quality of the classification model

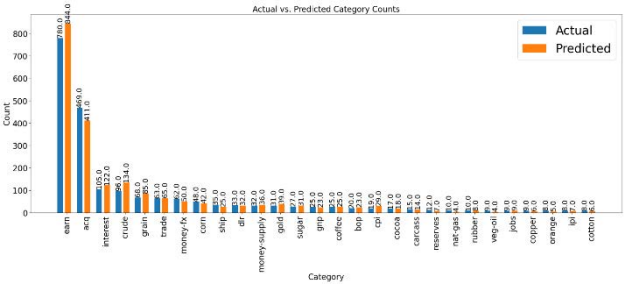

Figure 12 – Histogram comparison number of predicted and real data for k=15

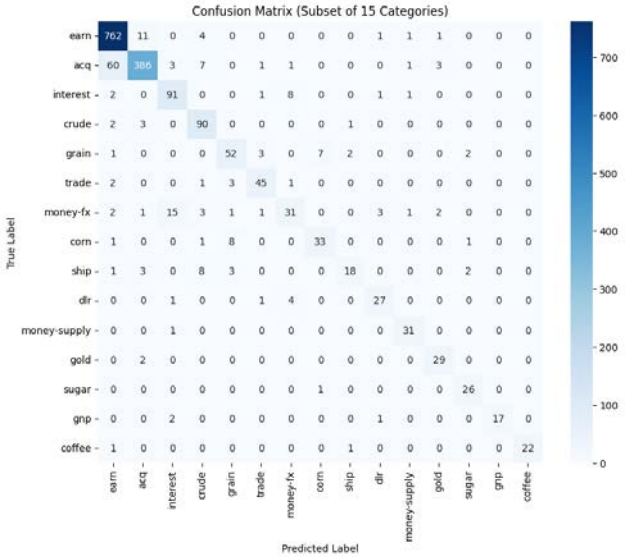

Figure 13 – Prediction matrix for k=15

DOI 10.15588/1607-3274-2023-3-9

As we can see from the Fig. 11, the results improved compared to the results in Fig. 8. In Fig. 12 it can be seen that again the greatest error belongs to the prediction of data in EARN, but compared to the results achieved at k = 10, the error has decreased. In accordance with the matrix of predictions in Fig. 13 we can also see that the algorithm was most often wrong in defining the EARN and CRUDE categories, instead of ACQ. The number of correct distributions has increased, although not significantly.

We calculate the assessment of the quality of the classification model at k = 20 (Fig. 14).

```
Accuracy:0.8387395736793327
Precision:0.8336147608484434
Recall:0.8387395736793327
F1 score:0.8289611340421243
```

Figure 14 – Evaluation of the quality of the classification model

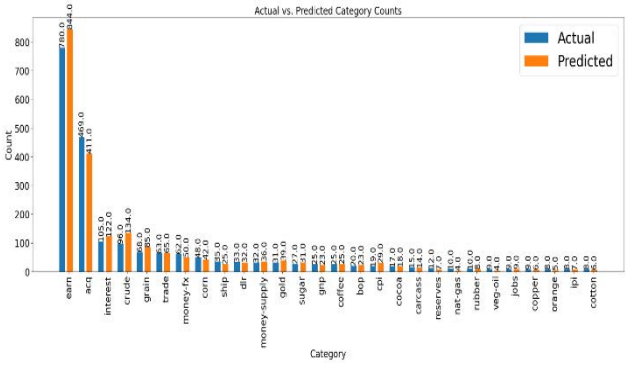

Figure 15 – Histogram comparison number of predicted and real data for k = 20

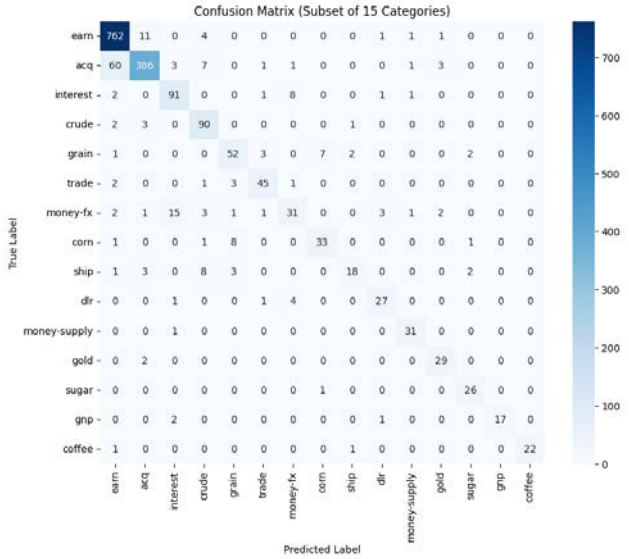

Figure 16 – Prediction matrix for k=20

As we can see from Fig. 14, the results remained the same in Fig. 11. This means that with a selected number of neighbors, the model has reached its maximum level of accuracy and it does not make sense to increase or decrease the number of neighbors. Accordingly, everything coincides with the results at k = 15.

The purpose of the experiment №2 is to study the effect of clustering on the algorithm k-NN. Clustering is a method of grouping similar objects into clusters based on their characteristics or distances to each other. In the context of k-NN, clustering can affect the results of an algorithm by changing the neighborhood of objects and hence determining their classification.

We will conduct a study on the parameters k = 5, 15, 20, c = 5, 15, 20, where k is the number of neighbors, and c is the number of clusters. We calculate the assessment of the quality of the classification model at k = 5 and c = 5 (Fig. 17).

```
Accuracy:0.8276181649675626
Precision:0.8236345856370154
Recall:0.8276181649675626
F1 score:0.8213364658704626
```

Figure 17 – Evaluation of the quality of the classification model

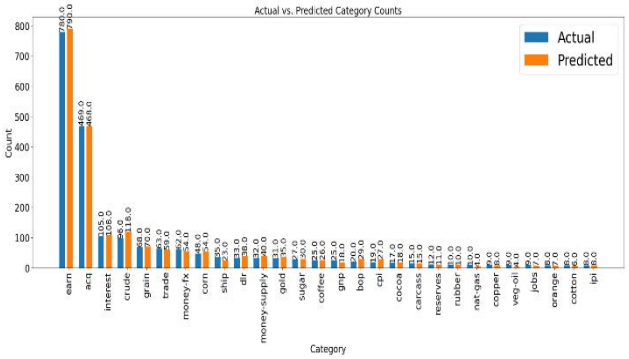

Figure 18 – Histogram comparing the number of predicted and real data for k=5 and c=5

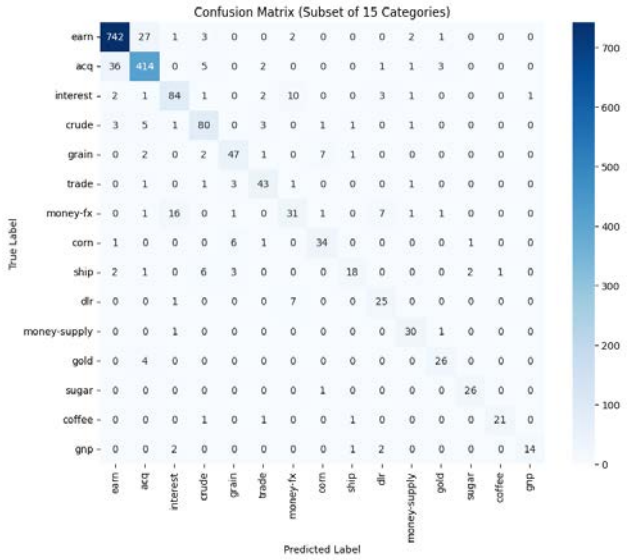

Figure 19 – Matrix of predictions for k = 5 and c = 5

As we can see from Fig. 17, the results are very good. If we compare the results of metrics with Fig. 5 and with Fig. 17, then with clustering there is a good increase in accuracy at k = 5. In Fig. 18 we can see that the attitude to categories has improved significantly with clustering than

DOI 10.15588/1607-3274-2023-3-9

without it, and the error has decreased accordingly. By the matrix of predictions in Fig. 19. We can also see that correct data allocation has improved a lot.

We calculate the assessment of the quality of the classification model at k = 15 and c = 15 (Fig. 20).

```
Accuracy:0.8419833178869324
Precision:0.836402372291527
Recall:0.8419833178869324
F1 score:0.8345115914215016
```

Figure 20 – Evaluation of the quality of the classification model

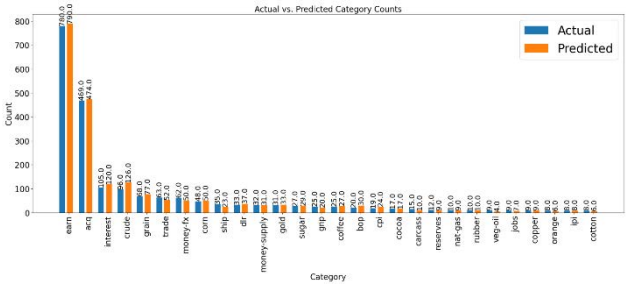

Figure 21 – Bar chart comparing the number of predicted and real data for k=15 and c=15

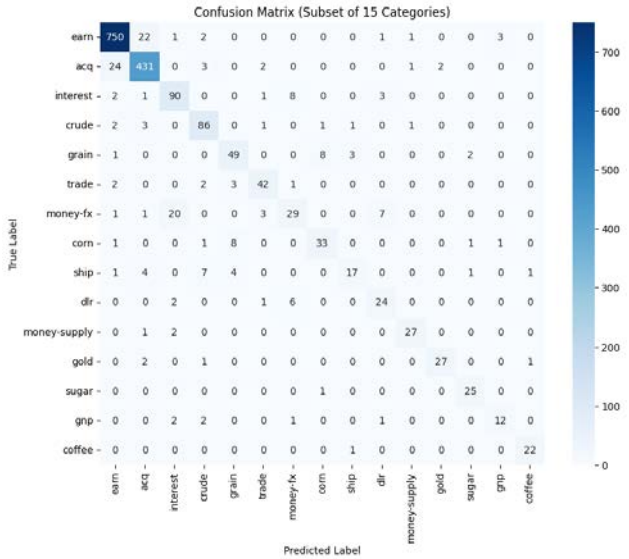

Figure 22 – Matrix of predictions for k = 15 and c = 15

As we can see from Fig. 20 results are very good. In Fig. 21 we can see that the attitude to categories has improved significantly with clustering than without it, and the predicted data almost coincides with the real data, which indicates a greater amount of properly distributed data. Following the matrix of predictions in Fig. 22 can also see that the correct distribution of data has improved a lot.

We calculate the quality assessment of the classification model at k = 20 and c = 20.

```
Accuracy:0.8456904541241891
Precision:0.8406501695176786
Recall:0.8456904541241891
F1 score:0.8374692034810864
```

Figure 23 – Assessment of the quality of the classification model

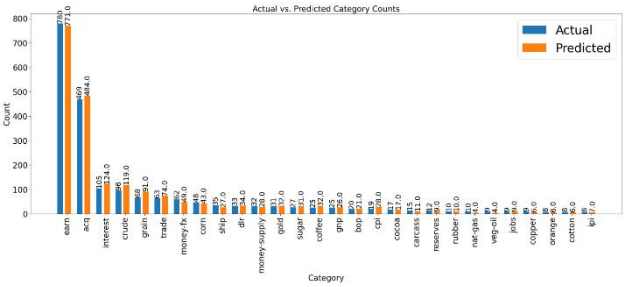

Figure 24 – Bar chart comparing the number of predicted and real data for k=20 and c=20

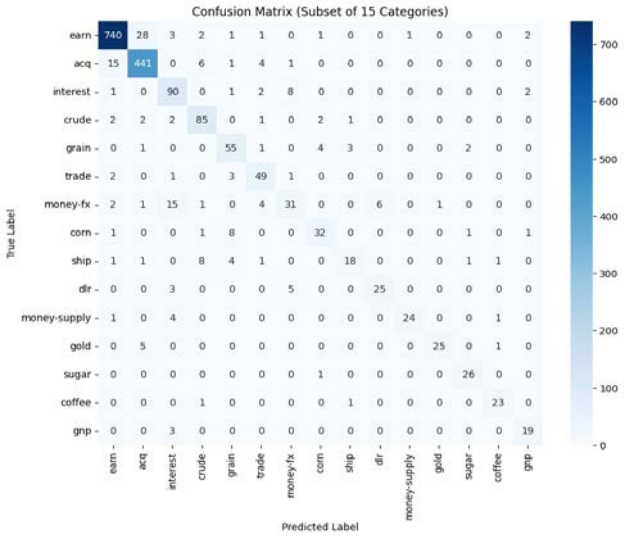

Figure 25 – Matrix of predictions for k = 20 and c = 20

The results, which are shown in Fig. 23–24 and in the matrix of predictions in Fig. 25, indicate very good results using clustering. From Fig. 23 we see that the accuracy of the model has again increased relative to k = 15 and c = 15. This means that clustering allows you to better determine the belonging of objects to the corresponding categories. In Fig. 24 shows that attitudes towards categories again improve significantly when clustering is used. Matrix of predictions in Fig. 25 also demonstrates that proper data allocation is greatly improved when clustering is used.

The experiment №3 aims to find hyperparameters that maximize the performance of the k-NN algorithm, as well as to understand the influence of hyperparameters on the classification results. The study can help identify which parameters are critical to achieving high accuracy and efficiency in a specific data context. We will use 15 neighbors for research.

We calculate the quality assessment of the classification model with the algorithm ‘ball_tree’ and the metric ‘manhattan’ at k = 15.

```
KNeighborsClassifier(algorithm='ball_tree', n_neighbors=15)
['earn' 'earn' 'earn' ... 'trade' 'cpi' 'crude']
Accuracy:0.8456904541241891
Precision:0.8406501695176786
Recall:0.8456904541241891
F1 score:0.8374692034810864
```

Figure 26 – Quality assessment of classification model with ‘ball_tree’ algorithm and ‘manhattan’ metric

DOI 10.15588/1607-3274-2023-3-9

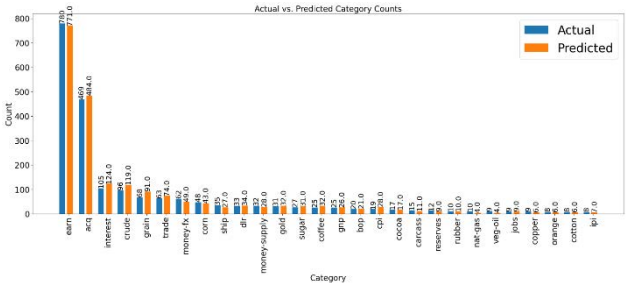

Figure 27 – Histogram comparing the number of predicted and real data with the ‘ball_tree’ algorithm and the ‘manhattan’ metric

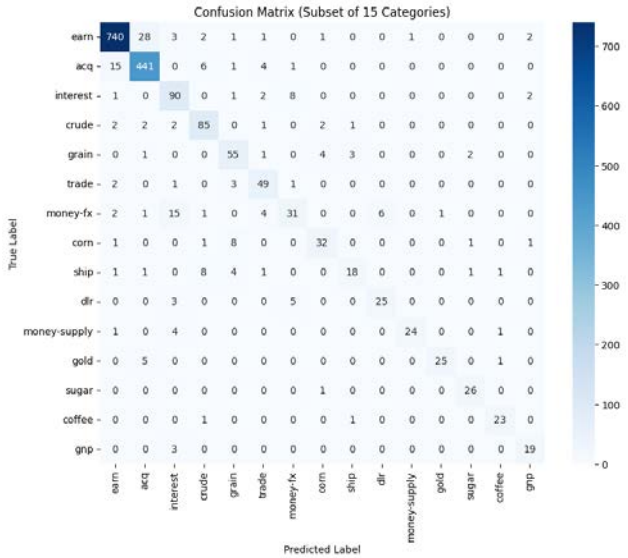

Figure 28 – Prediction Matrix with ‘ball_tree’ algorithm and ‘manhattan’ metric

As we can see from Fig. 26 results improved by comparing the usual *k*-NN with $k = 15$ in Fig. 11. In Fig. 27 we can see that, in general, the predicted data almost coincide with the real data, which indicates a more correct distribution of the data. Following the matrix of predictions in Fig. 28 We can also see that the correct distribution of data has improved a lot.

We calculate the quality assessment of the classification model with the algorithm ‘ball_tree’ and the metric ‘euclidean’ at $k = 15$.

```
Accuracy:0.8456904541241891
Precision:0.8406501695176786
Recall:0.8456904541241891
F1 score:0.8374692034810864
```

Figure 29 – Quality assessment of classification model with ‘ball_tree’ algorithm and ‘euclidean’ metric

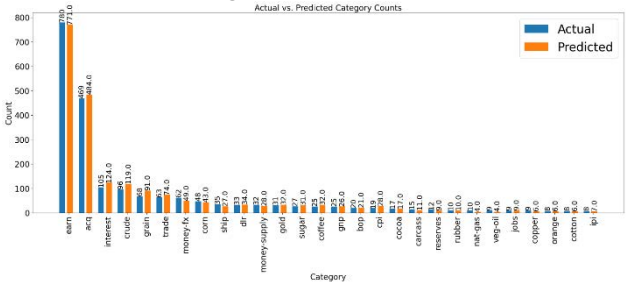

Figure 30 – Histogram comparing the number of predicted and real data with the ‘ball_tree’ algorithm and the ‘euclidean’ metric

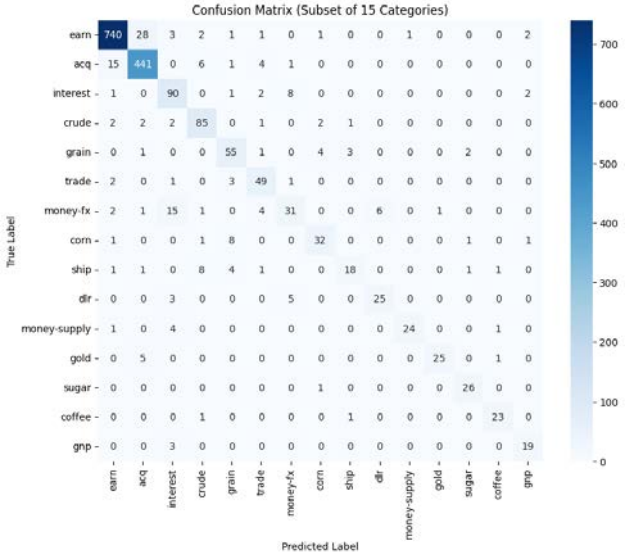

Figure 31 – Prediction matrix with ‘ball_tree’ algorithm and ‘euclidean’ metric

Comparing the results of the ‘ball_tree’ algorithm with different metrics, we can conclude that the introduction of these hyperparameters has increased the accuracy and efficiency of the model, but in two cases of using metrics, the result is the same, which may mean that both metrics measure the distance between two points with the same accuracy, or perhaps that the points are in a space where both metrics are equivalent.

We calculate the quality assessment of the classification model with the algorithm kd_tree’ and the metric ‘manhattan’ at $k = 15$.

```
KNeighborsClassifier(algorithm='kd_tree', n_neighbors=15)
['earn' 'earn' 'earn' ... 'palm-oil' 'cpi' 'crude']
Accuracy:0.8387395736793327
Precision:0.8352195686724123
Recall:0.8387395736793327
F1 score:0.8290827008957881
```

Figure 32 – Quality assessment of classification model with ‘kd_tree’ algorithm and ‘manhattan’ metric

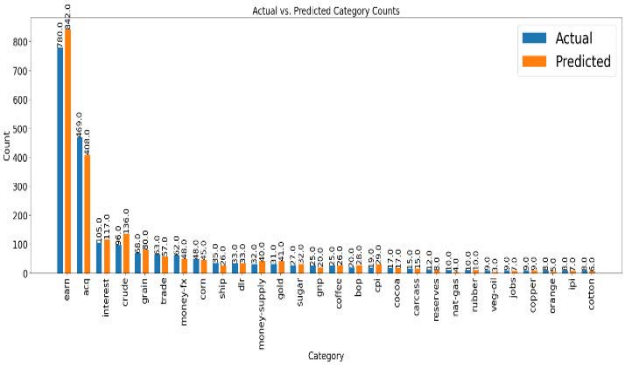

Figure 33 – Histogram comparing the number of predicted and real data with the ‘kd_tree’ algorithm and the ‘manhattan’ metric

DOI 10.15588/1607-3274-2023-3-9

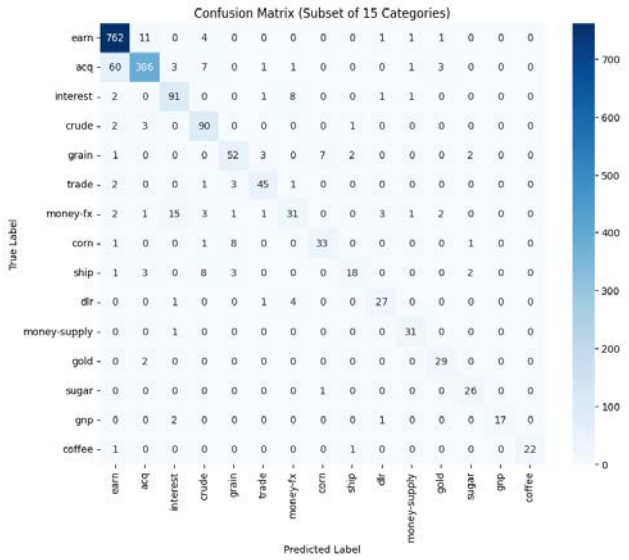

Figure 34 – Prediction matrix with ‘kd_tree’ algorithm and ‘manhattan’ metric

As you can see from Fig. 32–34, the application of ‘kd_tree’ with the ‘manhattan’ metric did not live up to expectations, since the results coincide with the use of the *k*-NN model without parameters at $k = 15$.

We calculate the quality assessment of the classification model with the algorithm kd_tree’ and the metric ‘euclidean’ at $k = 15$.

```
KNeighborsClassifier(algorithm='kd_tree', metric='euclidean', n_neighbors=15)
['earn' 'earn' 'earn' ... 'palm-oil' 'cpi' 'crude']
Accuracy:0.8387395736793327
Precision:0.8352195686724123
Recall:0.8387395736793327
F1 score:0.8290827008957881
```

Figure 35 – Evaluation of the quality of the classification model with the algorithm ‘kd_tree’ and the metric ‘euclidean’

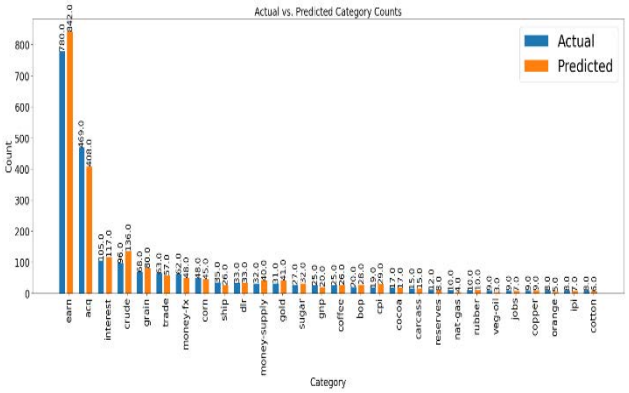

Figure 36 – Histogram comparing the number of predicted and real data with the ‘kd_tree’ algorithm and the ‘euclidean’ metric

As you can see from Fig. 35–37, the application of ‘kd_tree’ with the ‘euclidean’ metric as well as with ‘manhattan’ did not live up to expectations, since the results coincide with the use of the *k*-NN model without parameters at $k = 15$.

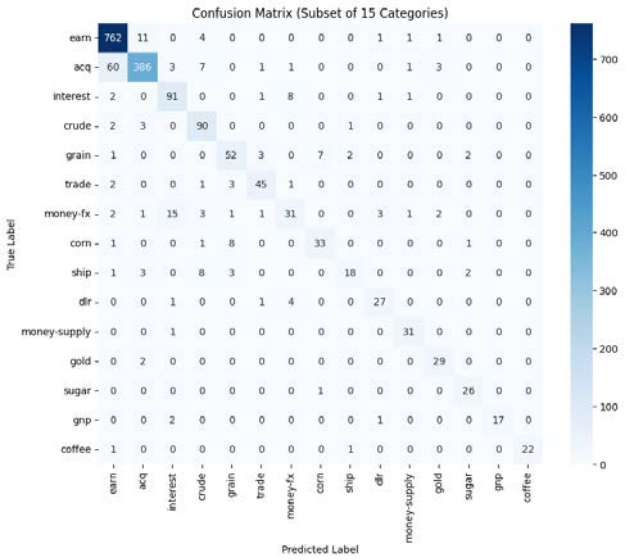

Figure 37 – Histogram comparing the number of predicted and real data with the ‘kd_tree’ algorithm and the ‘euclidean’ metric

5 RESULTS

In the previous section, the *k*-NN method for classifying text documents was implemented. Experiments have been conducted with various methods affecting the efficiency of *k*-NN, such as algorithm selection and metrics. Based on this, you can summarize the results.

In the first experiment, the results showed that the selected number of neighbors (parameter *k*) has a significant impact on the accuracy of classification. The best value of *k* is 15 and it achieves the maximum accuracy of classification of text documents, namely – 0.8387, which is equal to 83.87%. This means that increasing the number of neighbors does not significantly affect the results and does not bring additional improvements. This can be explained by the fact that too small *k* values can lose information, and too large *k* values can lead to overtraining of the model.

Therefore, for the classification of text documents, it is important to choose the optimal value of the parameter *k*, which provides the highest accuracy of classification. In this case, the use of $k = 15$ led to the maximum accuracy of classification of text documents, while at $k = 1$ the worst results are achieved, where the accuracy is – 0.7980 (79.80%).

In the second experiment, the use of clustering showed very good results for the classification of text documents. Maximum accuracy was achieved at $k = 20$ and is equal to 0.8457 (84.57%). Comparing the results when using the clusterless model *k*-NN in Fig. 4.13 and clustered in Fig. 4.22. With a value of $k = 20$, you can see how the accuracy and efficiency of classifying text documents have changed by better-determining similarities between documents and assigning them to appropriate categories.

The use of clustering changes the neighborhood of objects in space, that is, objects belonging to the same cluster become adjacent to each other. This allows the model to better distinguish objects from different categories

DOI 10.15588/1607-3274-2023-3-9

since internal similarities in clusters can be more pronounced than general similarities between all objects. Accordingly, the effectiveness and importance of this can be seen by comparing the results of models with and without clustering.

In the third experiment, which investigated the influence of hyperparameters on the *k*-NN algorithm, it was found that the choice of different algorithms and metrics can have a significant impact on the accuracy and efficiency of the model. This is achieved because different algorithms and metrics use different approaches to calculating distances between objects and determining their neighborhood. The choice of an algorithm, such as the Ball tree or *kd*-tree, affects the structure of the tree used to organize the data. In our case, the Ball tree works better, because when applied with Manhattan and Euclidean distance metrics, the maximum accuracy that has been achieved is 0.8457 (84.57%), which is on par with maximum accuracy when using clustering. Therefore, we can conclude that for datasets with a large number of features, the Ball tree works better. At this time, the *kd*-tree may be more efficient for datasets with fewer features, so in our case it was not very efficient and was able to achieve – 0.8387 (83.87%), which is not a bad result, but not very good either.

6 DISCUSSION

In our case, when using two different algorithms to find neighbors *k*-NN, metrics such as Manhattan and Euclidean distance were used. However, as can be seen from the experiments, there was no difference between them. This is because both metrics measure the distance between two points with the same precision, or the points may be in space where both metrics are equivalent, resulting in the fact that they give the same results.

So, summing up, in this case, the use of the *k*-NN method for the classification of text documents showed good results. *k*-NN takes into account the context of text documents using immediate neighbors and does not require complex data assumptions. These advantages make the *k*-NN method an attractive option for classifying text documents. However, to maximize classification accuracy, certain improvements need to be applied, such as choosing the optimal value of the *k* parameter, applying clustering, and using appropriate algorithms and metrics to improve the accuracy and efficiency of the model in our study. Based on experiments, the maximum results were shown by models *k*-NN at $k = 20$ with clustering and with hyperparameters, as an algorithm for finding neighbors – Ball tree at $k = 15$. At the same time, *k*-NN takes into account the context of text documents using immediate neighbors and does not require complex data assumptions. These advantages make the *k*-NN method an attractive option for classifying text documents.

However, to achieve maximum accuracy of classification, certain improvements must be applied. Using the optimal value of the *k* parameter, clustering, and selecting appropriate algorithms and metrics can significantly improve the quality and efficiency of the *k*-NN model.

DOI 10.15588/1607-3274-2023-3-9

In general, these experiments showed good results and confirmed the suitability of the *k*-NN nearest neighboring method for classifying text documents. In further research, it is recommended to pay attention to improving the model by optimizing parameters and using more complex algorithms to improve its efficiency.

So, summarizing all of the above, the nearest neighbors method is a very good method for classifying text documents. Given that the algorithm does not take much time, is flexible and is quite accurate, this makes it one of the best options for the classification task.

CONCLUSIONS

In this study, analysis and experiments were conducted using the *k*-NN nearest neighbor method to classify text documents. The results showed that the use of the *k*-NN method proved to be effective and a very good option for classifying text documents. The use of nearest neighbors allows the *k*-NN method to take into account the context of text documents and does not require complex data guesses. This makes it a flexible and versatile approach to classification.

In the case of researching the use of the nearest neighbors method *k*-NN to classify text documents by their topics, the **scientific novelty lies** in the fact that it offers the use of a method that is quite simple and effective to solve the complex problem of classifying text documents by their topics. The study proposes the use of clustering and dimensionality reduction to improve the quality of text classification. In addition, the study compares the efficiency of different types of term oscillation and different values of *k* in the *k*-NN method for classifying text documents. Thus, the study expands our understanding of how the nearest neighbors *k*-NN method can be applied to classify text documents by their topics and helps to improve methods for classifying texts.

The practical significance of the obtained results lies in a general review of the method of the nearest neighbors *k*-NN and the creation of a software solution for classifying text documents by their topics using this method. After all, the developed system can automatically classify text documents by their topics. It reduces classification errors, thereby improving the accuracy of the system. The study proposes developed software that implements the proposed indicators, and also experiments were conducted to study their properties. The results of the experiment allow for recommending the proposed indicators for use in practice, as well as determining the effective conditions for applying the proposed indicators.

Prospects for further research are to study the proposed algorithms for a wide class of practical problems.

ACKNOWLEDGEMENTS

The study was created within the framework of the project financed by the National Research Fund of Ukraine, registered No 30/0103 from 01.05.2023, “Methods and means of researching markers of aging and their influence on post-aging effects for prolonging the working period”, which is carried out at the Department of

Artificial Intelligence Systems of the Institute of Computer Sciences and Information of technologies of the National University “Lviv Polytechnic”.

REFERENCES

1. Tung A. K., Hou J., Han J. Spatial clustering in the presence of obstacles, *The 17th Intern. conf. on data engineering (ICDE’01)*. Heidelberg, 2001, pp. 359–367. DOI: 10.1109/ICDM.2002.1184042
2. Boehm C., Kailing K., Kriegel H., Kroeger P. Density connected clustering with local subspace preferences, *IEEE Computer Society. Proc. of the 4th IEEE Intern. conf. on data mining. Los Alamitos*, 2004, pp. 27–34. DOI: 10.1007/978-0-387-39940-9_605
3. Boyko N., Kmetyk-Podubinska K., Andrusiak I. Application of Ensemble Methods of Strengthening in Search of Legal Information, *Lecture Notes on Data Engineering and Communications Technologies*, 2021, Vol. 77, pp. 188–200. https://doi.org/10.1007/978-3-030-82014-5_13.
4. Boyko N., Hetman S., Kots I. Comparison of Clustering Algorithms for Revenue and Cost Analysis, *Proceedings of the 5th International Conference on Computational Linguistics and Intelligent Systems (COLINS 2021)*. Lviv, Ukraine, 2021, Vol. 1, pp. 1866–1877.
5. Procopiuc C. M., Jones M., Agarwal P. K., Murali T. M. A Monte Carlo algorithm for fast projective clustering, *ACM SIGMOD Intern. conf. on management of data*. Madison, Wisconsin, USA, 2002, pp. 418–427.
6. Sharma A., J. Nirmal Kumar S, Rana D., Setia S. A Review On Collaborative Filtering Using Knn Algorithm, *OPJU International Technology Conference on Emerging Technologies for Sustainable Development (OTCON)*, 2023, pp. 1–6. DOI: 10.1109/OTCON56053.2023.10113985
7. Faye G. C. Gamboa, Matthew B. Concepcion, Antolin J. Alipio, Dan Michael A. Cortez, Andrew G. Bitancor, Myra S.J. Santos, Francis Arlando L. Atienza, Mark Anthony S. Mercado Further Enhancement of KNN Algorithm Based on Clustering Applied to IT Support Ticket Routing, 3rd International Conference on Computing, Networks and Internet of Things (CNIOT), 2022, pp. 186–190. DOI: 10.1109/CNIOT55862.2022.00040
8. Yang J.-K., Huang K.-Ch., Chung Ch.-Y., Chen Yu-Chi, Wu T.-W. Efficient Privacy Preserving Nearest Neighboring Classification from Tree Structures and Secret Sharing, *IEEE International Conference on Communications*, 2022, pp. 5615–5620. DOI: 10.1109/ICC45855.2022.9838718
9. Zhang Yu., Zhou Y., Xiao M., Shang X. Comment Text Grading for Chinese Graduate Academic Dissertation Using Attention Convolutional Neural Networks, *7th International Conference on Systems and Informatics (ICSAI)*, 2021, pp. 1–6. DOI: 10.1109/ICSAI53574.2021.9664159
10. Rohwinasakti S., Irawan B., Setianingsih C. Sentiment Analysis on Online Transportation Service Products Using K-Nearest Neighbor Method, *International Conference on Computer, Information and Telecommunication Systems (CITS)*, 2021, pp. 1–6.
11. Javid J., Ali Mughal M., Karim M. Using kNN Algorithm for classification of Distribution transformers Health index, *International Conference on Innovative Computing (ICIC)*, 2021, pp. 1–6. DOI: 10.1109/ICIC53490.2021.9693013
12. Bansal A., Jain A. Analysis of Focussed Under-Sampling Techniques with Machine Learning Classifiers, *IEEE/ACIS 19th International Conference on Software Engineering Research, Management and Applications (SERA)*, 2021, pp. 91–96. DOI: 10.1109/SERA51205.2021.9509270
13. Bellad Sagar. C., Mahapatra A., Ghule S. Dilip, Shetty S. Sridhar, Sountharrajan S, Karthiga M, Suganya Prostate Cancer Prognosis-a comparative approach using Machine Learning Techniques, *5th International Conference on Intelligent Computing and Control Systems (ICICCS)*, 2021, pp. 1722–1728. DOI: 10.1109/ICICCS51141.2021.9432173
14. Pokharkar Swapnil R., Wagh Sanjeev J., Deshmukh Sachin N. Machine Learning Based Predictive Mechanism for Internet Bandwidth, *6th International Conference for Convergence in Technology (I2CT)*, 2021, pp. 1–4. DOI: 10.1109/I2CT51068.2021.9418164
15. Chaudhary K., Poirion O. B., Lu L., Garmire L. X. Deep learning based multi-omics integration robustly predicts survival in liver cancer, *Clin. Can. Res.*, 2017, 0853, pp. 1246–1259. doi: 10.1101/114892
16. Cheng B., Liu M., Zhang D., Musell B. C., Shen D. Domain Transfer Learning for MCI Conversion Prediction, *IEEE Trans. Biomed. Eng.*, 2015, Vol. 62 (7), pp. 1805–1817. doi: 10.1109/TBME.2015.2404809
17. Huang M., Yang W., Feng Q., Chen W., Weiner M. W., Aisen P. Longitudinal measurement and hierarchical classification framework for the prediction of Alzheimer’s disease, *Sci. Rep.*, 2017, Vol. 7, P. 39880. doi: 10.1038/srep39880
18. Hossain M. Z., Akhtar M. N., Ahmad R. B., Rahman M. A dynamic K-means clustering for data mining, *Indonesian Journal of Electrical Engineering and Computer Science*, 2017, Vol. 13 (2), pp. 521–526. DOI: http://doi.org/10.11591/ijeecs.v13.i2.pp521–526
19. Jothi R., Mohanty S. K., Ojha A. DK-means: a deterministic *k*-means clustering algorithm for gene expression analysis, *Pattern Analysis and Applications*, 2019, Vol. 22(2), pp. 649–667. DOI: 10.1007/s10044-017-0673-0
20. Polyakova M. V., Krylov V. N. Data normalization methods toimprovethe quality ofclassificationin the breast cancerdiagnostic system, *Applied Aspects of Information Technology*, 2022, Vol. 5(1), pp. 55–63. DOI: https://doi.org/10.15276/aait.05.2022.5

Received 15.05.2023.
Accepted 20.08.2023.

УДК 004.021

МЕТОД *k* НАЙБЛИЖЧИХ СУСІДІВ ДЛЯ КЛАСИФІКАЦІЇ ТЕКСТОВИХ ДОКУМЕНТІВ ЗА ЇХ ТЕМАТИКОЮ

Бойко Н. І. – канд. економ. наук, доцент, доцент кафедри Систем штучного інтелекту, Національний університет «Львівська політехніка», Львів, Україна.

Михайлишин В. Ю. – асистент кафедри Системи штучного інтелекту, Національний університет «Львівська політехніка», Львів, Україна.

АНОТАЦІЯ

Актуальність. Оптимізація методу найближчих сусідів *k*-NN для класифікації текстових документів за їх темою, а також розв’язок задачі на основі методу експериментальним шляхом.

Мета роботи є вивчення методу найближчих сусідів *k*-NN для класифікації текстових документів за їх темою. Завданням дослідження є на основі набору даних провести класифікацію текстових документів за їх темою за оптимальний час та з високою точністю.

Метод. Метод *k*-найближчих сусідів – це метричний алгоритм для автоматичної класифікації об’єктів або регресії. Алгоритм *k*-NN зберігає всі наявні дані та класифікує нову точку на основі відстані між новою точкою та всіма точками в нав-

DOI 10.15588/1607-3274-2023-3-9

чальному наборі. Для цього використовується певна метрика відстані, така як Евклідова відстань. У процесі навчання *k*-NN зберігає всі дані з навчального набору, тому він відноситься до «ледачих» алгоритмів, оскільки навчання відбувається в момент класифікації. Алгоритм не робить ніяких припущень про розподіл даних та він є непараметричним. Завдання алгоритму *k*-NN полягає в тому, щоб призначити тестовому документу *x* певну категорію на основі категорій *k* найближчих сусідів з навчального набору даних. Схожість між тестовим документом *x* та кожним з найближчих сусідів оцінюється балом категорії, до якої належить сусід. Якщо декілька з *k* найближчих сусідів належать до однієї категорії, то бал схожості цієї категорії для тестового документа *x* обчислюється як сума балів категорії для кожного з цих найближчих сусідів. Після цього, категорії ранжуються за балами, і тестовий документ призначається категорії з найвищим балом.

Результати. Успішно реалізовано метод *k*-NN для класифікації текстових документів. Було проведено експерименти з різними методами, що впливають на ефективність *k*-NN, такими як вибір алгоритму та метрики. Результати експериментів показали, що використання певних методів може покращити точність класифікації та ефективність моделі.

Висновки. Відображення результатів на різних метриках та алгоритмах показало, що вибір конкретного алгоритму та метрики може мати значний вплив на точність передбачень. Застосування алгоритму ball tree, а також використання різних метрик, таких як манхетівська або євклідова відстань, може призвести до покращення результатів. Використання кластеризації перед застосуванням *k*-NN показало позитивний вплив на результати та дозволяє краще групувати дані і зменшує вплив шуму або неправильно класифікованих точок, що призводить до покращення точності та розподілу класів.

КЛЮЧОВІ СЛОВА: метод, кластер, класифікація, текстовий документ, тема, алгоритм ball tree, метрика.

ЛІТЕРАТУРА

1. Tung A. K. Spatial clustering in the presence of obstacles / A. K. Tung, J. Hou, J. Han // The 17th Intern. conf. on data engineering (ICDE'01), Heidelberg. – 2001. – P. 359–367. DOI: 10.1109/ICDM.2002.1184042
2. Density connected clustering with local subspace preferences / [C. Boehm, K. Kailing, H. Kriegel, P. Kroeger] // IEEE Computer Society. Proc. of the 4th IEEE Intern. conf. on data mining. Los Alamitos. – 2004. – P. 27–34. DOI: 10.1007/978-0-387-39940-9_605
3. Boyko N. Application of Ensemble Methods of Strengthening in Search of Legal Information / N. Boyko, K. Kmetyk-Podubinska, I. Andrusiak // Lecture Notes on Data Engineering and Communications Technologies. – 2021. – Vol. 77. – P. 188–200. https://doi.org/10.1007/978-3-030-82014-5_13.
4. Boyko N. Comparison of Clustering Algorithms for Revenue and Cost Analysis / N. Boyko, S. Hetman, I. Kots // Proceedings of the 5th International Conference on Computational Linguistics and Intelligent Systems (COLINS 2021). Lviv, Ukraine. – 2021. – Vol. 1. – P. 1866–1877.
5. A Monte Carlo algorithm for fast projective clustering / [C. M. Procopiuc, M. Jones, P. K. Agarwal, T. M. Murali] // ACM SIGMOD Intern. conf. on management of data, Madison, Wisconsin, USA. – 2002. – P. 418–427.
6. A Review On Collaborative Filtering Using Knn Algorithm / [A. Sharma, J. Nirmal Kumar S, D. Rana, S. Setia] // OPJU International Technology Conference on Emerging Technologies for Sustainable Development (OTCON). – 2023. – P. 1–6. DOI: 10.1109/OTCON56053.2023.10113985
7. Gamboa Further Enhancement of KNN Algorithm Based on Clustering Applied to IT Support Ticket Routing / [C. Faye G. Gamboa, Matthew B. Concepcion, Antolin J. Alipio et al.] // 3rd International Conference on Computing, Networks and Internet of Things (CNIOT). – 2022. – P.186–190. DOI: 10.1109/CNIOT55862.2022.00040
8. Efficient Privacy Preserving Nearest Neighboring Classification from Tree Structures and Secret Sharing / [J.-K. Yang, K.-Ch. Huang, Ch.-Y. Chung et al.] // IEEE International Conference on Communications. – 2022. – P. 5615–5620. DOI: 10.1109/ICC45855.2022.9838718
9. Zhang Yu. Comment Text Grading for Chinese Graduate Academic Dissertation Using Attention Convolutional Neural Networks / [Y. Zhang, Y. Zhou, M. Xiao, X. Shang] // 7th International Conference on Systems and Informatics (ICSAI). – 2021. – P. 1–6. DOI: 10.1109/ICSAI53574.2021.9664159
10. Rohwinasakti S. Sentiment Analysis on Online Transportation Service Products Using *K*-Nearest Neighbor Method / S. Rohwinasakti, B. Irawan, C. Setianingsih // International Conference on Computer, Information and Telecommunication Systems (CITS). – 2021. – P.1–6.
11. Javid J. Using kNN Algorithm for classification of Distribution transformers Health index / J. Javid, M. Ali Mughal, M. Karim // International Conference on Innovative Computing (ICIC). – 2021. – P. 1–6. DOI: 10.1109/ICIC53490.2021.9693013
12. Bansal A. Analysis of Focussed Under-Sampling Techniques with Machine Learning Classifiers / A. Bansal, A. Jain // IEEE/ACIS 19th International Conference on Software Engineering Research, Management and Applications (SERA). – 2021. – P. 91–96. DOI: 10.1109/SERA51205.2021.9509270
13. Bellad Sagar.C. Prostate Cancer Prognosis-a comparative approach using Machine Learning Techniques / [Sagar.C. Bellad, A. Mahapatra, S. Dilip Ghule et al.] // 5th International Conference on Intelligent Computing and Control Systems (ICICCS). – 2021. – P. 1722–1728. DOI: 10.1109/ICICCS51141.2021.9432173
14. Pokharkar Swapnil R. Machine Learning Based Predictive Mechanism for Internet Bandwidth / Swapnil R. Pokharkar, Sanjeev J. Wagh, Sachin N. Deshmukh // 6th International Conference for Convergence in Technology (I2CT). – 2021. – P.1–4. DOI: 10.1109/I2CT51068.2021.9418164
15. Deep learning based multi-omics integration robustly predicts survival in liver cancer / [K. Chaudhary, O. B. Poirion, L. Lu, L. X. Garmire] // Clin. Can. Res. – 2017. – 0853. – P. 1246–1259. doi: 10.1101/114892
16. Domain Transfer Learning for MCI Conversion Prediction / [B. Cheng, M. Liu, D. Zhang et al.] // IEEE Trans. Biomed. Eng. – 2015. – Vol. 62 (7). – P. 1805–1817. doi: 10.1109/TBME.2015.2404809
17. Longitudinal measurement and hierarchical classification framework for the prediction of Alzheimer's disease / [M. Huang, W. Yang, Q. Feng et al.] // Sci. Rep. – 2017. – Vol. 7. – P. 39880. doi: 10.1038/srep39880
18. A dynamic K-means clustering for data mining / [M. Z. Hossain, M. N. Akhtar, R. B. Ahmad, M. Rahman] // Indonesian Journal of Electrical Engineering and Computer Science. – 2017. – Vol. 13 (2). – P. 521–526. DOI: http://doi.org/10.11591/ijeecs.v13.i2.pp521–526
19. Jothi R. DK-means: a deterministic k-means clustering algorithm for gene expression analysis / R. Jothi, S. K. Mohanty, A. Ojha // Pattern Analysis and Applications. – 2019. – Vol. 22(2). – P. 649–667. DOI: 10.1007/s10044-017-0673-0
20. Polyakova M. V. Data normalization methods toimprovethe quality ofclassificationin the breast cancerdiagnostic system / M. V. Polyakova, V. N. Krylov // Applied Aspects of Information Technology. – 2022. – Vol. 5(1). – P. 55–63. DOI: https://doi.org/10.15276/aait.05.2022.5

DOI 10.15588/1607-3274-2023-3-9